The Dissertation Committee for Pedro Metola Certifies that this is the approved version of the following dissertation:

Boronic Acids: Structural and Mechanistic Studies and Application as Macromolecular Sensing Systems

Committee:

Eric V. Anslyn, Supervisor

Brent L. Iverson

Michael J. Krische

Alan H. Cowley

Hung-Wen Liu

Boronic Acids: Structural and Mechanistic Studies and Application as Macromolecular Sensing Systems

by

Pedro Metola, B. S.

Dissertation

Presented to the Faculty of the Graduate School of

The University of Texas at Austin

in Partial Fulfillment

of the Requirements

for the Degree of

Doctor of Philosophy

The University of Texas at Austin

December 2013

Dedication

To the memory of my grandfather.

Acknowledgements

I would like to start by thanking Eric Anslyn for everything he has done for me. Nothing I write here can do justice to the debt I owe him both as a mentor and as a friend.

I would like to thank Anslyn group members past and present for support and advice. Without Mandy, Diana and Marco I would not have made it through candidacy. John Rainwater showed me the ropes and taught me the way of the turtle. In Leo Joyce I found a good friend and an example for how to behave inside and outside the lab. I am truly lucky to have spent these years in the company of great people.

Big thanks to our cousins in the Iverson lab, especially to Mike Alvey who helped me when I became a senior graduate student and Pam Keebles for his invaluable assistance in the last days of my degree.

For better or for worse, the people of Taos deserve a certain degree of recognition.

Finally, I would like to thank my father Luis Miguel, mother Mari Carmen, sisters Ane and Maria and the rest of my family for being 5000 miles away but always close by and available, for their unconditional support and for believing in me without ever really knowing what I was doing.

Boronic Acids: Structural and Mechanistic Studies and Application as Macromolecular Sensing Systems

Pedro Metola, Ph. D.

The University of Texas at Austin, 2013

Supervisor: Eric V. Anslyn

Boronic acids, particularly those that carry an *ortho*-aminomethyl group, have been extensively utilized in the field of molecular recognition in recent years thanks to their ability to reversibly bind to a wide variety of polyol substrates. They have been shown to form cyclic boronate esters rapidly upon reaction with 1,2- and 1,3-diols, catechols, carbohydrates and hydroxycarboxylic acids, making them attractive as potential sensing units. While they have found broad application in this forum, the mechanism by which they work is still up for debate. This work begins in Chapter 1 with a review of the fundamentals of ^{11}B NMR spectroscopy and its application on the analysis of boronic acid-containing systems.

The focus of Chapter 2 turns toward systems with an *o*-iminomethylphenylboronic acid moiety. This species can be formed easily through a three-component assembly, though physical understanding of this complex lags behind. With the fundamentals of ^{11}B NMR spectroscopy detailed previously, the results obtained when utilizing this technique to study both the structure and mode of interaction in these species will be presented.

In Chapter 3 we give a comprehensive review of the data and conclusions that have been published by different groups about one of the most successful fluorescent

sugar sensors of this kind, first introduced by Seiji Shinkai in 1994. Additionally, it delineates the experimental results obtained by our group when attempting to answer some of the remaining questions.

In Chapter 4 we report the use of the aforementioned multi-component assembly as an enantioselective sensor for α-chiral primary amines. Using circular dichroism, the *ee*% of these analytes could be accurately determined with this system. Additionally, enantio- and chemodiscrimination was possible by employing chemometric tools like PCA and LDA.

Finally, Chapter 5 is a compilation of efforts to expand the use of these sensing systems into synthetic organic chemistry research labs. In collaboration with Xumu Zhang at Rutgers University, we have implemented a previously developed system to analyze the product of an asymmetric hydrogenation of an imine to create a chiral amine. A proof of concept study on a novel automated circular dichroism plate reader prototype aimed to increasing sample throughput was completed at New York University with Professor Bart Kahr.

Table of Contents

List of Tables

List of Figures

List of Schemes

Chapter 1: ^{11}B NMR and its Uses in Molecular Recognition Involving Boronic Acids

1.1 Introduction

Boronic acids and boronate esters[1] serve a myriad of purposes, and the discovery of the Suzuki–Miyaura reaction[2] facilitated the widespread interest and application of organoboron compounds. This palladium-catalyzed C-C bond forming reaction initiated a renewed interest in the preparation of libraries of diversely functionalized boronic acids that would lead to valuable products. From this synthetic standpoint, Suzuki coupling reactions have been employed in the production of natural products[3-5] and the preparation of materials of interest.[6-10] The search for interesting starting materials for the Suzuki reaction produced a series of methods to prepare boronic acids so these species could be exploited in further applications. These compounds can be easily synthesized by ways of transmetalation or hydroboration reactions,[11-13] or through asymmetric conjugate addition.[14] Additionally, boronic acids and boronate esters have been shown to function as catalytic inhibitors in enzymes and other biologically relevant proteins,[15-21] in the building of macromolecular scaffolds[22-24] and as molecular recognition units with a special focus on sugars.[25-28] As highly versatile moieties, a profound and comprehensive understanding of their structural and electronic behavior is of relevance to the entire scientific community.

Boron-containing classes of molecules have been thoroughly studied *via* ^{11}B NMR, with the resulting chemical shift information correlated to different structural patterns.[29-31] The technique is not usually employed as a definitive characterization tool.

Rather it has been used to partially assign general structural features directly from measurements of chemical shift values, J coupling constants, and information obtained from ^{1}H-^{11}B NMR correlated two-dimensional spectra.[29] Even though spectral data for boronic acids and boronate esters has not been as extensively recorded, the difference in chemical shift between tricoordinated and tetracoordinated boron translates into a significant discrimination between spectroscopic signals. This allows for the use of ^{11}B NMR as a complementary technique to monitor and study behavior of boronic acid-based constructs or systems, particularly those where a change in coordination and hybridization accompanies a reaction or transformation of interest.

1.1.1 NMR Technique

Practical understanding of the particulars concerning ^{11}B NMR spectroscopy begins with the comparison of the boron nucleus to those nuclei that are traditionally studied: hydrogen and carbon. Table 1 contains parameters relevant to NMR spectroscopy for these nuclei.

Nucleus	Percent Abundance	Spin Number (I)	Gyromagnetic Ratio (γ)[a]	Relative Sensitivity[b]	Larmor Frequency[c]	Quadrupole moment[d]
^{1}H	99.99	1/2	26.75	1.00	400.00	0
^{13}C	1.07	1/2	6.73	1.70×10^{-04}	100.58	0
^{10}B	19.90	3	2.87	3.95×10^{-03}	42.98	1.11×10^{-01}
^{11}B	80.10	3/2	8.58	1.32×10^{-01}	128.34	3.55×10^{-02}

Table 1.1. Nuclear properties of hydrogen, carbon and boron isotopes

The ^{11}B nucleus, with a smaller quadrupole moment and nuclear spin, is more sensitive and yields sharper and less complex signals than ^{10}B. The ^{10}B nucleus splits protons attached to it into a heptet, while the ^{11}B nucleus leads to a quartet. In addition, ^{11}B has a greater nuclear magnetic momentum than the other active isotope, which generally translates into a higher signal/noise ratio. Given these factors, ^{11}B is generally the boron nucleus of choice for these types of experiments.[32]

However, the high natural abundance and relatively high sensitivity (when compared to ^{13}C for example) referenced in Table 1 do not necessarily translate into well resolved spectral signals. The aforementioned spin coupling of ^{1}H with ^{10}B and ^{11}B and quadrupole moments often lead to broad signals.[33] In fact, signals for both proton and boron in boron compounds in solution describe a width of between 30 and 60 Hz (at half maximum) consistently.[33] On the same practical note, there is another possible issue that must be considered when aiming to undertake ^{11}B NMR analysis: most glass equipment that is used in scientific settings is composed of boron-containing species. These borosilicates will have an effect on the output NMR spectra. The contribution of the glass from the NMR tubes to this interference is something that can be avoided by employing considerably more expensive quartz tubes. But one must keep in mind

[a] Gyromagnetic ratio expressed in 10^{7} rad $T^{-1}s^{-1}$

[b] Relative sensitivity when compared to ^{1}H

[c] Larmor frequency expressed in MHz at a magnetic field B = 9.4T

[d] Quadrupole moment xpressed in 10^{-24} cm^{2}

that most NMR probes also have a glass component and therefore readings are marred with a substantial background signal. Unless the facilities provide a probe that is specifically tailored for boron analysis, or can reliably account for the background footprint, quantitative studies are therefore not common in ^{11}B NMR spectroscopy.

The availability of X-ray crystallography instrumentation and data has made a significant difference to the way chemical shifts can be assigned to structural motifs or chemical environments around the boron atom. This solid state evidence provides a true image of the shape of the species under study and its binding modes, caution must be taken, however, since these details might not remain consistent when the molecule is in solution.

1.2 ^{11}B NMR Chemical Shifts

As a result of the ^{11}B NMR studies that have been carried out, lots of chemical shift values have been reported for a variety of boron-containing species. What follows is a compilation of chemical shifts corresponding to different common boranes and related species as recorded in the original bodies of work that analyzed them. The list includes one-boron compounds, polyboranes, carboranes and borates. All chemical shift values are given in relation to the external reference standard BF_3•Et_2O and rounded to within 0.1 ppm.

To delineate general trends, there exists a direct correlation between the π-donor ability of the groups around the boron atom and the frequencies for the ^{11}B resonances.[34] As the donating character of ligands increases, an upfield shift is observed, as evidenced by the systematic decrease of the ^{11}B signal that occurs when alkyl groups are substituted by electron-withdrawing ligands with increased back-bonding abilities in trialkylboranes.[34] This is a similar phenomenon to the switch to lower ppm values that can be observed upon addition of a fourth

group onto the p orbital that remains empty in tricoordinated boron compounds. As expected, factors that decrease π-bonding, like steric hindrance around the boron center, are prone to cause a positive displacement of the signal towards higher frequencies.[34]

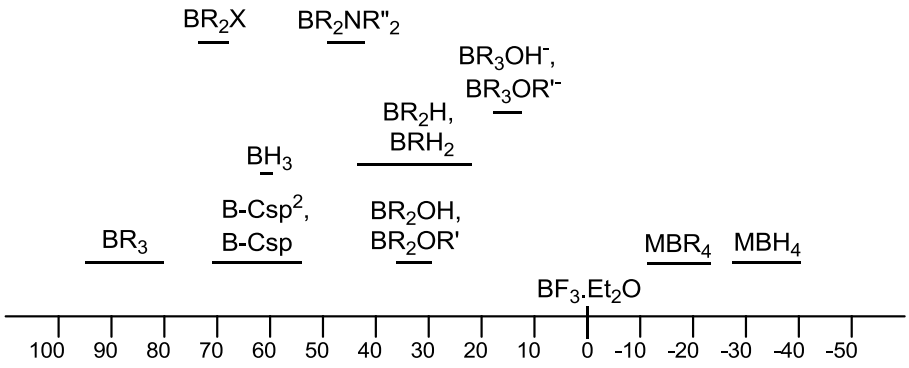

Figure 1.1. Relation of ^{11}B NMR resonances for different boron-containing species.

1.2.1 Tricoordinate Boranes and Trialkylboranes

The original borane (BH_3) and trialkylboranes have very well-defined resonance values. Trialkylboranes rarely show resonances outside the narrow low field range of 80-95 ppm regardless of the structure of the alkyl group. The chemical shifts of alkylboranes of the formula BRH_2 or BR_2H, however, cannot be as easily predicted and are highly dependent upon the structure of the alkyl groups around the boron atom.

Regarding cyclic boranes, the size of the ring has a direct effect on the position of the signal. In this construct, small rings show a pronounced downfield shift to higher ppm values. Five-member rings are on average 6 ppm further downfield than their six-member ring counterparts, which display approximately the same chemical shifts as acyclic alkylboranes.[34]

In any case, where there exists a B-H bond, the ^{11}B NMR spectrum will show a B-H coupling. This coupling will display the corresponding signal multiplicity as described earlier. The degree of B-H splitting and signal complexity increases with the number and electronegativity of the ligands.

Formation of a dimerized species is common in tricoordinated boranes without great steric hindrance. Their presence leads to a shift towards lower resonance frequencies and the possibility of more convoluted spectra by virtue of likely additional coupling interactions. Dative interactions with boron, where the two electrons forming the bond originate from another molecule (the solvent or a basic ligand), also lead to higher field frequencies.

Structure	Resonance (in ppm)	Reference
	+57.1	35
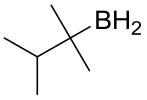	+24.0	36
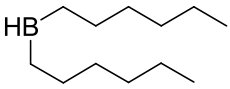	+30.5	37
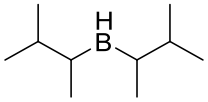	+30.0	38
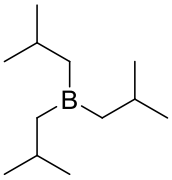	+87.1	39
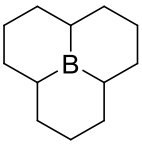	+71.2	40

Table 1.2. ^{11}B NMR chemical shifts for tricoordinated boranes and alkylboranes.

1.2.2 Unsaturation and Heteroatoms in Alkylboranes

Unsaturated substituents around boron have a dramatic effect on the ^{11}B chemical shifts over their saturated analogs. Ligands with π-bonds adjacent to the central boron atom are naturally more prone to donate into its empty p orbital due to orbital mixing. This can cause a consistent upfield shift of the ^{11}B resonance relative to the alkyl peaks. Alkyne ligands are also believed to contribute to this effect through anisotropy.

Similarly, the introduction of heteroatoms like oxygen, nitrogen or halogens results in lower ppm values for the borane resonances. The reasoning for this resides in the inter- or intramolecular donation of the lone pairs of the heteroatom into the empty p orbital of the of the central boron. This has the same effect as unsaturated systems, leading to upfield shifts of ^{11}B signals.

Structure	Resonance (in ppm)	Reference
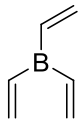	+55.2	41
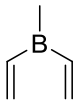	+64.4	41
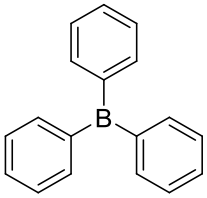	+60.2	41
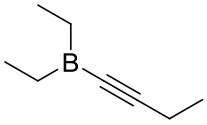	+72.9	42
	+60.1	43
	+75.5	43
	+78.8	44

Table 1.3. ^{11}B NMR chemical shifts for unsaturated and substituted alkylboranes.

	+47.1	45
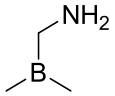	+48.4	46

Table 1.3. ^{11}B NMR chemical shifts for unsaturated and substituted alkylboranes (Cont.).

1.2.3 Boron Compounds with Oxygen-Ligands

Numerous boronates have been prepared that have oxygen atoms attached directly to the central boron atom. As expected of strong π-donors, introduction of hydroxyl or alkoxy groups shifts the ^{11}B signals upfield relative to the analogous trialkylborane. The structural features of the alkoxy group apparently have little influence on the final position of the resonances, with signals only slightly shifted upfield for aromatic or vinylic groups. Cyclic anhydrides of the boronic acids are known as boroxines, and show a moderate shift of resonances downfield towards higher ppm values.

Structure	Resonance (in ppm)	Reference
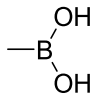	+31.9	43
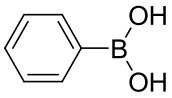	+28.4	47
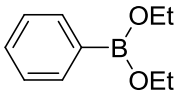	+28.6	48
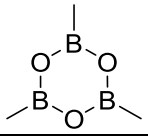	+33.2	43

Table 1.4. ^{11}B NMR chemical shifts for tricoordinated boranes bound to oxygen ligands.

1.2.4 Borohydrides, Alkylborohydrides and Tetraalkylborates

Another important boron-containing species is one where boron has four substituent groups. The original borohydrides (BH_4^-) can give more convoluted spectra than expected. This is largely based on whether the nature of these species is covalent or ionic, as the interactions of the counterion with the borohydride hydrogens will differ. Generally, this exchange between binding modes is fast on the NMR scale and only one type of hydrogen is observed. As expected, ^{11}B NMR resonances for borohydrides appear at higher field, -26 to -45 ppm. These species represent some of the furthest upfield chemical shifts for boron species. Effects that interfere with the solvation of the counterion, like the identity of the solvent, have a substantial effect on the position of the signals. When an alkyl group replaces one of the hydrogens, the resonances are shifted downfield to varying degrees. Tetraalkylborates appear between -15 and -22 ppm and

the dependence on counterion and solvent is much less pronounced in these cases. The behavior of four-coordinated boron species containing heteroatom-bound ligands are harder to predict. Most of these examples show that the upfield shift compared to tricoordinated boron is not as pronounced as in tetraalkylborates, which can be due to the differences in electronic donation between a purely covalent and more of a dative interaction.

Structure	Resonance (in ppm)	Reference
$Al(BH_4)_3$	-33.0	49
$Li\ BH_4$	-38.2	50
$Li(BEt_4)$	-17.5	51
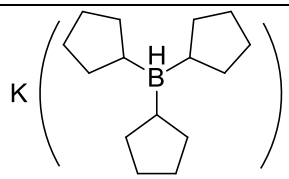	-10.7	40
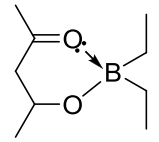	+14.2	52
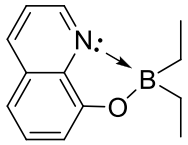	+14.4	52

Table 1.5. ^{11}B NMR chemical shifts for tetracoordinated boron species.

1.3 ^{11}B NMR IN BORONIC ACID SYSTEMS

Pizer and Tihal made the first significative contribution to the methodology of employing ^{11}B NMR spectroscopy as a means of confirming or validating mechanistic and/or kinetic hypothesis in the boronic acid area in 1992.[53,54] This technique was employed to complement the results obtained *via* pH titrations in order to describe the reaction pathways, equilibria and rate constants associated with the reaction of trigonal and four-coordinated methylboronic acid with several diols. He found that the tetrahedral boron was important for enhancing the binding affinity for diols. This important conclusion would help set the stage for future work on boronic acids The same group also took advantage of the power of ^{11}B NMR in 1996 to further study the different behaviors of the boron atom in trigonal vs. tetrahedral form in boronic acids. In particular, they focused on rates of interconversion between the two different species.

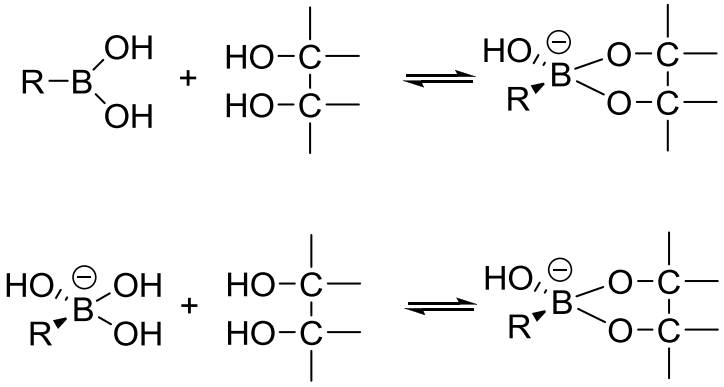

Scheme 1.1. Boronate ester formation reaction pathways studied by Pizer and Tihal.

In a simple, yet elegant, analysis of Lewis acid-base interactions between fluoride anions and boron, James et al. used ^{11}B-NMR to examine the change in boron hybridization upon complexation to a fluoride anion.[55] This process had the added allure of offering the possibility of a fluorescent sensor for fluoride anions based on **1.2**. The boron chemical shifts of **1.1** relative to a BMe_3 external reference, occur at 13.2 ppm. This represents a single sp^2 boron. In the case of **1.2** they observed two signals at 14.5 and 2.5 ppm, corresponding to one sp^2 free boron signal and one sp^3 boron signal due to coordination with the adjacent nitrogen atom), respectively. Upon addition of 1 equiv. of KF the boron signal of **1.1** shifts to 12.0 ppm and further shifts to 7.4 ppm after addition of 5 equiv. of KF due to a change in hybridization (sp^2 to sp^3) upon complexation with fluoride. For **1.2**, the signal at 14.5 ppm shifted to 13.5 ppm upon addition of 1 equiv. of KF. When 5 equiv. of KF were added to **1.2** only one signal at 2.5 ppm was observed. These data are indicative of a full switch from trigonal planar sp^2 boron to fully tetrahedral boron.

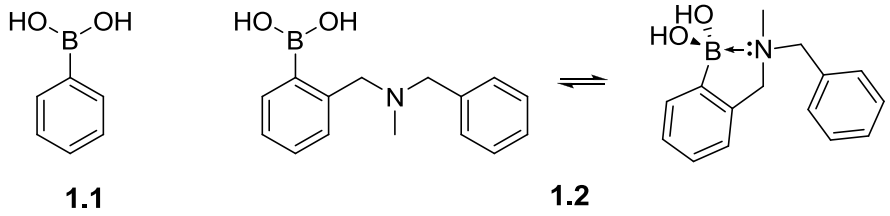

Figure 1.2. Boronic acid species studied by the James group.

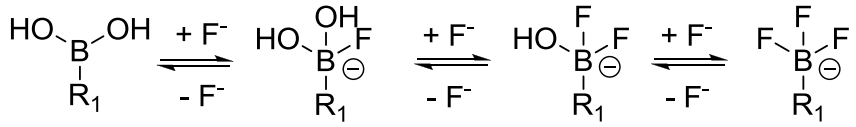

Scheme 1.2. Consecutive reactions of a boronic acid with fluoride anions.

In 1998, Todd et al. studied the thermodynamics and mode of coordination of the reaction of tetrahydroxyborate ($\mathbf{B^-}$) with three different carbohydrates (**1.3**, **1.4** and **1.5** in Figure 1.3, generalized as **L**) as a preliminary test to aid in the design of polymers capable of removing boron from aqueous solutions.[56] Quantification and determination of the boron-carbohydrate complexes were cleverly performed using ^{11}B-NMR spectroscopy due to the ease with which the various boron complexes can be distinguished based on chemical shifts. While the complex with **1.3** showed that borate monoesters of the **BL** type were the preferred mode of interaction, carbohydrate **1.4** favored borate diesters $\mathbf{BL_2}$ (Scheme 1.3). Interestingly, for the complex formed with **1.5** it was found that the product of complexation was a combination of intramolecular tetradentate borate diesters and oligomeric chains of **1.5** attached *via* intermolecular borate diesters.

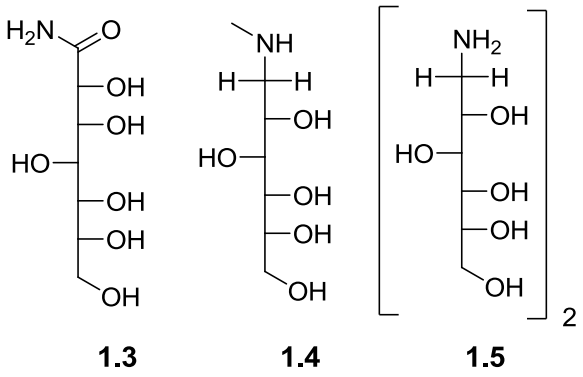

1.3 **1.4** **1.5**

Figure 1.3. Carbohydrates used by Todd as ligands for reaction with tetrahydroxyborate.

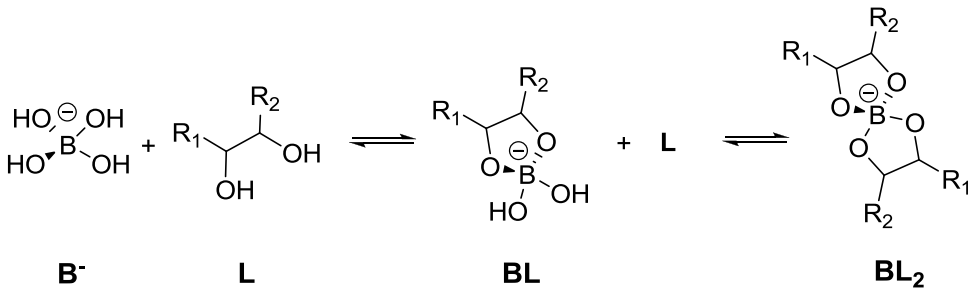

Scheme 1.3. Complexation reaction between borate and diol ligands.

The use of borate $\mathbf{B^-}$ in the reaction with hydroxyl-containing polymers like **PACL** (poly(1-(acrylamido)-1-deoxylactitol) was studied by Kurth et al.[57] Using ^{11}B-NMR spectroscopy they quantified the types of borate complexes formed and their binding constants. This study was placed within the framework of the investigation into factors (like presence of borax) affecting intrinsic viscosity of certain classes of polymers. This body of work focused on complexes formed between tetrahydroxyborate and three different ligands (Figure 1.4): **1.6** (subunit of **PACL**), the monomer **1.7** and **PACL**, with modes of interaction analogous as the ones described in schemes 1.3 and 1.4. Experiments of **B-1.6** and **B-1.7** complexes were performed first to help with peak assignments in the polymeric **B-PACL** complex due to foreseeable peak broadening. The α,ß bidentate, α,ß dimer and bidentate α,γ structures were recorded for the complexes with **1.6** and **1.7**. The polymeric **B-PACL** structure showed a broad α,ß peak and a dimeric α,ß peak. The boric acid/borate-**1.7** complex was shown to have the greatest binding affinity as indicated by a decreased amount of free boric acid/ borate present in the NMR.

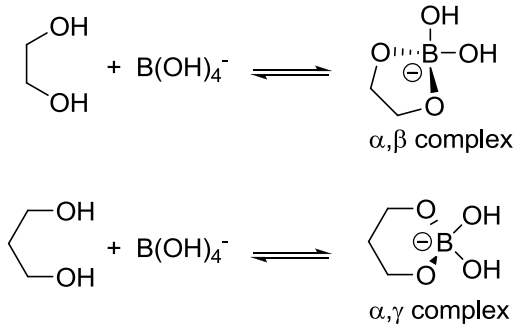

Scheme 1.4. Modes of complexation between borate and 1,2- and 1,3-diols.

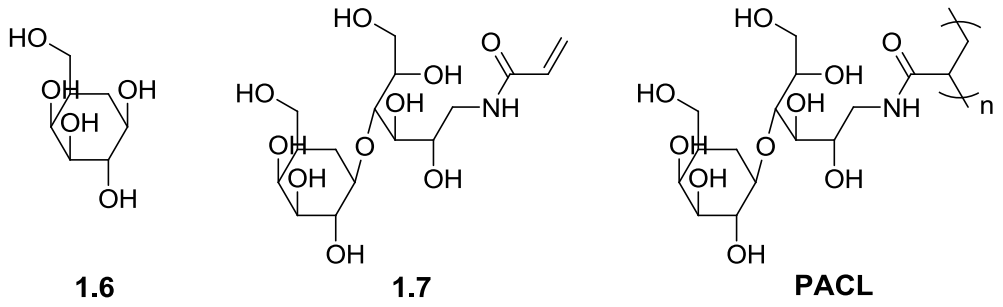

Figure 1.4. Ligands used by the Kurth lab.

Anslyn et al. used ^{11}B NMR spectroscopy in conjunction with molecular modeling and X-ray crystallography analysis to distinguish between the types of modes of interaction between the nitrogen and boron atoms in a series of molecules based on the *o*-aminomethyl phenylboronic acid moiety. This particular substructure is of special importance as it is the base for a number of efficient fluorescence polyol sensors.[25-28,58,59] The studies served to identify the factors involved in the formation of a dative B-N bond or the insertion of a molecule of solvent between the N and B atoms, with polar aprotic media such as acetonitrile or chloroform favoring the former case and polar protic solvents such as methanol promoting the latter. This work also deserves mention based on the fact that it established a clear differentiation between ^{11}B NMR signals for

the two different modes of tetrahedral boron. These shifts were determined to be 13-15 ppm for B-N bond **1.8** and 9-11 ppm for solvent inserted **1.9** (figure 1.5). These assignments were further corroborated by X-ray studies.[60]

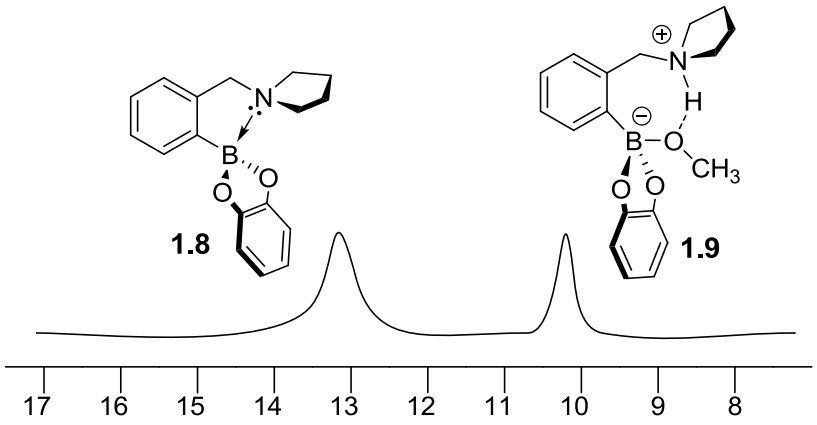

Figure 1.5. Modes of boron-nitrogen interaction in *o*-aminomethyl phenylboronic acid and their approximate resonances in ^{11}B NMR.

The complexation of boric acid with salicylic acid (**1.10**) was studied by Yoshimura et al. in 2008. Interestingly, ^{11}B-NMR spectra of boric acid and **1.10** in solution at pH 4 yielded three boron signals: one at ~20 ppm corresponding to the free boric acid, and two signals at 2.9 and 3.3 ppm. The authors reasoned that at higher pH **1.10** is present as the mono-anionic carboxylate **1.11** and the free boric acid as $B(OH)_3$ (Scheme 1.5). At lower pH, however, where it appears as both the neutral species and deprotonated, two complexations with boric acid were proposed. First, **1.11** can complex boric acid in a 1:1 ratio. This complexation leads to the monochelate **1.13,** which corresponds to the boron signal at 2.9 ppm. This monochelate can then undergo condensation with neutral **1.10** to yield the 1:2 bischelate **1.14** which corresponds to the boron signal at 3.3 ppm (Scheme 1.6). They then used this information to further study the complexation of boric acids with other salicylic acid derivatives.[61]

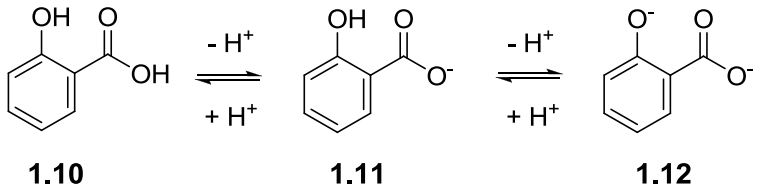

Scheme 1.5. Acid-base equilibrium for salicylic acid.

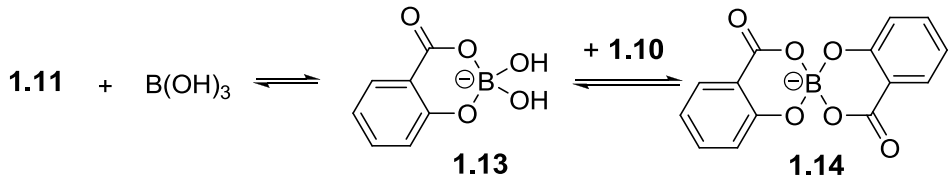

Scheme 1.6. Reaction of boric acid with saclicylic acid.

In a recent report by James et al., the structures of macrocyclic Schiff base complexes incorporating 2-formyl-aryl-boronic acids and 1,2-amino alcohols were explored.[24] Using ^{11}B-NMR spectroscopy the authors were able to determine the geometry of these complexes. In contrast to the phenyl-derived boracyclic complexes **1.15** (10.5-11.5 ppm), the furan-derived boracycles **1.16** were shown to have more tetrahedral character (4.6-5.4 ppm) owing to the incorporation of a more geometrically strained furan ring into the complex (Scheme 1.7). These studies facilitate future building and optimization of this type of self-assembling macromolecule.

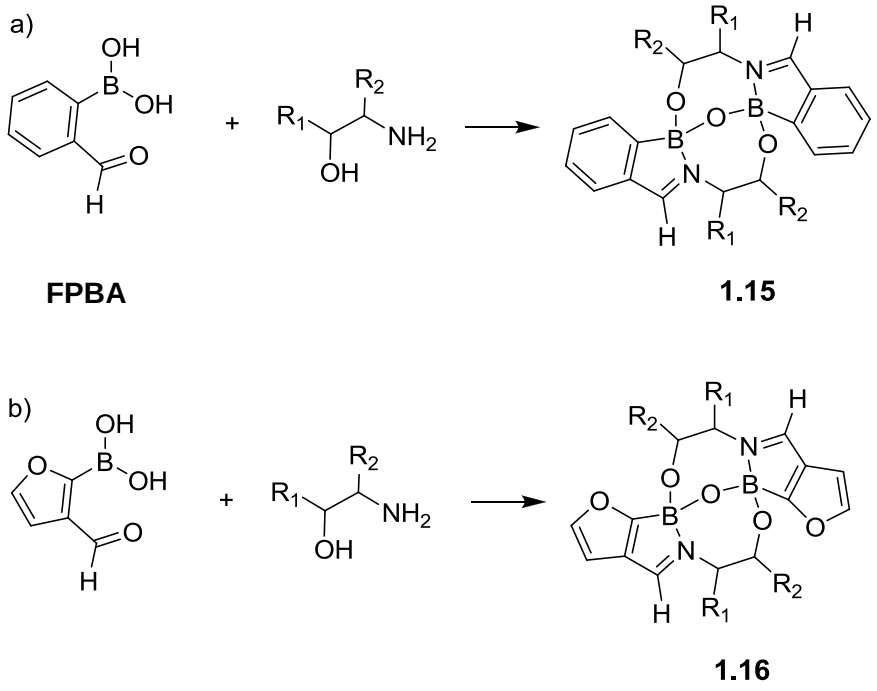

Scheme 1.7. Reaction of 1,2-aminoalcohols with a) 2-formylphenylboronic acid and b) 3-formyl-2-furanylboronic acid.

The rules affecting modes of interaction between boron and nitrogen were further studied by Anslyn et al. in 2009. They conducted a battery of analyses with the boronate ester formation reaction of several *o*-aminomethyl phenylboronic acids with different degrees of substitution around the nitrogen atom (Scheme 1.8). The experimental results showed a slight increase as a function of the number of substituents on the amine group in the ratio of B-N dative bond to solvent insertion in polar protic solvents. However, no real changes were observed in the overall preference for solvent insertion in polar protic solvents. Further, they found that the hydrogen atom from the inserted methanol was located closer to the amine than to the methanolic oxygen, indicating ionization of the solvent and the formation of a zwitterionic species.[62]

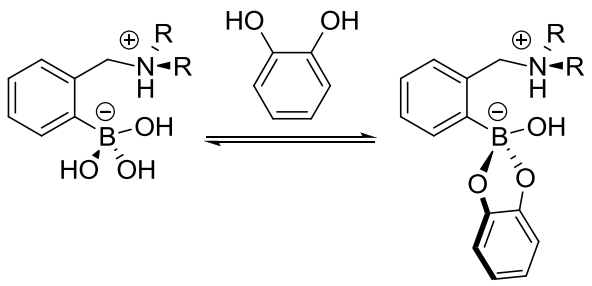

Scheme 1.8. Boronate ester formation involving o-aminomethyl phenylboronic acid.

To determine the interaction of phenylboronic acids with amines in water, Yatsimirsky et al. used ^{11}B-NMR spectroscopy to probe the charged state of the boron when in complex with an amine. At neutral pH (~7.0), 2-formylphenylboronic acid (**FPBA**) shows two boron resonances at 29.3 and 8.6 ppm. Acidification of the solution to pH 6.5 results in the complete disappearance of the 8.6 ppm peak. Hence, the peak at 29.3 ppm corresponds to the neutral boronic acid **FPBA**. Increasing the pH of the solution to pH 9.0 shows elimination of the 29.3 ppm signal. This means that the peak at 8.6 ppm corresponds to the anionic boron in **1.17**. In order to deduce which side of the complex equilibriurm between neutral **1.18** and zwitterionic **1.19** was favored, they looked at which of the two boron signals (neutral versus anionic) were present with increasing equivalents of amine. For both amines employed in the ^{11}B NMR aqueous titrations, disappearance of the neutral boron **FPBA** peak at 29.3 ppm, absence of peaks around the 13-16 ppm region, and a growing signal at around 9 ppm with increasing equivalents of amine gave clear evidence that the zwitterion **1.19** was present in solution.[63]

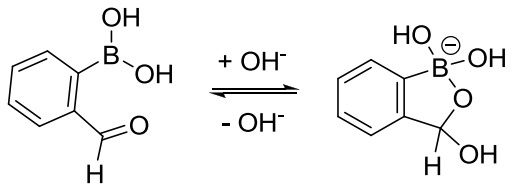

FPBA **1.17**

Scheme 1.9. Equilibrium between **FPBA** and its hemiacetal form.

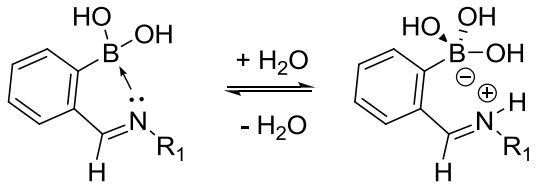

1.18 **1.19**

Scheme 1.10. Modes of boron-nitrogen interaction in o-iminomethylphenylboronic acids.

To fully study the stoichiometries, binding properties and formation constants of borate with 1,2-ethanediol and 1,3-propanediol, Yoshimura et al. employed ^{11}B-NMR spectroscopy in combination with computer-generated modeling. For borate-1,2-ethanediol interactions, there results showed that besides the formation of the well-known 1:1 (**1.20**) and 1:2 (**1.21**) borate-1,2-ethandiol complexes, two other complexes were found representing a monochelated complex 1:1 (**1.22**) and a bischelated complex 1:2 (**1.23**). For the borate-1,3-propanediol interactions, all the same types of complexes were found, 1:1 (**1.24**), 1:2 (**1.25**), 1:1 (**1.26**) and 1:2 (**1.27**).

Interestingly, upon mixing all three components, (borate, 1,2-ethandiol, 1,3-propanediol) a new boron signal appeared at ~5 ppm appeared. This was suggested to be a bischelate 1:2 complex, **1.28**, comprised of all three components.[64]

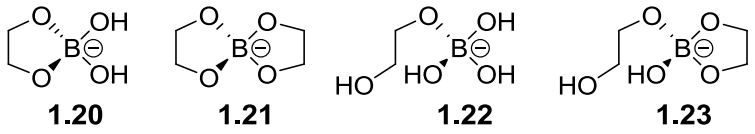

1.20 **1.21** **1.22** **1.23**

Figure 1.6. Complexes of borate with 1,2-ethanediol.

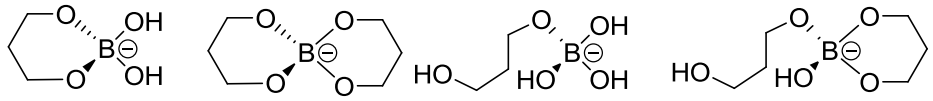

1.24 **1.25** **1.26** **1.27**

Figure 1.7. Complexes of borate with 1,3-propanediol.

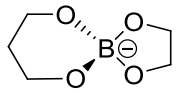

1.28

Figure 1.8. Complex of borate with 1,2-ethanediol and 1,3-propanediol.

Yatsimirsky et al. used various spectroscopic titration methods to determine the effect of substituents on boronic acids **1.29**, **1.30** and **1.31** with several diols.[65] The observed equilibrium constants (K_{obs}) were additionally determined by ^{11}B-NMR spectroscopy by titration of **1.32** into solutions of the three boronic acids. For this experiment, **1.29**, **1.30** and **1.31** all showed only one boron signal at 31.0, 31.8 and 31.6 ppm respectively. These signals corresponded to the free

boronic acid in the trigonal planar ester geometry. Titration of **1.32** into the solution of boronic acid at pH 5.5 showed the appearance of a new peak at 12.9, 13.4 and 13.5 ppm, for **1.29**, **1.30** and **1.31**, respectively. These chemical shifts indicated the formation of the tetrahedral ester complex. Unfortunately, the K_{obs} found using the ^{11}B-NMR titration experiment was significantly lower than the K_{obs} calculated using spectrophotometric titrations. The authors suggested that the quadrupolar interactions of ^{11}B nucleus and the aryl aromatic rings may lead to enhanced signal broadening which would disproportionate the NMR signal areas and the chemical concentrations.

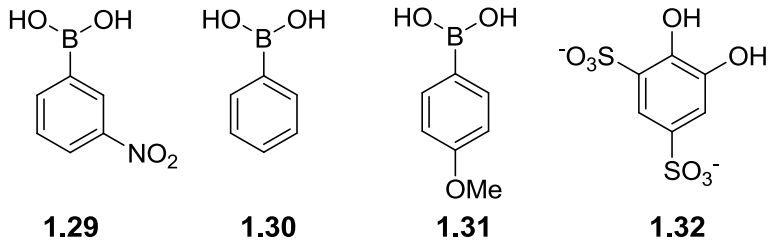

1.29 **1.30** **1.31** **1.32**

Figure 1.9. Boronic acid analytes and titrant used by Yatsimirsky.

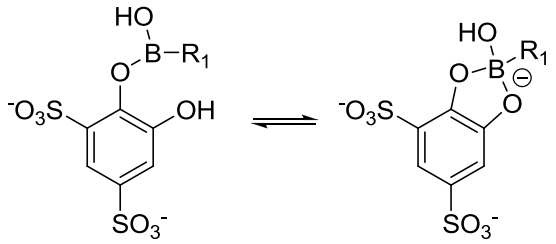

Scheme 1.11. Equilibrium between modes of complexation.

1.4 CONCLUSIONS

As it has been shown above, ^{11}B NMR spectroscopy is a valuable technique suited for the qualitative monitoring of electronic or structural changes in the chemical environment of a boron atom. Even more, in some cases the quantitative side of this spectroscopy can be employed to take advantage of the analysis of those changes. This review showcases the principles behind the technique and exemplifies successful and practical applications when studying different cases involving boronic acids.

1.5 REFERENCES

1. Hall, D. G. *Boronic Acids. Preparation and Applications in Organic Synthesis and Medicine*, Wiley-VCH: Weinheim, **2005**.

2. Miyaura, N.; Yamada, K.; Suzuki, A. *Tetrahedron Lett*. **1979**, *20*, 3437-3440.

3. Miyaura, N.; Suzuki, A. *Chem. Rev*. **1995**, *95*, 2457-2483.

4. Suzuki, A. *J. Organomet. Chem.* **1999**, *576*, 147-168.

5. Al-Zoubi, R. M.; Marion, O.; Hall, D. G. *Angew. Chem. Int. Ed*. **2008**, *47*, 2876-2879.

6. Côté, A. P.; Benin, A. I.; Ockwig, N. W.; O'Keeffe, M.; Matzger, A. J.; Yaghi, O. M. *Science* **2005**, *310*, 1166-1170.

7. El-Kaderi, H. M.; Hunt, J. R.; Mendoza-Cortés, J. L.; Côté, A. P.; Taylor, R. E.; O'Keeffe, M.; Yaghi, O. M. *Science* **2007**, *316*, 268-272.

8. Rambo, B. M.; Lavigne, J. *J. Chem. Mater*. **2007**, *19*, 3732-3739.

9. Korich, A. L.; Iovine, P. M. *Dalton Trans*. **2010**, *39*, 1423-1431.

10. Adamczyk-Woźniak, A.; Cyrański, M. K.; Jakubczyk, M.; Klimentowska, P.; Koll, A.; Kołodziejczak, J.; Pojmaj, G.; Żubrowska, A.; Żukowska, G. Z.; Sporzyński, A. *J. Phys. Chem. A* **2010**, *114*, 2324-2330.

11. Brown HC. *Organic Syntheses via Boranes. Vol. 1*. Milwaukee, WI: Aldrich Chemical; **1997**.

12. Brown HC, Zaidlewicz M. *Organic Syntheses via Boranes. Vol. 2*. Milwaukee, WI: Aldrich Chemical; **2001**.

13. Suzuki A, Brown HC. *Organic Syntheses via Boranes. Vol. 3*. Milwaukee, WI: Aldrich Chemical; **2003**.

14. Takaya, Y.; Ogasawara, M.; Hayashi, T.; Sakai, M.; Miyaura, N. *J. Am. Chem. Soc.* **1998**, *120*, 5579–5580.

15. Kettner, C.; Mersinger, L.; Knabb, R. *J. Biol. Chem*. **1990**, *265*, 18289-18297.

16. Spencer, J.; Burd, A. P.; Goodwin, C. A.; Mérette, S. A. M.; Scully, M. F.; Adatia, T.; Deadman, J. J. *Tetrahedron* **2002**, *58*, 1551-1556.

17. Strynadka, N. C. J.; Adachi, H.; Jensen, S. E.; Johns, K.; Sielecki, A.; Betzel, C.; Sutoh, K.; James, M. N. G. *Nature* **1992**, *359*, 700-705.

18. Flentke, G. R.; Munoz, E.; Huber, B. T.; Plaut, A. G.; Kettner, C. A.; Bachovchin, W. W. *Proc. Natl. Acad. Sci. U. S. A.* **1991**, *88*, 1556-1559.

19. Dunsdon, R. M.; Greening, J. R.; Jones, P. S.; Jordan, S.; Wilson, F. X. *Bioorg. Med. Chem. Lett.* **2000**, *10*, 1577-1579.

20. Bukhtiyarova, M.; Rizzo, C. J.; Kettner, C. A.; Korant, B. D.; Scarnati, H. T.; King, R. W. *Antiviral Chem. Chemother*. **2002**, *12*, 367-373.

21. Hiratake, J.; Oda, J. *Biosci. Biotech. Biochem*. **1997**, *61*, 211-218.

22. Arnal-Hérault, C.; Pasc, A.; Michau, M.; Cot, D.; Petit, E.; Barboiu, M. *Angew. Chem. Int. Ed.* **2007**, *46*, 8409-8413.

23. Hutin, M.; Bernardinelli, G.; Nitschke, J. R. *Chem. Eur. J.* **2008**, *14(15)*, 4585-4593.

24. Galbraith, E.; Kelly, A. M.; Fossey, J. S.; Kociok-Köhn, G.; Davidson, M. G.; Bull, S. D.; James, T. D. *New J. Chem*. **2009**, *33(1)*, 181-185.

25. James, T. D.; Sandanayake, K. R. A. S.; Shinkai, S. *J. Chem. Soc., Chem. Commun*. **1994**, 477.

26. James, T. D.; Sandanayake, K. R. A. S.; Shinkai, S. *Angew. Chem. Int. Ed*. **1994**, *33*, 2207.

27. James, T. D.; Sandanayake, K. R. A. S.; Shinkai, S. *Nature* **1995**, *374*, 345.

28. James, T. D. *Top Curr. Chem*. **2007**, *277*, 107-152.

29. Siedle, A. R. *Annu. Rep. NMR Spectrosc.* **1982**, *12*, 177-261.

30. Siedle, A. R. *Annu. Rep. NMR Spectrosc*. **1988**, *20*, 205-314.

31. Wrackmeyer, B. *Annu. Rep. NMR Spectrosc*. **1988**, *20*, 61-203.

32. Smith, W. L. *J. Chem. Ed*. **1977**, *54*, 469.

33. Eaton, G. R. *J. Chem. Ed*. **1969**, *46*, 547.

34. Nöth, H.; Wrackmeyer, B. *Nuclear Magnetic Resonance Spectroscopy of Boron Compounds*, Springer-Verlag: Berlin, **1978**.

35. Nöth, H.; Vahrenkamp, H. *Chem. Ber.* **1966**, *99*, 1049.

36. Brown, H. C.; B. Nazer, B.;Cha, J. S.;Sikorski, J. A. *J. Org. Chem*. **1986**, *51*, 5264.

37. Brown, H. C.; Cole, T. E.; Srebnick, M.; Kim, K. –W. *J. Org. Chem*. **1986**, *51*, 4925.

38. Chandrasekharan, J.; Brown, H. C. *J. Org. Chem*. **1985**, *50*, 518.

39. Mikhailov, B. M.; Kuimova, M. E. *Zh. Obshch. Khim*. **1971**, *41*, 1721.

40. Brown, H. C.; Kramer, G. W.; Hubbard, J. L.; Krishnamurthy, S. *J. Organometal. Chem*. **1980**, *188*, 1.

41. Good, C. D.; Ritter, D. M. Ritter *J. Am. Chem. Soc*. **1962**, *84*, 1162.

42. Brown, H. C.; Sinclair, J. A. *J. Organometal. Chem*. **1977**, *131*, 163.

43. DeMoor, J. E.; Van der Kelen, G. P. *J. Organomet. Chem*. **1966**, *6*, 235.

44. Paetzold, P. I.; Hansen, H. -J Z. *Inorg. Chem*. **1966**, *345*, 79.

45. Nöth, H.; Vahrenkamp, H. *Chem. Ber*. **1967**, *100*, 3353.

46. Schaeffer, R.; Todd, L. J. *J. Am. Chem. Soc.* **1965**, *87*, 488.

47. Dewar, M. J. S.; Jones, R. *J. Am. Chem. Soc*. **1967**, *89*, 4251.

48. Phillips, W. D; Miller, H. C.; Mutterties, E. L. *J. Am. Chem. Soc*. **1959**, *81*, 4496.

49. James, B. D.; Nanda, R. K.; Wallbridge, M. G. H. *J. Chem. Soc. A*, **1966**, 182.

50. Onak, T. P.; Landesman, H.; Willams, R. E. *J. Phys. Chem*. **1959**, *63*, 1533.

51. Thompson, R. J.; Davis, J. C. *J. Inorg. Chem*. **1965**, *4*, 1464.

52. Toporcer, L. H.; Dessy, R. E.; Green, S. I. E. *Inorg. Chem*. **1965**, *4*, 1649.
53. Pizer, R.; Tihal, C. *Inorg. Chem*. **1992**, *31*, 3243-3241.

54. Pizer, R.; Tihal, C. *Polyhedron* **1996**, *15(19)*, 3411-3416.

55. Cooper, C. R.; Spencer, N.; James, T. D. *Chem. Commun*. **1998**, 1365-1366.

56. Smith, B. M.; Owens, J. L.; Bowman, C. N.; Todd, P. *Carbohydr. Res.* **1998**, *308*, 173-179.

57. Wilson, M. E.; Najdi, S.; Krochta, J. M. Hsieh, J-L.; Kurth, M. *J. Macromolecules* **1998**, *31*, 4486-4492.

58. James, T. D.; Sandanayake, K. R. A.; Shinkai, S. *Angew. Chem. Int. Ed.* **1996**, *35(17)*, 1910-1922.

59. Fang, H.; Kaur, G.; Wang, B. *J. Fluoresc.* **2004**, *14(5)*, 481-489.

60. Zhu, L.; Shabbir, S. H.; Gray, M.; Lynch, V. M.; Sorey, S.; Anslyn, E. V. *J. Am. Chem. Soc.* **2006**, *128*, 1222-1232.

61. Miyazaki, Y.; Matsuo, H.; Fujimori, T.; Takemura, H.; Matsuoka, S.; Okobira, T.; Uezu, K.; Yoshimura, K. *Polyhedron*, **2008**, *27*, 2785-2790.

62. Collins, B. E.; Sorey, S.; Hargrove, A. E.; Shabbir, S. H.; Lynch, V. M.; Anslyn, E. V. *J. Org. Chem*. **2009**, *74*, 4055–4060.

63. Gutierrez-Moreno, N. J.; Medrano, F.; Yatsimirsky, A. K. *Org. Biomol. Chem.* **2012**, *10*, 6960-6972.

64. Miyazaki, Y.; Fujimori, T.; Okita, H.; Hirano, T.; Yoshimura, K. *Dalton Trans*. **2013**, *42*, 10473-10486.

65. Martinez-Aguirre, M. A.; Villamil-Ramos, R.; Guerrero-Alvarez, J. A.; Yatsimirsky, A. K. *J. Org. Chem*. **2013**, *78*, 4674-4684.

Chapter 2: Structural Studies on the N-B Interaction in *o*-Iminearylboronate Systems

2.1 INTRODUCTION

The high affinity of boronic acids for diols was first discovered in 1954[1]. Since this discovery, these species have become of great interest to the scientific community. They are remarkable for the way they are able to rapidly establish reversible covalent bonds with 1,2- and 1,3- diols through the formation of cyclic boronate esters. It is hence not surprising that based on the ubiquitous presence of polyols in nature, boronic acids have been a target of interest for the development of sensing systems aimed at biologically relevant analytes containing proximal hydroxyl groups.[2-25]

A series of papers from the Shinkai group describe a turn-on fluorescence sensing approach for sugars at biological conditions using derivatized boronic acid **2.1** (Scheme 2.1).[26-28] These studies laid the ground work for a breadth of sugar sensing in the subsequent years.[29-35] In this work receptor **2.1** registers an increase in fluorescence intensity upon binding of carbohydrates like fructose or glucose This binding leads to the formation of boronate ester **2.2**.

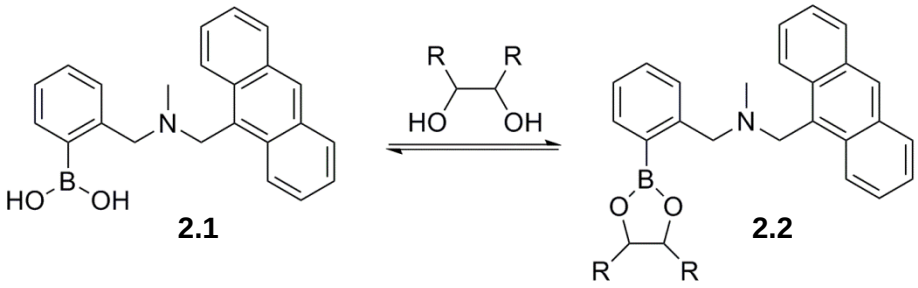

Scheme 2.1. Shinkai's fluorescent sensor reacting with a diol.

Upon the publication of these milestone studies it was understood that the incorporation of an aminomethyl group *ortho* to the boronic acid functionality leads to an increase in binding at physiological conditions.[36,37] In addition, it was observed to allow for tunability of the appended fluorophore. Although the precise mechanism of action of this methylamino group was not known at the time, a myriad of sensors have been designed based on structurally similar units. One consequence of the interest developed over such systems was a discovery by our group.[34] We reported the prevalence of two different types of interactions between the boronic acid functionality and the amine. Through the use of several coupled analytical techniques, such as ^{11}B NMR spectrosopy, X-Ray diffraction and computational modeling, it was determined that two different possibilities exist for these compounds. The first one involves a dative bond formed between the nitrogen and the boron, long envisioned as the main mode of B-N bond interaction. The other involves a single protic solvent inserted between the nitrogen and boron. By characterizing crystal structures for each of the different interaction modes and then subjecting each type of species to ^{11}B NMR analysis, it was possible to assign distinct ppm values to each of the two possible variants of tetrahedral boron. One of the main conclusions of this body of work was that aprotic solvents favor the B-N bond form while protic ones promote the formation of the solvent-inserted mode of interaction (Scheme 2.2).

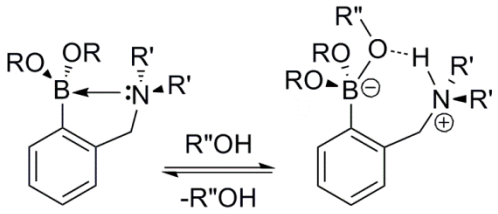

Scheme 2.2. Equilibrium between the two modes of boron-nitrogen coordination.

In a collaborative study by the James and the Bull groups, a three-component assembly system was employed to determine the enantiomeric excess (*ee*) of chiral amines *via* a ^{1}H NMR chiral shift strategy.[28,29] The enantio-discriminating unit is created from the reaction of *o*-formylphenylboronic acid (**FPBA**), enantiopure 1,1'-bi-2-naphthol (**BINOL**) and an α-chiral primary amine. This sensor evolves through the formation of a Schiff base and a boronate ester to give the product of the assembly (Scheme 2.3). The different diastereomers created in this reaction from the amine enantiomers are responsible for a characteristic ratio of peak intensities in ^{1}H NMR spectra. These intensities can be directly related to the enantiomeric composition of the original amine. This reaction is fast, highly efficient and relatively simple, requiring no purification steps.

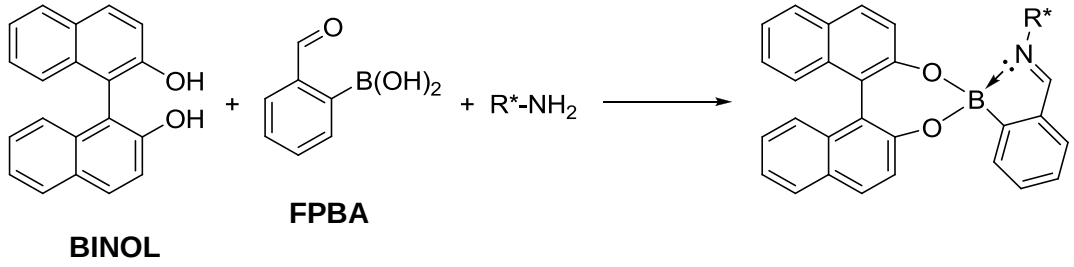

BINOL **FPBA**

Scheme 2.3. 3-component assembly developed by the James and Bull groups.

These unique properties, combined with the fact that both the imine formation and the boronate ester condensation involved in the assembly are reversible, confer this seemingly simple reaction with advantageous traits. For example, it has the potential to become a veritable playground for scientists interested in the field of dynamic multicomponent self-assemblies for tailored nano architectures, and for those who seek to create analytical assays thereof. As a testament to the applicability of these characteristics, a number of different studies based on this

type of assembly reaction have been subsequently developed. Some of these reports rely on the speed and ease of the assembly reaction to develop methods for the recognition, *ee* determination or discrimination of target amines or polyols.[40-44] Others have sought to exploit the reversibility and simplicity of the reaction to devise supramolecular architectures.[45-47]

As it has been noted, ^{11}B NMR spectroscopy was employed as an efficient tool to qualitatively discriminate between the structural identities based on the two main modes of boron-nitrogen interactions (Scheme 2.2). In the following pages we describe experiments undertaken to define the different parameters that determine the prevalence of one type of interaction or the other in the very versatile Bull-James assembly reaction. For this task we will apply our established ^{11}B NMR characterization methods to structural studies in different experimental conditions, with particular emphasis on the solvent used.

2.2 Results and Discussion

In an effort to better characterize the coordination modes and structures of the elements involved in the Bull-James assembly, a number of ^{11}B NMR titrations were performed. The ppm values for the boron resonances were referenced to numbers obtained and established in a prior body of work.[34-35] Peaks in the range of 25-35 ppm can be assigned to a boron atom in an arylboronic acid that displays trigonal planar geometry, while tetrahedral boron appears further upfield. For these species, previous examples show that signals attributed to a B-N bond phenomenon are around 15 ppm and those related to solvent insertion are generally around 10 ppm.

2.2.1 ^{11}B NMR Experiments Performed in Aprotic Solvents

In the first study using a polar aprotic solvent, one equivalent of **FPBA** and catechol were dissolved in CD_3CN and benzylamine added in increments of 0.2 equivalents, followed by recording the corresponding ^{11}B NMR spectra (Figure 2.1). It was observed that in the absence of benzylamine the spectra showed a dominant peak at approximately 30 ppm, corresponding to a species containing trigonal boron (the original *o*-formylphenylboronic acid **FPBA**). This signal starts to decrease as benzylamine is added and more imine is formed, until the predominant product is the one where a B-N bond is present (**2.3**). This complex has an associated characteristic ^{11}B NMR signal at around 14 ppm. This confirms that in a polar aprotic media, the assembly leads to the formation of a B-N bond between the imine nitrogen and the boron in the boronate ester as expected. X-ray analysis of a crystal grown with the original system with **BINOL** in CH_3CN showed this type of coordination; see the experimental section. Another observation that can be made on these results is that it seems evident boronate ester formation can happen in the absence of amine, although the addition of the latter clearly facilitates the process.

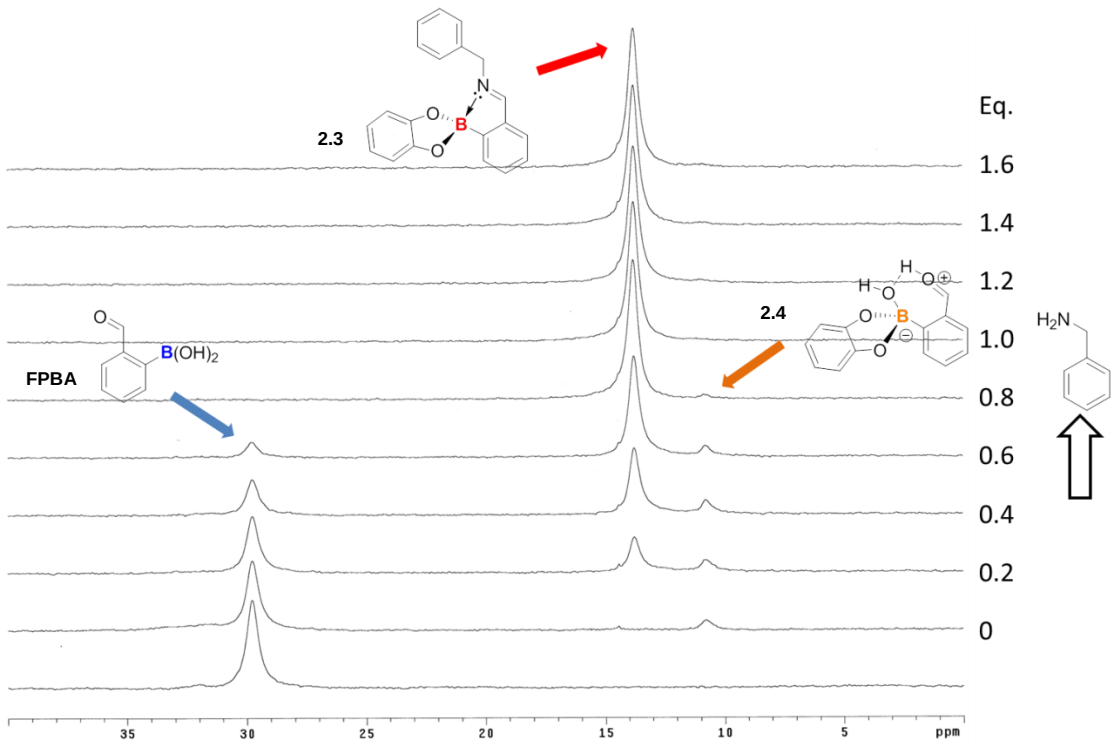

Figure 2.1. Addition of benzylamine (0-16 mM) into an equimolecular mixture of **FPBA** and catechol (10 mM) in CD_3CN. The first spectrum is **FPBA** alone.

In order to study the influence of the diol on the extent of assembly, a second series of experiments involved gradually increasing the concentration of catechol in the mixture (Figure 2.2). Starting with an equimolar mixture of **FPBA** and benzylamine, the dominant species was assigned to a B-N bonded free boronic acid **2.6** (15.5 ppm) with vestigial amounts of the imine species **2.5** in equilibrium where the boron atom does not have any interaction with the nitrogen (26.5 ppm). Throughout these experiments it becomes clear that the addition of catechol leads to the prevalence of the B-N bonded species **2.3** (14 ppm). The observation confirms the previous assumption[34] that this particular diol promotes the B-N bond coordination, perhaps by virtue of its rigidity and planarity, which forces the boronate ester to adopt an initial geometry more akin

to tetrahedral than other diols and makes the boron more electrophilic. In an analogous fashion as in the previous case, it can also be gathered from the spectra that imine formation occurs to a minimal extent when only the boronic acid and the amine are present, and that addition of catechol takes the assembly reaction to completion.

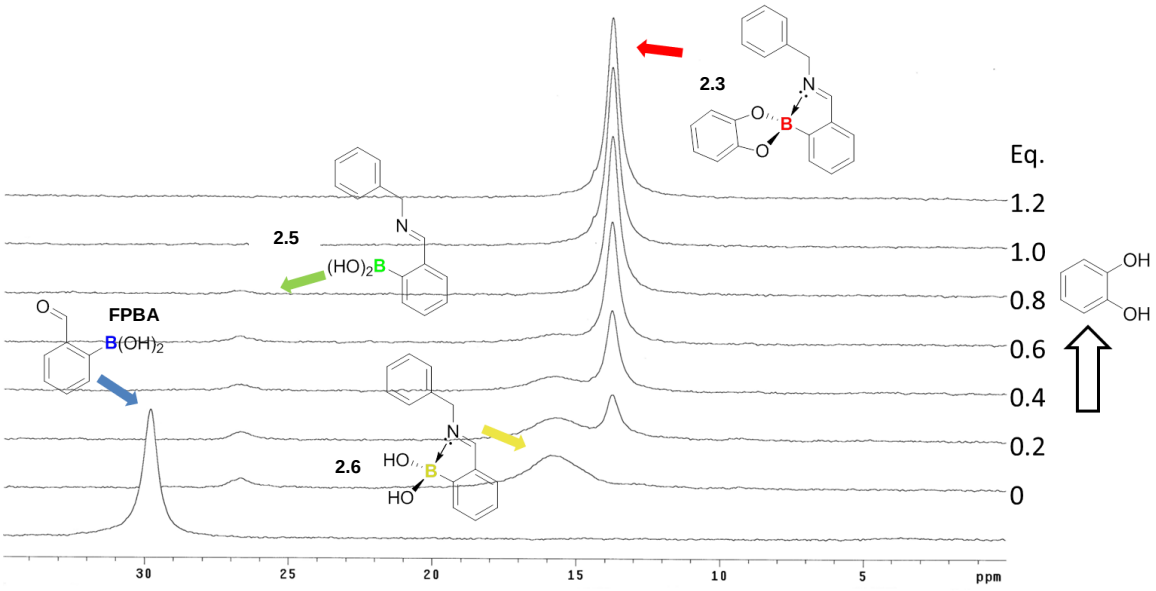

Figure 2.2. Addition of catechol (0-12 mM) into an equimolecular mixture of **FPBA** and benzylamine (10 mM) in CD_3CN. The first spectrum is **FPBA** alone.

In the last ^{11}B NMR titration in aprotic solvent, benzylamine was added incrementally from 0 to 1.6 equivalents to **FPBA**, and at the point where an equivalent of the amine had been added, an equivalent of catechol was added. Part of the explanation for the postulated assignment of peaks is shown in Scheme 2.4. As the amine is added, the addition product is structure **2.8**, but this is formed in the presence of an amine. This amine is expected to be basic enough to deprotonate **2.8** to create **2.7** (8 ppm) predominantly). As more amine is added, it is

consumed by the reaction with **FPBA** so that less amine is available in solution to deprotonate **2.8**. However, **2.8** does not dominate because its minor equilibrium species **2.9'** eliminates to give the solvent inserted species **2.9** (drawn in two ways depending on exactly where the proton resides). Compound **2.9**, responsible for the signal at 9 ppm, is a protonated iminium. Hence, once an equivalent of the amine is added benzyl ammonium hydroxide is created along with the B-N bonded imine **2.6** (15.5 ppm). Species **2.6** is expected to be in equilibrium with the open trigonal form **2.5** very much like it is the case for the conditions described in Figure 2.2. The spectral assignment of species **2.9** and **2.6** was confirmed by addition of one equivalent of H_2O to the postulated **2.6** solution. It was observed that the peak at 9 ppm (**2.9**) was regenerated. Finally, addition of one equivalent of catechol drives the reaction completely towards the B-N bonded boronate ester species **2.3** (14 ppm).

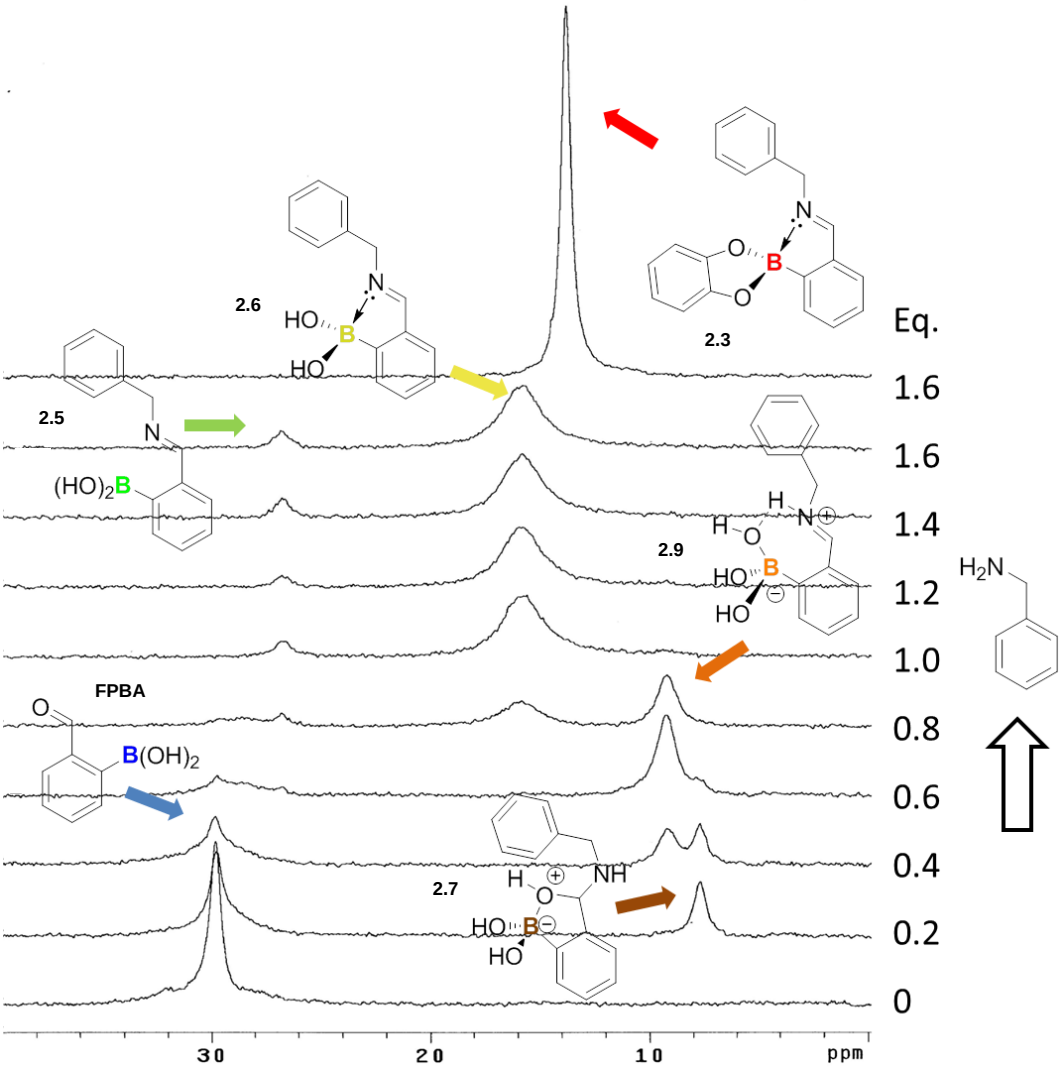

Figure 2.3. Addition of benzylamine (0-16 mM) into **FPBA** (10 mM) in CD_3CN with the addition of one equivalent (10 mM) of catechol at the end (top spectrum).

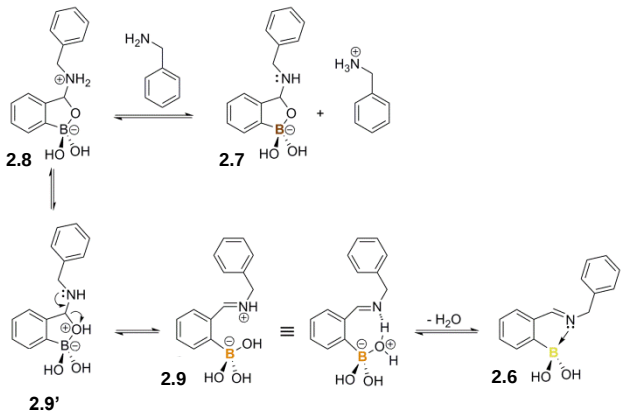

Scheme 2.4. Proposed mechanistic pathway for the reaction between **FPBA** and the amine.

These last two sets of experiments indicate that the assembly, originally believed to need all three components to proceed, is able to initiate condensation with only two of the pieces present. But the third element is necessary in order to drive the reaction to completion. The two individual condensations (boronate esterification and imine formation) add a degree of versatility to this system. They allow for an initial dynamic equilibration or scrambling step before addition of the third component and subsequent completion of the assembly.

2.2.2 ^{11}B NMR Experiments Performed in Protic Solvents

In order to investigate the structures that arise during assembly in a polar protic medium, **FPBA** and catechol were dissolved in CD_3OD and increments of benzylamine were added. The ^{11}B NMR spectra were recorded after each addition of benzylamine (Figure 2.4). The initial signal at 29.5 ppm corresponds to the solvated trigonal planar boron atom in species **2.10**, formed after incorporation of methoxy groups from the solvent into **FPBA**. When an equimolecular proportion of **FPBA** and catechol is mixed, a fraction of the trigonal methoxy

boronate ester becomes coordinated by catechol in an equilibrium. This coordination leads to a decrease in the original signal and the presence of the peak due to the tetrahedral boron **2.12** that this coordination creates (10 ppm). The phenoxide attached to boron in this species makes this atom more electrophilic, which we propose facilitates formation of hemiacetal **2.11** (14 ppm) or coordination of solvent, **2.12**. Once the amine is added, imine formation promotes insertion of a molecule of solvent between nitrogen and boron in **2.14**. Not too surprisingly, the boron resonance in this chemical environment appears at a similar frequency (10.5 ppm) as that of the species proposed to be the boronate ester with catechol (**2.4**) and methanol (**2.9**). Alongside the resonance assigned to the solvent-inserted form of the imine species, another peak (8.5 ppm) appears as soon as the amine is present. The ratio of this signal to that postulated for the solvent inserted form remains the same for all cases of this assembly in methanolic medium. We hypothesize that the 8.5 ppm resonance to belong to structure **2.13**, obtained from the deprotonation of imine **2.14**. It is also noteworthy that even with 5 equivalents of amine, not all of the initial boronic acid has been consumed, confirming that all species are in equilibrium.

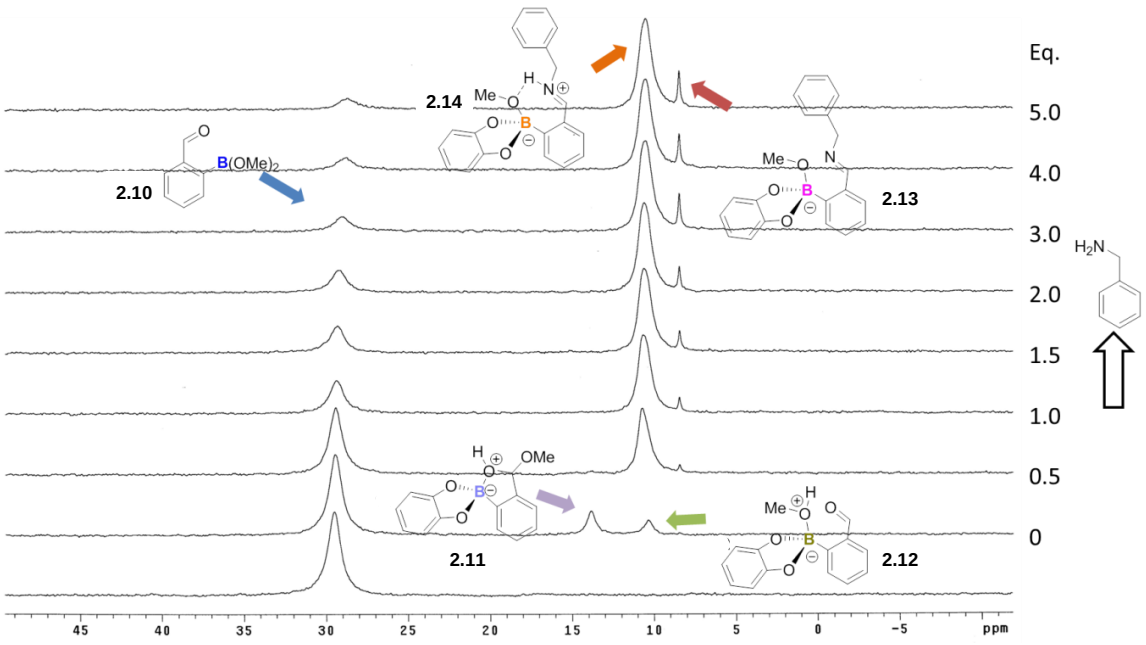

Figure 2.4. Addition of benzylamine (0-50 mM) into an equimolecular mixture of **FPBA** and catechol (10 mM) in CD_3OD. The first spectrum is **FPBA** alone.

In another experiment performed in deuterated methanol, increments of catechol were added to a 1:2 mixture of **FPBA** and benzylamine (Figure 2.5). As we learned from the previous series of experiments, a 1:2 proportion of the two components allows for the formation of the imine as the dominant product when combined with the diol. When only the initial two components were present in solution the peak corresponding to **2.10** (29.5 ppm) and that which is assumed to be due to solvent insertion upon a certain degree of imine formation **2.15** (11 ppm) could be observed. Upon addition of catechol the peaks for the solvent inserted imine with catechol coordinated to boron **2.14** (10.5 ppm) and its deprotonated version **2.13** (8.5 ppm) were observed. It is worth noting that the counterion for species **2.13** is protonated benzylamine after it reacts with **2.14**. Components **2.13** and **2.14** become the major species with only a remnant of

the original methanolic trigonal boron molecule **2.10** by the end of the titration, just as in the previous set (Figure 2.4).

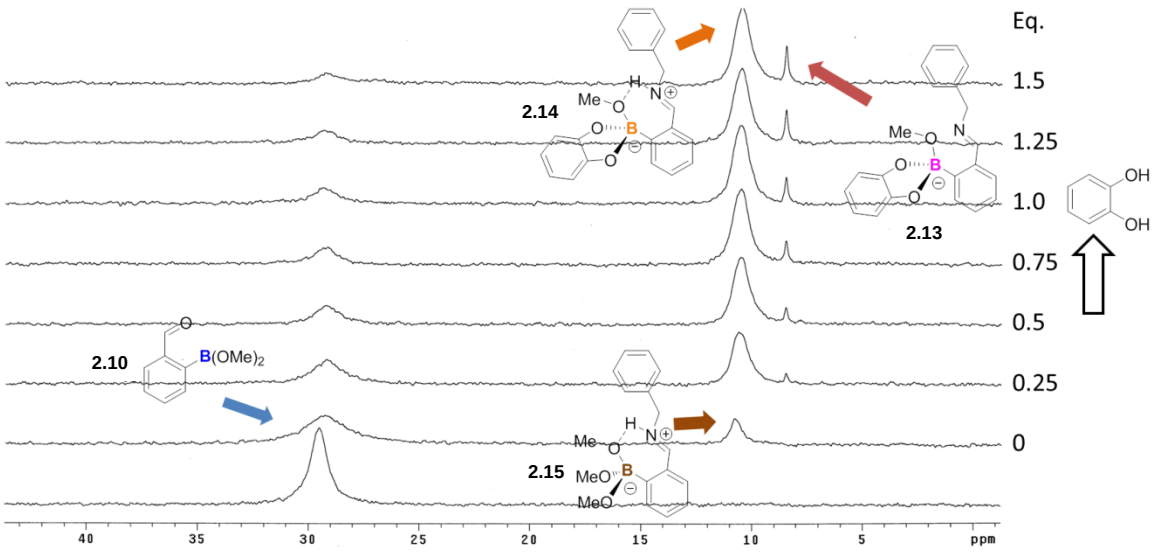

Figure 2.5. Addition of catechol (0-15 mM) into a mixture of **FPBA** (10 mM) and benzylamine (20 mM) in CD_3OD. The first spectrum is **FPBA** alone.

When the concentration of benzylamine was increased in a solution containing **FPBA** (Figure 2.6) the results were quite similar to those from the previous set of tests. The initial peak due to the trigonal boron in **2.10** (29.5 ppm) decreases as more amine is added, giving rise to the imine **2.15** with a solvent molecule inserted (11 ppm). The addition of one equivalent of catechol drives the reaction closer to completion and yields the characteristic signals assigned to structures **2.13** and **2.14** , where the boron is coordinated with catechol (8.5 ppm and 10.5 ppm respectively). These experiments, and particularly the initial spectra, provide further proof for the postulate that imine formation does not rely on the presence of the diol.

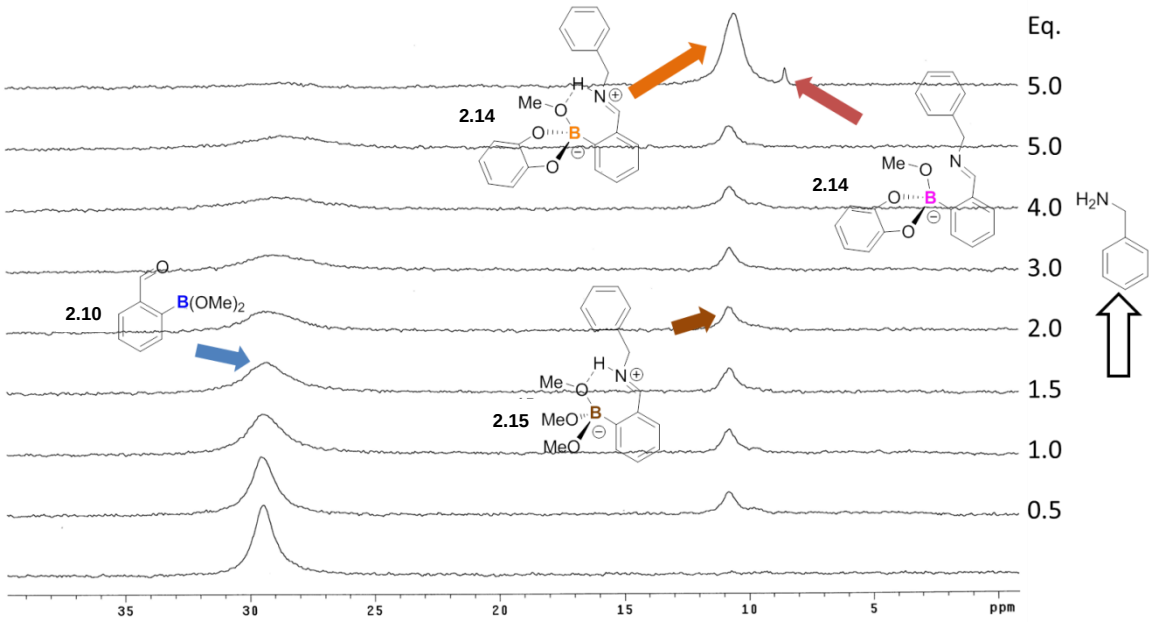

Figure 2.6. Addition of benzylamine (0-50 mM) into **FPBA** (10 mM) in CD_3OD with the addition of one equivalent (10mM) of catechol at the end (top spectrum).

Knowing that the binding constant for boronate ester formation is governed by the acidity of both diol and boronic acid,[48] we were interested in determining the effect that the acidity of the medium had on the binding mode and behavior of our system. With this objective in mind, we set up a series of experiments in a mixture of water and methanol that allowed for control of the solution pH (Figure 2.7). When the pH of the system (equimolecular amounts of **FPBA** and catechol and 2 equivalents of benzylamine) was increased, the trigonal planar methanolic boron **2.10** (30 ppm) and solvent-inserted imine **2.14** (10.5 ppm) present at low pH give way to other species. Deprotonation of **2.14** leading to **2.13** (8.5 ppm) is promoted by high pH values, which explains why this is the only example in the series of ^{11}B NMR spectra in polar protic solvent where the ratio of these two signals varies. This information was used to validate the initial

assignment for **2.13** in the previous 3 groups of experiments. The higher pH also makes catechol more nucleophilic which in turn produces a certain amount of structure **2.16**, where boron is surrounded by two molecules of catechol (9 ppm). Finally, as the deprotonation of the imine frees up the lone pair on nitrogen, it is possible to detect some B-N bonding (**2.3**, 14 ppm) at basic pH.

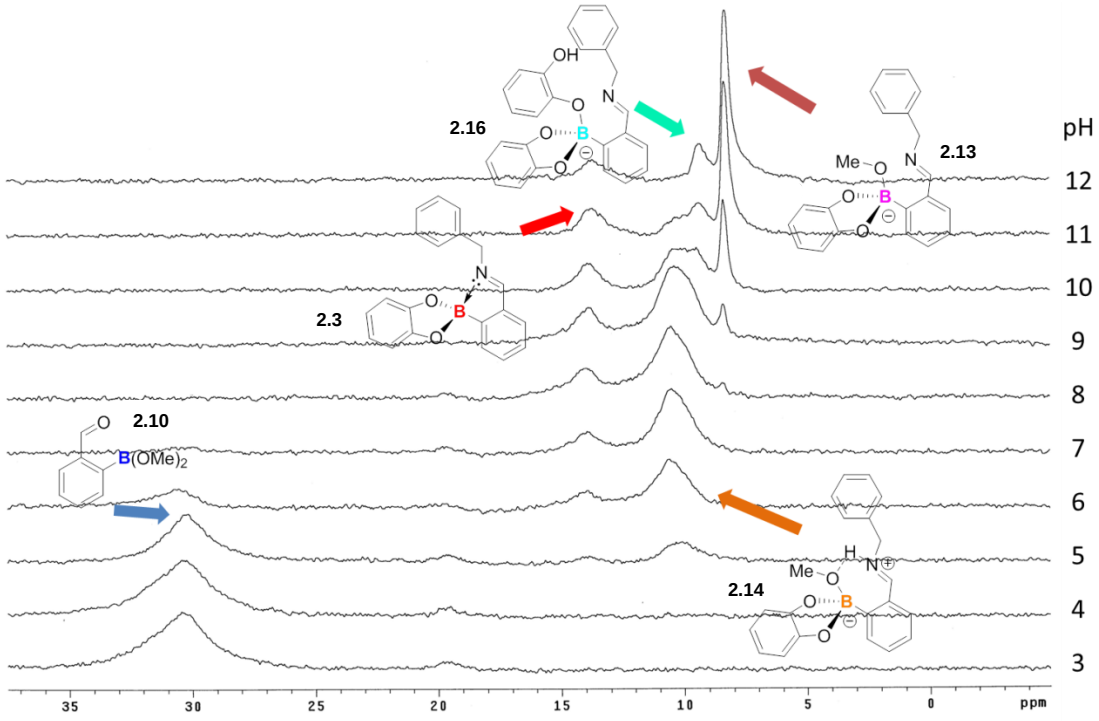

Figure 2.7. ^{11}B NMR spectra of a mixture of **FPBA** (10 mM), catechol (10 mM) and benzylamine (20 mM) in CD_3OD/D_2O (2:1) at varying pH's (3-12).

2.2.3 X-Ray Crystallography Studies

When crystal structures for the assembly product of an equimolar mixture of **FPBA** and catechol and two equivalents of benzylamine were obtained from CH_3CN and CH_3OH, the X-Ray analysis revealed the same molecule for both cases. In these structures, the mode of interaction between boron and nitrogen was B-N bond (Figure 2.8, see additional structures in experimental section). This is quite remarkable because in the case of ^{11}B NMR spectra taken in methanol this species was entirely absent or only marginally present. The most reasonable explanation that can be proposed for this phenomenom is that the solid state intermolecular packing forces in the crystal provide more stability to the system than the insertion of a molecule of the solvent.

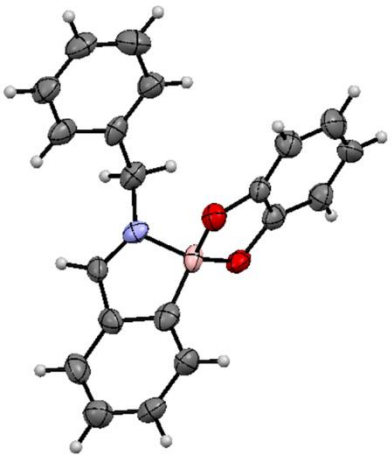

Figure 2.8. View of the assembly product of **FPBA**, catechol and benzylamine recrystalized from CH_3CN showing the presence of a B-N bond. Displacement ellipsoids are scaled to the 50% probability level. Heteroatoms: Nitrogen (blue), Oxygen (red) and Boron (pink).

2.2.4 Algebraic Expressions for the Assembly Equilibrium

As we noted earlier, completion of the assembly reaction depended upon the presence of all three components. But we also observed that binary mixtures could be present. These observations led us to realize that the mechanistic pathways for the reaction must be more complex than originally thought. We proposed the following system of reactions:

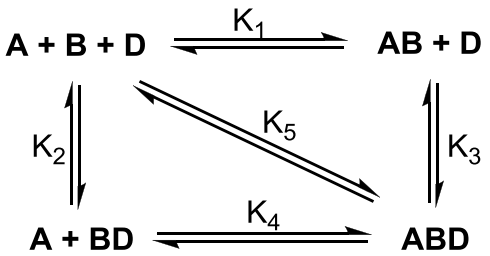

Scheme 2.5. Graphic representation of all the individual processes involved in the assembly reaction under study. Where A is the amine, B is **FPBA** and D represents the diol, AB is the imine product with free boronic acid, BD is the boronate ester with no imine and ABD is the final product of the assembly. $K_{1\text{-}5}$ are dissociation constants pertaining to each specific reaction.

Although our group has successfully solved the algebraic expressions that define some complex systems (including 1:2 binding cases),[49] this particular case involves more convoluted mathematics, with nonlinear equations and interdependence of the individual processes. It is for this reason that we enlisted the help of a mathematician and took advantage of the computing program of Wolfram Mathematica, combined with our knowledge of the chemical phenomena to arrive at the correct solution.

We began the process outlining the system of equations as defined by the dissociation constant expressions and mass balances (using capital letters for concentrations obviating the brackets for the sake of clarity):

$$A \times B = K_1 \times AB \quad (1)$$

$$B \times D = K_2 \times BD \quad (2)$$

$$AB \times D = K_3 \times ABD \quad (3)$$

$$A \times BD = K_4 \times ABD \quad (4)$$

$$A \times B \times D = K_5 \times ABD \quad (5)$$

$$AT = A + AB + ABD \quad (6)$$

$$BT = B + AB + BD + ABD \quad (7)$$

$$DT = D + BD + ABD \quad (8)$$

Our objective is to express ABD as a function of the constants K_i and AT;BT;DT. By substituting (1) in (3) we see that $K_1K_3A \times B \times D = ABD$. Similarly by substituting (2) in (4) we get $ABD = K_2K4A \times B \times D$. Combining this with (5) we get

$$K_1K_3 = K_2K_4 = K_5 \quad (*)$$

The physical reality of the situation demands that all of the constants are positive as well, so we move forward with this assumption.

Then we move on to the linear mass balance equations (6), (7) and (8). Substituting in what we already know we get

$$ABD = AT - A(1 + K_1^{-1} B) \quad (6')$$

$$ABD = BT - B(1 + K_1^{-1} A + K_2^{-1} D) \quad (7')$$

$$ABD = DT - D(1 + K_2^{-1} B) \quad (8')$$

Combining (6') with (8') we see that B can be expressed as a function of A and D and the relevant constants *via* the relationship

$$B = (K_2 - K_1 / (K_1K_2)) (AT - A) - (DT - D) \qquad (9)$$

Now using (9) with (6') we obtain the relationship

$$ABD = C \times A^2 + (C \times DT - C \times AT - 1)A - C \times (A \times D) + AT \qquad (10)$$

where $C = (K_2-K_1) / (K_1^2K_2)$

We can do similarly with (9) and (8') to get another quadratic form equal to ABD, but instead we'll take a different route which will result in a much simpler computation.

Using simple linear algebra on the system (7) and (9) we arrive at

$$(1 + C)AB + (1 - C)BD + ABD = BT \qquad (11)$$

with C as before.

Using (6) and (8) in (10) we can eliminate AB and BD by reducing the matrix

A	B	D	AB	BD	ABD	|	Total
1	0	0	1	0	1	|	AT
0	1	0	1	1	1	|	BT
0	0	1	0	1	1	|	DT
C	1	-C	0	0	0	|	C(AT – DT)

First we add the fourth row to the second, then we subtract the third row from the resulting new second row, then finally subtracting the first row from the resulting

$$-(C + 1)A + (C - 1)D - ABD = BT + (C - 1)(AT - DT) \qquad (11')$$

This naturally leads to

$$ABD = -(1 + C)A + (C - 1)D - BT + (C - 1)(DT - AT) \qquad (12)$$

which is a linear equation in terms of only A and D and the given constants.

Finally we may substitute the information in (12) into (10) to obtain

$$CA^2 + A + (C - 1)D - CAD + BT + DT = 0 \qquad (14)$$

This allows us to solve for D as a function of A yielding

$$D = (A^2 + A + BT + DT) / (1 - C + CA) \qquad (14')$$

Using (7') with (5) and applying (*) we get

$$ABD = DT - D - K_4(ABD / A) \qquad (15)$$

Rewriting this as

$$ABD = A(DT - D) / (K_4 + A) \qquad (15')$$

we can now substitute (14') into (15') and also into (12) to derive the final conclusion about A, which is

$A / (K_4 + A)((DTC(A - 1) - CA^2 - A - BT) / (1 - C + CA)) = ABD = -(1 + C)A + (C - 1)((CA^2 + A + BT + DT) / (1 - C + CA)) - BT + (C - 1)(DT - AT)$ (16)

It is clear from the dependence of the right hand side on AT that this cannot be an identity, hence can be numerically solved for A in terms of the given constants. But then, using either side of (16) we automatically have the value of ABD in terms of the given constants. A cursory inspection shows that this expression is as reduced as it can be, and by looking at the difference of the two sides of (16) we are left with a cubic expression for A.

We write, for convenience, the equation that we have reduced all of this to, namely $c_3A^3+c_2A^2+c_1A+c_0 = 0$

where

$c_0 = ATK_4 - 2BTK_4 - 2ATCK_4 + 2BTCK_4 + ATC^2K_4 - 2DTK_4 + 3CDTK_4 - C^2DTK_4$

$c_1 = AT - BT - 2ATC + 2BTC + ATC^2 - 2DT + 4CDT - C^2DT - 2K_4 + CK_4 + ATCK_4 - BTCK_4 + C^2K_4 - ATC^2K_4 - CDT K_4 + C^2DT K_4$

$c_2 = -1 + C + ATC - BTC + C^2 - ATC^2 - 2CDT + C^2DT + 2C^2K_4$

$c_3 = C + 2C^2$

From here we can use either the cubic equation and a truncated binomial series or use Newton's method or other basic numerical analysis results to get a rapidly converging set of values for A, and use physical constraints to judge which root(s) to use. From general theory, it is likely that this polynomial only has one real root, so in a "typical" situation we won't even have to choose. An easy way to test whether the polynomial has multiple roots or not is with its

discriminant, however the formula for it in terms of the given constants is quite large. Instead we recommend inputting the values for K_1; K_3; K_4; AT; BT; DT and then computing it using the usual formula $\Delta = 18c_0c_1c_2c_3 - 4c_3^2c_0 + c_2^2c_1^2 - 4c_3c_1^3 - 27c_3^2c_0^2$. The main use of this in practice is, for example, if we are using Newton's method, then we will know whatever our iterations produce is the only real root, and so it must be correct. We need not worry about getting the "wrong" root of the polynomial for our application.

2.3 CONCLUSIONS

Upon completion of these structural experiments we observed that polar aprotic media leads to a prevalence of the B-N bond binding mode. Conducting the assembly reaction in a polar protic solvent favors solvent insertion. However, from the X-ray diffraction data and the pH titration experiments, we can deduce that there are certain conditions where a B-N bond can be promoted even when in polar protic media. This solvent effect is similar to what our group has previously reported concerning the behavior of similar compounds containing amine moieties in lieu of the imine. The experiments conducted also gave information concerning the existence of individual binary equilibria prior to the formation of the 3-component assembly, casting doubt on the existing notion that all three elements are needed for the condensations to initiate. Inspired by that observation, we performed the necessary algebraic operations to define the mathematical derivation of the chemical process of this assembly reaction. The final expression that was obtained encompasses all individual equilibria and relates final concentration of the assembly product to initial concentration of the three original components and equilibrium constants. As a generic equation for a three-component reaction, it can be applied to any such system in order to determine rate constants or calculate concentrations at equilibrium.

2.4 EXPERIMENTAL DETAILS

2.4.1 Materials and Methods

All reagents and solvents were used as purchased from commercial sources. ^{11}B NMR spectra were collected on Varian INOVA 500 with a sweep width of 51250 Hz, 66k of data points, a 90º pulse width and a 2.2 second recycle time, using BF_3•OEt_2 as an external reference. Each spectrum was processed with 10 Hz line broadening, and a second order polynomial fitting routine was used to remove ^{11}B background. The temperature for these experiments was regulated at 27ºC. All pH measurements were made using an Orion 720A pH meter.

2.4.2 General procedure for ^{11}B NMR titrations

All the ^{11}B NMR experiments were done with quartz NMR tubes (Wilmad). Stock solutions of **FPBA** (0.1 M) benzylamine (0.1 M) and catechol (0.1 M) in CD_3CN (or CD_3OD) were prepared. Each of the (up to) ten NMR tubes was loaded with 100 μL of the solution of **FPBA** (0.1 M) first, then the corresponding amounts of amine and catechol solutions were added as specified on each set of spectra. CD_3CN (or CD_3OD) was then added to take the total volume to 1.0 mL. For example, for the case of the experiments corresponding to Figure 2.1, all ten tubes contained the initial 100 μL of **FPBA** 0.1 M. Then all but the first tube received 100 μL of catechol 0.1 M followed by 0, 20 μL, 40 μL, 60 μL, 80 μL, 100 μL, 120 μL, 140 μL, and 160 μL of benzylamine solution (0.1 M) respectively and the final volume was adjusted to 1 mL with CD_3CN. Therefore, each of the last 9 tubes contained 10 mM of **FPBA** and 10 mM of catechol,

with 0, 2 mM, 4 mM, 6 mM, 8 mM, 10 mM, 12 mM, 140 mM, and 160 mM of benzylamine respectively.

2.4.3 General procedure for ^{11}B NMR – pH profiles

Solutions of **FPBA** (0.1 mL, 0.1 M in CD_3OD/D_2O (2:1)), catechol (0.1 mL, 0.1 M in CD_3OD/D_2O (2:1)), benzylamine (0.2 mL, 0.1 M in CD_3OD/D_2O (2:1)) and HEPES (0.25 mL, 0.1 M in CD_3OD/D_2O (2:1)) were added in 10 vials and their pH values were adjusted with NaOH (2 M) or HCl (2 M) in a range from 3 – 12. The total volume of the samples was adjusted to 1.0 mL with CD_3OD/D_2O (2:1). The final concentrations for **FPBA**, catechol, benzylamine and HEPES were 10 mM, 10 mM, 20 mM and 25 mM, respectively.

2.4.4 X-ray crystal structure determination

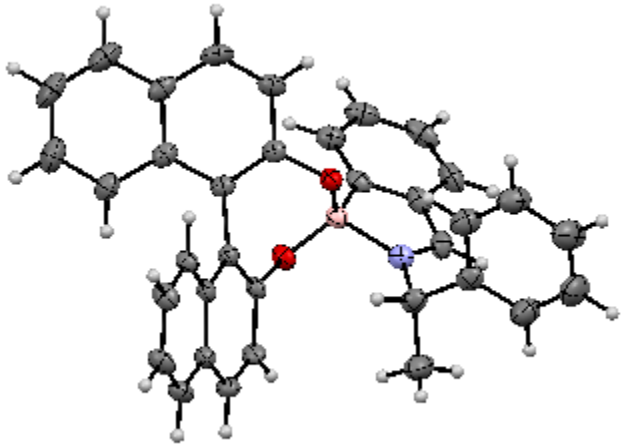

Figure 2.9. View of the assembly product of **FPBA**, (*R*)-**BINOL** and (*S*)-methylbenzylamine recrystalized from CH_3CN showing the presence of a B-N bond. Displacement ellipsoids are scaled to the 50% probability level. Heteroatoms: Nitrogen (blue), Oxygen (red) and Boron (pink).

Empirical formula	C35 H26 B N O2	
Formula weight	503.38	
Temperature	150(2) K	
Wavelength	0.71073 A	
Crystal system,	Orthorhombic,	
Space group	P 21 21 21	
Unit cell dimensions	a = 9.14300(10) A	alpha = 90 deg.
	b = 16.5180(2) A	beta = 90 deg.
	c = 17.5310(3) A	gamma = 90 deg.
Volume	2647.60(6) $Å^3$	
Z	4	
Calculated density	1.263 Mg/m^3	
Absorption coefficient	0.077 mm^{-1}	
F(000)	1056	
Crystal size	0.40 x 0.16 x 0.15 mm^3	
Theta range for data collection	3.22 to 27.47°.	
Limiting indices	-11<=h<=11, -21<=k<=21, -22<=l<=22	
Reflections collected	44235 [R(int) = 0.0668]	
Completeness to theta = 27.47°	99.6 %	
Absorption correction	None	
Max. and min. transmission	1.00 and 0.653	
Refinement method	Full-matrix least-squares on F^2	
Data / restraints / parameters	6054 / 0 / 353	
Goodness-of-fit on F^2	1.036	
Final R indices [I>2sigma(I)]	R1 = 0.0427, wR2 = 0.0862	
R indices (all data)	R1 = 0.0648, wR2 = 0.0933	
Absolute structure parameter	0.1(10)	
Largest diff. peak and hole	0.291 and -0.176 $e.A^{-3}$	

Table 2.1. Crystal data and structure refinement for the structure in Figure 2.9.

	x	y	z	U(eq)
C(1)	5918(2)	4043(1)	1817(1)	27(1)
C(2)	5362(2)	3830(1)	1115(1)	32(1)
C(3)	3992(2)	3459(1)	1061(1)	39(1)
C(4)	3173(2)	3305(1)	1707(1)	40(1)
C(5)	3686(2)	3513(1)	2419(1)	36(1)
C(6)	5069(2)	3878(1)	2461(1)	30(1)
C(7)	5843(2)	4129(1)	3143(1)	31(1)
C(8)	8102(2)	4733(1)	3619(1)	32(1)
C(9)	7439(3)	5478(1)	4003(1)	48(1)
C(10)	8490(2)	4046(1)	4161(1)	33(1)
C(11)	8090(2)	4034(1)	4921(1)	45(1)
C(12)	8501(3)	3399(1)	5390(1)	56(1)
C(13)	9329(3)	2771(1)	5106(1)	56(1)
C(14)	9705(2)	2764(1)	4338(1)	48(1)
C(15)	9304(2)	3398(1)	3877(1)	42(1)
C(16)	8838(2)	5702(1)	1923(1)	22(1)
C(17)	8723(2)	6444(1)	2323(1)	27(1)
C(18)	9931(2)	6890(1)	2481(1)	28(1)
C(19)	11337(2)	6606(1)	2277(1)	24(1)
C(20)	12620(2)	7047(1)	2465(1)	29(1)
C(21)	13972(2)	6750(1)	2297(1)	32(1)

Table 2.2. Atomic coordinates (x 10^4) and equivalent isotropic displacement parameters (Å ^{2} x 10^3) for the structure in Figure 2.9. U(eq) is defined as one third of the trace of the orthogonalized U^{ij} tensor.

C(22)	14110(2)	5995(1)	1928(1)	31(1)
C(23)	12897(2)	5570(1)	1715(1)	25(1)
C(24)	11469(2)	5866(1)	1866(1)	21(1)
C(25)	10172(2)	5436(1)	1643(1)	22(1)
C(26)	10211(2)	4723(1)	1121(1)	23(1)
C(27)	10927(2)	4753(1)	393(1)	27(1)
C(28)	11580(2)	5471(1)	93(1)	33(1)
C(29)	12295(2)	5464(1)	-591(1)	46(1)
C(30)	12376(2)	4757(2)	-1030(1)	53(1)
C(31)	11716(2)	4069(1)	-780(1)	46(1)
C(32)	10970(2)	4048(1)	-69(1)	33(1)
C(33)	10234(2)	3341(1)	183(1)	37(1)
C(34)	9473(2)	3334(1)	850(1)	31(1)
C(35)	9474(2)	4025(1)	1322(1)	24(1)
B	7440(2)	4459(1)	2088(1)	25(1)
N	7100(1)	4445(1)	3007(1)	28(1)
O(1)	7573(1)	5277(1)	1796(1)	26(1)
O(2)	8764(1)	3977(1)	2012(1)	25(1)

Table 2.2. Atomic coordinates (x 10^4) and equivalent isotropic displacement parameters (Å ^{2} x 10^3) for the structure in Figure 2.9. U(eq) is defined as one third of the trace of the orthogonalized U^{ij} tensor. (Cont.)

C(1)-C(2)	1.379(2)	C(19)-C(20)	1.419(2)
C(1)-C(6)	1.397(2)	C(19)-C(24)	1.424(2)
C(1)-B	1.623(2)	C(20)-C(21)	1.362(2)
C(2)-C(3)	1.398(2)	C(21)-C(22)	1.410(2)
C(3)-C(4)	1.381(3)	C(22)-C(23)	1.365(2)
C(4)-C(5)	1.376(3)	C(23)-C(24)	1.419(2)
C(5)-C(6)	1.403(2)	C(24)-C(25)	1.436(2)
C(6)-C(7)	1.451(3)	C(25)-C(26)	1.493(2)
C(7)-N	1.285(2)	C(26)-C(35)	1.381(2)
C(8)-N	1.488(2)	C(26)-C(27)	1.435(2)
C(8)-C(10)	1.522(3)	C(27)-C(32)	1.419(2)
C(8)-C(9)	1.529(3)	C(27)-C(28)	1.428(2)
C(10)-C(11)	1.382(3)	C(28)-C(29)	1.366(2)
C(10)-C(15)	1.394(3)	C(29)-C(30)	1.399(3)
C(11)-C(12)	1.385(3)	C(30)-C(31)	1.359(3)
C(12)-C(13)	1.378(3)	C(31)-C(32)	1.421(3)
C(13)-C(14)	1.390(3)	C(32)-C(33)	1.419(3)
C(14)-C(15)	1.373(3)	C(33)-C(34)	1.361(3)
C(16)-O(1)	1.3711(17)	C(34)-C(35)	1.410(2)
C(16)-C(25)	1.386(2)	C(35)-O(2)	1.3747(19)
C(16)-C(17)	1.415(2)	B-O(1)	1.449(2)
C(17)-C(18)	1.356(2)	B-O(2)	1.455(2)
C(18)-C(19)	1.414(2)	B-N	1.642(2)

Table 2.3. Selected bond lengths [Å] and angles [°] for the structure in Figure 2.9.

C(2)-C(1)-C(6)	117.80(15)	O(1)-C(16)-C(17)	117.46(12)
C(2)-C(1)-B	133.31(16)	C(25)-C(16)-C(17)	120.97(14)
C(6)-C(1)-B	108.89(15)	C(18)-C(17)-C(16)	120.74(14)
C(1)-C(2)-C(3)	120.19(18)	C(17)-C(18)-C(19)	120.60(14)
C(4)-C(3)-C(2)	120.76(18)	C(18)-C(19)-C(20)	121.55(14)
C(5)-C(4)-C(3)	120.88(16)	C(18)-C(19)-C(24)	119.27(14)
C(4)-C(5)-C(6)	117.50(18)	C(20)-C(19)-C(24)	119.17(14)
C(1)-C(6)-C(5)	122.87(17)	C(21)-C(20)-C(19)	120.97(14)
C(1)-C(6)-C(7)	109.81(14)	C(20)-C(21)-C(22)	119.98(15)
C(5)-C(6)-C(7)	127.31(17)	C(23)-C(22)-C(21)	120.46(15)
N-C(7)-C(6)	113.53(16)	C(22)-C(23)-C(24)	121.28(14)
N-C(8)-C(10)	110.84(14)	C(23)-C(24)-C(19)	117.95(14)
N-C(8)-C(9)	109.27(15)	C(23)-C(24)-C(25)	122.55(13)
C(10)-C(8)-C(9)	114.69(15)	C(19)-C(24)-C(25)	119.47(13)
C(11)-C(10)-C(15)	118.34(18)	C(16)-C(25)-C(24)	118.29(14)
C(11)-C(10)-C(8)	123.43(17)	C(16)-C(25)-C(26)	119.22(13)
C(15)-C(10)-C(8)	118.23(16)	C(24)-C(25)-C(26)	122.49(13)
C(10)-C(11)-C(12)	120.72(19)	C(35)-C(26)-C(27)	118.58(14)
C(13)-C(12)-C(11)	120.4(2)	C(35)-C(26)-C(25)	119.37(14)
C(12)-C(13)-C(14)	119.46(19)	C(27)-C(26)-C(25)	121.96(14)
C(15)-C(14)-C(13)	119.87(19)	C(32)-C(27)-C(28)	117.34(15)
C(14)-C(15)-C(10)	121.18(19)	C(32)-C(27)-C(26)	119.47(15)
O(1)-C(16)-C(25)	121.52(13)	C(28)-C(27)-C(26)	123.17(15)

Table 2.4. Bond lengths [Å] and angles [°] for the structure in Figure 2.9.

C(29)-C(28)-C(27)	121.12(17)	O(1)-B-O(2)	114.12(13)
C(28)-C(29)-C(30)	120.96(19)	O(1)-B-C(1)	111.31(14)
C(31)-C(30)-C(29)	119.77(18)	O(2)-B-C(1)	117.04(13)
C(30)-C(31)-C(32)	121.09(19)	O(1)-B-N	112.05(13)
C(33)-C(32)-C(27)	119.01(15)	O(2)-B-N	103.87(13)
C(33)-C(32)-C(31)	121.37(17)	C(1)-B-N	96.78(12)
C(27)-C(32)-C(31)	119.60(17)	C(7)-N-C(8)	123.14(15)
C(34)-C(33)-C(32)	121.14(16)	C(7)-N-B	110.98(14)
C(33)-C(34)-C(35)	119.79(16)	C(8)-N-B	125.86(13)
O(2)-C(35)-C(26)	120.22(14)	C(16)-O(1)-B	119.42(12)
O(2)-C(35)-C(34)	117.97(14)	C(35)-O(2)-B	116.21(12)
C(26)-C(35)-C(34)	121.75(15)		

Table 2.4. Bond lengths [Å] and angles [°] for the structure in Figure 2.9 (Cont.).

	U11	U22	U33	U23	U13	U12
C(1)	23(1)	20(1)	39(1)	2(1)	-1(1)	4(1)
C(2)	28(1)	30(1)	38(1)	-3(1)	-5(1)	3(1)
C(3)	33(1)	30(1)	54(1)	-8(1)	-13(1)	4(1)
C(4)	21(1)	26(1)	72(2)	3(1)	-11(1)	-3(1)
C(5)	28(1)	30(1)	50(1)	12(1)	0(1)	-2(1)

Table 2.5. Anisotropic displacement parameters ($Å^2 \times 10^3$) for the structure in Figure 2.9. The anisotropic displacement factor exponent takes the form: $-2\pi^2[h^2 a^{*2} U^{11} + ... + 2 h k a^* b^* U^{12}]$

C(6)	22(1)	27(1)	41(1)	8(1)	0(1)	1(1)
C(7)	25(1)	35(1)	34(1)	6(1)	4(1)	1(1)
C(8)	31(1)	34(1)	31(1)	-6(1)	-2(1)	-4(1)
C(9)	67(1)	40(1)	37(1)	-6(1)	2(1)	11(1)
C(10)	29(1)	39(1)	31(1)	-6(1)	-6(1)	-5(1)
C(11)	52(1)	50(1)	33(1)	-5(1)	1(1)	7(1)
C(12)	79(2)	57(1)	32(1)	2(1)	-3(1)	6(1)
C(13)	82(2)	45(1)	41(1)	0(1)	-19(1)	10(1)
C(14)	60(1)	40(1)	43(1)	-8(1)	-9(1)	11(1)
C(15)	43(1)	45(1)	37(1)	-7(1)	-5(1)	6(1)
C(16)	19(1)	20(1)	28(1)	2(1)	2(1)	-2(1)
C(17)	24(1)	25(1)	33(1)	-2(1)	8(1)	5(1)
C(18)	32(1)	22(1)	30(1)	-5(1)	5(1)	2(1)
C(19)	26(1)	21(1)	24(1)	1(1)	1(1)	-1(1)
C(20)	33(1)	22(1)	34(1)	-3(1)	-5(1)	-2(1)
C(21)	27(1)	26(1)	44(1)	-1(1)	-6(1)	-7(1)
C(22)	20(1)	29(1)	45(1)	4(1)	0(1)	2(1)
C(23)	23(1)	21(1)	30(1)	0(1)	0(1)	1(1)
C(24)	22(1)	20(1)	23(1)	4(1)	0(1)	0(1)
C(25)	20(1)	21(1)	24(1)	1(1)	1(1)	0(1)
C(26)	18(1)	26(1)	25(1)	-3(1)	-2(1)	4(1)
C(27)	20(1)	36(1)	25(1)	-3(1)	-2(1)	4(1)

Table 2.5. Anisotropic displacement parameters ($Å^2 \times 10^3$) for the structure in Figure 2.9. The anisotropic displacement factor exponent takes the form: $-2\pi^2[h^2 a^{*2} U^{11} + ... + 2 h k a^* b^* U^{12}]$ (Cont.).

C(28)	28(1)	42(1)	28(1)	1(1)	2(1)	0(1)
C(29)	42(1)	64(1)	31(1)	7(1)	8(1)	-2(1)
C(30)	48(1)	84(2)	26(1)	-2(1)	11(1)	9(1)
C(31)	47(1)	63(1)	30(1)	-13(1)	1(1)	12(1)
C(32)	29(1)	45(1)	23(1)	-7(1)	-4(1)	8(1)
C(33)	39(1)	35(1)	35(1)	-15(1)	-8(1)	7(1)
C(34)	30(1)	26(1)	37(1)	-6(1)	-6(1)	-1(1)
C(35)	18(1)	26(1)	26(1)	-1(1)	-2(1)	3(1)
B	23(1)	22(1)	31(1)	1(1)	3(1)	0(1)
N	25(1)	29(1)	31(1)	-1(1)	-2(1)	1(1)
O(1)	17(1)	24(1)	37(1)	1(1)	0(1)	-1(1)
O(2)	22(1)	23(1)	31(1)	1(1)	2(1)	1(1)

Table 2.5. Anisotropic displacement parameters ($Å^2 \times 10^3$) for the structure in Figure 2.9. The anisotropic displacement factor exponent takes the form: $-2\pi^2[h^2 a^{*2} U^{11} + ... + 2 h k a^* b^* U^{12}]$ (Cont.).

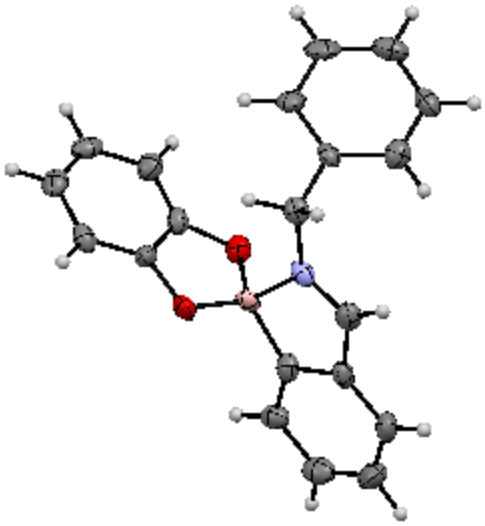

Figure 2.10. View of the assembly product of **FPBA**, catechol and benzylamine recrystalized from CH_3OH showing the presence of a B-N bond. Displacement ellipsoids are scaled to the 50% probability level. Heteroatoms: Nitrogen (blue), Oxygen (red) and Boron (pink).

Empirical formula	C20 H16 B N O2	
Formula weight	313.15	
Temperature	153(2) K	
Wavelength	0.71075 Å	
Crystal system	Triclinic	
Space group	P1	
Unit cell dimensions	a = 9.270(4) Å	α= 99.082(8)°.
	b = 10.764(4) Å	β= 96.647(8)°.
	c = 16.417(6) Å	γ = 90.248(8)°.
Volume	1606.2(10) $Å^3$	
Z	4	

Table 2.6. Crystal data and structure refinement for the structure in Figure 2.10.

Density (calculated)	1.295 Mg/m^3
Absorption coefficient	0.082 mm^{-1}
F(000)	656
Crystal size	0.16 x 0.10 x 0.05 mm^3
Theta range for data collection	3.14 to 25.00°.
Index ranges	-11<=h<=11, -11<=k<=12, -19<=l<=19
Reflections collected	13578
Independent reflections	5635 [R(int) = 0.1100]
Completeness to theta = 25.00°	99.7 %
Absorption correction	Semi-empirical from equivalents
Max. and min. transmission	1.00 and 0.653
Refinement method	Full-matrix least-squares on F^2
Data / restraints / parameters	5635 / 3 / 865
Goodness-of-fit on F^2	1.042
Final R indices [I>2sigma(I)]	R1 = 0.0700, wR2 = 0.1349
R indices (all data)	R1 = 0.1307, wR2 = 0.1647
Largest diff. peak and hole	0.291 and -0.286 $e.Å^{-3}$

Table 2.6. Crystal data and structure refinement for the structure in Figure 2.10 (Cont.).

	x	y	z	U(eq)		x	y	z	U(eq)
O1	9304(5)	11327(4)	4071(3)	28(1)	C1	9679(8)	11544(6)	3329(4)	25(2)
O2	11335(5)	10157(4)	3729(3)	28(1)	C2	9013(9)	12329(7)	2822(5)	33(2)
N1	9168(6)	9024(5)	4135(4)	28(2)	C3	9577(9)	12360(7)	2078(5)	38(2)
B1	10216(9)	10313(7)	4300(5)	25(2)	C4	10731(9)	11659(7)	1863(5)	38(2)
					C5	11425(9)	10876(7)	2390(5)	33(2)

Table 2.7. Atomic coordinates (x 10^4) and equivalent isotropic displacement parameters ($Å^2$x 10^3) for the structure in Figure 2.10. U(eq) is defined as one third of the trace of the orthogonalized U^{ij} tensor.

C6	10877(8)	10838(7)	3118(5)	31(2)
C7	10696(8)	10309(6)	5280(5)	27(2)
C8	11611(8)	11090(8)	5873(5)	33(2)
C9	11736(10)	10891(8)	6695(5)	46(2)
C10	10997(11)	9921(8)	6923(5)	50(2)
C11	10052(9)	9132(8)	6346(5)	38(2)
C12	9948(8)	9338(7)	5541(5)	28(2)
C13	9045(9)	8621(7)	4823(5)	34(2)
C14	8448(8)	8469(7)	3329(5)	33(2)
C15	9367(8)	7518(7)	2874(4)	27(2)
C16	9764(8)	7692(7)	2121(5)	36(2)
C17	10566(9)	6794(8)	1675(5)	42(2)
C18	10947(9)	5705(8)	1979(5)	40(2)
C19	10549(8)	5517(7)	2744(5)	37(2)
C20	9767(8)	6422(7)	3193(5)	34(2)
O3	6279(5)	6267(4)	3734(3)	29(1)
O4	4239(5)	5267(4)	4079(3)	30(1)
	x	y	z	U(eq)
N2	4161(6)	7609(5)	4149(4)	27(2)
B2	5195(9)	6393(7)	4309(5)	24(2)
C21	5826(8)	5265(6)	3132(5)	26(2)
C22	6390(9)	4858(7)	2419(5)	34(2)
C23	5741(9)	3801(7)	1899(5)	34(2)
C24	4553(9)	3201(7)	2114(5)	33(2)
C25	3946(8)	3638(7)	2845(5)	30(2)
C26	4598(8)	4674(6)	3344(4)	25(2)
C27	5677(8)	6875(6)	5280(5)	28(2)
C28	6591(8)	6382(8)	5868(5)	32(2)
C29	6803(9)	7012(8)	6686(5)	39(2)
C30	6045(10)	8081(8)	6916(5)	43(2)
C31	5105(9)	8599(7)	6343(5)	37(2)
C32	4967(8)	7965(6)	5546(5)	29(2)
C33	4047(8)	8352(7)	4827(5)	31(2)
C34	3411(7)	7770(7)	3336(4)	26(2)
C35	4351(8)	8473(6)	2873(5)	26(2)
C36	4783(8)	9719(7)	3165(5)	33(2)
C37	5596(8)	10370(7)	2726(5)	34(2)
C38	6006(9)	9812(8)	1980(5)	39(2)
C39	5597(9)	8570(8)	1679(5)	40(2)
C40	4754(9)	7893(7)	2115(5)	35(2)
O5	10005(5)	7247(4)	7831(3)	29(1)
O6	12206(5)	6294(4)	8180(3)	31(1)
N3	9926(7)	4903(5)	7764(4)	26(1)
B3	10877(9)	6119(8)	7613(5)	28(2)
C41	10650(8)	7815(7)	8593(5)	27(2)
C42	10140(9)	8812(7)	9098(5)	36(2)

Table 2.7. Atomic coordinates (x 10^4) and equivalent isotropic displacement parameters (Å^{2}x 10^3) for the structure in Figure 2.10. U(eq) is defined as one third of the trace of the orthogonalized U^{ij} tensor (Cont.).

C43	11003(10)	9205(8)	9873(5)	41(2)
C44	12278(9)	8641(8)	10084(5)	38(2)
C45	12805(9)	7644(7)	9548(5)	38(2)
C46	11950(8)	7256(6)	8792(4)	25(2)
C47	10957(8)	5681(6)	6644(5)	28(2)
C48	11651(8)	6166(7)	6049(5)	32(2)
C49	11467(10)	5546(8)	5238(5)	41(2)
C50	10624(10)	4465(8)	4994(5)	48(2)
C51	9944(9)	3957(7)	5557(5)	34(2)
C52	10137(8)	4562(6)	6389(4)	25(2)
C53	9522(8)	4167(6)	7076(5)	28(2)
C54	9534(8)	4696(7)	8558(4)	27(2)
C55	10670(8)	3934(7)	9008(5)	28(2)
C56	11495(9)	4469(7)	9737(5)	35(2)
C57	12474(10)	3770(8)	10156(5)	43(2)
C58	12667(9)	2523(8)	9853(5)	39(2)
C59	11868(9)	1990(7)	9119(5)	39(2)
C60	10843(8)	2698(6)	8696(5)	27(2)
O7	7177(5)	2380(4)	8128(3)	26(1)
O8	5023(5)	1184(4)	7747(3)	29(1)
N4	4879(6)	3475(5)	7660(4)	25(1)
B4	5871(9)	2220(7)	7525(6)	25(2)
C61	6928(8)	1693(7)	8738(4)	27(2)
C62	7758(8)	1673(8)	9476(5)	36(2)
C63	7276(9)	890(7)	10005(5)	37(2)
C64	6010(9)	174(7)	9764(5)	34(2)
C65	5178(9)	212(7)	9010(5)	36(2)
C66	5654(8)	977(7)	8508(5)	27(2)
C67	5980(7)	2200(6)	6582(5)	26(2)
C68	6663(9)	1427(7)	5980(5)	35(2)
C69	6520(10)	1616(8)	5175(5)	45(2)
C70	5658(10)	2556(8)	4915(5)	47(2)
C71	4955(9)	3361(7)	5477(5)	37(2)
C72	5125(8)	3141(7)	6291(5)	28(2)
C73	4507(8)	3881(7)	6971(5)	32(2)
C74	4421(8)	4059(6)	8476(5)	27(2)
C75	5554(8)	4993(7)	8963(5)	31(2)
C76	6193(9)	4798(8)	9719(5)	39(2)
C77	7190(10)	5702(9)	10190(5)	53(3)
C78	7520(9)	6761(8)	9869(5)	41(2)
C79	6853(9)	6969(7)	9132(5)	38(2)
C80	5867(8)	6070(7)	8662(5)	31(2)

Table 2.7. Atomic coordinates (x 10^4) and equivalent isotropic displacement parameters ($Å^2$x 10^3) for the structure in Figure 2.10. U(eq) is defined as one third of the trace of the orthogonalized U^{ij} tensor (Cont.).

O1-C1	1.359(8)	C10-C11	1.391(12)	N2-C33	1.279(9)
O1-B1	1.454(9)	C10-H10	0.95	N2-C34	1.468(9)
O2-C6	1.363(9)	C11-C12	1.367(10)	N2-B2	1.662(10)
O2-B1	1.471(10)	C11-H11	0.95	B2-C27	1.606(11)
N1-C13	1.289(10)	C12-C13	1.471(10)	C21-C22	1.349(10)
N1-C14	1.447(9)	C13-H13	0.95	C21-C26	1.405(10)
N1-B1	1.659(9)	C14-C15	1.499(10)	C22-C23	1.397(11)
B1-C7	1.619(11)	C14-H14A	0.99	C22-H22	0.95
C1-C2	1.376(10)	C14-H14B	0.99	C23-C24	1.383(12)
C1-C6	1.395(10)	C15-C16	1.370(11)	C23-H23	0.95
C2-C3	1.388(11)	C15-C20	1.399(10)	C24-C25	1.399(11)
C2-H2	0.95	C16-C17	1.390(11)	C24-H24	0.95
C3-C4	1.359(12)	C16-H16	0.95	C25-C26	1.368(10)
C3-H3	0.95	C17-C18	1.377(11)	C25-H25	0.95
C4-C5	1.407(11)	C17-H17	0.95	C27-C32	1.382(10)
C4-H4	0.95	C18-C19	1.392(11)	C27-C28	1.382(10)
C5-C6	1.357(10)	C18-H18	0.95	C28-C29	1.397(11)
C5-H5	0.95	C19-C20	1.386(11)	C28-H28	0.95
C7-C8	1.385(10)	C19-H19	0.95	C29-C30	1.376(12)
C7-C12	1.400(10)	C20-H20	0.95	C29-H29	0.95
C8-C9	1.391(12)	O3-C21	1.371(8)	C30-C31	1.391(11)
C8-H8	0.95	O3-B2	1.449(9)	C30-H30	0.95
C9-C10	1.369(13)	O4-C26	1.352(8)	C31-C32	1.368(10)
C9-H9	0.95	O4-B2	1.471(9)	C31-H31	0.95

Table 2.8. Bond lengths [Å] and angles [°] for the structure in Figure 2.10 (Cont.).

C32-C33 1.490(11)	C41-C42 1.370(11)	C54-H54B 0.99
C33-H33 0.95	C41-C46 1.378(10)	C55-C60 1.365(10)
C34-C35 1.497(10)	C42-C43 1.424(11)	C55-C56 1.383(11)
C34-H34A 0.99	C42-H42 0.95	C56-C57 1.375(11)
C34-H34B 0.99	C43-C44 1.365(12)	C56-H56 0.95
C35-C36 1.392(10)	C43-H43 0.95	C57-C58 1.376(11)
C35-C40 1.393(10)	C44-C45 1.404(11)	C57-H57 0.95
C36-C37 1.363(11)	C44-H44 0.95	C58-C59 1.378(11)
C36-H36 0.95	C45-C46 1.395(10)	C58-H58 0.95
C37-C38 1.372(11)	C45-H45 0.95	C59-C60 1.410(10)
C37-H37 0.95	C47-C48 1.394(11)	C59-H59 0.95
C38-C39 1.386(11)	C47-C52 1.401(10)	C60-H60 0.95
C38-H38 0.95	C48-C49 1.383(11)	O7-C61 1.374(8)
C39-C40 1.394(12)	C48-H48 0.95	O7-B4 1.464(9)
C39-H39 0.95	C49-C50 1.378(12)	O8-C66 1.367(9)
C40-H40 0.95	C49-H49 0.95	O8-B4 1.477(10)
O5-C41 1.371(9)	C50-C51 1.357(11)	N4-C73 1.287(9)
O5-B3 1.482(9)	C50-H50 0.95	N4-C74 1.495(9)
O6-C46 1.367(8)	C51-C52 1.408(10)	N4-B4 1.639(9)
O6-B3 1.448(9)	C51-H51 0.95	B4-C67 1.560(11)
N3-C53 1.288(9)	C52-C53 1.441(11)	C61-C62 1.361(10)
N3-C54 1.443(9)	C53-H53 0.95	C61-C66 1.389(10)
N3-B3 1.642(10)	C54-C55 1.532(10)	C62-C63 1.409(11)
B3-C47 1.596(11)	C54-H54A 0.99	C62-H62 0.95

Table 2.8. Bond lengths [Å] and angles [°] for the structure in Figure 2.10 (Cont.).

C63-C64	1.384(11)	C76-H76	0.95	C3-C2-H2	121.8
C63-H63	0.95	C77-C78	1.377(12)	C4-C3-C2	121.9(8)
C64-C65	1.386(10)	C77-H77	0.95	C4-C3-H3	119.1
C64-H64	0.95	C78-C79	1.345(11)	C2-C3-H3	119.1
C65-C66	1.359(10)	C78-H78	0.95	C3-C4-C5	121.5(8)
C65-H65	0.95	C79-C80	1.401(11)	C3-C4-H4	119.2
C67-C72	1.398(10)	C79-H79	0.95	C5-C4-H4	119.2
C67-C68	1.400(10)	C80-H80	0.95	C6-C5-C4	117.0(8)
C68-C69	1.360(11)	C1-O1-B1	105.8(6)	C6-C5-H5	121.5
C68-H68	0.95	C6-O2-B1	105.3(6)	C4-C5-H5	121.5
C69-C70	1.382(12)	C13-N1-C14	125.2(6)	C5-C6-O2	128.6(7)
C69-H69	0.95	C13-N1-B1	110.7(6)	C5-C6-C1	121.2(7)
C70-C71	1.385(12)	C14-N1-B1	124.1(6)	O2-C6-C1	110.1(7)
C70-H70	0.95	O1-B1-O2	106.5(6)	C8-C7-C12	117.8(7)
C71-C72	1.385(10)	O1-B1-C7	117.6(6)	C8-C7-B1	132.6(7)
C71-H71	0.95	O2-B1-C7	118.9(6)	C12-C7-B1	109.6(6)
C72-C73	1.443(11)	O1-B1-N1	106.8(5)	C7-C8-C9	119.2(8)
C73-H73	0.95	O2-B1-N1	109.2(6)	C7-C8-H8	120.4
C74-C75	1.516(10)	C7-B1-N1	96.7(5)	C9-C8-H8	120.4
C74-H74A	0.99	O1-C1-C2	127.4(7)	C10-C9-C8	121.2(8)
C74-H74B	0.99	O1-C1-C6	110.6(6)	C10-C9-H9	119.4
C75-C76	1.360(11)	C2-C1-C6	122.0(7)	C8-C9-H9	119.4
C75-C80	1.372(10)	C1-C2-C3	116.4(8)	C9-C10-C11	121.1(8)
C76-C77	1.410(12)	C1-C2-H2	121.8	C9-C10-H10	119.5

Table 2.8. Bond lengths [Å] and angles [°] for the structure in Figure 2.10 (Cont.).

C11-C10-H10	119.5	C16-C17-H17	119.9	C21-C22-C23	118.1(8)
C12-C11-C10	116.9(8)	C17-C18-C19	119.7(8)	C21-C22-H22	121
C12-C11-H11	121.6	C17-C18-H18	120.1	C23-C22-H22	121
C10-C11-H11	121.6	C19-C18-H18	120.1	C24-C23-C22	120.5(8)
C11-C12-C7	123.8(7)	C20-C19-C18	120.0(8)	C24-C23-H23	119.8
C11-C12-C13	126.9(7)	C20-C19-H19	120	C22-C23-H23	119.8
C7-C12-C13	109.3(7)	C18-C19-H19	120	C23-C24-C25	121.6(7)
N1-C13-C12	113.4(7)	C19-C20-C15	119.9(8)	C23-C24-H24	119.2
N1-C13-H13	123.3	C19-C20-H20	120.1	C25-C24-H24	119.2
C12-C13-H13	123.3	C15-C20-H20	120.1	C26-C25-C24	116.9(7)
N1-C14-C15	112.2(6)	C21-O3-B2	106.0(6)	C26-C25-H25	121.6
N1-C14-H14A	109.2	C26-O4-B2	106.2(5)	C24-C25-H25	121.6
C15-C14-H14A	109.2	C33-N2-C34	124.4(6)	O4-C26-C25	128.5(7)
N1-C14-H14B	109.2	C33-N2-B2	111.6(6)	O4-C26-C21	110.1(6)
C15-C14-H14B	109.2	C34-N2-B2	123.9(6)	C25-C26-C21	121.4(7)
H14A-C14-H14B	107.9	O3-B2-O4	106.5(6)	C32-C27-C28	117.3(7)
C16-C15-C20	119.6(7)	O3-B2-C27	119.7(6)	C32-C27-B2	110.5(6)
C16-C15-C14	119.9(7)	O4-B2-C27	117.9(6)	C28-C27-B2	132.1(7)
C20-C15-C14	120.5(7)	O3-B2-N2	109.0(6)	C27-C28-C29	119.7(8)
C15-C16-C17	120.6(8)	O4-B2-N2	106.1(6)	C27-C28-H28	120.1
C15-C16-H16	119.7	C27-B2-N2	96.1(5)	C29-C28-H28	120.1
C17-C16-H16	119.7	C22-C21-O3	128.4(7)	C30-C29-C28	120.2(8)
C18-C17-C16	120.2(8)	C22-C21-C26	121.5(7)	C30-C29-H29	119.9
C18-C17-H17	119.9	O3-C21-C26	110.1(6)	C28-C29-H29	119.9

Table 2.8. Bond lengths [Å] and angles [°] for the structure in Figure 2.10 (Cont.).

C29-C30-C31	121.6(8)	C36-C37-C38	120.7(8)	C42-C41-C46	122.9(7)
C29-C30-H30	119.2	C36-C37-H37	119.7	O5-C41-C46	110.2(6)
C31-C30-H30	119.2	C38-C37-H37	119.7	C41-C42-C43	115.8(8)
C32-C31-C30	115.8(7)	C37-C38-C39	119.2(8)	C41-C42-H42	122.1
C32-C31-H31	122.1	C37-C38-H38	120.4	C43-C42-H42	122.1
C30-C31-H31	122.1	C39-C38-H38	120.4	C44-C43-C42	121.7(8)
C31-C32-C27	125.3(7)	C38-C39-C40	120.9(8)	C44-C43-H43	119.1
C31-C32-C33	125.3(7)	C38-C39-H39	119.6	C42-C43-H43	119.1
C27-C32-C33	109.4(7)	C40-C39-H39	119.6	C43-C44-C45	121.6(8)
N2-C33-C32	112.0(7)	C35-C40-C39	119.1(8)	C43-C44-H44	119.2
N2-C33-H33	124	C35-C40-H40	120.4	C45-C44-H44	119.2
C32-C33-H33	124	C39-C40-H40	120.4	C46-C45-C44	116.4(7)
N2-C34-C35	111.2(6)	C41-O5-B3	105.0(5)	C46-C45-H45	121.8
N2-C34-H34A	109.4	C46-O6-B3	105.7(5)	C44-C45-H45	121.8
C35-C34-H34A	109.4	C53-N3-C54	123.6(6)	O6-C46-C41	111.0(6)
N2-C34-H34B	109.4	C53-N3-B3	111.5(6)	O6-C46-C45	127.5(7)
C35-C34-H34B	109.4	C54-N3-B3	124.9(6)	C41-C46-C45	121.4(7)
H34A-C34-H34B	108	O6-B3-O5	106.0(6)	C48-C47-C52	117.8(7)
C36-C35-C40	118.9(7)	O6-B3-C47	119.6(7)	C48-C47-B3	133.8(7)
C36-C35-C34	121.4(7)	O5-B3-C47	115.7(6)	C52-C47-B3	108.4(6)
C40-C35-C34	119.7(7)	O6-B3-N3	110.9(6)	C49-C48-C47	118.9(8)
C37-C36-C35	121.1(8)	O5-B3-N3	106.7(6)	C49-C48-H48	120.6
C37-C36-H36	119.4	C47-B3-N3	97.0(6)	C47-C48-H48	120.6
C35-C36-H36	119.4	C42-C41-O5	126.9(7)	C50-C49-C48	122.6(8)

Table 2.8. Bond lengths [Å] and angles [°] for the structure in Figure 2.10 (Cont.).

C50-C49-H49	118.7	C57-C56-H56	119.6	C67-B4-N4	96.8(5)
C48-C49-H49	118.7	C55-C56-H56	119.6	C62-C61-O7	127.6(7)
C51-C50-C49	120.3(8)	C56-C57-C58	120.5(8)	C62-C61-C66	122.0(7)
C51-C50-H50	119.9	C56-C57-H57	119.7	O7-C61-C66	110.4(6)
C49-C50-H50	119.9	C58-C57-H57	119.7	C61-C62-C63	117.3(7)
C50-C51-C52	118.1(7)	C57-C58-C59	118.8(8)	C61-C62-H62	121.3
C50-C51-H51	121	C57-C58-H58	120.6	C63-C62-H62	121.3
C52-C51-H51	121	C59-C58-H58	120.6	C64-C63-C62	119.9(7)
C47-C52-C51	122.4(7)	C58-C59-C60	120.8(8)	C64-C63-H63	120
C47-C52-C53	111.1(6)	C58-C59-H59	119.6	C62-C63-H63	120
C51-C52-C53	126.5(7)	C60-C59-H59	119.6	C63-C64-C65	121.8(8)
N3-C53-C52	111.7(6)	C55-C60-C59	119.3(7)	C63-C64-H64	119.1
N3-C53-H53	124.1	C55-C60-H60	120.3	C65-C64-H64	119.1
C52-C53-H53	124.1	C59-C60-H60	120.3	C66-C65-C64	117.6(7)
N3-C54-C55	112.1(6)	C61-O7-B4	106.2(5)	C66-C65-H65	121.2
N3-C54-H54A	109.2	C66-O8-B4	106.3(5)	C64-C65-H65	121.2
C55-C54-H54A	109.2	C73-N4-C74	123.9(6)	C65-C66-O8	128.5(7)
N3-C54-H54B	109.2	C73-N4-B4	111.5(6)	C65-C66-C61	121.4(7)
C55-C54-H54B	109.2	C74-N4-B4	124.5(6)	O8-C66-C61	110.2(6)
H54A-C54-H54B	107.9	O7-B4-O8	105.4(6)	C72-C67-C68	115.4(7)
C60-C55-C56	119.6(7)	O7-B4-C67	120.7(7)	C72-C67-B4	110.0(6)
C60-C55-C54	119.3(7)	O8-B4-C67	116.7(6)	C68-C67-B4	134.5(7)
C56-C55-C54	121.0(7)	O7-B4-N4	109.7(6)	C69-C68-C67	121.4(8)
C57-C56-C55	120.9(8)	O8-B4-N4	106.3(6)	C69-C68-H68	119.3

Table 2.8. Bond lengths [Å] and angles [°] for the structure in Figure 2.10 (Cont.).

C67-C68-H68	119.3	N4-C73-H73	124.2	C78-C77-C76	119.2(8)
C68-C69-C70	121.2(9)	C72-C73-H73	124.2	C78-C77-H77	120.4
C68-C69-H69	119.4	N4-C74-C75	111.8(6)	C76-C77-H77	120.4
C70-C69-H69	119.4	N4-C74-H74A	109.3	C79-C78-C77	120.8(8)
C69-C70-C71	120.5(8)	C75-C74-H74A	109.3	C79-C78-H78	119.6
C69-C70-H70	119.7	N4-C74-H74B	109.3	C77-C78-H78	119.6
C71-C70-H70	119.7	C75-C74-H74B	109.3	C78-C79-C80	119.9(8)
C72-C71-C70	116.7(7)	H74A-C74-H74B	107.9	C78-C79-H79	120
C72-C71-H71	121.7	C76-C75-C80	120.2(7)	C80-C79-H79	120
C70-C71-H71	121.7	C76-C75-C74	119.8(7)	C75-C80-C79	120.0(7)
C71-C72-C67	124.8(7)	C80-C75-C74	119.8(7)	C75-C80-H80	120
C71-C72-C73	125.3(7)	C75-C76-C77	119.7(8)	C79-C80-H80	120
C67-C72-C73	109.9(7)	C75-C76-H76	120.1		
N4-C73-C72	111.5(6)	C77-C76-H76	120.1		

Table 2.8. Bond lengths [Å] and angles [°] for the structure in Figure 2.10 (Cont.).

	U11	U22	U33	U23	U13	U12
O1	27(3)	20(3)	36(3)	5(2)	8(2)	1(2)
O2	19(3)	32(3)	35(3)	6(2)	8(2)	2(2)
N1	21(4)	24(3)	38(4)	5(3)	3(3)	-3(3)
B1	21(5)	17(4)	38(5)	9(4)	1(4)	-6(3)

Table 2.9. Anisotropic displacement parameters ($Å^2 x\ 10^3$) for the structure in Figure 2.10. The anisotropic displacement factor exponent takes the form: $-2\pi^2[\ h^2\ a^{*2}U^{11} + ...\ + 2\ h\ k\ a^*\ b^*\ U^{12}\ ]$

C1	30(4)	20(4)	25(4)	3(3)	7(3)	-3(3)
C2	31(5)	32(5)	38(5)	9(4)	3(4)	-3(4)
C3	51(6)	28(4)	35(5)	5(4)	-3(4)	-5(4)
C4	40(5)	39(5)	30(5)	-2(4)	0(4)	-14(4)
C5	30(5)	38(5)	29(5)	-2(4)	1(4)	-8(4)
C6	29(5)	19(4)	40(5)	-3(4)	-6(4)	-4(3)
C7	25(4)	17(4)	40(5)	0(3)	9(4)	4(3)
C8	30(5)	37(5)	32(5)	-1(4)	5(4)	2(4)
C9	52(6)	46(6)	35(5)	0(4)	-6(4)	12(4)
C10	67(7)	44(6)	36(5)	8(4)	-5(5)	10(5)
C11	38(5)	43(5)	37(5)	16(4)	12(4)	15(4)
C12	29(4)	23(4)	35(5)	9(4)	7(4)	2(3)
C13	38(5)	22(4)	42(5)	9(4)	1(4)	-4(3)
C14	19(4)	22(4)	56(6)	10(4)	-5(4)	-5(3)
C15	27(4)	26(4)	25(4)	5(3)	0(3)	-7(3)
C16	35(5)	36(5)	38(5)	11(4)	0(4)	-2(4)
C17	48(6)	52(6)	25(5)	-1(4)	7(4)	-6(4)
C18	43(6)	38(5)	37(5)	-6(4)	7(4)	2(4)
C19	23(4)	31(5)	55(6)	1(4)	-5(4)	5(3)
C20	32(5)	28(4)	43(5)	8(4)	1(4)	-6(4)
O3	24(3)	27(3)	34(3)	4(2)	0(2)	1(2)
O4	36(3)	21(3)	33(3)	8(2)	8(2)	-4(2)

Table 2.9. Anisotropic displacement parameters ($Å^2 x\ 10^3$) for the structure in Figure 2.10. The anisotropic displacement factor exponent takes the form: $-2\pi^2[\ h^2\ a^{*2}U^{11} + ... + 2\ h\ k\ a^*\ b^*\ U^{12}\ ]$ (Cont.).

N2	22(3)	25(3)	34(4)	10(3)	1(3)	-2(3)
B2	26(5)	24(5)	26(5)	8(4)	12(4)	0(4)
C21	24(4)	20(4)	31(5)	3(3)	-1(4)	4(3)
C22	36(5)	33(5)	32(5)	2(4)	0(4)	2(4)
C23	36(5)	44(5)	22(4)	10(4)	2(4)	15(4)
C24	35(5)	31(4)	30(5)	3(4)	-10(4)	3(4)
C25	25(4)	23(4)	40(5)	9(4)	-2(4)	2(3)
C26	33(4)	22(4)	19(4)	2(3)	5(3)	3(3)
C27	24(4)	23(4)	36(5)	2(3)	1(4)	0(3)
C28	31(5)	38(5)	29(4)	10(4)	2(4)	-5(4)
C29	34(5)	49(5)	34(5)	13(4)	-3(4)	-5(4)
C30	54(6)	44(5)	28(5)	-2(4)	5(4)	-9(4)
C31	49(6)	20(4)	39(5)	-1(4)	7(4)	-4(4)
C32	33(5)	19(4)	37(5)	5(3)	12(4)	4(3)
C33	28(4)	29(4)	37(5)	4(4)	11(4)	1(3)
C34	15(4)	27(4)	35(5)	6(3)	3(3)	1(3)
C35	29(4)	21(4)	29(5)	11(3)	0(4)	3(3)
C36	28(5)	32(4)	36(5)	2(4)	3(4)	4(3)
C37	34(5)	28(4)	42(5)	14(4)	-2(4)	-3(4)
C38	34(5)	54(6)	34(5)	23(4)	7(4)	6(4)
C39	46(6)	56(6)	23(5)	18(4)	1(4)	12(4)
C40	49(5)	37(5)	19(4)	7(4)	-2(4)	7(4)

Table 2.9. Anisotropic displacement parameters ($Å^2 x\ 10^3$) for the structure in Figure 2.10. The anisotropic displacement factor exponent takes the form: $-2\pi^2[\ h^2\ a^{*2}U^{11} + ...\ + 2\ h\ k\ a^*\ b^*\ U^{12}\ ]$ (Cont.).

O5	28(3)	25(3)	30(3)	-1(2)	-6(2)	6(2)
O6	26(3)	28(3)	38(3)	3(2)	-2(2)	1(2)
N3	32(4)	22(3)	25(4)	9(3)	1(3)	1(3)
B3	29(5)	28(5)	27(5)	5(4)	-1(4)	-1(4)
C41	31(5)	22(4)	30(4)	9(3)	0(4)	-4(3)
C42	42(5)	25(4)	45(5)	12(4)	12(4)	-1(4)
C43	56(6)	35(5)	30(5)	-5(4)	12(4)	-13(4)
C44	39(5)	41(5)	33(5)	1(4)	4(4)	-6(4)
C45	29(5)	40(5)	41(5)	7(4)	-11(4)	-4(4)
C46	24(4)	24(4)	27(4)	3(3)	4(3)	-3(3)
C47	27(4)	24(4)	37(5)	10(3)	7(4)	3(3)
C48	27(5)	30(4)	36(5)	-1(4)	-1(4)	4(3)
C49	54(6)	41(5)	32(5)	6(4)	18(4)	5(4)
C50	59(6)	46(6)	37(5)	0(4)	13(5)	8(5)
C51	41(5)	30(5)	30(5)	1(4)	2(4)	0(4)
C52	37(5)	19(4)	18(4)	1(3)	0(3)	1(3)
C53	24(4)	18(4)	41(5)	2(4)	-1(4)	2(3)
C54	25(4)	25(4)	32(5)	7(3)	4(3)	-4(3)
C55	21(4)	31(4)	36(5)	13(4)	9(4)	8(3)
C56	46(5)	27(4)	31(5)	-1(4)	14(4)	10(4)
C57	49(6)	61(6)	22(5)	2(4)	14(4)	15(5)
C58	46(5)	41(5)	35(5)	12(4)	14(4)	10(4)

Table 2.9. Anisotropic displacement parameters ($Å^2 x\ 10^3$) for the structure in Figure 2.10. The anisotropic displacement factor exponent takes the form: $-2\pi^2[\ h^2\ a^{*2}U^{11} + ...\ + 2\ h\ k\ a^*\ b^*\ U^{12}\ ]$ (Cont.).

C59	42(5)	35(5)	44(5)	6(4)	18(4)	2(4)
C60	29(5)	19(4)	32(5)	1(3)	1(4)	-2(3)
O7	23(3)	28(3)	27(3)	7(2)	0(2)	1(2)
O8	29(3)	28(3)	30(3)	7(2)	-2(2)	-2(2)
N4	23(3)	22(3)	29(4)	4(3)	2(3)	-1(3)
B4	18(5)	17(4)	40(5)	5(4)	1(4)	8(3)
C61	34(5)	29(4)	23(4)	12(3)	13(4)	2(3)
C62	23(4)	50(5)	36(5)	12(4)	-4(4)	6(4)
C63	39(5)	47(5)	27(5)	20(4)	-1(4)	4(4)
C64	38(5)	36(5)	33(5)	16(4)	12(4)	11(4)
C65	42(5)	31(5)	34(5)	3(4)	2(4)	3(4)
C66	27(4)	29(4)	27(4)	9(4)	4(4)	2(3)
C67	18(4)	25(4)	34(4)	3(3)	10(3)	6(3)
C68	40(5)	30(5)	38(5)	11(4)	13(4)	2(4)
C69	49(6)	48(6)	38(5)	9(4)	9(4)	-10(4)
C70	64(6)	48(6)	30(5)	11(4)	0(5)	-19(5)
C71	39(5)	37(5)	34(5)	10(4)	-2(4)	-1(4)
C72	33(5)	23(4)	26(4)	0(3)	-2(4)	0(3)
C73	30(5)	25(4)	41(5)	15(4)	-7(4)	2(3)
C74	25(4)	25(4)	33(4)	7(3)	3(3)	2(3)
C75	29(5)	26(4)	35(5)	-4(4)	11(4)	2(3)
C76	44(5)	45(5)	30(5)	11(4)	2(4)	-9(4)

Table 2.9. Anisotropic displacement parameters ($Å^2 x\ 10^3$) for the structure in Figure 2.10. The anisotropic displacement factor exponent takes the form: $-2\pi^2[\ h^2\ a^{*2}U^{11} + ...\ + 2\ h\ k\ a^*\ b^*\ U^{12}\ ]$ (Cont.).

C77	60(7)	61(6)	34(5)	10(5)	-10(5)	-4(5)
C78	32(5)	44(5)	42(5)	-8(4)	7(4)	-2(4)
C79	43(5)	24(4)	50(6)	14(4)	6(5)	-4(4)
C80	29(5)	30(4)	38(5)	8(4)	10(4)	7(3)

Table 2.9. Anisotropic displacement parameters ($Å^2 x\ 10^3$) for the structure in Figure 2.10. The anisotropic displacement factor exponent takes the form: $-2\pi^2[\ h^2\ a^{*2}U^{11} + ...\ + 2\ h\ k\ a^*\ b^*\ U^{12}\ ]$ (Cont.).

	x	y	z	U(eq)
H2	8210	12823	2973	40
H3	9145	12886	1709	46
H4	11077	11700	1345	45
H5	12240	10395	2243	40
H8	12148	11753	5721	40
H9	12344	11438	7106	55
H10	11132	9786	7484	60
H11	9504	8480	6504	45
H13	8431	7930	4863	41
H14A	8210	9142	2992	39
H14B	7524	8058	3402	39
H16	9488	8433	1901	43
H17	10853	6932	1158	51
H18	11478	5084	1669	48
H19	10812	4769	2957	45
H20	9504	6299	3718	41
H22	7204	5277	2274	41
H23	6118	3493	1393	40
	x	y	z	U(eq)
H24	4139	2474	1758	40
H25	3119	3234	2988	35
H28	7074	5618	5717	38
H29	7473	6701	7085	47
H30	6166	8476	7480	51
H31	4592	9345	6495	44
H33	3446	9066	4867	37
H34A	2506	8234	3414	31

Table 2.10. Hydrogen coordinates ($x\ 10^4$) and isotropic displacement parameters ($Å^2 x\ 10^3$) for the structure in Figure 2.10.

H34B	3144	6933	3005	31
H36	4507	10123	3679	39
H37	5882	11219	2939	41
H38	6563	10273	1673	46
H39	5896	8173	1168	48
H40	4459	7048	1899	42
H42	9265	9215	8942	43
H43	10683	9878	10252	49
H44	12823	8931	10607	46
H45	13695	7254	9692	45
H48	12240	6910	6198	39
H49	11940	5879	4834	50
H50	10518	4073	4429	57
H51	9355	3215	5395	41
H53	8896	3451	7028	34
H54A	8584	4242	8474	33
H54B	9427	5519	8910	33
H56	11383	5332	9950	41
H57	13022	4150	10659	52
H58	13339	2037	10144	47
H59	12010	1136	8896	47
H60	10279	2319	8197	33
H62	8627	2168	9628	43
H63	7820	852	10528	44
H64	5702	-357	10124	40
H65	4308	-279	8851	43
H68	7238	756	6137	41
H69	7022	1092	4785	54
H70	5547	2652	4345	57
H71	4384	4029	5313	44
H73	3902	4581	6917	38
H74A	4255	3389	8807	33
H74B	3493	4493	8377	33
H76	5969	4056	9929	47
H77	7630	5581	10724	63
H78	8227	7353	10171	49
H79	7050	7725	8931	46
H80	5415	6205	8135	38

Table 2.10. Hydrogen coordinates (x 10^4) and isotropic displacement parameters ($Å^2$x 10^3) for the structure in Figure 2.10 (Cont.).

C1-O1-B1-O2	11.7(7)	O1-C1-C6-C5	178.3(6)	C11-C12-C13-N1	-179.7(7)
C1-O1-B1-C7	147.9(6)	C2-C1-C6-C5	-1.3(11)	C7-C12-C13-N1	1.3(9)
C1-O1-B1-N1	-104.9(6)	O1-C1-C6-O2	-1.3(8)	C13-N1-C14-C15	-92.6(9)
C6-O2-B1-O1	-12.4(7)	C2-C1-C6-O2	179.2(6)	B1-N1-C14-C15	90.1(8)
C6-O2-B1-C7	-148.0(6)	O1-B1-C7-C8	-68.7(11)	N1-C14-C15-C16	-119.7(7)
C6-O2-B1-N1	102.6(6)	O2-B1-C7-C8	62.1(11)	N1-C14-C15-C20	63.3(9)
C13-N1-B1-O1	-115.7(7)	N1-B1-C7-C8	178.4(8)	C20-C15-C16-C17	-0.3(11)
C14-N1-B1-O1	61.9(9)	O1-B1-C7-C12	108.0(7)	C14-C15-C16-C17	-177.4(7)
C13-N1-B1-O2	129.6(7)	O2-B1-C7-C12	-121.2(7)	C15-C16-C17-C18	1.3(12)
C14-N1-B1-O2	-52.8(8)	N1-B1-C7-C12	-4.9(7)	C16-C17-C18-C19	-1.3(12)
C13-N1-B1-C7	5.8(7)	C12-C7-C8-C9	-0.8(11)	C17-C18-C19-C20	0.3(12)
C14-N1-B1-C7	-176.6(6)	B1-C7-C8-C9	175.7(8)	C18-C19-C20-C15	0.7(11)
B1-O1-C1-C2	172.8(7)	C7-C8-C9-C10	1.5(13)	C16-C15-C20-C19	-0.6(11)
B1-O1-C1-C6	-6.7(7)	C8-C9-C10-C11	-2.6(14)	C14-C15-C20-C19	176.4(6)
O1-C1-C2-C3	-178.1(6)	C9-C10-C11-C12	2.7(13)	C21-O3-B2-O4	9.8(7)
C6-C1-C2-C3	1.4(11)	C10-C11-C12-C7	-2.1(12)	C21-O3-B2-C27	146.7(6)
C1-C2-C3-C4	-0.4(11)	C10-C11-C12-C13	179.1(8)	C21-O3-B2-N2	-104.3(6)
C2-C3-C4-C5	-0.8(12)	C8-C7-C12-C11	1.1(12)	C26-O4-B2-O3	-10.1(7)
C3-C4-C5-C6	0.9(11)	B1-C7-C12-C11	-176.1(7)	C26-O4-B2-C27	-147.9(6)
C4-C5-C6-O2	179.5(7)	C8-C7-C12-C13	-179.9(7)	C26-O4-B2-N2	105.9(6)
C4-C5-C6-C1	0.1(10)	B1-C7-C12-C13	2.9(8)	C33-N2-B2-O3	-129.9(6)
B1-O2-C6-C5	-170.9(7)	C14-N1-C13-C12	177.6(6)	C34-N2-B2-O3	53.2(8)
B1-O2-C6-C1	8.5(7)	B1-N1-C13-C12	-4.8(9)	C33-N2-B2-O4	115.8(6)

Table 2.11. Torsion angles [°] for the structure in Figure 2.10.

C34-N2-B2-O4	-61.2(8)	N2-B2-C27-C28	-178.2(8)	C36-C37-C38-C39	-0.7(11)
C33-N2-B2-C27	-5.6(7)	C32-C27-C28-C29	-2.3(11)	C37-C38-C39-C40	1.4(11)
C34-N2-B2-C27	177.5(6)	B2-C27-C28-C29	-179.4(7)	C36-C35-C40-C39	1.0(11)
B2-O3-C21-C22	172.6(7)	C27-C28-C29-C30	3.5(12)	C34-C35-C40-C39	178.3(6)
B2-O3-C21-C26	-6.0(8)	C28-C29-C30-C31	-3.0(13)	C38-C39-C40-C35	-1.5(11)
O3-C21-C22-C23	179.8(7)	C29-C30-C31-C32	1.2(12)	C46-O6-B3-O5	14.1(7)
C26-C21-C22-C23	-1.7(11)	C30-C31-C32-C27	0.0(12)	C46-O6-B3-C47	147.0(7)
C21-C22-C23-C24	0.2(11)	C30-C31-C32-C33	-178.9(7)	C46-O6-B3-N3	-101.4(6)
C22-C23-C24-C25	1.3(11)	C28-C27-C32-C31	0.6(12)	C41-O5-B3-O6	-14.5(7)
C23-C24-C25-C26	-1.2(10)	B2-C27-C32-C31	178.2(7)	C41-O5-B3-C47	-149.5(7)
B2-O4-C26-C25	-174.5(7)	C28-C27-C32-C33	179.6(7)	C41-O5-B3-N3	103.8(6)
B2-O4-C26-C21	6.6(8)	B2-C27-C32-C33	-2.7(8)	C53-N3-B3-O6	-130.9(7)
C24-C25-C26-O4	-179.2(6)	C34-N2-C33-C32	-178.4(6)	C54-N3-B3-O6	51.3(9)
C24-C25-C26-C21	-0.3(11)	B2-N2-C33-C32	4.6(8)	C53-N3-B3-O5	114.0(7)
C22-C21-C26-O4	-179.1(6)	C31-C32-C33-N2	177.7(7)	C54-N3-B3-O5	-63.7(8)
O3-C21-C26-O4	-0.4(8)	C27-C32-C33-N2	-1.3(9)	C53-N3-B3-C47	-5.5(7)
C22-C21-C26-C25	1.9(11)	C33-N2-C34-C35	94.0(8)	C54-N3-B3-C47	176.8(6)
O3-C21-C26-C25	-179.4(6)	B2-N2-C34-C35	-89.5(7)	B3-O5-C41-C42	-171.8(8)
O3-B2-C27-C32	120.6(7)	N2-C34-C35-C36	-64.5(8)	B3-O5-C41-C46	9.6(8)
O4-B2-C27-C32	-107.2(7)	N2-C34-C35-C40	118.3(7)	O5-C41-C42-C43	178.4(7)
N2-B2-C27-C32	4.6(7)	C40-C35-C36-C37	-0.4(11)	C46-C41-C42-C43	-3.2(11)
O3-B2-C27-C28	-62.2(11)	C34-C35-C36-C37	-177.6(7)	C41-C42-C43-C44	1.7(11)
O4-B2-C27-C28	70.0(11)	C35-C36-C37-C38	0.3(11)	C42-C43-C44-C45	0.0(12)

Table 2.11. Torsion angles [°] for the structure in Figure 2.10 (Cont.).

C43-C44-C45-C46 -0.5(12)	B3-C47-C52-C53 -1.1(8)	C66-O8-B4-C67 148.5(6)
B3-O6-C46-C41 -8.7(8)	C50-C51-C52-C47 2.2(11)	C66-O8-B4-N4 -104.9(6)
B3-O6-C46-C45 168.9(7)	C50-C51-C52-C53 -179.4(7)	C73-N4-B4-O7 130.4(7)
C42-C41-C46-O6 -179.4(7)	C54-N3-C53-C52 -176.8(6)	C74-N4-B4-O7 -51.3(9)
O5-C41-C46-O6 -0.8(8)	B3-N3-C53-C52 5.4(8)	C73-N4-B4-O8 -116.1(7)
C42-C41-C46-C45 2.9(11)	C47-C52-C53-N3 -2.9(9)	C74-N4-B4-O8 62.2(8)
O5-C41-C46-C45 -178.5(6)	C51-C52-C53-N3 178.6(7)	C73-N4-B4-C67 4.4(8)
C44-C45-C46-O6 -178.2(7)	C53-N3-C54-C55 91.9(8)	C74-N4-B4-C67 -177.3(6)
C44-C45-C46-C41 -0.9(11)	B3-N3-C54-C55 -90.6(8)	B4-O7-C61-C62 -171.6(8)
O6-B3-C47-C48 -57.0(12)	N3C54-C55-C60 -68.4(9)	B4-O7-C61-C66 8.2(8)
O5-B3-C47-C48 71.7(11)	N3-C54-C55-C56 113.2(8)	O7-C61-C62-C63 179.9(7)
N3-B3-C47-C48 -175.9(8)	C60-C55-C56-C57 -0.9(12)	C66-C61-C62-C63 0.1(12)
O6-B3-C47-C52 122.5(7)	C54-C55-C56-C57 177.5(8)	C61-C62-C63-C64 0.4(12)
O5-B3-C47-C52 -108.8(7)	C55-C56-C57-C58 0.9(13)	C62-C63-C64-C65 -0.6(13)
N3-B3-C47-C52 3.6(7)	C56-C57-C58-C59 0.4(13)	C63-C64-C65-C66 0.3(12)
C52-C47-C48-C49 1.7(11)	C57-C58-C59-C60 -1.6(13)	C64-C65-C66-O8 -179.2(7)
B3-C47-C48-C49 -178.8(8)	C56-C55-C60-C59 -0.3(12)	C64-C65-C66-C61 0.1(11)
C47-C48-C49-C50 -0.1(12)	C54-C55-C60-C59 -178.7(7)	B4-O8-C66-C65 172.4(8)
C48-C49-C50-C51 -0.6(13)	C58-C59-C60-C55 1.6(12)	B4-O8-C66-C61 -6.9(8)
C49-C50-C51-C52 -0.4(12)	C61-O7-B4-O8 -12.0(7)	C62-C61-C66-C65 -0.3(12)
C48-C47-C52-C51 -2.9(11)	C61-O7-B4-C67 -146.8(6)	O7-C61-C66-C65 179.8(6)
B3-C47-C52-C51 177.6(7)	C61-O7-B4-N4 102.1(6)	C62-C61-C66-O8 179.1(7)
C48-C47-C52-C53 178.5(6)	C66-O8-B4-O7 11.6(7)	O7-C61-C66-O8 -0.8(9)

Table 2.11. Torsion angles [°] for the structure in Figure 2.10 (Cont.).

O7-B4-C67-C72	-122.7(7)	C68-C67-C72-C71	-1.7(12)	C74-C75-C76-C77	-176.7(8)
O8-B4-C67-C72	107.3(7)	B4-C67-C72-C71	-178.5(7)	C75-C76-C77-C78	-1.1(14)
N4-B4-C67-C72	-4.9(8)	C68-C67-C72-C73	-179.0(6)	C76-C77-C78-C79	3.1(14)
O7-B4-C67-C68	61.3(12)	B4-C67-C72-C73	4.2(9)	C77-C78-C79-C80	-3.4(13)
O8-B4-C67-C68	-68.7(11)	C74-N4-C73-C72	179.3(6)	C76-C75-C80-C79	0.3(12)
N4-B4-C67-C68	179.1(8)	B4-N4-C73-C72	-2.4(8)	C74-C75-C80-C79	176.4(7)
C72-C67-C68-C69	1.6(12)	C71-C72-C73-N4	-178.3(8)	C78-C79-C80-C75	1.7(12)
B4-C67-C68-C69	177.5(8)	C67-C72-C73-N4	-1.1(9)		
C67-C68-C69-C70	-2.0(13)	C73-N4-C74-C75	-95.0(8)		
C68-C69-C70-C71	2.2(14)	B4-N4-C74-C75	87.0(8)		
C69-C70-C71-C72	-2.1(12)	N4-C74-C75-C76	-118.9(8)		
C70-C71-C72-C67	2.0(12)	N4-C74-C75-C80	65.0(9)		
C70-C71-C72-C73	178.8(7)	C80-C75-C76-C77	-0.6(13)		

Table 2.11. Torsion angles [°] for the structure in Figure 2.10 (Cont.).

Empirical formula	C20 H16 B N O2	
Formula weight	313.15	
Temperature	153(2) K	
Wavelength	0.71073 Å	
Crystal system	Triclinic	
Space group	P1	
Unit cell dimensions	a = 9.2987(12) Å	α= 99.348(6)°.
	b = 10.7865(15) Å	β= 96.773(7)°.
	c = 16.512(2) Å	γ = 90.053(7)°.
Volume	1622.4(4) $Å^3$	
Z	4	
Density (calculated)	1.282 Mg/m^3	
Absorption coefficient	0.082 mm^{-1}	
F(000)	656	
Crystal size	0.41 x 0.12 x 0.04 mm	
Theta range for data collection	2.11 to 27.56°.	
Index ranges	-11<=h<=11, -14<=k<=14, -21<=l<=21	
Reflections collected	12489	
Independent reflections	12493	
Completeness to theta = 27.56°	96.4 %	
Absorption correction	None	
Refinement method	Full-matrix least-squares on F^2	
Data / restraints / parameters	12493 / 3 / 866	
Goodness-of-fit on F^2	1.058	
Final R indices [I>2sigma(I)]	R1 = 0.1169, wR2 = 0.1934	
R indices (all data)	R1 = 0.2918, wR2 = 0.2648	
Largest diff. peak and hole	0.441 and -0.341 $e.Å^{-3}$	

Table 2.12. Crystal data and structure refinement for the structure in Figure 2.8.

	x	y	z	U(eq)
O1	6199(9)	7005(9)	4343(5)	46(3)
O2	8399(8)	6030(8)	4683(5)	37(2)
N1	8488(10)	8373(10)	4751(6)	37(3)
B1	7544(16)	7143(14)	4892(9)	34(4)
C1	7433(15)	7597(16)	5888(9)	42(4)
C2	6756(14)	7133(18)	6477(9)	40(4)
C3	6898(17)	7690(18)	7264(11)	62(5)
C4	7740(16)	8800(16)	7530(8)	51(4)
C5	8469(18)	9344(16)	6962(9)	47(5)
C6	8276(17)	8722(16)	6143(9)	41(4)
C7	8909(14)	9130(13)	5447(9)	45(4)
C8	8889(14)	8608(14)	3932(8)	48(4)
C9	7793(15)	9344(19)	3520(9)	43(4)
C10	6953(17)	8791(18)	2772(9)	49(5)
C11	5991(17)	9530(20)	2355(10)	57(5)
C12	5795(16)	10746(16)	2652(9)	44(4)
C13	6528(15)	11306(15)	3386(10)	45(4)
C14	7530(17)	10618(19)	3812(10)	51(5)
C15	6431(16)	6038(16)	3726(9)	44(4)
C16	5647(16)	5604(16)	2971(9)	45(4)
C17	6140(18)	4640(20)	2455(10)	57(6)
C18	7434(17)	4063(18)	2658(10)	54(5)
C19	8227(15)	4472(16)	3429(8)	35(4)
C20	7754(15)	5470(16)	3929(8)	31(4)
O3	1225(9)	10910(8)	4381(5)	41(2)
O4	3393(9)	12121(8)	4767(5)	39(2)
N2	3540(10)	9779(10)	4840(6)	34(3)
B2	2542(14)	11064(14)	4984(9)	33(4)
C21	2428(14)	11101(16)	5931(8)	39(4)

Table 2.13. Atomic coordinates (x 10^4) and equivalent isotropic displacement parameters ($Å^2$x 10^3) for the structure in Figure 2.8. U(eq) is defined as one third of the trace of the orthogonalized U^{ij} tensor.

C22	1746(17)	11862(19)	6498(9)	50(5)
C23	1925(16)	11648(14)	7327(8)	44(4)
C24	2766(16)	10713(15)	7596(9)	52(4)
C25	3465(16)	9950(18)	7027(10)	49(5)
C26	3300(16)	10111(17)	6225(9)	39(4)
C27	3864(15)	9425(13)	5520(8)	40(4)
C28	3963(13)	9231(12)	4030(8)	43(3)
C29	2868(17)	8322(15)	3554(11)	46(5)
C30	2556(16)	7210(20)	3833(10)	51(5)
C31	1590(16)	6359(16)	3394(9)	50(5)
C32	915(18)	6500(20)	2627(10)	64(5)
C33	1214(18)	7600(20)	2324(10)	61(5)
C34	2216(18)	8469(17)	2769(9)	51(5)
C35	1484(15)	11602(13)	3760(8)	35(4)
C36	613(17)	11578(17)	3031(9)	51(4)
C37	1109(18)	12411(17)	2507(10)	51(5)
C38	2396(18)	13132(18)	2731(8)	45(5)
C39	3209(17)	13101(18)	3483(10)	49(5)
C40	2745(16)	12313(17)	4005(10)	41(4)
O5	4181(9)	8030(8)	8430(5)	36(2)
O6	2118(8)	7021(8)	8783(5)	43(2)
N3	4245(10)	5671(10)	8362(6)	35(3)
B3	3237(14)	6861(16)	8208(10)	44(4)
C41	2719(15)	6428(16)	7250(7)	34(4)
C42	1838(17)	6900(20)	6651(10)	54(5)
C43	1638(16)	6290(17)	5845(10)	55(5)
C44	2370(19)	5203(18)	5602(9)	65(5)
C45	3311(16)	4714(16)	6172(9)	41(4)
C46	3450(16)	5357(17)	6977(9)	41(4)
C47	4349(13)	4950(14)	7683(8)	41(4)

Table 2.13. Atomic coordinates (x 10^4) and equivalent isotropic displacement parameters ($Å^2$x 10^3) for the structure in Figure 2.8. U(eq) is defined as one third of the trace of the orthogonalized U^{ij} tensor (Cont.).

C48	4987(13)	5499(14)	9163(7)	40(3)
C49	4038(15)	4808(17)	9641(8)	38(4)
C50	3655(16)	3578(16)	9329(9)	38(4)
C51	2810(17)	2911(16)	9776(10)	55(5)
C52	2428(17)	3504(18)	10523(10)	52(5)
C53	2796(16)	4700(20)	10830(9)	50(5)
C54	3579(15)	5388(16)	10389(9)	41(4)
C55	3825(16)	8610(16)	9166(9)	39(4)
C56	4443(16)	9622(17)	9670(9)	46(4)
C57	3846(18)	10081(19)	10387(9)	54(5)
C58	2654(17)	9473(19)	10614(9)	49(5)
C59	2034(15)	8434(15)	10089(9)	41(4)
C60	2577(15)	8048(14)	9381(8)	37(4)
O7	7092(9)	3137(8)	8772(5)	39(2)
O8	9109(9)	1950(8)	8426(5)	42(2)
N4	9262(10)	4256(10)	8361(6)	40(3)
B4	8208(16)	2949(15)	8219(10)	44(5)
C61	7770(15)	2967(15)	7235(9)	40(4)
C62	6798(15)	2204(17)	6634(9)	37(4)
C63	6647(15)	2406(17)	5821(9)	50(5)
C64	7444(17)	3386(16)	5604(9)	58(5)
C65	8361(19)	4171(19)	6158(8)	53(5)
C66	8485(17)	3971(15)	6971(9)	39(4)
C67	9394(14)	4674(13)	7687(9)	41(4)
C68	10006(14)	4812(12)	9183(8)	45(4)
C69	9087(16)	5776(16)	9626(10)	46(5)
C70	8638(15)	6886(17)	9326(10)	42(4)
C71	7910(15)	7779(14)	9776(10)	46(4)
C72	7513(15)	7618(16)	10529(10)	51(5)
C73	7900(18)	6500(20)	10833(10)	60(6)

Table 2.13. Atomic coordinates (x 10^4) and equivalent isotropic displacement parameters ($Å^2$x 10^3) for the structure in Figure 2.8. U(eq) is defined as one third of the trace of the orthogonalized U^{ij} tensor (Cont.).

C74	8696(18)	5605(19)	10390(10)	51(5)
C75	7589(15)	2459(16)	9392(9)	41(4)
C76	6996(15)	2389(16)	10117(9)	44(4)
C77	7697(19)	1590(20)	10647(8)	56(6)
C78	8899(17)	914(17)	10437(10)	47(4)
C79	9448(15)	960(15)	9694(9)	38(4)
C80	8735(15)	1766(17)	9187(10)	42(5)

Table 2.13. Atomic coordinates (x 10^4) and equivalent isotropic displacement parameters ($Å^2$x 10^3) for the structure in Figure 2.8. U(eq) is defined as one third of the trace of the orthogonalized U^{ij} tensor (Cont.).

O1-C15	1.371(17)	C7-H7A	0.95	C17-C18	1.39(2)		
O1-B1	1.447(16)	C8-C9	1.46(2)	C17-H17A	0.95		
O2-C20	1.362(15)	C8-H8A	0.99	C18-C19	1.40(2)		
O2-B1	1.458(15)	C8-H8B	0.99	C18-H18A	0.95		
N1-C7	1.315(15)	C9-C14	1.41(3)	C19-C20	1.35(2)		
N1-C8	1.504(15)	C9-C10	1.42(2)	C19-H19A	0.95		
N1-B1	1.653(18)	C10-C11	1.39(2)	O3-C35	1.405(15)		
B1-C1	1.65(2)	C10-H10A	0.95	O3-B2	1.476(15)		
C1-C2	1.38(2)	C11-C12	1.34(2)	O4-C40	1.376(18)		
C1-C6	1.42(2)	C11-H11A	0.95	O4-B2	1.502(16)		
C2-C3	1.33(2)	C12-C13	1.365(19)	N2-C27	1.247(14)		
C2-H2A	0.95	C12-H12A	0.95	N2-C28	1.470(15)		
C3-C4	1.41(2)	C13-C14	1.39(2)	N2-B2	1.669(17)		
C3-H3A	0.95	C13-H13A	0.95	B2-C21	1.57(2)		
C4-C5	1.42(2)	C14-H14A	0.95	C21-C22	1.36(2)		
C4-H4A	0.95	C15-C16	1.378(19)	C21-C26	1.45(2)		
C5-C6	1.40(2)	C15-C20	1.40(2)	C22-C23	1.42(2)		
C5-H5A	0.95	C16-C17	1.35(2)	C22-H22A	0.95		
C6-C7	1.48(2)	C16-H16A	0.95	C23-C24	1.37(2)		

Table 2.14. Bond lengths [Å] and angles [°] for the structure in Figure 2.8.

C23-H23A	0.95	N3-B3	1.626(19)	C59-H59A	0.95
C24-C25	1.37(2)	B3-C41	1.59(2)	O7-C75	1.389(17)
C24-H24A	0.95	C41-C42	1.37(2)	O7-B4	1.454(17)
C25-C26	1.353(19)	C41-C46	1.38(2)	O8-C80	1.387(17)
C25-H25A	0.95	C42-C43	1.38(2)	O8-B4	1.426(18)
C26-C27	1.43(2)	C42-H42A	0.95	N4-C67	1.284(16)
C27-H27A	0.95	C43-C44	1.38(2)	N4-C68	1.482(15)
C28-C29	1.47(2)	C43-H43A	0.95	N4-B4	1.685(18)
C28-H28A	0.99	C44-C45	1.38(2)	B4-C61	1.63(2)
C28-H28B	0.99	C44-H44A	0.95	C61-C62	1.41(2)
C29-C30	1.39(3)	C45-C46	1.39(2)	C61-C66	1.42(2)
C29-C34	1.40(2)	C45-H45A	0.95	C62-C63	1.386(19)
C30-C31	1.34(2)	C46-C47	1.48(2)	C62-H62A	0.95
C30-H30A	0.95	C47-H47A	0.95	C63-C64	1.41(2)
C31-C32	1.37(2)	C48-C49	1.52(2)	C63-H63A	0.95
C31-H31A	0.95	C48-H48A	0.99	C64-C65	1.36(2)
C32-C33	1.40(3)	C48-H48B	0.99	C64-H64A	0.95
C32-H32A	0.95	C49-C50	1.37(2)	C65-C66	1.38(2)
C33-C34	1.38(2)	C49-C54	1.405(19)	C65-H65A	0.95
C33-H33A	0.95	C50-C51	1.41(2)	C66-C67	1.470(19)
C34-H34A	0.95	C50-H50A	0.95	C67-H67A	0.95
C35-C36	1.366(19)	C51-C52	1.38(2)	C68-C69	1.50(2)
C35-C40	1.38(2)	C51-H51A	0.95	C68-H68A	0.99
C36-C37	1.45(2)	C52-C53	1.33(3)	C68-H68B	0.99
C36-H36A	0.95	C52-H52A	0.95	C69-C74	1.39(2)
C37-C38	1.40(2)	C53-C54	1.38(2)	C69-C70	1.41(3)
C37-H37A	0.95	C53-H53A	0.95	C70-C71	1.35(2)
C38-C39	1.38(2)	C54-H54A	0.95	C70-H70A	0.95
C38-H38A	0.95	C55-C56	1.34(2)	C71-C72	1.38(2)
C39-C40	1.41(2)	C55-C60	1.42(2)	C71-H71A	0.95
C39-H39A	0.95	C56-C57	1.39(2)	C72-C73	1.41(3)
O5-C55	1.351(17)	C56-H56A	0.95	C72-H72A	0.95
O5-B3	1.506(17)	C57-C58	1.41(2)	C73-C74	1.38(2)
O6-C60	1.389(16)	C57-H57A	0.95	C73-H73A	0.95
O6-B3	1.481(16)	C58-C59	1.38(2)	C74-H74A	0.95
N3-C47	1.269(15)	C58-H58A	0.95	C75-C80	1.35(2)
N3-C48	1.458(14)	C59-C60	1.334(19)	C75-C76	1.388(18)

Table 2.14. Bond lengths [Å] and angles [°] for the structure in Figure 2.8 (Cont.).

C76-C77 1.43(2)		C5-C6-C7	125.3(15)	C18-C17-H17A	119.1
C76-H76A	0.95	C1-C6-C7	112.0(13)	C17-C18-C19	118.9(16)
C77-C78 1.38(2)		N1-C7-C6	110.7(13)	C17-C18-H18A	120.6
C77-H77A	0.95	N1-C7-H7A	124.6	C19-C18-H18A	120.5
C78-C79 1.39(2)		C6-C7-H7A	124.6	C20-C19-C18	118.9(15)
C78-H78A	0.95	C9-C8-N1	111.7(11)	C20-C19-H19A	120.5
C79-C80 1.42(2)		C9-C8-H8A	109.3	C18-C19-H19A	120.6
C79-H79A	0.95	N1-C8-H8A	109.3	C19-C20-O2	127.5(14)
		C9-C8-H8B	109.3	C19-C20-C15	121.9(13)
		N1-C8-H8B	109.3	O2-C20-C15	110.5(13)
C15-O1-B1	104.7(10)	H8A-C8-H8B	107.9	C35-O3-B2	106.1(9)
C20-O2-B1	104.4(10)	C14-C9-C10	116.4(16)	C40-O4-B2	105.4(11)
C7-N1-C8	122.3(11)	C14-C9-C8	123.5(14)	C27-N2-C28	128.3(12)
C7-N1-B1	112.6(10)	C10-C9-C8	120.2(17)	C27-N2-B2	108.6(11)
C8-N1-B1	125.1(10)	C11-C10-C9	119.4(18)	C28-N2-B2	123.0(11)
O1-B1-O2	108.1(11)	C11-C10-H10A	120.3	O3-B2-O4	105.3(10)
O1-B1-C1	117.1(11)	C9-C10-H10A	120.3	O3-B2-C21	120.3(11)
O2-B1-C1	115.7(11)	C12-C11-C10	122.0(16)	O4-B2-C21	116.1(11)
O1-B1-N1	110.5(10)	C12-C11-H11A	119	O3-B2-N2	109.6(10)
O2-B1-N1	107.6(10)	C10-C11-H11A	119	O4-B2-N2	107.1(9)
C1-B1-N1	97.0(10)	C11-C12-C13	120.8(15)	C21-B2-N2	97.6(11)
C2-C1-C6	117.6(14)	C11-C12-H12A	119.6	C22-C21-C26	116.9(13)
C2-C1-B1	135.1(14)	C13-C12-H12A	119.6	C22-C21-B2	133.8(15)
C6-C1-B1	107.3(14)	C12-C13-C14	119.2(16)	C26-C21-B2	109.3(12)
C3-C2-C1	122.1(16)	C12-C13-H13A	120.4	C21-C22-C23	118.7(16)
C3-C2-H2A	119	C14-C13-H13A	120.4	C21-C22-H22A	120.7
C1-C2-H2A	119	C13-C14-C9	122.1(15)	C23-C22-H22A	120.7
C2-C3-C4	121.1(16)	C13-C14-H14A	119	C24-C23-C22	123.6(14)
C2-C3-H3A	119.4	C9-C14-H14A	118.9	C24-C23-H23A	118.2
C4-C3-H3A	119.4	O1-C15-C16	131.7(15)	C22-C23-H23A	118.2
C3-C4-C5	120.5(14)	O1-C15-C20	110.0(12)	C25-C24-C23	117.9(15)
C3-C4-H4A	119.8	C16-C15-C20	118.2(15)	C25-C24-H24A	121.1
C5-C4-H4A	119.8	C17-C16-C15	120.1(16)	C23-C24-H24A	121
C6-C5-C4	115.9(16)	C17-C16-H16A	119.9	C26-C25-C24	120.3(17)
C6-C5-H5A	122	C15-C16-H16A	119.9	C26-C25-H25A	119.9
C4-C5-H5A	122	C16-C17-C18	121.7(16)	C24-C25-H25A	119.9
C5-C6-C1	122.8(15)	C16-C17-H17A	119.1	C25-C26-C27	130.9(17)

Table 2.14. Bond lengths [Å] and angles [°] for the structure in Figure 2.8 (Cont.).

C25-C26-C21	122.7(15)	C36-C37-H37A	118.9	C41-C46-C47	109.7(13)
C27-C26-C21	106.5(12)	C39-C38-C37	120.2(16)	C45-C46-C47	124.7(16)
N2-C27-C26	117.8(14)	C39-C38-H38A	119.9	N3-C47-C46	112.5(13)
N2-C27-H27A	121.1	C37-C38-H38A	119.9	N3-C47-H47A	123.8
C26-C27-H27A	121.1	C38-C39-C40	118.8(16)	C46-C47-H47A	123.8
N2-C28-C29	112.1(11)	C38-C39-H39A	120.6	N3-C48-C49	112.0(10)
N2-C28-H28A	109.2	C40-C39-H39A	120.6	N3-C48-H48A	109.2
C29-C28-H28A	109.2	O4-C40-C35	112.0(15)	C49-C48-H48A	109.2
N2-C28-H28B	109.2	O4-C40-C39	128.5(15)	N3-C48-H48B	109.2
C29-C28-H28B	109.2	C35-C40-C39	119.5(15)	C49-C48-H48B	109.2
H28A-C28-H28B	107.9	C55-O5-B3	105.5(11)	H48A-C48-H48B	107.9
C30-C29-C34	117.1(16)	C60-O6-B3	105.8(10)	C50-C49-C54	120.2(16)
C30-C29-C28	120.9(16)	C47-N3-C48	125.0(12)	C50-C49-C48	118.1(13)
C34-C29-C28	121.7(16)	C47-N3-B3	110.6(11)	C54-C49-C48	121.7(16)
C31-C30-C29	121.4(16)	C48-N3-B3	124.4(11)	C49-C50-C51	118.9(15)
C31-C30-H30A	119.3	O6-B3-O5	105.8(11)	C49-C50-H50A	120.6
C29-C30-H30A	119.3	O6-B3-C41	117.9(11)	C51-C50-H50A	120.6
C30-C31-C32	122.3(18)	O5-B3-C41	116.1(12)	C52-C51-C50	118.9(16)
C30-C31-H31A	118.8	O6-B3-N3	110.4(11)	C52-C51-H51A	120.5
C32-C31-H31A	118.9	O5-B3-N3	107.7(9)	C50-C51-H51A	120.5
C31-C32-C33	117.6(17)	C41-B3-N3	98.3(11)	C53-C52-C51	122.5(17)
C31-C32-H32A	121.2	C42-C41-C46	115.3(14)	C53-C52-H52A	118.7
C33-C32-H32A	121.2	C42-C41-B3	136.0(16)	C51-C52-H52A	118.7
C34-C33-C32	120.3(16)	C46-C41-B3	108.5(13)	C52-C53-C54	119.7(16)
C34-C33-H33A	119.9	C41-C42-C43	121.7(18)	C52-C53-H53A	120.2
C32-C33-H33A	119.9	C41-C42-H42A	119.1	C54-C53-H53A	120.1
C33-C34-C29	120.9(17)	C43-C42-H42A	119.1	C53-C54-C49	119.7(17)
C33-C34-H34A	119.5	C42-C43-C44	120.9(16)	C53-C54-H54A	120.2
C29-C34-H34A	119.6	C42-C43-H43A	119.6	C49-C54-H54A	120.2
C36-C35-C40	125.6(15)	C44-C43-H43A	119.5	C56-C55-O5	129.4(15)
C36-C35-O3	124.9(14)	C45-C44-C43	119.8(15)	C56-C55-C60	119.0(15)
C40-C35-O3	109.5(12)	C45-C44-H44A	120.1	O5-C55-C60	111.5(13)
C35-C36-C37	113.7(16)	C43-C44-H44A	120.1	C55-C56-C57	119.1(16)
C35-C36-H36A	123.1	C44-C45-C46	116.6(16)	C55-C56-H56A	120.5
C37-C36-H36A	123.1	C44-C45-H45A	121.7	C57-C56-H56A	120.4
C38-C37-C36	122.2(14)	C46-C45-H45A	121.7	C56-C57-C58	121.2(17)
C38-C37-H37A	118.9	C41-C46-C45	125.5(15)	C56-C57-H57A	119.4

Table 2.14. Bond lengths [Å] and angles [°] for the structure in Figure 2.8 (Cont.).

C58-C57-H57A	119.4	C62-C63-H63A	120.2	C72-C71-H71A	119.4
C59-C58-C57	118.9(16)	C64-C63-H63A	120.2	C71-C72-C73	118.5(15)
C59-C58-H58A	120.6	C65-C64-C63	123.3(16)	C71-C72-H72A	120.7
C57-C58-H58A	120.5	C65-C64-H64A	118.4	C73-C72-H72A	120.7
C60-C59-C58	118.9(15)	C63-C64-H64A	118.4	C74-C73-C72	120.4(17)
C60-C59-H59A	120.5	C64-C65-C66	116.6(18)	C74-C73-H73A	119.8
C58-C59-H59A	120.6	C64-C65-H65A	121.7	C72-C73-H73A	119.8
C59-C60-O6	127.4(14)	C66-C65-H65A	121.7	C73-C74-C69	120.6(18)
C59-C60-C55	122.7(14)	C65-C66-C61	123.7(15)	C73-C74-H74A	119.7
O6-C60-C55	109.7(12)	C65-C66-C67	127.8(16)	C69-C74-H74A	119.7
C75-O7-B4	103.1(10)	C61-C66-C67	108.4(13)	C80-C75-O7	110.9(13)
C80-O8-B4	103.8(11)	N4-C67-C66	112.6(13)	C80-C75-C76	121.2(15)
C67-N4-C68	124.4(12)	N4-C67-H67A	123.7	O7-C75-C76	127.8(14)
C67-N4-B4	113.3(11)	C66-C67-H67A	123.7	C75-C76-C77	116.8(15)
C68-N4-B4	122.2(11)	N4-C68-C69	111.2(11)	C75-C76-H76A	121.6
O8-B4-O7	109.0(12)	N4-C68-H68A	109.4	C77-C76-H76A	121.6
O8-B4-C61	116.2(12)	C69-C68-H68A	109.4	C78-C77-C76	121.1(15)
O7-B4-C61	119.3(12)	N4-C68-H68B	109.4	C78-C77-H77A	119.5
O8-B4-N4	107.4(10)	C69-C68-H68B	109.4	C76-C77-H77A	119.4
O7-B4-N4	109.3(10)	H68A-C68-H68B	108	C77-C78-C79	121.3(16)
C61-B4-N4	93.8(11)	C74-C69-C70	117.7(17)	C77-C78-H78A	119.3
C62-C61-C66	116.9(14)	C74-C69-C68	118.9(15)	C79-C78-H78A	119.3
C62-C61-B4	131.5(14)	C70-C69-C68	123.4(16)	C78-C79-C80	116.1(15)
C66-C61-B4	111.6(12)	C71-C70-C69	121.6(16)	C78-C79-H79A	122
C63-C62-C61	119.8(16)	C71-C70-H70A	119.2	C80-C79-H79A	121.9
C63-C62-H62A	120.1	C69-C70-H70A	119.2	C75-C80-O8	111.3(15)
C61-C62-H62A	120.1	C70-C71-C72	121.3(16)	C75-C80-C79	123.4(15)
C62-C63-C64	119.5(15)	C70-C71-H71A	119.4	O8-C80-C79	125.3(14)

Table 2.14. Bond lengths [Å] and angles [°] for the structure in Figure 2.8 (Cont.).

	U^{11}	U^{22}	U^{33}	U^{23}	U^{13}	U^{12}
O1	43(6)	35(6)	53(6)	-4(5)	-6(5)	-1(4)
O2	36(5)	24(5)	49(6)	5(4)	-7(4)	1(4)
N1	40(7)	26(7)	43(7)	4(6)	4(5)	12(5)
B1	44(10)	21(9)	38(9)	6(7)	8(8)	8(7)
C1	32(9)	35(10)	54(9)	-7(8)	0(7)	6(8)
C2	34(9)	40(10)	41(9)	-4(9)	-5(7)	-10(8)
C3	52(11)	67(14)	75(13)	29(11)	9(9)	-7(10)
C4	68(11)	56(12)	26(8)	-3(8)	4(7)	18(9)
C5	67(11)	28(10)	37(9)	-10(8)	-7(8)	9(8)
C6	48(10)	28(10)	47(9)	15(8)	2(7)	16(8)
C7	39(8)	22(8)	69(10)	-7(8)	3(7)	3(6)
C8	47(9)	46(10)	53(9)	13(8)	11(7)	-3(8)
C9	25(8)	53(12)	53(9)	16(9)	0(7)	-6(8)
C10	57(10)	54(11)	38(8)	3(8)	14(8)	13(9)
C11	43(10)	82(16)	45(9)	15(10)	-6(7)	10(10)
C12	46(9)	36(10)	53(10)	13(8)	15(8)	9(8)
C13	46(9)	32(9)	67(11)	29(9)	20(8)	18(8)
C14	46(11)	47(12)	58(10)	-6(10)	16(8)	-4(9)
C15	39(9)	36(10)	59(10)	14(9)	3(8)	-6(8)
C16	41(9)	36(10)	58(10)	22(9)	-14(8)	-12(8)
C17	66(13)	75(15)	35(9)	12(10)	22(8)	-17(11)

Table 2.15. Anisotropic displacement parameters ($Å^2 x\ 10^3$) for the structure in Figure 2.8. The anisotropic displacement factor exponent takes the form: $-2\pi^2[\ h^2\ a^{*2}U^{11} + ...\ + 2\ h\ k\ a^*\ b^*\ U^{12}\ ]$

C18	49(10)	45(12)	67(11)	3(9)	15(9)	17(9)
C19	41(9)	34(10)	27(7)	3(7)	-8(6)	-4(8)
C20	35(9)	25(9)	28(8)	-10(7)	-2(6)	-5(7)
O3	36(5)	40(6)	47(5)	9(5)	4(4)	-6(4)
O4	43(5)	28(6)	38(5)	-6(4)	-9(4)	3(4)
N2	29(6)	30(7)	40(7)	-5(6)	7(5)	-5(5)
B2	20(8)	21(9)	57(10)	12(8)	-4(7)	-6(7)
C21	29(8)	37(10)	47(9)	-2(8)	4(7)	-9(8)
C22	61(12)	41(12)	41(9)	-6(9)	4(8)	8(10)
C23	58(10)	27(9)	45(9)	-8(7)	16(7)	-5(8)
C24	55(10)	48(11)	52(10)	7(9)	8(8)	-3(9)
C25	37(9)	57(13)	52(10)	24(9)	-10(7)	6(8)
C26	36(9)	52(11)	30(8)	14(8)	1(7)	-11(8)
C27	58(10)	28(8)	35(9)	15(7)	-5(7)	-3(7)
C28	35(8)	31(8)	64(9)	4(7)	13(6)	0(7)
C29	44(9)	11(8)	86(12)	6(8)	21(8)	6(7)
C30	27(9)	53(13)	59(10)	-19(10)	-15(8)	16(9)
C31	51(10)	44(11)	57(11)	8(9)	14(8)	-5(8)
C32	62(11)	58(13)	56(11)	-30(10)	0(9)	6(10)
C33	77(13)	68(14)	35(9)	8(9)	-2(8)	-14(10)
C34	75(12)	38(11)	36(8)	0(8)	2(8)	-3(9)
C35	47(9)	21(9)	36(8)	4(7)	5(7)	7(7)

Table 2.15. Anisotropic displacement parameters ($Å^2 x\ 10^3$) for the structure in Figure 2.8. The anisotropic displacement factor exponent takes the form: $-2\pi^2[\ h^2\ a^{*2}U^{11} + ...\ + 2\ h\ k\ a^*\ b^*\ U^{12}\ ]$ (Cont.).

C36	49(10)	61(12)	45(9)	15(9)	2(8)	9(8)
C37	62(12)	43(12)	50(10)	24(9)	-10(8)	17(10)
C38	76(12)	47(11)	11(7)	4(7)	2(7)	18(9)
C39	58(11)	28(10)	68(11)	16(9)	28(9)	3(9)
C40	30(9)	31(10)	53(10)	-9(8)	-9(7)	3(7)
O5	50(6)	27(5)	29(5)	-1(4)	0(4)	-1(4)
O6	29(5)	35(6)	62(6)	-2(5)	6(4)	-1(4)
N3	43(7)	24(7)	39(7)	12(6)	-4(5)	-3(5)
B3	20(8)	41(11)	72(12)	7(9)	15(8)	-4(8)
C41	44(9)	42(10)	14(6)	6(7)	-6(6)	-8(8)
C42	64(12)	56(13)	44(10)	10(10)	5(9)	-10(11)
C43	51(11)	45(11)	62(11)	11(9)	-17(8)	-6(9)
C44	80(13)	70(14)	40(10)	6(10)	-3(9)	-32(11)
C45	42(9)	33(11)	50(10)	9(8)	5(7)	9(8)
C46	30(8)	40(12)	51(10)	1(9)	5(7)	-11(8)
C47	30(8)	42(9)	46(8)	-1(8)	-1(7)	-5(7)
C48	25(7)	56(10)	40(7)	12(7)	-4(6)	-8(7)
C49	30(8)	47(11)	33(8)	2(8)	1(6)	12(8)
C50	50(11)	27(10)	35(8)	5(8)	-5(7)	-2(8)
C51	71(12)	33(10)	59(11)	16(9)	-4(9)	6(9)
C52	57(10)	48(12)	55(11)	21(10)	8(8)	6(9)
C53	49(10)	63(13)	41(10)	15(10)	9(8)	15(10)

Table 2.15. Anisotropic displacement parameters ($Å^2 x\ 10^3$) for the structure in Figure 2.8. The anisotropic displacement factor exponent takes the form: $-2\pi^2[\ h^2\ a^{*2}U^{11} + ...\ + 2\ h\ k\ a^*\ b^*\ U^{12}\ ]$ (Cont.).

C54	41(9)	36(10)	43(9)	4(8)	1(7)	-2(8)
C55	36(9)	27(10)	52(10)	10(8)	-10(7)	-11(8)
C56	44(9)	47(11)	45(9)	7(9)	-1(7)	-13(9)
C57	63(11)	68(13)	23(8)	-3(9)	-15(7)	-2(10)
C58	55(11)	56(13)	38(9)	16(9)	3(8)	14(10)
C59	34(9)	43(11)	51(9)	26(9)	-5(7)	-4(7)
C60	48(10)	21(8)	41(9)	5(7)	-2(7)	17(8)
O7	41(6)	36(6)	41(5)	12(5)	4(4)	2(4)
O8	36(5)	37(6)	55(6)	11(5)	12(4)	8(4)
N4	34(6)	39(8)	45(7)	7(6)	-2(5)	6(6)
B4	36(10)	24(10)	68(12)	-7(8)	5(9)	-9(8)
C61	41(9)	26(9)	53(9)	7(8)	7(7)	9(8)
C62	50(10)	23(9)	39(9)	3(8)	10(7)	6(9)
C63	46(10)	65(13)	35(9)	-1(8)	3(7)	16(9)
C64	79(12)	52(12)	51(11)	24(10)	15(9)	29(10)
C65	80(13)	62(14)	15(8)	2(8)	4(7)	18(10)
C66	55(10)	12(8)	52(10)	9(7)	2(8)	4(7)
C67	40(8)	34(9)	51(9)	12(7)	8(7)	9(7)
C68	38(8)	18(8)	78(10)	5(7)	3(7)	10(6)
C69	35(9)	22(9)	74(11)	16(8)	-28(8)	-15(7)
C70	30(9)	35(10)	64(10)	2(9)	22(8)	-5(8)
C71	42(9)	27(10)	60(11)	-4(8)	-14(8)	-5(7)

Table 2.15. Anisotropic displacement parameters ($Å^2 x\ 10^3$) for the structure in Figure 2.8. The anisotropic displacement factor exponent takes the form: $-2\pi^2[\ h^2\ a^{*2}U^{11} + ...\ + 2\ h\ k\ a^*\ b^*\ U^{12}\ ]$ (Cont.).

C72	33(9)	43(11)	64(11)	-26(10)	-8(8)	-2(8)
C73	69(13)	58(14)	49(10)	2(10)	-6(9)	-7(11)
C74	67(11)	49(12)	44(10)	25(9)	10(8)	-5(9)
C75	32(9)	48(11)	43(9)	5(9)	5(7)	-3(8)
C76	38(9)	48(11)	49(9)	12(9)	9(7)	-16(8)
C77	77(14)	72(14)	13(8)	1(9)	-9(8)	-17(12)
C78	55(10)	35(10)	55(10)	24(8)	4(8)	-10(9)
C79	37(9)	18(8)	57(10)	5(8)	-7(7)	-8(7)
C80	26(9)	36(11)	67(11)	11(9)	19(8)	-10(8)

Table 2.15. Anisotropic displacement parameters ($Å^2 x\ 10^3$) for the structure in Figure 2.8. The anisotropic displacement factor exponent takes the form: $-2\pi^2[\ h^2\ a^{*2}U^{11} + ...\ + 2\ h\ k\ a^*\ b^*\ U^{12}\ ]$ (Cont.).

	x	y	z	U(eq)
H2A	6168	6393	6317	48
H3A	6423	7333	7653	75
H4A	7819	9187	8093	61
H5A	9053	10086	7128	56
H7A	9534	9843	5496	54
H8A	9833	9065	4020	57
H8B	8996	7794	3572	57
H10A	7046	7926	2559	59
H11A	5458	9163	1846	68
H12A	5138	11223	2347	53
H13A	6354	12156	3603	54

Table 2.16. Hydrogen coordinates ($x\ 10^4$) and isotropic displacement parameters ($Å^2 x\ 10^3$) for the structure in Figure 2.8.

H14A	8056	11017	4315	61
H16A	4759	5984	2814	54
H17A	5583	4343	1938	69
H18A	7777	3401	2280	64
H19A	9084	4057	3598	42
H22A	1160	12525	6341	59
H23A	1438	12179	7719	53
H24A	2860	10600	8158	62
H25A	4069	9306	7195	58
H27A	4465	8722	5567	48
H28A	4898	8803	4112	52
H28B	4104	9912	3710	52
H30A	3037	7054	4346	61
H31A	1366	5637	3620	60
H32A	268	5866	2314	77
H33A	726	7743	1811	73
H34A	2466	9180	2538	61
H36A	-238	11064	2880	61
H37A	545	12470	1997	61
H38A	2707	13642	2364	54
H39A	4067	13604	3645	58
H42A	1353	7661	6796	65
H43A	988	6622	5450	66
H44A	2224	4794	5043	78
H45A	3837	3974	6022	50
H47A	4938	4229	7635	49
H48A	5276	6331	9492	49
H48B	5878	5018	9079	49
H50A	3955	3184	8820	46
H51A	2508	2066	9566	66
H52A	1882	3044	10830	62

Table 2.16. Hydrogen coordinates (x 10^4) and isotropic displacement parameters ($Å^2$x 10^3) for the structure in Figure 2.8 (Cont.).

H53A	2522	5071	11350	60
H54A	3804	6250	10592	49
H56A	5277	10017	9536	55
H57A	4250	10821	10732	65
H58A	2283	9771	11120	59
H59A	1233	8001	10231	50
H62A	6249	1555	6788	45
H63A	6010	1886	5413	60
H64A	7335	3504	5043	70
H65A	8891	4825	5996	64
H67A	10012	5362	7656	49
H68A	10934	5210	9115	55
H68B	10226	4140	9519	55
H70A	8852	7007	8796	51
H71A	7669	8533	9568	55
H72A	6989	8245	10838	62
H73A	7611	6357	11344	72
H74A	8980	4868	10609	61
H76A	6165	2851	10255	53
H77A	7330	1522	11152	67
H78A	9359	407	10807	56
H79A	10255	479	9536	46

Table 2.16. Hydrogen coordinates (x 10^4) and isotropic displacement parameters ($Å^2$x 10^3) for the structure in Figure 2.8 (Cont.).

C15-O1-B1-O2	-14.4(14)	C4-C5-C6-C7	178.9(14)
C15-O1-B1-C1	-147.3(13)	C2-C1-C6-C5	2(2)
C15-O1-B1-N1	103.0(11)	B1-C1-C6-C5	-177.6(14)
C20-O2-B1-O1	15.0(14)	C2-C1-C6-C7	-178.5(13)
C20-O2-B1-C1	148.6(13)	B1-C1-C6-C7	2.1(17)
C20-O2-B1-N1	-104.2(11)	C8-N1-C7-C6	176.0(11)
C7-N1-B1-O1	129.0(11)	B1-N1-C7-C6	-6.0(14)
C8-N1-B1-O1	-53.0(15)	C5-C6-C7-N1	-177.9(14)
C7-N1-B1-O2	-113.3(11)	C1-C6-C7-N1	2.4(17)
C8-N1-B1-O2	64.7(14)	C7-N1-C8-C9	-91.5(15)
C7-N1-B1-C1	6.6(13)	B1-N1-C8-C9	90.7(15)
C8-N1-B1-C1	-175.4(11)	N1-C8-C9-C14	68.5(19)
O1-B1-C1-C2	59(2)	N1-C8-C9-C10	-113.3(15)
O2-B1-C1-C2	-71(2)	C14-C9-C10-C11	3(2)
N1-B1-C1-C2	176.0(16)	C8-C9-C10-C11	-175.2(15)
O1-B1-C1-C6	-122.0(13)	C9-C10-C11-C12	-2(3)
O2-B1-C1-C6	108.6(14)	C10-C11-C12-C13	-1(3)
N1-B1-C1-C6	-4.7(14)	C11-C12-C13-C14	3(2)
C6-C1-C2-C3	-1(2)	C12-C13-C14-C9	-2(2)
B1-C1-C2-C3	177.7(17)	C10-C9-C14-C13	-1(2)
C1-C2-C3-C4	1(3)	C8-C9-C14-C13	177.0(14)
C2-C3-C4-C5	-1(3)	B1-O1-C15-C16	-168.6(16)
C3-C4-C5-C6	1(2)	B1-O1-C15-C20	8.3(16)
C4-C5-C6-C1	-1(2)	O1-C15-C16-C17	178.1(15)

Table 2.17. Torsion angles [°] for the structure in Figure 2.8.

C20-C15-C16-C17	1(2)	O3-B2-C21-C22	-60(2)
C15-C16-C17-C18	-1(3)	O4-B2-C21-C22	69(2)
C16-C17-C18-C19	2(3)	N2-B2-C21-C22	-177.9(16)
C17-C18-C19-C20	-4(3)	O3-B2-C21-C26	122.5(13)
C18-C19-C20-O2	-177.5(15)	O4-B2-C21-C26	-108.8(14)
C18-C19-C20-C15	5(3)	N2-B2-C21-C26	4.4(13)
B1-O2-C20-C19	172.7(16)	C26-C21-C22-C23	0(2)
B1-O2-C20-C15	-10.0(16)	B2-C21-C22-C23	-177.5(15)
O1-C15-C20-C19	178.7(14)	C21-C22-C23-C24	1(3)
C16-C15-C20-C19	-4(2)	C22-C23-C24-C25	0(2)
O1-C15-C20-O2	1.1(18)	C23-C24-C25-C26	-1(2)
C16-C15-C20-O2	178.5(13)	C24-C25-C26-C27	-177.7(15)
C35-O3-B2-O4	13.1(12)	C24-C25-C26-C21	2(3)
C35-O3-B2-C21	146.5(13)	C22-C21-C26-C25	-1(2)
C35-O3-B2-N2	-101.7(11)	B2-C21-C26-C25	176.9(14)
C40-O4-B2-O3	-12.3(13)	C22-C21-C26-C27	178.4(13)
C40-O4-B2-C21	-148.0(12)	B2-C21-C26-C27	-3.6(16)
C40-O4-B2-N2	104.3(11)	C28-N2-C27-C26	-179.3(12)
C27-N2-B2-O3	-130.2(11)	B2-N2-C27-C26	2.5(16)
C28-N2-B2-O3	51.5(14)	C25-C26-C27-N2	-179.9(16)
C27-N2-B2-O4	116.1(11)	C21-C26-C27-N2	0.6(18)
C28-N2-B2-O4	-62.2(14)	C27-N2-C28-C29	93.9(16)
C27-N2-B2-C21	-4.2(12)	B2-N2-C28-C29	-88.1(14)
C28-N2-B2-C21	177.5(10)	N2-C28-C29-C30	-64.5(17)

Table 2.17. Torsion angles [°] for the structure in Figure 2.8 (Cont.).

N2-C28-C29-C34	122.5(15)	C60-O6-B3-O5	-11.5(14)
C34-C29-C30-C31	-5(2)	C60-O6-B3-C41	-143.4(13)
C28-C29-C30-C31	-178.0(14)	C60-O6-B3-N3	104.8(11)
C29-C30-C31-C32	4(3)	C55-O5-B3-O6	13.0(14)
C30-C31-C32-C33	-3(2)	C55-O5-B3-C41	145.9(12)
C31-C32-C33-C34	3(3)	C55-O5-B3-N3	-105.1(12)
C32-C33-C34-C29	-5(3)	C47-N3-B3-O6	130.2(12)
C30-C29-C34-C33	5(2)	C48-N3-B3-O6	-52.9(15)
C28-C29-C34-C33	178.6(15)	C47-N3-B3-O5	-114.8(12)
B2-O3-C35-C36	171.1(14)	C48-N3-B3-O5	62.2(15)
B2O3-C35-C40	-9.4(14)	C47-N3-B3-C41	6.2(13)
C40-C35-C36-C37	-1(2)	C48-N3-B3-C41	-176.9(11)
O3-C35-C36-C37	178.3(12)	O6-B3-C41-C42	61(2)
C35-C36-C37-C38	2(2)	O5-B3-C41-C42	-66(2)
C36-C37-C38-C39	-2(3)	N3-B3-C41-C42	179.4(17)
C37-C38-C39-C40	2(2)	O6-B3-C41-C46	-124.6(14)
B2-O4-C40-C35	7.0(16)	O5-B3-C41-C46	108.3(15)
B2-O4-C40-C39	-172.5(15)	N3-B3-C41-C46	-6.2(14)
C36-C35-C40-O4	-179.1(14)	C46-C41-C42-C43	4(2)
O3-C35-C40-O4	1.4(17)	B3-C41-C42-C43	178.0(16)
C36-C35-C40-C39	0(2)	C41-C42-C43-C44	-3(3)
O3-C35-C40-C39	-179.0(13)	C42-C43-C44-C45	0(3)
C38-C39-C40-O4	178.8(15)	C43-C44-C45-C46	1(2)
C38-C39-C40-C35	-1(2)	C42-C41-C46-C45	-3(2)

Table 2.17. Torsion angles [°] for the structure in Figure 2.8 (Cont.).

B3-C41-C46-C45	-178.6(14)	C60-C55-C56-C57	0(2)
C42-C41-C46-C47	-179.7(13)	C55-C56-C57-C58	3(3)
B3-C41-C46-C47	4.6(16)	C56-C57-C58-C59	-3(3)
C44-C45-C46-C41	1(2)	C57-C58-C59-C60	-1(2)
C44-C45-C46-C47	177.0(14)	C58-C59-C60-O6	179.0(13)
C48-N3-C47-C46	179.1(11)	C58-C59-C60-C55	4(2)
B3-N3-C47-C46	-4.0(15)	B3-O6-C60-C59	-169.4(14)
C41-C46-C47-N3	-0.3(17)	B3-O6-C60-C55	5.9(15)
C45-C46-C47-N3	-177.2(14)	C56-C55-C60-C59	-4(2)
C47-N3-C48-C49	-95.3(16)	O5-C55-C60-C59	178.3(13)
B3-N3-C48-C49	88.2(15)	C56-C55-C60-O6	-179.8(13)
N3-C48-C49-C50	65.9(17)	O5-C55-C60-O6	2.6(17)
N3-C48-C49-C54	-115.2(14)	C80-O8-B4-O7	-12.9(14)
C54-C49-C50-C51	-1(2)	C80-O8-B4-C61	-151.3(12)
C48-C49-C50-C51	178.2(12)	C80-O8-B4-N4	105.4(12)
C49-C50-C51-C52	-2(2)	C75-O7-B4-O8	13.6(13)
C50-C51-C52-C53	2(2)	C75-O7-B4-C61	150.5(13)
C51-C52-C53-C54	1(3)	C75-O7-B4-N4	-103.4(12)
C52-C53-C54-C49	-3(2)	C67-N4-B4-O8	114.4(12)
C50-C49-C54-C53	3(2)	C68-N4-B4-O8	-62.9(15)
C48-C49-C54-C53	-175.8(13)	C67-N4-B4-O7	-127.5(12)
B3-O5-C55-C56	172.9(16)	C68-N4-B4-O7	55.2(15)
B3-O5-C55-C60	-9.8(16)	C67-N4-B4-C61	-4.6(13)
O5-C55-C56-C57	177.5(16)	C68-N4-B4-C61	178.1(10)

Table 2.17. Torsion angles [°] for the structure in Figure 2.8 (Cont.).

O8-B4-C61-C62	73.4(19)	N4-C68-C69-C70	-61.8(18)
O7-B4-C61-C62	-60(2)	C74-C69-C70-C71	3(2)
N4-B4-C61-C62	-175.1(14)	C68-C69-C70-C71	-174.5(13)
O8-B4-C61-C66	-108.9(14)	C69-C70-C71-C72	-3(2)
O7-B4-C61-C66	117.1(14)	C70-C71-C72-C73	1(2)
N4-B4-C61-C66	2.5(14)	C71-C72-C73-C74	2(2)
C66-C61-C62-C63	4(2)	C72-C73-C74-C69	-2(3)
B4-C61-C62-C63	-178.6(14)	C70-C69-C74-C73	0(2)
C61-C62-C63-C64	-1(2)	C68-C69-C74-C73	177.3(15)
C62-C63-C64-C65	-1(2)	B4-O7-C75-C80	-9.2(15)
C63-C64-C65-C66	0(3)	B4-O7-C75-C76	174.8(15)
C64-C65-C66-C61	3(2)	C80-C75-C76-C77	3(2)
C64-C65-C66-C67	179.8(15)	O7-C75-C76-C77	178.2(14)
C62-C61-C66-C65	-5(2)	C75-C76-C77-C78	-1(2)
B4-C61-C66-C65	176.9(14)	C76-C77-C78-C79	-2(3)
C62-C61-C66-C67	177.8(12)	C77-C78-C79-C80	2(2)
B4-C61-C66-C67	-0.2(17)	O7-C75-C80-O8	1.4(18)
C68-N4-C67-C66	-177.6(11)	C76-C75-C80-O8	177.7(13)
B4-N4-C67-C66	5.2(16)	O7-C75-C80-C79	-178.6(13)
C65-C66-C67-N4	179.8(15)	C76-C75-C80-C79	-2(2)
C61-C66-C67-N4	-3.2(17)	B4-O8-C80-C75	7.3(16)
C67-N4-C68-C69	91.7(16)	B4-O8-C80-C79	-172.7(14)
B4-N4-C68-C69	-91.3(14)	C78-C79-C80-C75	0(2)
N4-C68-C69-C74	120.8(14)	C78-C79-C80-O8	179.9(14

Table 2.17. Torsion angles [°] for the structure in Figure 2.8 (Cont.).

2.5 REFERENCES

1. Kuivila, H. G.; Keough, A. H.; Soboczenski, E. J. *J. Org. Chem.* **1954**, *19*, 780-783.

2. James, T. D.; Sandanayake, K. R. A. S.; Shinkai, S. *Angew. Chem., Int. Ed. Engl.* **1996**, *35*, 1910–1922.

3. Yang, W.; Gao, X.; Wang, B. *Med. Res. Rev.* **2003**, *23(3)*, 346-368.

4. Secor, K. E.; Glass, T. E. *Org. Lett.* **2004**, *6*, 3727–3730.

5. Maue, M.; Schrader, T. *Angew. Chem., Int. Ed.* **2005**, *44*, 2265–2270.

6. Paugam, M.-F.; Valencia, L. S.; Bogges, B.; Smith, B. D. *J. Am. Chem. Soc.* **1994**, *116*, 11203–11204.

7. Paugam, M.-F.; Bien, J. T.; Smith, B. D.; Chrisstoffels, L. A. J.; de Jong, F.; Reinhoudt, D. N. *J. Am. Chem. Soc.* **1996**, *118*, 9820–9825.

8. Gray, C. W., Jr.; Houston, T. A. *J. Org. Chem.* **2002**, *67*, 5426–5428.

9. Zhu, L.; Anslyn, E. V. *J. Am. Chem. Soc.* **2004**, *126*, 3676–3677.

10. Wiskur, S. L.; Lavigne, J. J.; Matzger, A.; Tobey, S. L.; Lynch, V. M.; Anslyn, E. V. *Chem.-Eur. J.* **2004**, *10*, 3792–3804.

11. Nguyen, B. T.; Wiskur, S. L.; Anslyn, E. V. *Org. Lett.* **2004**, *6*, 2499–2501.

12. Zhao, J.; Fyles, T. M.; James, T. D. *Angew. Chem., Int. Ed.* **2004**, *43*, 3461–3464.

13. Zhao, J.; Davidson, M. G.; Mahon, M. F.; Kociok-Kohn, G.; James, T. D. *J. Am. Chem. Soc.* **2004**, *126*, 16179–16186.

14. Zhu, L.; Zhong, Z.; Anslyn, E. V. *J. Am. Chem. Soc*. **2005**, *127*, 4260–4269.

15. Wright, A. T.; Griffin, M. J.; Zhong, Z.; McCleskey, S. C.; Anslyn, E. V.; McDevitt, J. T. *Angew. Chem., Int. Ed.* **2005**, *44*, 6375–6378.

16. James, T. D.; Linnane, P.; Shinkai, S. *Chem. Commun.* **1996**, 281–288.

17. Wang, W.; Gao, X.; Wang, B. *Curr. Org. Chem.* **2002**, *6*, 1285–1317.

18. Striegler, S. *Curr. Org. Chem*. **2003**, *7*, 81–102.

19. Fang, H.; Kaur, G.; Wang, B. *J. Fluoresc.* **2004**, *14*, 481–489.

20. Phillips, M. D.; James, T. D. *J. Fluoresc.* **2004**, *14*, 549–559.

21. Cao, H.; Heagy, M. D. *J. Fluoresc*. **2004**, *14*, 569–584.

22. Hall, D. G. *Boronic Acids. Preparation and Applications in Organic Synthesis and Medicine*, Wiley-VCH: Weinheim, **2005**.

23. Yang, W.; Lin, L.; Wang, B. *Tett. Lett.* **2005**, *46*, 7981–7984.

24. Gamsey, S.; Miller, A.; Olmstead, M. M.; Beavers, C. M.; Hirayama, L. C.; Pradhan, S.; Wessling, R. A.; Singaram, B. *J. Am. Chem. Soc*. **2007**, *129*, 1278–1286.

25. Zhang, T.; Anslyn, E. V. *Org. Lett.* **2007**, *9*, 1627–1629.

26. James, T. D.; Sandanayake, K. R. A. S.; Shinkai, S. *J. Chem. Soc. Chem. Commun.* **1994**, 477.

27. James, T. D.; Sandanayake, K. R. A. S.; Shinkai, S. *Angew. Chem. Int. Ed.* **1994**, *33*, 2207.

28. James, T. D.; Sandanayake, K. R. A. S.; Shinkai, S. *Nature,* **1995**, *374*, 345-347.

29. Franzen, S.; Ni, W.; Wang, B. *J. Phys. Chem. B* **2003**, *107*, 12942−12948

30. Ni, W.; Kaur, G.; Springsteen, G.; Wang, B.; Franzen, S. *Bioorg. Chem*. **2004**, *32*, 571−581.

31. Springsteen, G.; Deeter, S.; Gao, X.; Wang, B. *Tetrahedron*, **2002**, *58*, 5291–5300.

32. James, T. D. *Creative Chemical Sensor Systems*. Springer Berlin Heidelberg, **2007**.

33. Wiskur, S. L.; Lavigne, J. J.; Ait-Haddou, H.; Lynch, V.; Chiu, Y. H.; Canary, J. W.; Anslyn, E. V. *Org. Lett.* **2001**, *3(9)*, 1311-1314.

34. Zhu, L.; Shabbir, S. H.; Gray, M.; Lynch, V. M.; Sorey, S.; Anslyn, E. V. *J. Am. Chem. Soc.* **2006**, *128*, 1222-1232.

35. Collins, B. E.; Sorey, S.; Hargrove, A. E.; Shabbir, S. H.; Lynch, V. M.; Anslyn, E. V. *J. Org. Chem*. **2009**, *74*, 4055–4060.

36. Wulff, G. *Pure Appl. Chem.* **1982**, *54*, 2093-2102

37. Wulff, G.; Lauer, M.; Böhnke, H. *Angew. Chem. Int. Ed*. **1984**, *23(9)*, 741–742.

38. Perez-Fuertes, Y.; Kelly, A. M.; Johnson, A. L.; Arimori, S.; Bull, S. D.; James, T. D. *Org. Lett*. **2006**, *8*, 609–612.

39. Kelly, A. M.; Perez-Fuertes, Y.; Arimori, S.; Bull, S. D.; James, T. D. *Org. Lett.* **2006**, *8*, 1971–1974.

40. Mirri, G.; Bull, S. D.; Horton, P. N.; James, T. D.; Male L.; Tucker, J. H. R. *J. Am. Chem. Soc.* **2010**, *132*, 8903-8905.

41. Kelly, A. M.; Pérez-Fuertes, Y.; Fossey, J. S.; Yeste, S. L.; Bull, S. D.; James, T. D. *Nat. Protoc.* **2008**, *3(2)*, 215-219.

42. Perez-Fuertes, Y.; Kelly, A. M.; Fossey, J. S.; Powell, M. E.; Bull, S. D.; James, T. D. *Nat. Protoc.* **2008**, *3*, 210–214.

43. Yeste, S. L.; Powell, M. E.; Bull, S. D.; James, T. D. *J. Org. Chem.* **2008**, *74(1)*, 427-430.

44. Metola, P.; Anslyn, E. V.; James, T. D.; Bull, S. D. *Chem. Sci.* **2011**, *3(1)*, 156-161. Reproduced by permission of The Royal Society of Chemistry

45. Hutin, M.; Bernardinelli, G.; Nitschke, J. R. *Chem.-Eur. J.* **2008**, *14(15)*, 4585-4593.

46. Galbraith, E.; Kelly, A. M.; Fossey, J. S.; Kociok-Köhn, G.; Davidson, M. G.; Bull, S. D.; James, T. D. *New J. Chem.* **2009**, *33(1)*, 181-185.

47. Arnal-Hérault, C.; Pasc, A.; Michau, M.; Cot, D.; Petit, E.; Barboiu, M. *Angew. Chem. Int. Ed*. **2007**, *46(44)*, 8409-8413.

48. Martinez-Aguirre, M. A.; Villamil-Ramos, R.; Guerrero-Alvarez, J. A.; Yatsimirsky, A. K. *J. Org. Chem.* **2013**, *78*, 4674-4684.

49. Hargrove, A. E.; Zhong, Z.; Sessler, J. L.; Anslyn, E. V. *New J. Chem*. **2012**, *34(2)*, 348-354.

Chapter 3: Concerning the Mechanism of Boronate Ester Formation and Fluorescent Switch in *o*-Aminomethyl Phenylboronic Acids

3.1 INTRODUCTION

As it has been discussed in the previous chapters, boronic acids are extensively utilized in synthetic receptors for the molecular recognition and sensing of carbohydrates, as well as various other vicinal diol-containing compounds.[1-16] The practical detection of carbohydrates is commonly pursued in disease diagnostics, such as diabetes.[17-22] From a basic-science standpoint, carbohydrates present a challenge for molecular recognition due to their high solvation energies in water[23-25] and their great structural diversity.[26] Yet, boronic acids are able to overcome this solvation limitation because the binding event does not replace the solvent as with non-covalent binding, but rather interchanges covalent bonds. Thus, in the field of host-guest chemistry, boronate ester formation is recognized as a very unique reaction. It is one of the few rapidly reversible binding motifs that involve the making and breaking of covalent bonds (Scheme 3.1).[27-32]

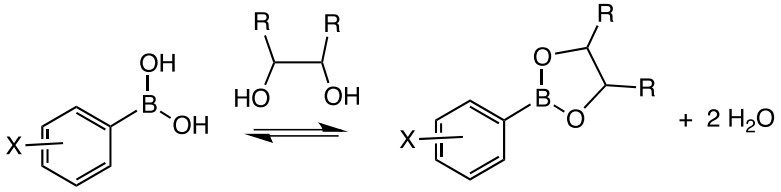

Scheme 3.1. Boronate ester formation.

Since the bonds formed in boronate esters are covalent in nature, boronic acids are able to bind their target diols in competitive media such as water and alcohols, whereas

receptors that rely on more traditional supramolecular interactions, such as H-bonds, electrostatics or solvophobicity often require multiple binding interactions in order to achieve reasonable affinities.[33-35] Importantly, the incorporation of a boronic acid into most any scaffold reliably imparts high to moderate millimolar binding affinities to vicinal diol, catechol, and α-hydroxycarboxylate-containing guests in competitive media without further structural manipulation.

However, phenylboronic acid itself is limited in its utility because it only shows significant binding a few pH units above physiological pH.[36,37] As a result of this high pH requirement for binding, several decades passed between when the reaction was discovered by the scientific community and its modification into a suitable biologically compatible system.

Lorand,[38] as well as Wulff,[36,39] delineated substituent effects for phenylboronic acids binding various diol species in early studies. Most significantly, they found that placement of an aminomethyl group on the *ortho* position to the boronic acid was found as a structural motif that leads to significantly improved binding at neutral pH.[40] This discovery set the stage for the use of this structural motif that continues to receive broad application to this day.[41-43]

3.2 Boronate Ester Formation and B-N Bonding

Established now as a series of landmark studies by Shinkai and James, the use of anthracene-based receptors such as **3.1** to signal the presence of various carbohydrates in neutral aqueous media *via* a fluorescence turn-on response (Scheme 3.2) was reported in 1994.[44-46] Simply put, formation of the boronate ester with the polyol-containing sugars

led to a great fluorescent signal increase. It was clear that the *o*-aminomethyl group in **3.1** not only improved the thermodynamics of binding at neutral pH, but also in some manner modulated the fluorescence of the receptor in the presence and absence of sugars.

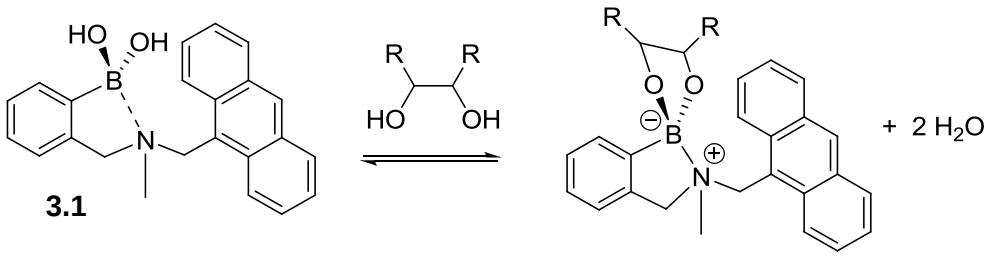

Scheme 3.2. Boronate ester condensation reaction with formation of a B-N bond.

Years later the authors put forth a hypothesis associated with **3.1**, that could be applied to any *o*-aminomethyl phenylboronic acids, to explain the role of the amino-group in binding and optical signaling.[47] Their postulate involved a weak dative bond to the boron atom from the amine nitrogen, resulting in sp^3 hybridization at B at neutral pH, represented by the dashed B-N line shown in compound **3.1**.[47] In contrast, the boron in phenylboronic acid ($PhB(OH)_2$) is sp^2 at neutral pH. This is a fact that has been established using ^{11}B NMR.[48] Upon boronate ester formation, a five membered ring involving the B atom is created with either structure **3.1** or phenylboronic acid. Shinkai and James reasoned this ring would be strained with an sp^2 boron relative to sp^3.[49] Hence, the B-N bond was postulated to stabilize the boronate adduct with *o*-aminomethyl phenylboronic acids because pyramidalization of the boron is induced by the Lewis acid-base coordination with the neighboring nitrogen. In essence, the two interactions reinforce each other; B-N bonds are stronger with a pyramidalized B, while boronate ester formation is stabilized by B-N bonding. In addition, diols, catechols, and α-

hydrocarboxylates are more electron-withdrawing ligands for boron than are hydroxyl groups. Therefore, the boron is more electrophilic upon creation of boronate esters, hence creating a stronger Lewis acid-base interaction.[2,49] For these reasons, the strength of the B-N bond in the ester was proposed to increase relative to the acid (solid B-N line in Scheme 3.2).

The modulation of the B-N bond strength also explains the turn-on of fluorescence found for structure **3.1** and analogs.[44-46] Photo-induced electron transfer (PET)[50,51] from the nitrogen lone-pair electrons in **3.1** was postulated to quench the emission of anthracene because this lone pair was not strongly coordinated to boron. However, upon boronate ester formation, the energy of the N donor electron pair to B drops due to stronger coordination, making the lone pair on nitrogen less available and lowering the extent of PET. Hence, PET quenching is decreased upon ester formation, which results in a turn-on of fluorescence.

In summary, one potential role of an *o*-aminomethyl group on a phenylboronic acid is for the amine to act as a Lewis base that datively coordinates the boron. This enhances the affinity of the boronic acid toward diol binding at neutral pH, and modulates the energy of the nitrogen lone pair to alter the extent of PET quenching of neighboring fluorophores. Irrespective of the actual role of the *o*-aminomethyl group, the discovery of a class of compounds such as **3.1**, and the associated proposed mechanism, remains a landmark study in the history of supramolecular sensors.[e]

[e] Although boronate ester formation is not technically supramolecular based upon the original definition by Jean-Marie Lehn because it involves covalent bonds, this binding interaction has become a staple of the field. A recent definition of Supramolecular Analytical Chemistry accepts this interaction within the purview of this area of research. See Lehn, J. M. *Angew. Chem. Int. Ed.* **1988**, *27(1)*, 89-112 and reference[66].

3.3 ALTERNATIVE EXPLANATION: pK_A SWITCH

Wang put forth an alternative mechanism to the B-N dative bond theory in 2003 and 2004.[52,53] He noted that crystal structures of boronic acids actually have shorter B-N bond lengths than those in corresponding boronate esters. In his first paper analyzing the B-N bond mechanism, he and Franzen used density functional theory (DFT) for computational modeling, and found that relative changes in the B-N bond strength upon ester formation were not significant enough to show the large changes in PET quenching necessary to explain the behavior of **3.1** with sugars. The DFT results revealed that B-N bond formation was not efficient enough to tie up the nitrogen lone pair. In this paper, they noted that protonation of the amine was a more likely explanation for the arresting of the PET quenching found with sugars, but they did not delineate a detailed proposal. The reason that protonation of the amine was proposed to dominate is that a N-H bond is far stronger than a B-N bond

In a subsequent analysis, Wang proposed what has now come to be known as the "pK_a switch" or "hydrolysis/solvolysis" mechanism. The critical feature of this proposal is given in Scheme 3.3.[53] He proposed that B-N bonding exists in the boronic acid, while the boronate ester chelates a solvent between the boron and the amine (called "hydrolysis"). This leads to protonation of the amine; the reason this is called a pK_a switch is covered below. For purposes of this dissertation, we note that the product in Scheme 3.3 has a solvent molecule inserted between the amine nitrogen and boron. This has turned out to be an important structural postulate given by Wang.

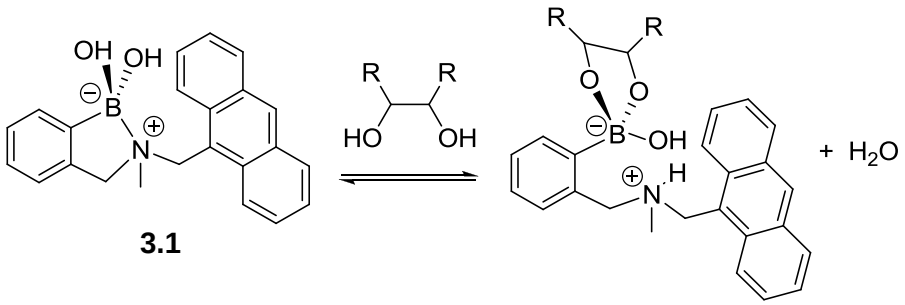

Scheme 3.3. Boronate ester condensation reaction with solvent insertion.

Wang also pointed out other issues that were inconsistent with the B-N bond strength modulation postulate. First, the emission intensity of the assembled sensor is independent of the pK_a of the boronate ester, even though the pK_a varies as a function of which sugar is used. In fact, it is well documented with phenylboronic acid that the lowering of the pK_a of the boronic acid depends upon which sugar is added to the solution.[38,54] Because the strength of the B-N bond should modulate the extent of PET, and because each sugar has a different electron withdrawing ability, the electrophilicity of different boronate esters should vary. Accordingly, the fluorescence response of the system should also vary with different sugars. The earlier work by James and Cooper showed that the change in fluorescence is not dependent upon the sugar,[55] and Wang reconfirmed this experimentally with four different carbohydrates.[53]

Wang further noted that sugars which form trivalent binding of the boron should not modulate the fluorescence if a B-N bond occurs. The hydrolysis mechanism would still show a fluorescence change, as is experimentally observed. A third valency of a trivalent sugar would break the B-N bond, while the hydrolysis mechanism simply has the third valency taking the place of the hydroxyl in the boronate ester. We will return to this point later.

One last piece of experimental data used by Wang to support the hydrolysis mechanism relied on an earlier experiment by Anslyn that revealed that the B-N bond is formed during pH titrations of compounds analogous to those of structure **3.1**. The evidence for the B-N bond was ^{11}B NMR analysis of pH titrations, which only showed pyramidalization of B around pHs of 5-6. These titrations, in hindsight, should now be interpreted in a different fashion. This reinterpretation is a large focus of this treatise, and will be covered below following examination of pH titrations and further structural analyses we performed in order to gain a better understanding.

3.4 pH Titrations Performed

pH Titrations are among the data that can be rationalized with either the B-N bond or hydrolysis mechanisms.[53] There are two types of pH titrations often performed: fluorescent or ^{11}B NMR. In fluorescence titrations of **3.1** alone, a large emission drop between pHs of 5 to 6 is observed. Another smaller decrease in fluorescence occurs above pH 11. In contrast, the first fluorescence decrease is minor in the presence of a sugar, with a large decrease occurring at higher pH. Figure 3.1A shows a pH titration we performed in a 1:2 methanol/water mixture. This titration reproduces all the essential features found in earlier titrations.[45] The same low and high pH inflections were found around pH 6 and 11, as well as the fluorescence differences with and without the sugar fructose. Figure 3.1B is an overlay of similar pH titrations using many different sugars, all of which show similar features.

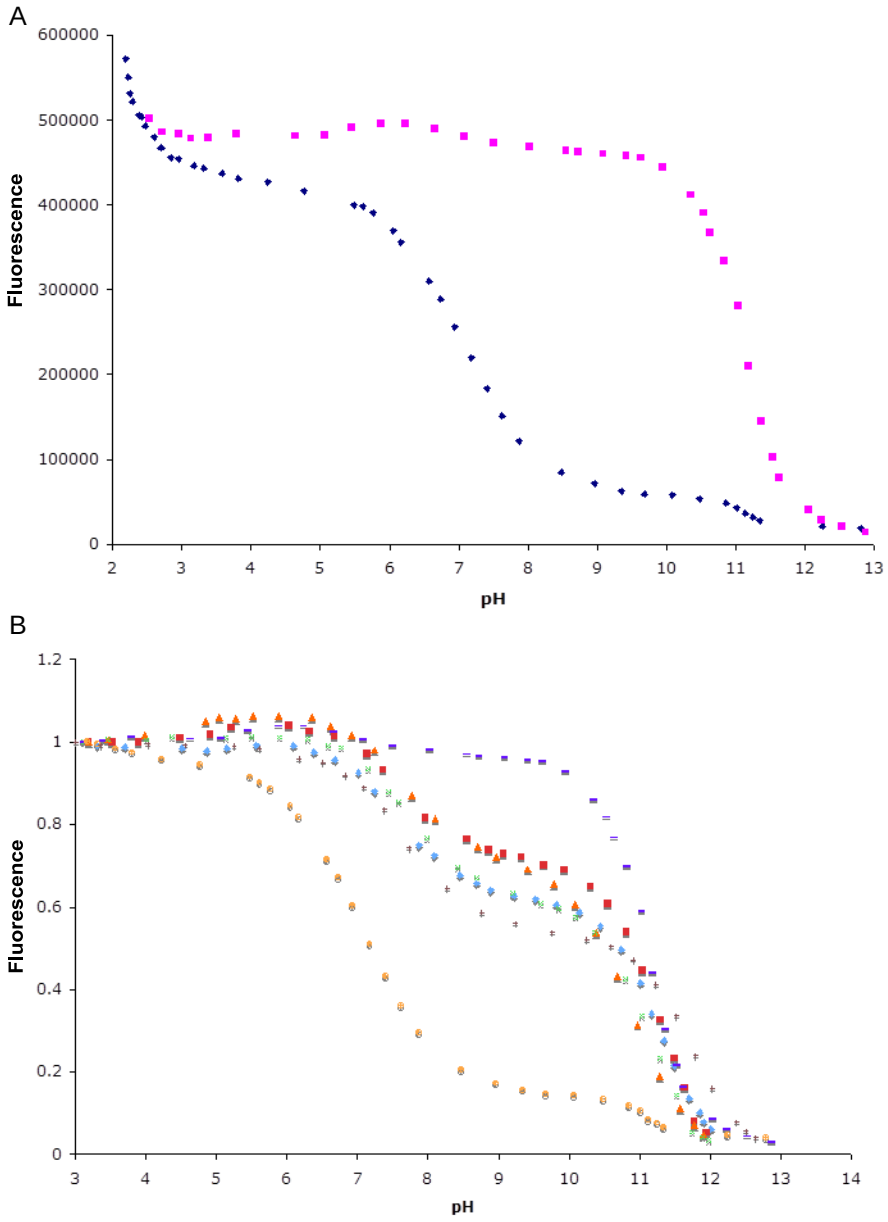

Figure 3.1. A) pH titrations of **3.1** (1 μM) on its own (◆) and in the presence of D-fructose (50 mM) (■), in 2:1 H_2O:CH_3OH with 50 mM NaCl. B) Analogous pH titrations of **3.1** in 2:1 H_2O:CH_3OH alone (●) and in the presence of 50 mM D-mannose (◆), D-galactose (■), L-sorbose (▲), D-glucose (×), inositol (+), and D-fructose (–).

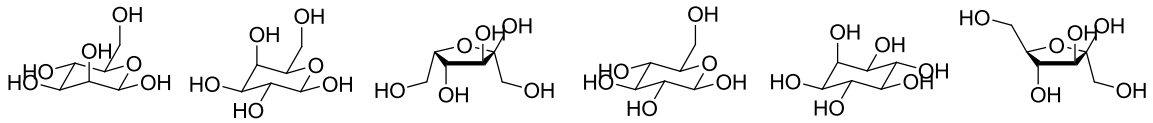

With the postulate of a B-N bond formation in mind, it is logical to assign pK_{a1} to the deprotonation of the ammonium ion. This value is lowered in comparison to a standard alkyl ammonium (9-11) due to the resulting coordination with boron (Scheme 3.4A). The coordination of nitrogen to boron replaces, and is in competition with, protonation. The lowering of the pK_a is analogous to that observed for ammoniums in the presence of metals, due to metal-amine coordination.[56] pK_{a2} therefore would be hydroxylation of the boron with subsequent breaking of the B-N bond. This pK_a is in the standard range of that for boronic acids. Note that hydroxylation of a boronic acid is accompanied by the release of a proton, and hence is a Brønsted acid dissociation reaction that has an associated pK_a value (Scheme 3.5).

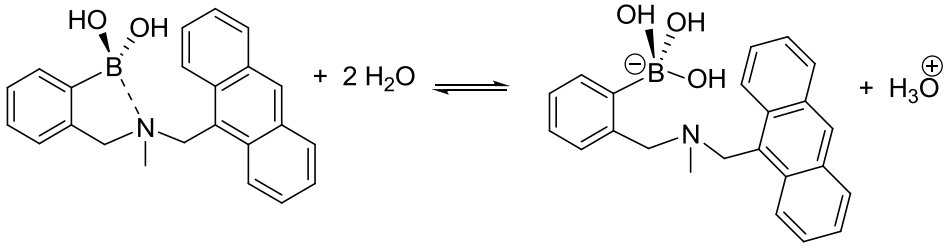

Scheme 3.5. Hydroxylation of boronic acid **3.1**.

Continuing with the postulate of B-N bonding, deprotonation of the ammonium of the boronic acid leads to liberation of the nitrogen lone-pair (pK_{a1}). This lone pair is then weakly coordinated to boron (Scheme 3.4A), therefore quenching the anthracene

fluorescence emission. Hydroxylation of the boron in the boronic acid only slightly increases quenching (pK_{a2}). On the other hand, addition of a sugar leads to boronate ester formation (Scheme 3.4B), and therefore deprotonation of the ammonium (pK_{a1}) replaces a strong N-H bond with a strong dative N-B bond, essentially not affecting the ability of the nitrogen to be involved in PET. Hydroxylation of the boron in the boronate ester, however, does free up the amine's lone pair, leading to quenching of the anthracene emission (pK_{a2}).

To whatever extent the B-N bonding mechanism does operate, the first pK_a in Scheme 3.4B must reflect an even more complicated scenario. The reason is that the binding constants of *o*-aminomethyl phenylboronic acids increase dramatically as the pH is raised above the first pK_a, due to the pyramidalizing the B atom upon ester binding (discussed above). While the pH is increasing during a titration of **3.1** in the presence of a sugar, binding of that sugar is also increasing in equilibrium with the deprotonation reactions. Hence, the slight fluorescence modulation seen for pK_{a1} reflects not just a deprotonation reaction but also sugar binding. When a sugar is present, pK_{a2} simply involves the deprotonation accompanying hydroxylation of boron because boronate ester formation is essentially complete before and after this deprotonation. Hence, Scheme 3.4 shows equilibrium arrows connecting individual species in parts A and B, while the red arrows depict the general flow of structures created when raising the pH in the presence of a sugar. Note that the structures on the upper right and lower left are presumed not to be present to a significant extent under neutral pH conditions. This scheme depicts what occurs when the B-N bonding mechanism is operating.

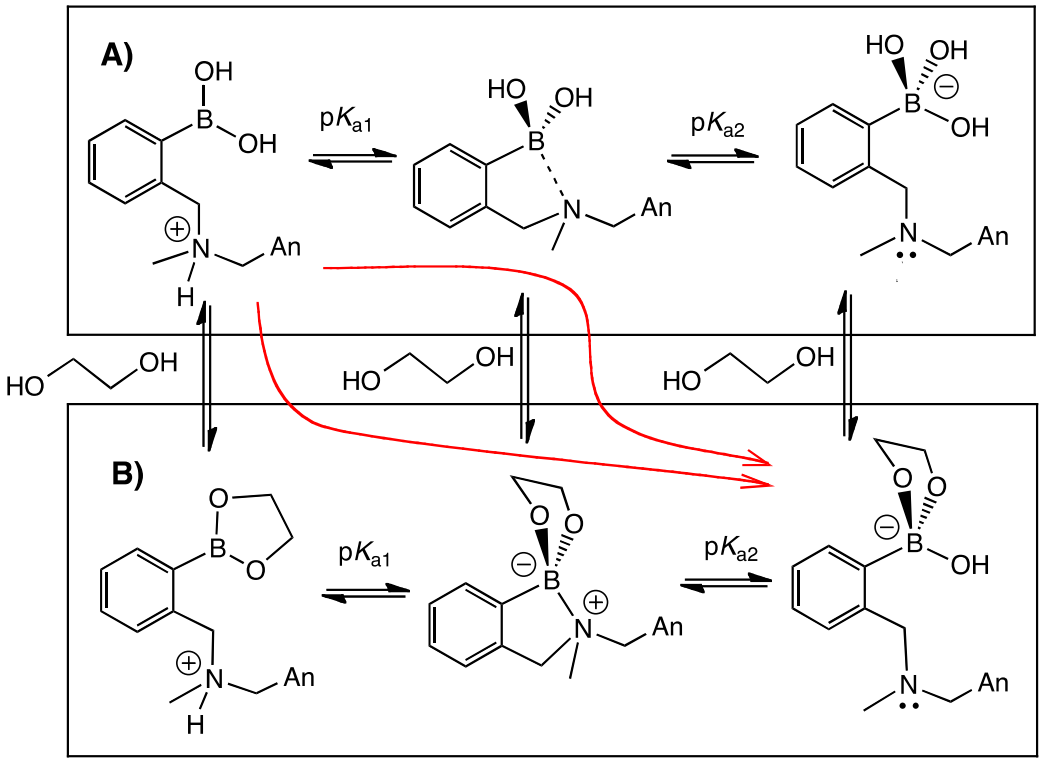

Scheme 3.4. B-N Bonding Scheme - The structures involved with *o*-aminomethyl phenylboronic acids as a function of pH (low to high pH given from left to right) and the absence (A) and presence (B) of a diols, such as a sugar, α-hydroxy carboxylate, and catechol.

Scheme 3.6 depicts the individual species that would be involved in the hydrolysis pathway, displayed in a manner consistent with Scheme 3.4. Let us walk through each intermediate, examine the proper pK_a assignment, and contrast this with Scheme 3.4. As with the B-N bond mechanism, Scheme 3.6 shows that at low pH the amine is protonated. In the presence of a diol there is little binding with the boronic acid. As the pH is increased in the absence of a sugar, pK_{a1} would be deprotonation of the amine to make a B-N bond, while pK_{a2} is hydroxylation of the boron. This is exactly the

same as Scheme 3.4, the only difference being a postulated difference in the strength of the B-N interaction.

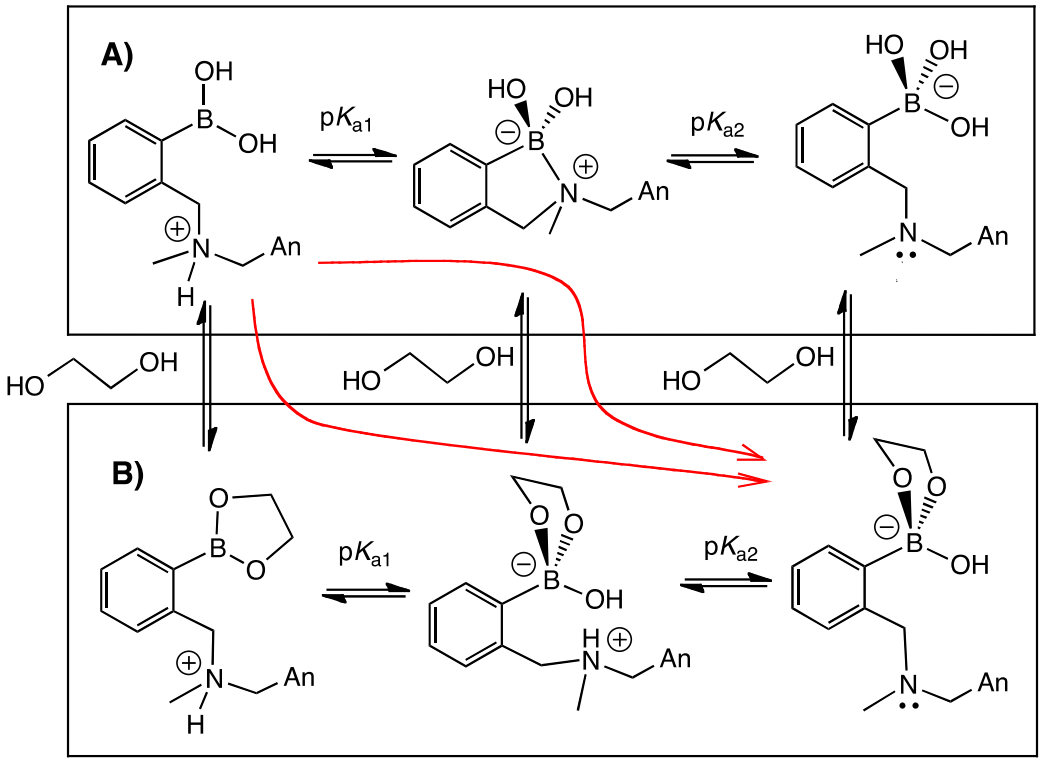

Scheme 3.6. Hydrolysis (pK_a switch) Mechanism Scheme - The structures involved with *o*-aminomethyl phenylboronic acids as a function of pH (low to high pH given from left to right) and the absence (A) and presence (B) of a diols, such as a sugar, α-hydroxy carboxylate, and catechol.

However, in the presence of a sugar the proposal is very different from Scheme 3.4. As the pH is increased the sugar binds along with hydrolysis of the boron. The two equilibria are occurring simultaneously, and therefore the first pK_a is a combined thermodynamic effect of both equilibria (just as was noted for the first pK_a of Scheme

3.4B). Logically, it must follow that the second pK_a would be deprotonation of the ammonium ion. The slightly elevated value relative to a normal ammonium can be explained by its proximity to the negative boron center. Note that in the absence of the diol the first and second pK_a values are deprotonation of the amine and hydroxylation of the boron, respectively. The presence of a diol reverses the order; the first and second pK_a values are hydroxylation and amine deprotonation, respectively. This mechanistic postulate is therefore called a "pK_a switch". Importantly, it should be noted that if the pK_a values actually do switch, then it is a coincidence that pK_{a1} of Scheme 3.6A and pK_{a1} of Scheme 3.6B are nearly the same. The analogous is true for pK_{a2} of Scheme 3.6A and pK_{a2} of Scheme 3.6B. This coincidence may exist, but given the data presented in the next section, the pK_a values can be interpreted differently.

One of the last pieces of evidence that Wang used to support his hydrolysis mechanism (Scheme 3.6) is a comparison of the logic behind Scheme 3.4 and 3.6 based upon some work by Anslyn from 2001. Wang's support for the formation of the strong B-N bond with boronic acids derivatives was stated as "there are ample literature results proving that the first pK_a is the deprotonation of the amine '(ammonium actually)' with concomitant formation of a B-N bond". At the time this statement was correct due to Anslyn's interpretation of his own work, which was referenced as the "literature precedent". These experiments were pH titrations on structures similar to compound **3.1** (**3.2** and **3.3**)[57] which were followed by ^{11}B NMR. As seen in chapter 1 ^{11}B NMR spectroscopy is very sensitive to the hybridization of B. Accordingly, trigonal planar boron (as with boronic acids or esters at low pH) can be readily distinguished from tetrahedral boron (as with B-N bonded structures or hydrolysis).[48]

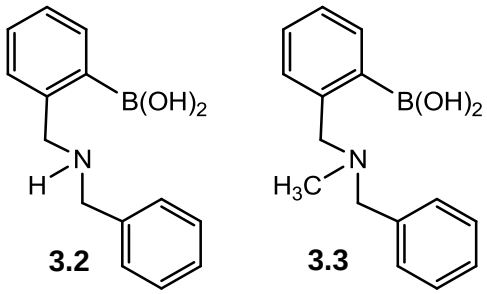

Figure 3.2. Analogues to **3.1** used in the studies by Anslyn et al.

The goal of the 2001 Anslyn experiments was to determine if the pK_a values of secondary and tertiary amines proximal to the boronic acids were similar or not. With a secondary amine, deprotonation could lead to a standard covalent B-N bond rather than a dative B-N bond interaction (Scheme 3.7).[57] This possibility had been suggested to Anslyn by a reviewer of one of his Angew. Chemie papers,[58] and hence he set out to test if this was occurring. He found nearly identical pK_a values for *o*-aminomethyl phenylboronic acids involving tertiary and secondary amines, which thereby rules out the equilibria shown in Scheme 3.7. Further, the ^{11}B NMR results showed that trigonal planar boronic acid derivatives are not formed at pHs above the first pK_a.

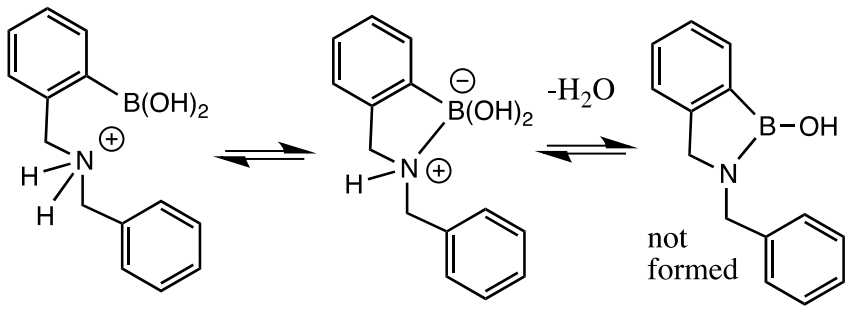

Scheme 3.7. Amine-containing analogues to **3.1** studied by Anslyn et al.

To further explore if the pK_a values will switch between boronic acids and boronate esters, Anslyn examined the ^{11}B NMR of **3.4** in the presence of saturating amounts of different diols in 2006. He found at most half of a pK_a unit difference for both the first and second pK_a values between this boronic acid and the various boronate esters.[59] In addition, Figure 3.1B similarly shows that the first and second pK_a values of **3.1** do not change significantly in the presence of several different sugars. Taken together, these studies show that acid/base reactions of the *o*-aminomethyl phenyl boronate esters are not significantly different than those of their corresponding boronic acids. This fact indicates that the increased electrophilicity of the boronate esters upon diol binding does not lead to differences in pK_a, thereby questioning whether a "pK_a switch" as postulated by Wang is actually operative.

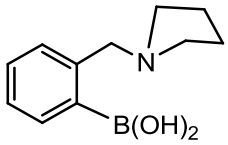

3.4

Figure 3.3. **3.1** analogue used by Anslyn et al. for ^{11}B NMR studies.

With the clarity of hindsight, it is obvious that there is a problem with Anslyn's interpretation of his 2001 ^{11}B NMR experiments.[57] They really only reveal trigonal planar versus tetrahedral boron, and therefore are not able to distinguish B-N bonds from other structures containing an sp^3 boron. In 2001 Anslyn interpreted the first pK_a to result in B-N bond formation upon pyramidilization of the boron because B-N bonding was the prevailing thought at the time. But given the benefit of hindsight and the experiments

discussed immediately below, there is a better interpretation that involves solvent insertion in both the boronic acids and boronate esters.

3.5 Structural Studies and ^{11}B NMR Studies

To distinguish the B-N bond or the pK_a switch mechanisms, Anslyn performed a series of X-ray crystallographic and ^{11}B NMR studies. The ^{11}B NMR spectra of titrations of **3.4** with catechol, hydrobenzoin, and α-hydroxyisobutyric acid were examined.[59] The chemical shifts of the products created during titration were correlated with those found for purified boronate esters for which crystal structures were obtained. Hence, they were confident in the assignment of B-N bonded and solvent inserted structures. The conclusion was that solvent insertion dominates over B-N bond formation for the boronic acid **3.4** and all the boronate esters created. A small extent of B-N bond formation was found when using catechol, meaning that B-N bonds and solvent-inserted products can co-exist in equilibria. Further, computational studies in this same paper found that solvent insertion dominates over B-N bond formation for both boronic acids and boronate esters.[59]

More recent, advanced computational results from Larkin led to a similar conclusion.[60] Using both second-order Moller-Plesset perturbation theory and density functional theory, both with explicit solvation models, Larkin found that the solvent-inserted species are lower in energy than B-N dative bonded species. They also found that B-N bonding and solvent insertion are both lower in energy than no interaction between the *o*-aminomethyl group and the boronic acid or boronate ester in a protic

media. Lastly, the results found that any B-N bonding leads energetically downhill to species involving solvent insertion.

It was so found experimentally and computationally that solvent insertion dominates over B-N bonding for both *o*-aminomethyl boronic acids and boronate esters. This, paired with experiments revealed that the first and second pK_a values for boronic acids and boronate esters are not significantly different, led to the conclusion that there is no conversion of B-N bonds for boronic acids to solvent-inserted species for boronate esters. Hence, the pK_a switch postulate is not correct, although the notion of a "hydrolysis" mechanism is correct.

We should, however, also recall that Wang's pK_a switch postulate was based upon Anslyn's misinterpretation of this ^{11}B NMR data. It was primarily put forth to explain the large difference in fluorescence emission for boronic acid **3.1** and its boronate esters in the presence of sugars. Further, recall that the original Shinkai explanation involved a difference in strengths of the B-N bond to explore what modulates the emission of **3.1**. This also must not be correct because solvent insertion dominates with both boronic acids and boronate esters. Hence, the modulation of the emission of **3.1** upon binding sugars is a phenomenon that still needs an explanation (vide infra).

3.6 Further Support for Solvent Insertion of Boronic Acids and Boronate Esters

All the studies from Wang, James, Shinkai, and Anslyn indicate that the boron is tetrahedral at pH values above the first pK_a. The issue we have discussed to this point is whether that tetrahedral structure involves a B-N dative bond or inserted solvent, and it is

clear that solvent insertion dominates in protic media. Hence, the boron is tetravalent (having three bonds to oxygen atoms and one to a phenyl ring) at pH values above the first pK_a. Actually, this was also supported by crystal structures of boronic acids with sugars that can act as trivalent ligands, supplying three oxygens to the boron. In these cases, the inserted solvent is replaced by an OH group from the sugar itself. This is well accepted for fructose[61] and is the most common explanation of why the furanose sugars, fructose and sorbital, routinely have the largest affinities to many boronic acids, creating structures such as **3.5**.

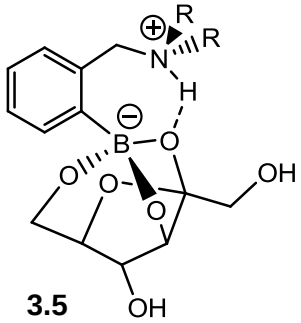

3.5

Figure 3.4. Glucose binding mode with arylboronic acids.

Norrild found that glucose rearranges to its furanose form when binding with a bis-boronic acid receptor (Scheme 3.8), as revealed by a series of coupling constant measurements.[62] The postulate is that the driving force is to exploit the energetically favorable trivalent interaction by glucose. Hence, other sugars that dominantly exist in pyranose forms likely also rearrange to their furanose forms when complexing boronic acid-based receptors. A hydroxyl group is used to replace the inserted solvent. But the binding energy for such configurations will pay the energy cost associated with the

rearrangement, and hence give lower binding constants than sugars that dominantly exist in furanose forms.

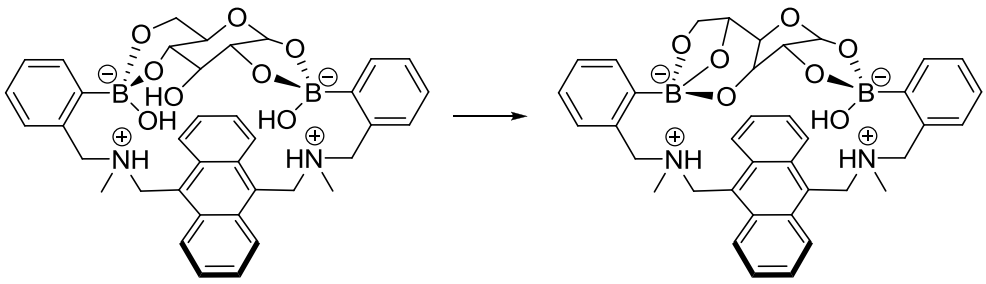

Scheme 3.8. Reaction studied by Norrild et al.

3.7 The Role of the *Ortho*-Amino Methyl Group in Thermodynamics and pK_A Values

It is now well established that solvent insertion is the manner by which both boronic acids and boronate esters are pyramidalized in protic solvents, as a tetrahedral boronate anion. Interestingly, this is exactly the same as found for simple phenylboronic acid. At pHs near or above the pK_a, the anionic tetrahedral boronate ester is readily formed in the presence of a sugar and the question arises as to the role that the aminomethyl group plays. This functional group increases diol-binding affinity of phenylboronic acids at neutral pH, and this is the primary reason that the group is so widely adopted. In some manner this group also plays a role in modulating the emission of appended fluorophores. Exactly how the group performs these functions, however, requires examination and discussion.

The *o*-aminomethyl group must lower the pK_a of the proximal boronic acid group. It could simply act as a proximal electron-withdrawing group towards the boron that makes the phenylboronic acid act as it normally does, except at a lower pH. Solvent may simply insert upon first deprotonation, and have no other significance. This possibility for the aminomethyl group requires us to reinterpret the first and second pK_a values of these compounds (Scheme 3.9).

Phenylboronic acid itself has a pK_a of 8.8, yet the first pK_a of *o*-aminomethyl phenylboronic acid compounds are between 5 and 7 depending upon the solvent. Scheme 3.4 shows the earliest interpretation of this pK_a, assigning it to the deprotonation of the ammonium leading to a B-N bond. Scheme 3.6 shows a second interpretation, involving solvent insertion with boronate esters and B-N bonding with boronic acids. These are both reasonable interpretations, but in light of the fact that solvent insertion occurs with boronic acids and boronate esters, we must now conclude that the first pK_a corresponds to hydroxylation (or alkoxylation in an alcohol solvent) of the boronic acid. This event leads directly to a solvent-inserted structure (Scheme 3.9A). Hence, the proximity of the positively charged ammonium group depresses the pK_a of the boronic acid to around 5-7 from the common values of 9-10. This occurs irrespective of whether the boron atom is part of a boronic acid or a boronate ester because the first pK_a values do not significantly vary between these two species (discussed above). With this conclusion in mind, the second pK_a value of *o*-aminomethyl phenylboronic acids or boronate esters must be the deprotonation of the amine, occurring at pH values of around 11-12. This second pK_a is raised 1-2 units above that of normal ammonium groups due to the proximity of the negatively charged boronate.

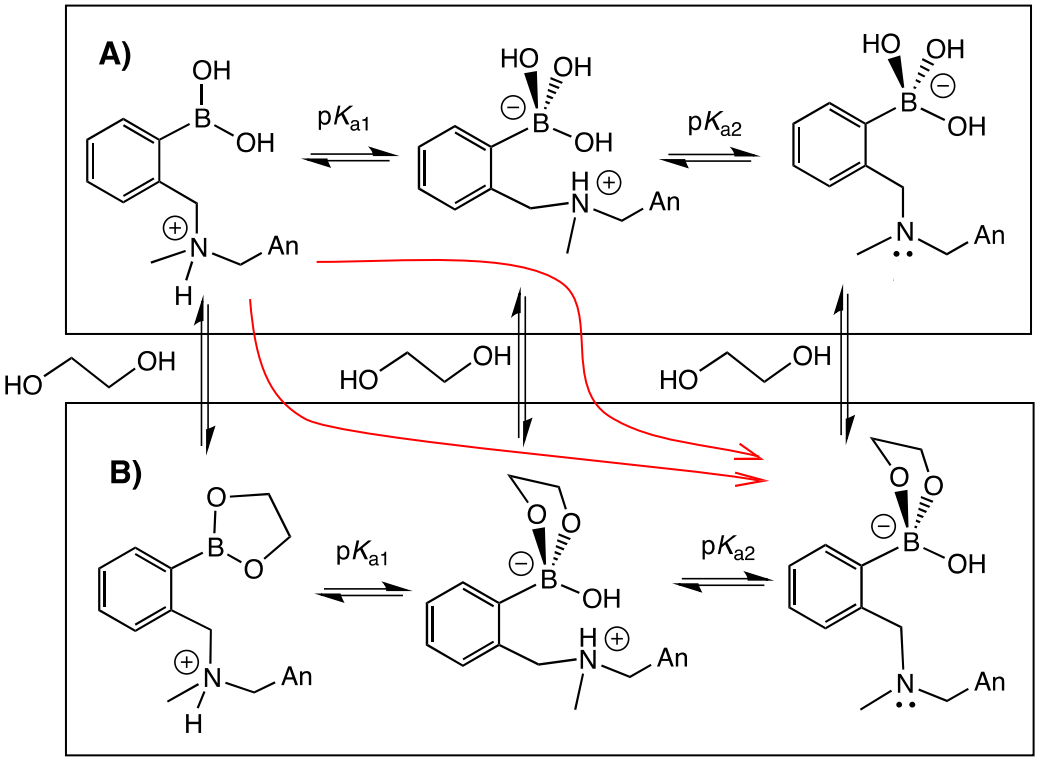

Scheme 3.9. Solvent Insertion Scheme - The structures involved with *o*-aminomethyl phenylboronic acids as a function of pH (low to high pH given from left to right) and the absence (A) and presence (B) of a diols, such as a sugar, α-hydroxy carboxylate, and catechol.

The situation, however, is actually even more complicated. Although solvent insertion dominates in all cases yet studied, Anslyn showed that with certain diols some small level of B-N bonding does exist in equilibrium with solvent insertion in protic media. When there is a significant level of B-N bonding, the first and second thermodynamic pK_a values represent mixed deprotonation events (Scheme 3.4 and 3.9 simultaneously). In these cases, the first and second pK_a values involve both boron hydroxylation/alkoxylation and ammonium deprotonation.

3.8 The Role of the *Ortho*-Amino Methyl Group in the Mechanism of Boronate Ester Formation

If the ammonium of the *o*-aminomethyl group perturbs the pK_a values of the boronic acids and boronate esters, it is logical that it could also play a key role in the mechanism of boronate ester formation. For example, consider what steps need to be involved when starting with a solvent-inserted boronic acid and transitioning to a solvent-inserted boronate ester (Scheme 3.10). The inserted solvent first needs to be expelled, then replaced by an alcohol of the diol or saccharide, followed by bond rotations and further stepwise replacements of inserted solvent(s) leading to a fully bound guest. Because the first replacement of the inserted solvent by the guest is intermolecular, it is likely slow relative to the subsequent steps that are intramolecular and chelate the diol or saccharide to the boron atom.

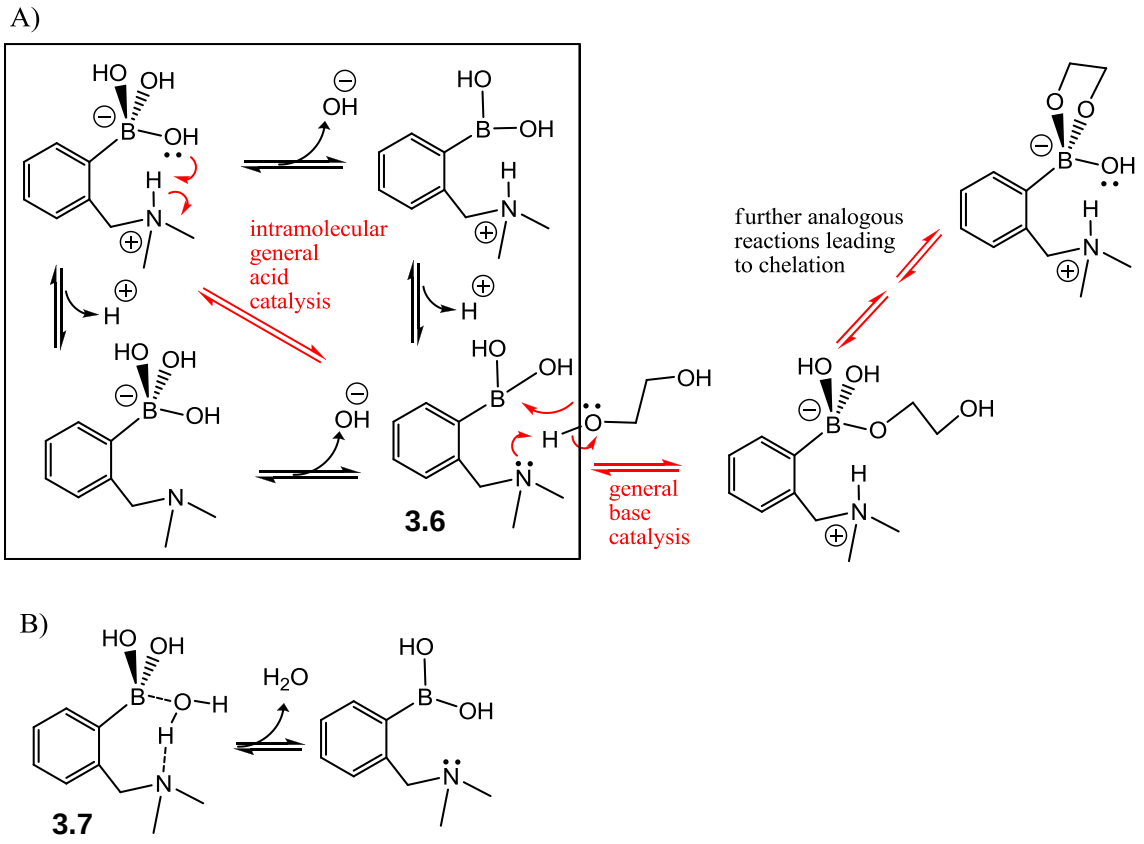

Scheme 3.10. A) The proposed mechanism for boronate ester formation at pH between the first and second pK_a values, based upon kinetics, crystal structures, and isotope effects. The red arrows show the dominant pathway, involving general acid-catalyzed expulsion of an inserted solvent with a general base-catalyzed delivery of the guest. B) The possibility of losing the inserted solvent in a single step if that solvent is not highly ionized between the N and B.

The release of an inserted solvent would lead to species **3.6** in Scheme 3.10A. This could happen in two steps: ammonium deprotonation and loss of hydroxide/alkoxide from the boron, in any order. These two possibilities are shown in the upper right and lower left corners of the box. Either way, this would require loss of a very poor leaving

group at neutral pH. Alternatively, the solvent can be lost in one step by simple decomplexation from the boron (see the intramolecular "general acid catalysis" pathway). This would involve creating an *o*-aminomethyl phenylboronic acid in a high-energy state (**3.6**) because it does not possess the preferred boronic acid and amine protonation states at the operating pH.

Interestingly, this dilemma between stepwise and single-step loss of the inserted solvent is dependent on the ionization state of the inserted solvent. The loss of the inserted solvent should have a dependence upon the extent to which that solvent is deprotonated when bound between the boron and nitrogen. If the solvent is fully deprotonated when inserted, thereby creating a zwitterionic boronate anion and ammonium cation, its single step departure as a neutral species requires a proton transfer simultaneously with departure (as shown in the pathway that is color-coded with red arrows in Scheme 3.10A). If the solvent is not ionized when inserted, it can simply depart with no proton transfer (Scheme 3.10B). The former possibility, protonation concerted with leaving group departure, is defined as general-acid catalysis. This sequence and can be analyzed by classic experiments such as isotope effects.

Any of the alternatives for loss of solvent, such as stepwise or a single-step, with the single step either involving proton transfer or not, all create high-energy intermediates. The diol-containing guest subsequently reacts with the newly created high-energy intermediate. This means there is a step that creates an intermediate prior to reaction with the guest, which is a mechanism that should show saturation kinetics. Yet, saturation kinetics for such systems had not been found previously.[63] Alternatively, a mechanism where the solvent-inserted *o*-aminomethyl phenylboronic acid directly reacts with the guest would consistently show second order kinetics as with an S_N2 reaction,

first order in both boronic acid and guest. Although this later alternative does not seem reasonable, there have not been kinetics experiments reported to date to rule it out.

3.8.1 Probing the mechanism

In an effort to understand this mechanism better we studied the kinetics of the reaction of **3.1** with fructose, both at low and high fructose concentrations.[64] At low concentrations of fructose the kinetics appeared second order, and the y-intercept of the kinetic plots revealed ratios of k_1 and k_{-1}. The reaction appeared analogous to an S_N2 mechanism, except for the fact that there was a non-zero y-intercept, which is indicative of equilibrium kinetics.

At high fructose concentrations of 0.015 M (1500 equivalents) or more, we found saturation kinetics (Figure 3.5). At these concentrations of fructose, the kinetics shows that a mechanism involving a rate-determining step prior to reaction with the guest is operative. It was proposed that this first step is loss of the inserted solvent to create **3.6** (Scheme 3.10). Such a mechanism is analogous to an S_N1 reaction, where leaving group departure leads to a reactive intermediate that takes on a nucleophile. Unlike S_N1 chemistry that appears first order at low concentrations of nucleophile, the boronic acid mechanism requires hundreds of equivalents of fructose to reach saturation. This makes perfect sense, given that the reverse step that competes with the first insertion of guest (fructose in this exact case) is insertion of a solvent molecule. The solvent is in incredibly large excess over fructose (being in the range of several molar, while fructose is only mM). This competing re-insertion of solvent is analogous to the common ion effect in S_N1 mechanisms,[65] but with boronic acids the "common ion" is the solvent. By

fitting the kinetic data, we were able to estimate that fructose is around 1000 times better nucleophile when adding to **3.6** than the solvent (see experimental section).

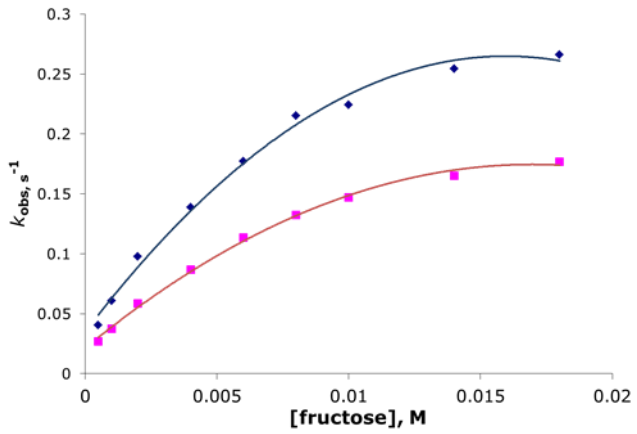

Figure 3.5. Observed rate constants for the reaction of **3.1** (10 μM) with fructose in 2:1 H_2O:CH_3OH (◆) and in 2:1 D_2O:CD_3OD (■) at pH(D) = 8.7 and [NaCl] = 50 mM showing saturation of the kinetics as fructose is increased in concentration.

Additionally, we addressed the issue of whether the inserted solvent is significantly ionized or retains substantial O-H bonding (**3.7**, Scheme 3.10B). The loss of solvent from either possibility is delineated in Scheme 3.10, the first undergoing general acid-catalyzed loss of the solvent, while the second is a simple decomplexation. The former involves the movement of a proton, and hence should have an isotope effect while the second possibility would have nearly no isotope effect. A crystal structure of solvent-inserted species **3.8** with the proper resolution to find the position of the hydrogen between the O and N atoms shows a shorter H-N bond than O-H bond, supporting some extent of ionization of the inserted solvent.[66] Consistent with this finding, we uncovered a direct isotope effect of 1.42 for the reaction of **3.1** with fructose. This value is smaller

than what may be expected, but is clearly a substantial effect that shows cleavage of a weak bond with hydrogen. This is confirming evidence that the general acid-catalyzed pathway for expulsion of the inserted solvent occurs. It should be noted that if the expulsion is general acid-catalyzed, then the reverse solvent insertion reaction, would be general base-catalyzed (as noted in Scheme 3.10A).

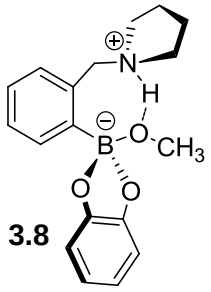

3.8

Figure 3.6. Compound used for X-ray crystal structural analyses.

There are two possibilities for why the isotope effect on the rate-determining step involving solvent loss from **3.1** is small. First, the isotope effect could be smaller than a standard primary kinetic isotope effect because the extent of proton transfer to liberate the solvent is minimal due to a lack of full ionization (such as structure **3.7**). As stated, the less ionized the solvent, the lower the expected size of the isotope effect. A second possibility is that the stepwise pathways depicted in the box of Scheme 3.10 are occurring simultaneously with the general acid-catalyzed path. This would mean that only a fraction of pathways involved in departure of solvent would be expected to show an isotope effect.

3.9 Effect of the Aminomethyl Group on the Fluroescence of 3.1

The remaining unsolved aspect concerning the reactivity of **3.1**, and other similar boronic acid-based fluorescence sensors, is how the *o*-aminomethyl group influences the emission of an appended fluorophore. We covered above that the original postulate put forth by Shinkai and James is not consistent with structural data, nor is the pK_a switch notion of Wang. In the following pages we attempt to put forth novel reasoning and discuss the experimental work we performed to investigate their validity.

One possible answer is in the relative ratio of the B-N species and in the solvent insertion species in a boronic acid as compared to the boronic ester. Several lines of evidence support this postulate. First, in the structural studies performed by our group in 2006, the free boronic acid species showed a small percentage of B-N bond species in a protic solvent, while the solvent insertion species dominates. On the other hand, no B-N bond was observed with the boronic/boronate ester species. The small percentage of the B-N species in the boronic acid form could contribute the fluorescent switch by going through the pK_a switch mechanism as postulated by Wang. Then there is the question of whether the small percentage of the B-N species in the boronic acid form would be enough to contribute to the observed fluorescent changes. This leads to the second line of evidence that we can discuss in light of a series of our own results. With all the fluorescent studies using **3.1**, one typically observes fluorescent intensity changes of about three-fold, as seen in Figure 3.7 for the addition of fructose. However, the 9-aminomethyl anthracene system has been studied extensively as a pH-sensitive fluorescent sensor. In those studies, like the one we present in Figure 3.8, one typically sees fluorescent intensity changes of close to thirty-fold. This is also true in our fluorescent pH titration work, where fluorescent changes of more than ten-fold were

observed over the pH range (Figure 3.1A in this study and Figure 1 of the paper by Wang[53]). What this could mean is that while the solvent insertion species dominates in structural forms, a small percentage of B-N formation in the boronic acid form could be the reason for the fluorescent intensity changes. This then raises another issue: with catechol boronate ester one does see the B-N bond species. One would not expect to see much change because the B-N species in the boronic acid form would not be expected to convert to the solvent insertion species (percentage wise). In fact, we saw that addition of the catechol leads to a decrease in the intensity of the fluorescent signal (Figure 3.7).

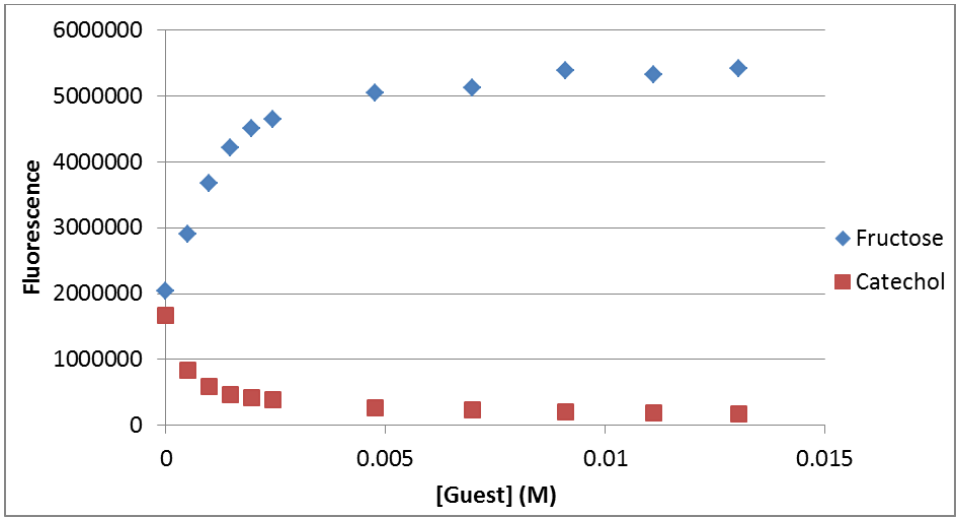

Figure 3.7. Fluorescence titrations of D-fructose (◆) and catechol (■) into **3.1** (100 μM) in 2:1 H_2O:CH_3OH with 50 mM NaCl.

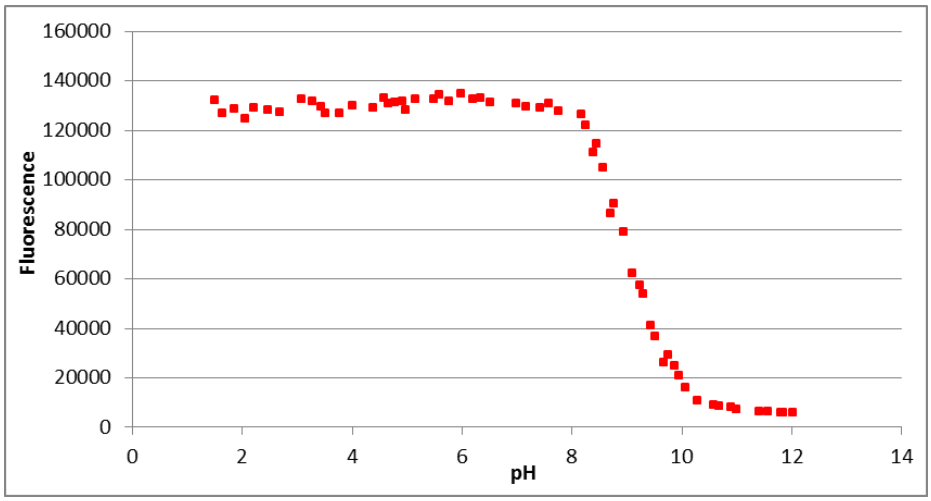

Figure 3.8. pH fluorescence titrations of 9-methylaminomethyl anthracene (10 μM) in 2:1 H_2O:CH_3OH with 50 mM NaCl.

Although initial results made this hypothesis very promising, it was abandoned after two sets of experiments. Firstly, we obtained a crystal structure and determined through X-ray analysis that there exists no B-N interaction of any type (Figure 3.9). Secondly, and more importantly, we found no evidence of any B-N bond in the free boronic acid form of **3.1** using ^{11}B NMR spectroscopy (Figure 3.10A). To validate our peak assignment we added catechol, as it is known to promore B-N bond formation, to the sample containing **3.1** and registered the presence of a new peak at 14.4 ppm (Figure 3.10B) This value is within the range of resonances traditionally assigned to this type of coordination.

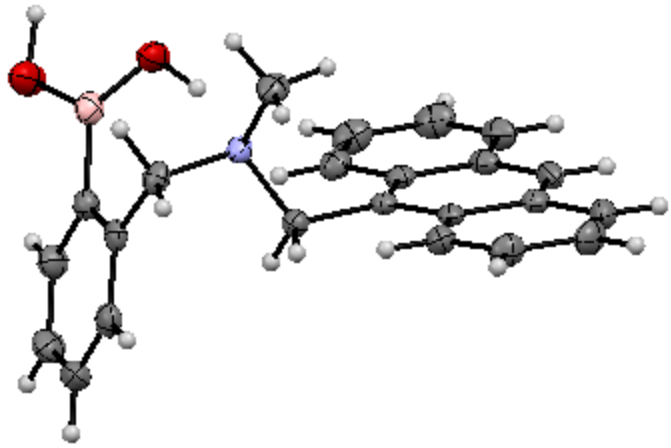

Figure 3.9. View of **3.1** crystalized from CH_3CN showing no interaction between B and N. Displacement ellipsoids are scaled to the 50% probability level. Heteroatoms: Nitrogen (blue), Oxygen (red) and Boron (pink).

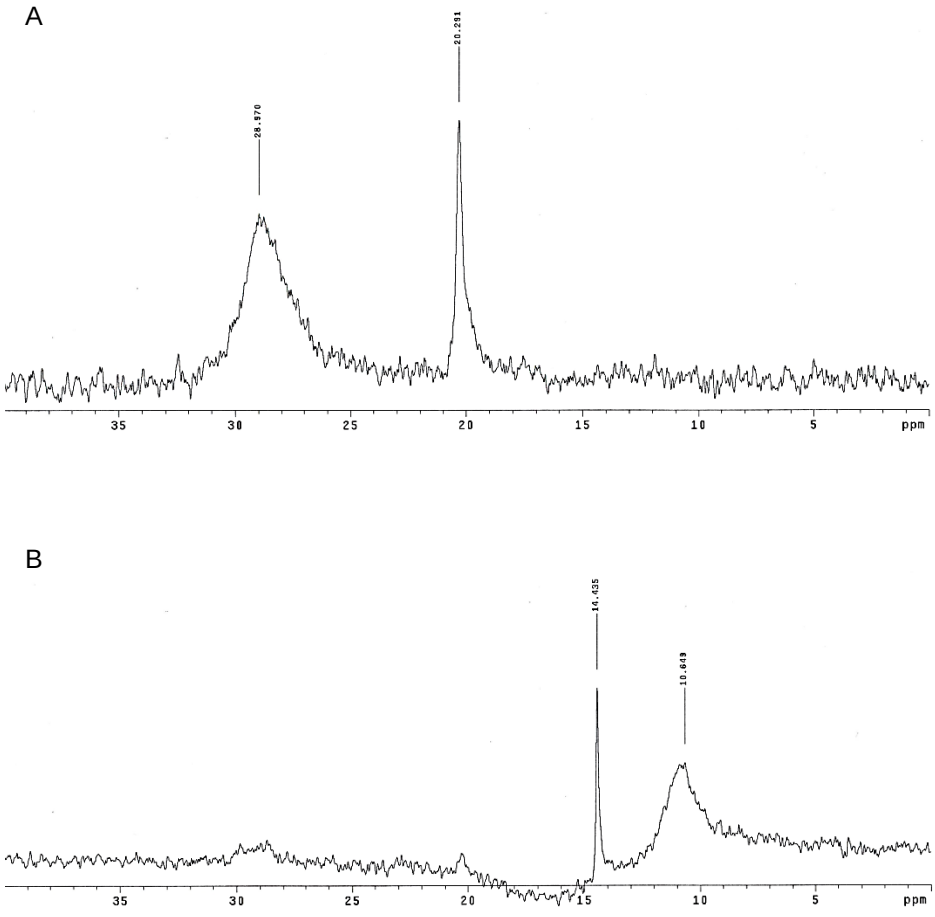

Figure 3.10. ^{11}B NMR spectra of **3.1** in CD_3CN (10 mM) A) on its own and B) after adding 2 equivalents of catechol.

Having refuted our original idea, we aimed to reconcile all the experimental data we had accumulated throughout the composition of this work. The original B-N postulate focused upon PET quenching of an appended fluorophore by the nitrogen lone pair, which becomes lower in energy upon boronate ester formation due to a stronger dative interaction. The argument in the pK_a switch approach focused on the increased strength of

a N-H bond relative to a B-N bond. Our current hypothesis combines these ideas, where the increased electrophilicity of a boronate ester relative to a boronic acid affects the extent of ionization of the inserted solvent. The idea is that with a boronic acid, the inserted solvent has more character of an intact solvent. There is significant O-H bonding and little proton transfer from the solvent to the amine. Hence, the lone pair of the amine is still available for PET quenching of an appended fluorophore. Alternatively, when a boronate ester is formed from a saccharide or other more electron-withdrawing diol species, the boron is more electrophilic. Hence, the inserted solvent (or a third chelated alcohol from the saccharide) is ionized to a greater extent, with a larger contribution from an anionic boronate and a protonated amine. With a greater extent of proton transfer to the amine, less PET quenching would occur, and therefore the fluorescence of **3.1** is higher upon sugar binding.

This explanation could predict that each sugar should result in a different level of fluorescence turn-on when binding with **3.1** because each sugar is different in its electron withdrawing capabilities toward their respective boronate ester. However, each sugar gives nearly identical fluorescence turn-on, except for fructose (see Figure 3.1 herein). Wang originally cited this experimental observation as one that is not consistent with the B-N bonding hypothesis, because in this postulate each sugar should also give a different extent of fluorescence turn-on.[53]

However, we now note that the extent of fluorescence turn-on is not absolutely the same. Figure 3.1 was created with the sugars at the same concentration during the titrations, and we find that the fluorescence response is not absolutely identical. Hence, while the B-N bonding hypothesis has been ruled out for structural reasons (vide supra), the idea of differing extents of proton transfer to the amine from the inserted solvent should not be ruled out on the basis of the turn-on response being identical for all sugars.

In fact, it could be that an extent of proton transfer beyond some critical level is all that is needed to achieve a near maximum fluorescence turn-on upon binding a sugar, and that any greater extent of proton transfer resulting from a more electron withdrawing sugar doesn't give a significantly greater emission response.

Currently, there is one experiment that does lend some credence to the idea that the extent of proton transfer from the inserted solvent to the amine is the determining factor in turning on the fluorescence of **3.1** upon sugar binding. We have found that the fluorescence quenching of **3.1** is lowered in deuterated water/methanol mixtures, as is also the boronate esters of **3.1**. As mentioned above, crystal structure analysis of **3.8** reveals that the bridging H is closer to nitrogen than oxygen, supporting significant ionization of the inserted solvent. Hence, a potential surface such as shown in Figure 3.11 best depicts the motion and position of this hydrogen. Because the well representing the N-H---O is lower in energy than the well for N---H-O, and given the lower zero-point energy for deuterium, a deuterium in this position would even further accentuate the population imbalance, favoring a full-fledged N-D bond. If there is a greater extent of nitrogen bonding to deuterium than hydrogen in the deuterated solvent relative to protio solvent, then we would expect less quenching of an appended fluorophore in the deuterated solvent and therefore higher emission. As just described, this is exactly what is experimentally determined. However, as with the original two postulates for the role that the *o*-aminomethyl group plays, this hypothesis awaits further experimental and computational analysis for verification.

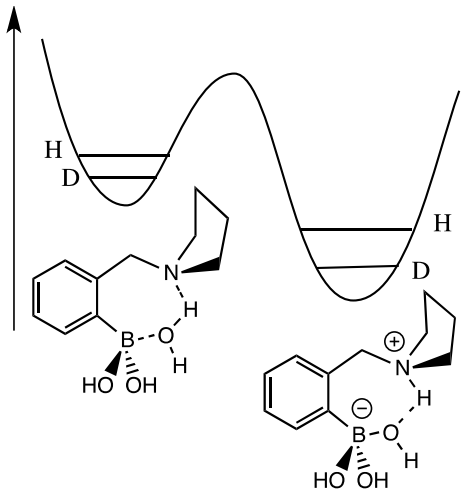

Figure 3.11. Potential energy surface showing the ZPEs for a solvent inserted *o*-aminomethyl phenylboronic acid (or ester) with a bridging solvent and an ionized solvent, respectively.

3.10 CONCLUSIONS

This chapter delineates a historical account of the ideas and concepts put forth by Shinkai/James and Wang of the role of the *o*-aminomethyl group in phenylboronic acids, covering both the B-N bond and the pK_a switch postulates, respectively. Both concepts can explain the effect on the thermodynamics and emission properties of boronate esters relative to boronic acids. However, with evidence from ^{11}B NMR from our group, logic concerning pK_a values, crystal structures from Norrild, and computations from Larkin, it is clear that neither postulate is supported by all the data. Instead, solvent insertion consistently dominates the structures of both boronic acids and boronate esters. Hence, the upshot is that the *o*-aminomethyl group lowers the pK_a of the proximal boronic acid due to its electron withdrawing nature and a field effect from the ammonium ion. In

doing so the structure created for such boronic acids and boronate esters exists with a solvent inserted between the boron and nitrogen atoms. Consequently, this arrangement of atoms facilitates leaving group departure, because the ammonium group acts as a general acid catalyst in liberating the inserted solvent. This conclusion is supported by both kinetics and isotope effect studies. Thus, the *o*-aminomethyl group both improves the thermodynamics of boronate ester formation, and facilitates the kinetics of exchange at the boron center.

The last remaining issue for debate is the exact manner in which the *o*-aminomethyl group is involved in modulating the emission of an appended fluorophore. A new postulate involving the extent of ionization of the inserted solvent was put forth, which awaits additional experimental and computational analysis.

3.11 EXPERIMENTAL DETAILS

3.11.1 Materials and Methods

All reagents were purchased from Aldrich Chemical Co., Acros Organics, or Atlantic Scientific Co., Inc. and used without further purification. NMR spectra were recorded on a Varian INOVA 500 or a Varian UNITY+300 instrument. Stopped-flow kinetic experiments were performed on a KinTek Corp. SF-2004 instrument with a PMT detector fitted with a 400 nm long-pass filter. All kinetic data were fit to either a single or double exponential equation using KinTek_Explorer software. Fluorescence data were recorded on a Photon Technology international QuantaMaster Cuvet-Based spectrofluorometer. All pH measurements were made using an Orion 720A pH meter. All reported association constant data was iteratively fit to a 1:1 binding equation using Microsoft Origin 5.0. ^{11}B NMR spectra were collected on Varian INOVA 500 with a sweep width of 51250 Hz, 66k of data points, a 90º pulse width and a 2.2 second recycle time, using $BF_3 \bullet OEt_2$ as an external reference. Each spectrum was processed with 10 Hz line broadening, and a second order polynomial fitting routine was used to remove ^{11}B background. The temperature for these experiments was regulated at 25ºC.

3.11.2 Fluorescence pH Titrations

Two separate solutions of **3.1** (10μM) were prepared using 2:1 H_2O:CH_3OH with 50 mM NaCl and either NaOH or HCl (50 mM). To a quartz fluorescence cuvette were added 2.0 mL of the acidic solution of **3.1** and a small stir bar. The basic solution was added iteratively, and the pH measured after each addition. In titrations with **3.1** and a diol, the diol was added to both solutions so that it was maintained at a constant concentration of 0.1 M. The pH measurements made in deuterated solvents were prepared with D_2O and CH_3OD and NaOD and DCl were used for pH adjustment. Under these conditions, a greater volume of basic solution was necessary to affect pH change throughout the necessary pH region. When necessary, titration solution was removed from the cuvette in 1 mL aliquots. The spectra were monitored using λ_{ex} = 368 nm and λ_{em} = 390-500 nm. The analogous was followed for the pH titration of 9-methylaminomethyl anthracene, with λ_{ex} = 368 nm and λ_{em} = 380-500 nm.

3.11.3 Procedure for Stopped-Flow Kinetics

All reaction solutions were prepared from stock solutions of **3.1** (10 mM in methanol) and D-fructose (1 M in 2:1 H_2O:CH_3OH). These were used to prepare dilute solutions at double the concentration desired for analysis. In early experiments where buffer was used, the pH of the buffer was adjusted separately and used to dilute the stock solutions to the desired concentrations. When buffer was not used, the necessary aliquots

of host or fructose were added to a volumetric flask, which was then filled nearly full with solvent. The pH of each individual solution was adjusted using solutions of NaOH (50 mM) and HCl (50 mM) in 2:1 H_2O:CH_3OH. After appropriate pH adjustment, the flask was filled to volume with solvent.

3.11.4 Procedure for Fluorescence Kinetics

All reaction solutions were prepared from stock solutions of **3.1** (10 mM in methanol), sugars (1 M in 2:1 H_2O:CH_3OH) or catechol (0.1 M in 2:1 H_2O:CH_3OH). These were used to prepare dilute solutions at double the concentration desired for analysis. The necessary aliquots of the desired reagent were added to a volumetric flask, which was then filled nearly full with solvent. The pH of each individual solution was adjusted using solutions of NaOH (50 mM) and HCl (50 mM) in 2:1 H_2O:CH_3OH. After appropriate pH adjustment, the flask was filled to volume with solvent. To perform the kinetic experiments, a 1.0 mL aliquot of the fluorescent reagent was first added to a quartz fluorescence cuvette with a stir bar. A 1.0 mL aliquot of the second reagent was added rapidly *via* syringe with simultaneous initiation of the data collection.

3.11.5 Kinetic Analysis

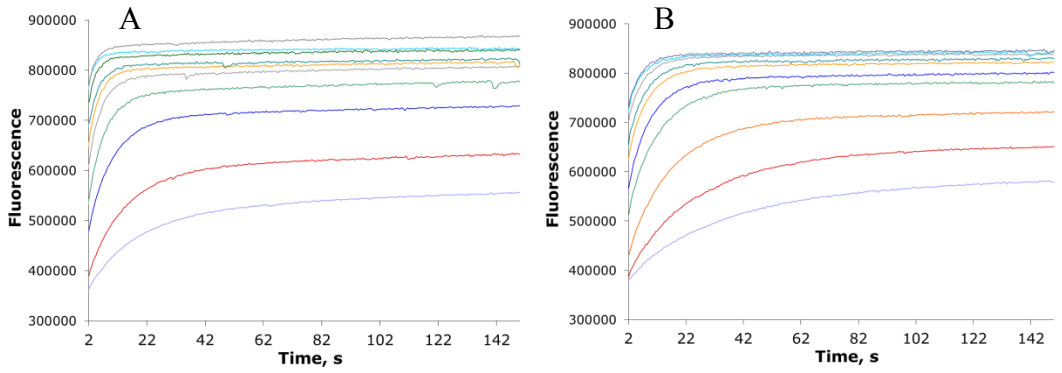

Figure 3.12. Kinetic traces following reaction between **3.1** (10 μM) and D-fructose (0.5, 1, 2, 4, 6, 8, 10, 14, 18, and 20 mM) in A) 2:1 H_2O:CH_3OH and B) 2:1 D_2O:CH_3OD at pH(D) 8.7 with 50 mM NaCl.

3.11.6 Calculation of Total Nucleophilic Oxygen Atoms

For a 2:1 H_2O:CH_3OH mixture we used densities $\rho(H_2O)$ = 1 g/mL and $\rho(CH_3OH)$ = 0.7918 g/mL and molecular masses $MW(H_2O)$ = 18.00 g/mol and $MW(CH_3OH)$ = 32.04 g/mol.

Concentration of pure water

$$\frac{1\ g(H_2O)}{1\ mL(H_2O)} \times \frac{1\ mol(H_2O)}{18\ g(H_2O)} \times \frac{1\ mL}{1\ L} = 55.5\ M(H_2O)$$

Concentration of pure methanol

$$\frac{0.7918\ g(CH_3OH)}{1\ mL(CH_3OH)} \times \frac{1\ mol(CH_3OH)}{32.04\ g(CH_3OH)} \times \frac{1\ mL}{1\ L} = 8.2\ M(CH_3OH)$$

Concentration of O nucleophiles in mixture

$$55.5\ M(H_2O) \times \frac{2}{3} + 8.2\ M(CH_3OH) \times \frac{1}{3} = 45.2\ M$$

3.11.7 X-ray crystal structure determination

Empirical formula	C23 H22 B N O2	
Formula weight	355.22	
Temperature	153(2) K	
Wavelength	0.71073 Å	
Crystal system	monoclinic	
Space group	P 21/n	
Unit cell dimensions	a = 9.8642(7) Å	α= 90°.
	b = 12.4840(7) Å	β= 98.445(4)°.
	c = 15.7552(9) Å	γ = 90°.
Volume	1919.1(2) $Å^3$	
Z	4	
Density (calculated)	1.229 Mg/m^3	
Absorption coefficient	0.077 mm^{-1}	

Table 3.1. Crystal data and structure refinement for the structure in Figure 3.9.

F(000)	752
Crystal size	0.530 x 0.370 x 0.340 mm
Theta range for data collection	2.620 to 27.495°.
Index ranges	-12<=h<=12, -16<=k<=16, -20<=l<=20
Reflections collected	30758
Independent reflections	4365 [R(int) = 0.0597]
Completeness to theta = 25.242°	99.5 %
Absorption correction	Semi-empirical from equivalents
Max. and min. transmission	1.00 and 0.855
Refinement method	Full-matrix least-squares on F^2
Data / restraints / parameters	4365 / 0 / 253
Goodness-of-fit on F^2	1.052
Final R indices [I>2sigma(I)]	R1 = 0.0495, wR2 = 0.1217
R indices (all data)	R1 = 0.0809, wR2 = 0.1407
Extinction coefficient	n/a
Largest diff. peak and hole	0.298 and -0.224 e.$Å^{-3}$

Table 3.1. Crystal data and structure refinement for the structure in Figure 3.9. (Cont.)

	x	y	z	U(eq)		x	y	z	U(eq)
C1	2803(2)	5920(1)	6617(1)	25(1)	C6	3924(2)	5246(2)	6857(1)	30(1)
C2	2832(2)	6941(1)	7010(1)	22(1)	C7	1695(2)	7737(1)	6758(1)	25(1)
C3	3931(2)	7226(2)	7623(1)	27(1)	C8	524(2)	8847(2)	5634(1)	30(1)
C4	5028(2)	6541(2)	7844(1)	31(1)	C9	3016(2)	8750(1)	5870(1)	21(1)
C5	5028(2)	5552(2)	7448(1)	34(1)	C10	3162(2)	9277(1)	5027(1)	20(1)
					C11	3376(2)	8626(1)	4329(1)	21(1)

Table 3.2. Atomic coordinates (x 10^4) and equivalent isotropic displacement parameters ($Å^2$x 10^3) for the structure in Figure 3.9. U(eq) is defined as one third of the trace of the orthogonalized U^{ij} tensor.

C12	3397(2)	7483(2)	4376(1)	27(1)	C20	3176(2)	12660(2)	4716(1)	33(1)
C13	3564(2)	6874(2)	3685(1)	34(1)	C21	2926(2)	12205(2)	5502(1)	31(1)
C14	3753(2)	7353(2)	2904(1)	35(1)	C22	2917(2)	11125(1)	5610(1)	25(1)
C15	3776(2)	8429(2)	2826(1)	31(1)	C23	3150(2)	10405(1)	4943(1)	20(1)
C16	3591(2)	9106(2)	3529(1)	24(1)	N1	1719(1)	8158(1)	5882(1)	21(1)
C17	3605(2)	10219(2)	3464(1)	26(1)	O1	856(1)	6173(1)	5342(1)	32(1)
C18	3391(2)	10877(1)	4143(1)	23(1)	O2	1284(2)	4448(1)	5921(1)	40(1)
C19	3404(2)	12018(2)	4065(1)	30(1)	B1	1581(2)	5509(2)	5930(1)	26(1)

Table 3.2. Atomic coordinates (x 10^4) and equivalent isotropic displacement parameters ($Å^2$x 10^3) for the structure in Figure 3.9. U(eq) is defined as one third of the trace of the orthogonalized U^{ij} tensor (Cont.).

C1-C6	1.397(3)	C6-H6	0.95
C1-C2	1.415(3)	C7-N1	1.480(2)
C1-B1	1.583(3)	C7-H7A	0.99
C2-C3	1.388(3)	C7-H7B	0.99
C2-C7	1.508(2)	C8-N1	1.464(2)
C3-C4	1.383(3)	C8-H8A	0.98
C3-H3	0.95	C8-H8B	0.98
C4-C5	1.383(3)	C8-H8C	0.98
C4-H4	0.95	C9-N1	1.480(2)
C5-C6	1.379(3)	C9-C10	1.507(2)
C5-H5	0.95	C9-H9A	0.99

Table 3.3. Bond lengths [Å] and angles [°] for the structure in Figure 3.9.

C9-H9B	0.99	C22-C23	1.427(2)
C10-C11	1.409(2)	C22-H22	0.95
C10-C23	1.414(2)	O1-B1	1.365(2)
C11-C12	1.429(2)	O1-H1O	1.00(3)
C11-C16	1.439(2)	O2-B1	1.356(2)
C12-C13	1.357(3)	O2-H2O	1.08(4)
C12-H12	0.95	C6-C1-C2	117.38(17)
C13-C14	1.404(3)	C6-C1-B1	118.88(16)
C13-H13	0.95	C2-C1-B1	123.74(16)
C14-C15	1.350(3)	C3-C2-C1	119.91(17)
C14-H14	0.95	C3-C2-C7	119.27(16)
C15-C16	1.425(3)	C1-C2-C7	120.81(16)
C15-H15	0.95	C4-C3-C2	121.26(18)
C16-C17	1.394(3)	C4-C3-H3	119.4
C17-C18	1.390(3)	C2-C3-H3	119.4
C17-H17	0.95	C5-C4-C3	119.36(18)
C18-C19	1.430(3)	C5-C4-H4	120.3
C18-C23	1.443(2)	C3-C4-H4	120.3
C19-C20	1.346(3)	C6-C5-C4	119.95(19)
C19-H19	0.95	C6-C5-H5	120
C20-C21	1.417(3)	C4-C5-H5	120
C20-H20	0.95	C5-C6-C1	122.10(18)
C21-C22	1.360(3)	C5-C6-H6	119
C21-H21	0.95	C1-C6-H6	119

Table 3.3. Bond lengths [Å] and angles [°] for the structure in Figure 3.9 (Cont.).

N1-C7-C2	111.50(14)	C13-C12-C11	121.34(18)
N1-C7-H7A	109.3	C13-C12-H12	119.3
C2-C7-H7A	109.3	C11-C12-H12	119.3
N1-C7-H7B	109.3	C12-C13-C14	120.74(19)
C2-C7-H7B	109.3	C12-C13-H13	119.6
H7A-C7-H7B	108	C14-C13-H13	119.6
N1-C8-H8A	109.5	C15-C14-C13	120.65(18)
N1-C8-H8B	109.5	C15-C14-H14	119.7
H8A-C8-H8B	109.5	C13-C14-H14	119.7
N1-C8-H8C	109.5	C14-C15-C16	120.90(19)
H8A-C8-H8C	109.5	C14-C15-H15	119.6
H8B-C8-H8C	109.5	C16-C15-H15	119.6
N1-C9-C10	115.13(14)	C17-C16-C15	121.99(17)
N1-C9-H9A	108.5	C17-C16-C11	118.98(16)
C10-C9-H9A	108.5	C15-C16-C11	119.03(17)
N1-C9-H9B	108.5	C18-C17-C16	121.88(17)
C10-C9-H9B	108.5	C18-C17-H17	119.1
H9A-C9-H9B	107.5	C16-C17-H17	119.1
C11-C10-C23	120.12(16)	C17-C18-C19	121.22(17)
C11-C10-C9	118.69(15)	C17-C18-C23	119.64(16)
C23-C10-C9	121.12(15)	C19-C18-C23	119.14(17)
C10-C11-C12	122.59(16)	C20-C19-C18	121.55(18)
C10-C11-C16	120.10(16)	C20-C19-H19	119.2
C12-C11-C16	117.31(16)	C18-C19-H19	119.2

Table 3.3. Bond lengths [Å] and angles [°] for the structure in Figure 3.9 (Cont.).

C19-C20-C21	119.82(18)	C10-C23-C18	119.25(16)
C19-C20-H20	120.1	C22-C23-C18	116.84(15)
C21-C20-H20	120.1	C8-N1-C7	109.57(14)
C22-C21-C20	120.83(18)	C8-N1-C9	111.49(14)
C22-C21-H21	119.6	C7-N1-C9	108.81(14)
C20-C21-H21	119.6	B1-O1-H1O	111.1(18)
C21-C22-C23	121.82(18)	B1-O2-H2O	113.5(19)
C21-C22-H22	119.1	O2-B1-O1	119.72(19)
C23-C22-H22	119.1	O2-B1-C1	117.71(17)
C10-C23-C22	123.91(16)	O1-B1-C1	122.55(17)

Table 3.3. Bond lengths [Å] and angles [°] for the structure in Figure 3.9 (Cont.).

	U11	U22	U33	U23	U13	U12
C1	26(1)	21(1)	27(1)	5(1)	4(1)	0(1)
C2	26(1)	21(1)	21(1)	6(1)	8(1)	0(1)
C3	34(1)	26(1)	22(1)	3(1)	7(1)	-3(1)
C4	30(1)	35(1)	27(1)	8(1)	-3(1)	-6(1)
C5	31(1)	30(1)	41(1)	9(1)	-2(1)	6(1)
C6	32(1)	21(1)	36(1)	4(1)	1(1)	3(1)
C7	26(1)	22(1)	29(1)	1(1)	11(1)	0(1)

Table 3.4. Anisotropic displacement parameters ($Å^2 x\ 10^3$) for the structure in Figure 3.9. The anisotropic displacement factor exponent takes the form: $-2\pi^2[\ h^2\ a^{*2}U^{11} + ...\ + 2\ h\ k\ a^*\ b^*\ U^{12}\ ]$

C8	22(1)	24(1)	43(1)	4(1)	4(1)	4(1)
C9	21(1)	21(1)	23(1)	1(1)	2(1)	-1(1)
C10	14(1)	23(1)	22(1)	1(1)	0(1)	-1(1)
C11	14(1)	24(1)	25(1)	-1(1)	1(1)	0(1)
C12	23(1)	26(1)	32(1)	0(1)	6(1)	1(1)
C13	29(1)	28(1)	45(1)	-9(1)	9(1)	1(1)
C14	30(1)	40(1)	35(1)	-13(1)	8(1)	0(1)
C15	27(1)	43(1)	25(1)	-3(1)	5(1)	-1(1)
C16	17(1)	31(1)	23(1)	-2(1)	1(1)	0(1)
C17	21(1)	36(1)	21(1)	7(1)	1(1)	-1(1)
C18	16(1)	24(1)	27(1)	3(1)	-1(1)	-1(1)
C19	26(1)	29(1)	31(1)	12(1)	0(1)	-3(1)
C20	35(1)	18(1)	46(1)	4(1)	1(1)	-2(1)
C21	32(1)	23(1)	37(1)	-5(1)	3(1)	0(1)
C22	24(1)	26(1)	25(1)	1(1)	2(1)	-2(1)
C23	13(1)	23(1)	24(1)	3(1)	-1(1)	-2(1)
N1	18(1)	17(1)	27(1)	3(1)	3(1)	2(1)
O1	31(1)	22(1)	40(1)	2(1)	-6(1)	-3(1)
O2	44(1)	21(1)	50(1)	2(1)	-11(1)	-1(1)
B1	28(1)	19(1)	32(1)	2(1)	6(1)	2(1)

Table 3.4. Anisotropic displacement parameters ($Å^2 x\ 10^3$) for the structure in Figure 3.9. The anisotropic displacement factor exponent takes the form: $-2\pi^2[\ h^2 a^{*2} U^{11} + ... + 2\ h\ k\ a^*\ b^*\ U^{12}\ ]$ (Cont.).

	x	y	z	U(eq)
H3	3929	7904	7897	33
H4	5775	6748	8263	38
H5	5789	5084	7583	41
H6	3925	4555	6606	36
H7A	801	7387	6784	30
H7B	1792	8339	7172	30
H8A	573	9466	6020	44
H8B	-314	8441	5674	44
H8C	515	9094	5043	44
H9A	3789	8246	6019	26
H9B	3093	9308	6320	26
H12	3291	7142	4901	32
H13	3552	6115	3730	41
H14	3867	6915	2427	42
H15	3918	8740	2296	38
H17	3765	10537	2939	31
H19	3578	12330	3542	35
H20	3183	13416	4648	40
H21	2762	12661	5959	37
H22	2751	10841	6145	30
H1O	1240(30)	6910(30)	5386(19)	81(9)
H2O	480(40)	4220(30)	5410(20)	110(12)

Table 3.5. Hydrogen coordinates (x 10^4) and isotropic displacement parameters ($Å^2$x 10^3) for the structure in Figure 3.9.

C6-C1-C2-C3	-1.6(3)	C14-C15-C16-C17	-179.71(19)
B1-C1-C2-C3	178.36(17)	C14-C15-C16-C11	-0.1(3)
C6-C1-C2-C7	177.18(16)	C10-C11-C16-C17	1.0(3)
B1-C1-C2-C7	-2.9(3)	C12-C11-C16-C17	-178.79(17)
C1-C2-C3-C4	1.9(3)	C10-C11-C16-C15	-178.63(16)
C7-C2-C3-C4	-176.81(17)	C12-C11-C16-C15	1.6(3)
C2-C3-C4-C5	-0.3(3)	C15-C16-C17-C18	178.39(17)
C3-C4-C5-C6	-1.8(3)	C11-C16-C17-C18	-1.2(3)
C4-C5-C6-C1	2.2(3)	C16-C17-C18-C19	-179.84(17)
C2-C1-C6-C5	-0.5(3)	C16-C17-C18-C23	0.1(3)
B1-C1-C6-C5	179.60(19)	C17-C18-C19-C20	178.94(18)
C3-C2-C7-N1	108.76(18)	C23-C18-C19-C20	-1.0(3)
C1-C2-C7-N1	-70.0(2)	C18-C19-C20-C21	0.5(3)
N1-C9-C10-C11	-71.5(2)	C19-C20-C21-C22	0.2(3)
N1-C9-C10-C23	111.45(18)	C20-C21-C22-C23	-0.3(3)
C23-C10-C11-C12	-179.88(17)	C11-C10-C23-C22	178.90(16)
C9-C10-C11-C12	3.1(3)	C9-C10-C23-C22	-4.1(3)
C23-C10-C11-C16	0.3(2)	C11-C10-C23-C18	-1.4(2)
C9-C10-C11-C16	-176.75(15)	C9-C10-C23-C18	175.57(15)
C10-C11-C12-C13	177.94(17)	C21-C22-C23-C10	179.45(18)
C16-C11-C12-C13	-2.3(3)	C21-C22-C23-C18	-0.2(3)
C11-C12-C13-C14	1.4(3)	C17-C18-C23-C10	1.2(2)
C12-C13-C14-C15	0.2(3)	C19-C18-C23-C10	-178.81(16)
C13-C14-C15-C16	-0.8(3)	C17-C18-C23-C22	-179.09(16)

Table 3.6. Torsion angles [°] for the structure in Figure 3.9.

C19-C18-C23-C22	0.9(2)	C6-C1-B1-O2	33.1(3)
C2-C7-N1-C8	174.63(15)	C2-C1-B1-O2	-146.81(18)
C2-C7-N1-C9	-63.24(18)	C6-C1-B1-O1	-145.05(19)
C10-C9-N1-C8	-56.09(19)	C2-C1-B1-O1	35.0(3)
C10-C9-N1-C7	-177.06(14)		

Table 3.6. Torsion angles [°] for the structure in Figure 3.9 (Cont.).

D-H...A	d(D-H)	d(H...A)	d(D...A)	<(DHA)
O1-H1O...N1	1.00(3)	1.77(3)	2.716(2)	157(3)
O2-H2O...O1#1	1.08(4)	1.71(4)	2.789(2)	176(3)

Symmetry transformations used to generate equivalent atoms: #1 -x,-y+1,-z+1

Table 3.7. Hydrogen bonds for the structure in Figure 3.9 [Å and °].

3.12 REFERENCES

1 James, T. D.; Shinkai, S.; *Top. Curr. Chem*. **2002**, *218*, 159–200.

2 James, T. D.; Phillips, M. D.; Shinkai, S. *Boronic Acids in Saccharide Recognition*, RSC Publishing, Cambridge, **2006**.

3 James, T. D.; Sandanayake, K. R. A.; Shinkai, S. *Angew. Chem. Int. Ed*. **2003**, *35(17),* 1910-1922.

4 Jin, S.; Cheng, Y.; Reid, S.; Li, M.; Wang, B. *Med. Res. Rev*. **2010**, *30*, 171–257.

5 Hall, D. G. *Boronic Acids: Preparation and Applications in Organic Synthesis and Medicine*, Wiley-VCH, Weinheim, **2005**.

6 Wright, A. T.; Griffin, M. J.; Zhong, Z.; McCleskey, S. C.; Anslyn, E. V.; McDevitt, J. T. *Angew. Chem. Int. Ed*. **2005**, *44,* 6375–6378.

7 Zaubitzer, F.; Buryak, A.; Severin, K.; *Chem. Eur. J.* **2006**, *12*, 3928–3934.

8 Bicker, K. L.; Sun, J.; Harrell, M.; Zhang, Y.; Pena, M. M.; Thompson, P. R.; Lavigne, J. J. *Chem. Sci.* **2012**, *3*, 1147–1156.

9 Gray Jr, C. W.; Houston, T. A. *J. Org. Chem*. **2002**, *67(15),* 5426-5428.

10 Wang W.; Gao X.; Wang B. *Curr. Org. Chem*. **2002**, *6(14)*, 1285-1317.

11 Lee, J. W.; Lee, J.-S.; Chang, Y.-T. *Angew. Chem. Int. Ed*. **2006**, *45*, 6485–6487.

12 Schiller, A.; Wessling, R. A.; Singaram, B. *Angew. Chem. Int. Ed*. **2007**, *46*, 6457–6459.

13 Edwards, N. Y.; Sager, T. W.; McDevitt, J. T.; Anslyn, E. V. *J. Am. Chem. Soc*. **2007**, *129*, 13575–13583.

14 Musto, C. J.; Lim, S. H.; Suslick, K. S. *Anal. Chem*. **2009**, *81*, 6526–6533.

15 Zhang, X.; You, L.; Anslyn, E. V.; Qian, X. *Chem. Eur. J.* **2012**, *18*, 1102–1110.

16 Springsteen, G.; Wang, B. *Tetrahedron* **2002**, *58(26)*, 5291-5300.

17 Yasuda, H.; Kurokawa, T.; Fuji, Y.; Yamashita, A.; Ishibashi, S. *Biochim. Biophys. Acta* **1990**, *1021*, 114.

18 Fedoak, R. N.; Gershon, M. D.; Field, M. *Gastroenterology* **1989**, *96*, 37.

19 Mallia, A. K.; Hermanson, G. T.; Krohn, R. I.; Fujimoto, E. K.; Smith, P. K. *Anal. Lett.* **1981**, *14(8)*, 649-661.

20 Fang, H.; Kaur, G.; Wang, B. *J. Fluorescence* **2004**, *14(5)*, 481-489.

21 Yang, W.; Gao, S.; Gao, X.; Karnati, V.R.; Ni, W.; Wang, B.; Hooks, W.B.; Carson, J.; Weston, B. *Bioorg. Med. Chem. Lett*. **2002**, *12*, 2175-2177.

22 Dai, C.; Cazares, L.H.; Wang, L.; Chu, Y.; Troyer, D.A.; Semmes, O.J.; Drake, R.R. Wang, B. *Chem. Commun.* **2011**, *47*, 10338-10340.

23 Goldberg, R. N.; Tewari, Y. B. *J. Phys. Chem. Ref. Data* **1989**, *18*, 809−880.

24 Cesàro, A. *Thermodynamic Data for Biochemistry and Biotechnology*; Hinz, H. J., Ed.; Springer-Verlag: Berlin, **1986**.

25 Franks, F. *Pure Appl. Chem.* **1987**, *59*, 1189–1202.

26 Varki, A.; Cummings, R. D.; Esko, J. D. et al., editors. *Essentials of Glycobiology.* 2nd edition. Cold Spring Harbor (NY): Cold Spring Harbor Laboratory Press; **2009**.

27 Moulin, E.; Cormosw, G.; Giuseppone, N. *Chem. Soc. Rev*. **2012**, *41*,1031.

28 Lehn, J.-M. *Chem. Soc. Rev*. **2007**, *36*, 151.

29 Lehn, J.-M. *Supramolecular Chemistry: Concepts and Perspectives*; VCH: Weinheim, **1995**.

30 Rowan, S. J.; Cantrill, S. J.; Cousins, G. R. L.; Sanders, J. K. M.; Stoddart, J. F. *Angew. Chem., Int. Ed*. **2002**, *41*,898.

31 Corbett, P. T.; Vial, L.; West, K. R.; Wietor, J.-L.; Sanders, J. K. M.; Otto, S. *Chem. Rev*. **2006**, *106*, 3652.

32 Cougnon, F. B. L.; Sanders, J. K. M. *Acc. Chem. Res*., Article ASAP

33 Nagai, Y.; Kobayashi, K.; Toi, H.; Aoyama, Y. *Bull. Chem. Soc. Jpn.* **1993**, *66*, 2965−2971.

34 Huang, C. Y.; Cabell, L. A.; Anslyn, E. V. *J. Am. Chem. Soc.* **1994**, *116(7),* 2778-2792.

35 Ferrand, Y.; Crump, M. P.; Davis, A. P. *Science*, **2007**, *318(5850)*, 619-622.

36 G. Wulff; *Pure Appl. Chem.* **1982**, *54*, 2093-2102.

37 Weith, H.; Wiebers, J.; Gilham, P. *Biochem*. **1970**, *9*, 4396.

38 Lorand, J. P.; Edwards, J. O. *J. Org. Chem*. **1959**, *24(6)*, 769-774.

39 Wulff, G., Dederichs, W., Grotstollen, R., Jupe, C. *On the chemistry of binding sites, Part II: Specific binding of substances to polymers by fast and reversible covalent interactions, in Affinity Chromatography and Related Techniques*, Gribnau, T. C. J., Visser, J., Nivard, R. J. F., Eds., Elsevier, Amsterdam, **1982**.

40 Wulff, G.; Lauer, M.; Böhnke, H. *Angew. Chem. Int. Ed*. **1984**, *23(9)*, 741–742.

41 Xing, Z.; Wang, H. C.; Cheng, Y.; Zhu, C.; James, T. D.; Zhao, J. *Eur. J. Org. Chem.* **2012**, *6*, 1223-1229.

42 Li, H.; Liu, Y.; Liu, J.; Liu, Z. *Chem. Commun*. **2011**, *47(28)*, 8169-8171.

43 Kitamura, M.; Suzuki, T.; Abe, R.; Ueno, T.; Aoki, S. *Inorg. Chem.* **2011**, *50(22)*, 11568-11580.

44 James, T. D.; Sandanayake, K. R. A. S.; Shinkai, S. J. Chem. Soc., Chem. Commun. **1994**, 477.

45 James, T. D.; Sandanayake, K. R. A. S.; Shinkai, S. *Angew. Chem. Int. Ed*. **1994**, *33*, 2207.

46 James, T. D.; Sandanayake, K. R. A. S.; Shinkai, S. *Nature* **1995**, *374*, 345.

47 James, T. D.; Linnane, P.; Shinkai, S. *Chem. Commun*. **1996**, *3*, 281-288.

48 Nöth, H.; Wrackmeyer, B. *Nuclear Magnetic Resonance Spectroscopy of Boron Compounds*, Springer-Verlag: Berlin, **1978**. .

49 James, T. D. *Top. Curr. Chem*. **2007**, *277*, 107-152.

50 de Silva, A. P.; Gunnlaugsson, T.; Rice, T. E. *Analyst*, **1996**, *121(12)*, 1759-1762.

51 Bissell, R.; Prasanna de Silva, A.; Nimal Gunaratne, H.; Mark Lynch, P.; Maguire, G.; McCoy, C.; Samankumara Sandanayake, K. *Top. Curr. Chem*. **1993**, *168*, 223-264.

52 Franzen, S.; Ni, W.; Wang, B. *J. Phys. Chem. B* **2003**, *107*, 12942−12948.

53 Ni, W.; Kaur, G.; Springsteen, G.; Wang, B.; Franzen, S. *Bioorg. Chem.* **2004**, *32*, 571−581.

54 Springsteen, G.; Deeter, S.; Gao, X.; Wang, B. *Tetrahedron*, **2002**, *58*, 5291–5300.

55 Cooper, C. R.; James, T. D. *Chem. Lett* **1998**, 883–884.

56 Chaberek, S.; Courtney, R. C.; Martell, A. E. *J. Am. Chem. Soc*. **1952**, *74*, 5057.

57 Wiskur, S.L.; Lavigne, J.J.; Ait-Haddou, H.; Lynch, V.; Chiu, Y.H.; Canary, J.W.; Anslyn, E.V. *Org. Lett*., **2001**, *3*, 1311-1314.

58 Lavigne, J. J.; Anslyn, E. V. *Angew. Chem., Int. Ed.* **1999**, *38(24)*, 3666-3669.

59 Zhu, L.; Shabbir, S.H.; Gray, M.; Lynch, V.M.; Sorey, S.; Anslyn, E.V. *J. Am. Chem. Soc.* **2006**, *128*, 1222-1232.

60 Larkin, J.D.; Fossey, J.S.; James, T.D.; Brooks, B.R.; Bock, C.W. *J. Phys. Chem. A* **2010**, *114*, 12531-12539.

61 Norrild, J. C.; Eggert, H. *J. Chem. Soc., Perkin Trans. 2*, **1996**, *12*, 2583-2588.

62 Bielecki, M.; Eggert, H.; Norrild, J. C. *J. Chem. Soc., Perkin Trans. 2*, **1999**, *3*, 449-456.

63 Matsumura, T.; Iwatsuki, S.; Ishihara, K. *Inorg. Chem. Commun*. **2005**, *8(8),* 713-716.

64 Collins, B. E.; Metola, P.; Anslyn, E. V. *Supramol. Chem.* **2013**, *25(2)*, 79-86.

65 Anslyn, E. V.; Dougherty, D. A. Chapter 11. *Modern physical organic chemistry*. University Science Books. **2006**.

66 Collins, B. E.; Sorey, S.; Hargrove, A. E.; Shabbir, S. H.; Lynch, V. M.; Anslyn, E. V. *J. Org. Chem.* **2009** *74(11)*, 4055-4060.

Chapter 4: Circular Dichroism of Multi-Component Assemblies for Chiral Amine Recognition and Rapid *Ee* Determination

4.1 INTRODUCTION

The traditional method for obtaining and optimizing asymmetric catalysis is characterized by a trial and error process. A potential catalyst is synthesized, its efficiency evaluated, and the results used to redesign the original compound. This process undergoes iterative cycles until a satisfactory degree of selectivity in the products is obtained.[1-3] The current industry standard techniques for analysis of chiral products are chiral HPLC and GC.[4-8] Although these chromatographic methods provide highly accurate values of enantiomeric excess (*ee*), they are not easily amenable to rapid screening of hundreds to thousands of reactions. Using these techniques, the analysis of the *ee* becomes a rate-limiting process when such large numbers of reactions are considered. In contrast, optical techniques are in general simple, affordable, and fast.[9-13] Therefore, exploiting optical techniques for the aforementioned purpose has the potential to allow rapid and inexpensive screening of large numbers of asymmetric reactions, hastening the optimization of reaction conditions and catalyst structure.

4.1.1 Chiral Primary Amines

Both pharmaceutical and agricultural chemists employ α-chiral amines as versatile building blocks and intermediates in the synthesis of target products.[14] Methods

for the preparation of chiral amines continue to be developed, with chiral transition metal catalysts often being used for the enantioselective hydrogenation of imines.[15-20] It is for these types of transformations that an improvement in efficiency could be derived directly from the application of simple and rapid methods for the analysis of the enantiopurity of α-chiral primary amines.

4.1.2 Circular Dichroism and Previous Efforts

Circular dichroism (CD) is a spectroscopic technique that measures the difference in absorbance between left- and right-circularly polarized light upon interaction with a sample.[21] Due to the inherent chirality of circularly polarized light, its interaction with different enantiomers will lead to asymmetric electronic transitions, allowing for the differentiation between said enantiomers. Exciton coupled circular dichroism (ECCD) is a particular CD method that takes advantage of the phenomenon that is present when two chromophores that are in proximity to each other and asymmetrically oriented.[21] This situation leads to a coupling of the transition states of the two chromophores and translates into a signal in CD. This method can be used quite effectively to assign absolute configurations, as the sign of this signal (also called the Cotton effect) can be related to the dihedral angle between the two groups: positive dihedral angles producing positive values of CD as one goes from higher to lower wavelengths and vice versa (Fig. 4.1).

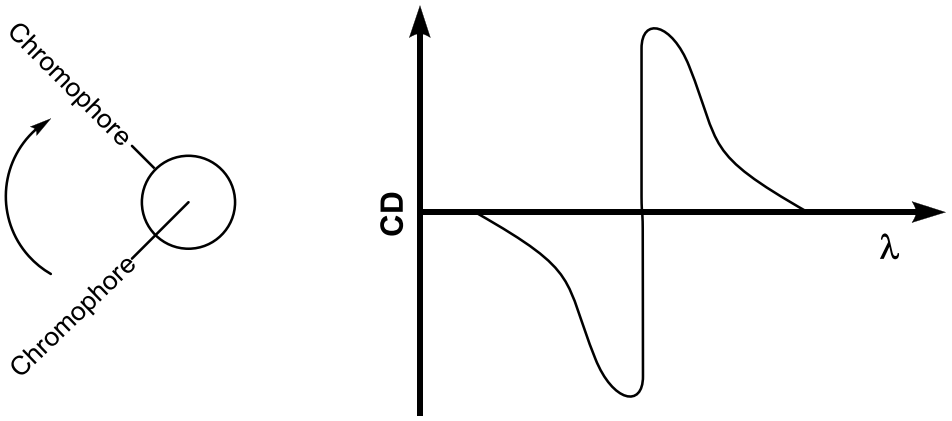

Figure 4.1. Positive dihedral angle between chromophores translates into a positive Cotton effect for an ECCD couplet.

CD is also suited for *ee* analysis since it relies on the chirality of the light source and does not necessarily require a chiral derivatization step (i.e. chiral shift reagents in NMR spectroscopy). The fact that it is an optical technique makes it even more alluring for the purposes of designing rapid *ee* determination methods.

Our group has recently published a method for the analysis of *ee* and total concentration of α-chiral amines in which the target amine is converted into a diimine **4.3**, that when complexed with chiral Cu(I) host **4.1** gives a distinctive signal change in CD (Scheme 4.1).[22] This method, however, has several limitations: a derivatization step that can take up to two hours, a low signal intensity, short wavelengths for λ_{max} values, and the requirement of a preformed metal-complex host. It was thus evident that room for improvement was still possible, and one approach to devise a better system is described herein.

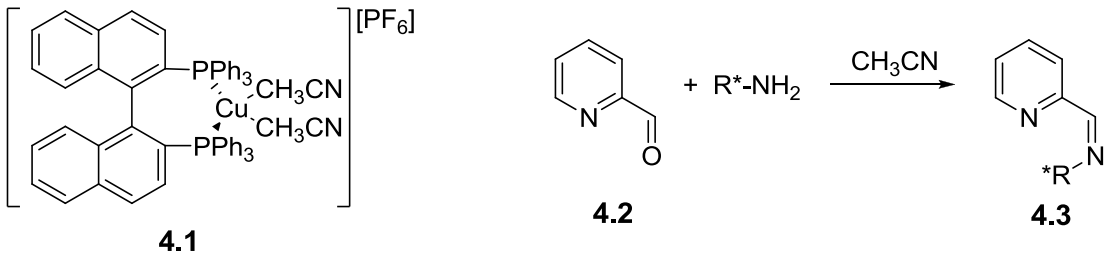

Scheme 4.1. Host employed as receptor and derivatization reaction for primary amines to form the Schiff base guests.

4.1.3 Derivatization Reaction and Initial Hypothesis

While pursuing the goal mentioned above our interest was piqued by an assembly process studied by the Bull and James groups.[23,24] As has been explained in chapter 2, in the Bull-James system an α-chiral primary amine, *o*-formyl phenylboronic acid (**FPBA**), and enantiopure 1,1'-bi-2-naphthol (**BINOL**) assemble rapidly upon mixing. This leads to characteristic ^{1}H NMR spectroscopic shifts for each enantiomer of the amine, as the reaction produces diastereomers that can be differentiated through NMR spectroscopy (Scheme 4.2). This system has also been used for electrochemical *ee* determination: the sensor can be made redox-active thanks to the introduction of a ferrocene unit.[25]

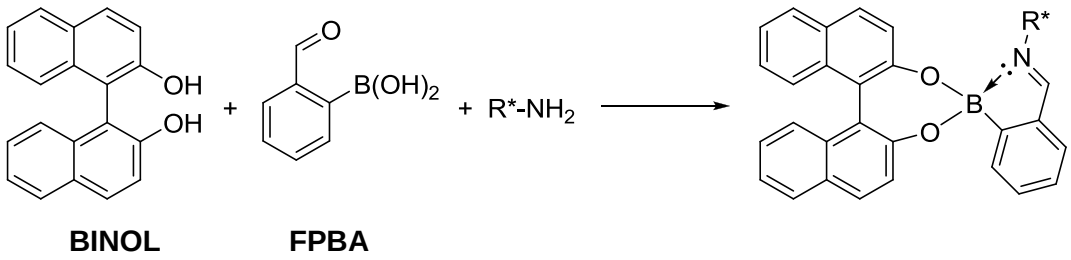

Scheme 4.2. Assembly developed by the Bull and James groups.

We hypothesized that upon formation of the assembly the twist angle of **BINOL** would be altered, which in turn would translate into a modulated ECCD signal that could be monitored through CD spectroscopy. Alternatively, formation of an imine-coordinated boronate ester could give rise to an induced CD signal by virtue of the chiral derivatization of the aryl boronic acid. Working with these postulates, we set up a series of experiments using several different **BINOL** derivatives as host for the analysis of α-chiral primary amines (Fig. 4.2). Having a collection of hosts readily available through this fast three-component assembly would allow us to utilize chemometric tools such as principal component analysis (PCA) and linear discriminant analysis (LDA) to process the data collected. The fact that CD spectroscopy, especially in combination with a plate loader, is able to perform rapid analysis, coupled with the speed of the assembly reaction and its relative simplicity, made the proposed system a promising approach.

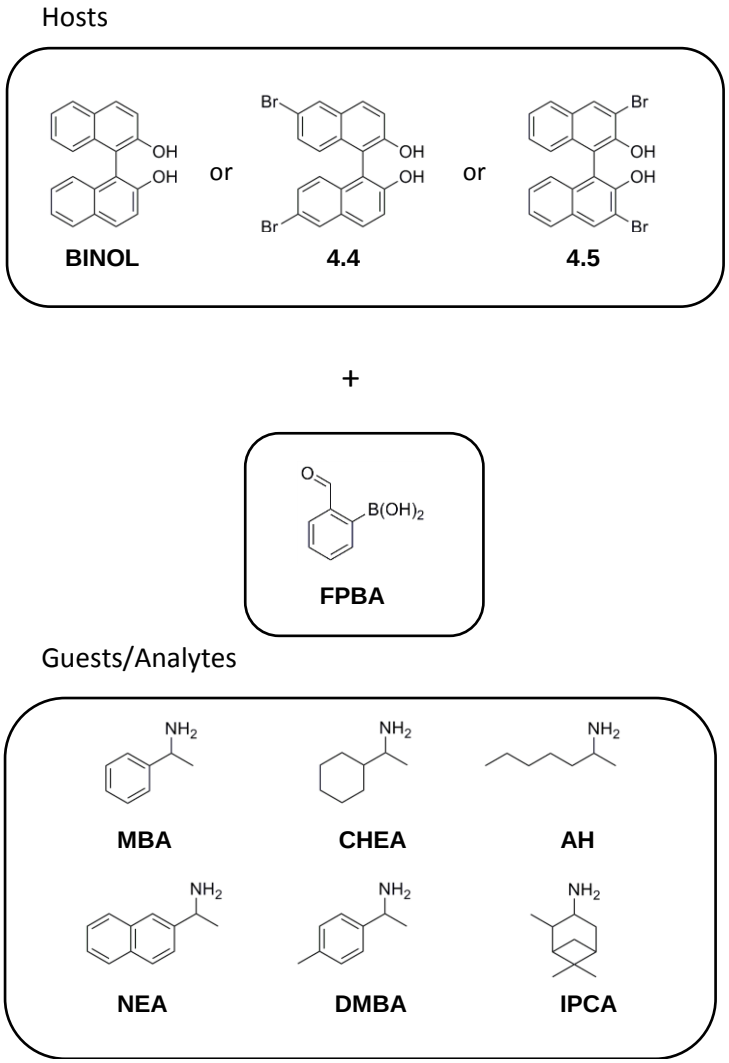

Figure 4.2. Structures of the compounds used as hosts and guests/analytes.

4.2 RESULTS AND DISCUSSION

4.2.1 CD Titrations

The Bull-James ^{1}H-NMR chiral shift protocol was originally carried out in chloroform. In order to obtain a satisfactory CD response upon assembly, the procedure was transitioned to acetonitrile because its spectral cut-off point at 195 nm makes acetonitrile a more suitable solvent for CD spectroscopy than chloroform. Further, the assembly was simultaneously confirmed in acetonitrile by ^{1}H-NMR spectroscopy. The CD tests using equimolecular amounts of (*S*)-**BINOL** and **FPBA** (this combination herein referred to as the "host"), along with an equivalent of α–methyl benzylamine (**MBA**) relative to **FPBA** (Fig. 4.3A) showed a difference in the signal with (*R*)- or (*S*)-**MBA** upon assembly. In contrast, no CD signal modulation occurs when only (*S*)-**BINOL** is combined with **FPBA** ("*S*-Host"), indicating that there is either no condensation or that the torsion angle of (*S*)-**BINOL** is not modified to a significant extent when condensation occurs. The effect of the two enantiomers of **MBA** on the (*S*)-**BINOL** CD signal between 250 and 270 nm occurs in opposite directions, which could mean that the chirality of the amine induces twists in the dihedral angle of (*S*)-**BINOL** in opposite directions. Alternatively, the CD spectra of enantiomeric imine coordinated boronic acids would add or substract from the **BINOL** CD spectra if the two spectra overlapped. When using the enantimeric host (*R*)-**BINOL** (Fig. 4.3B) in an analogous experiment the changes in the signal are of the same intensity as with (*S*)-**BINOL**, but in

opposite sign. This confirms the expected behaviour of a symmetrical system.

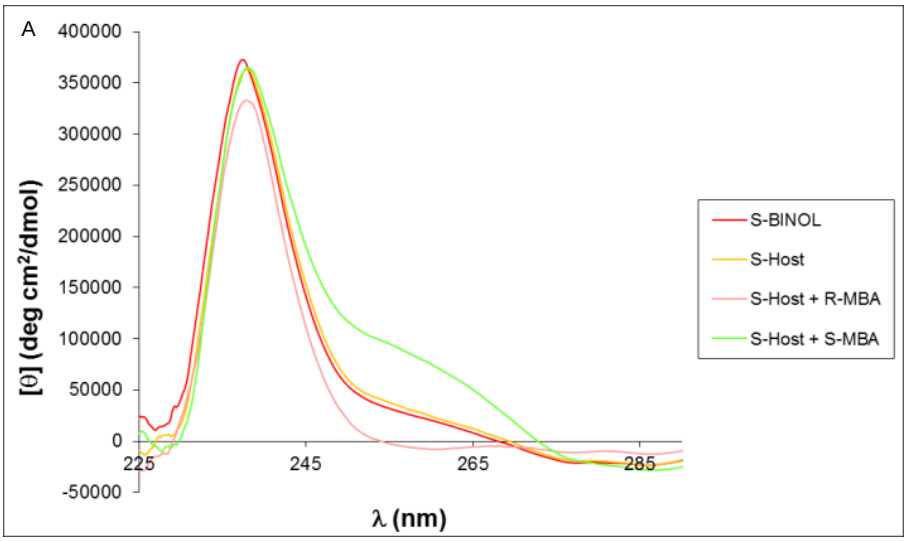

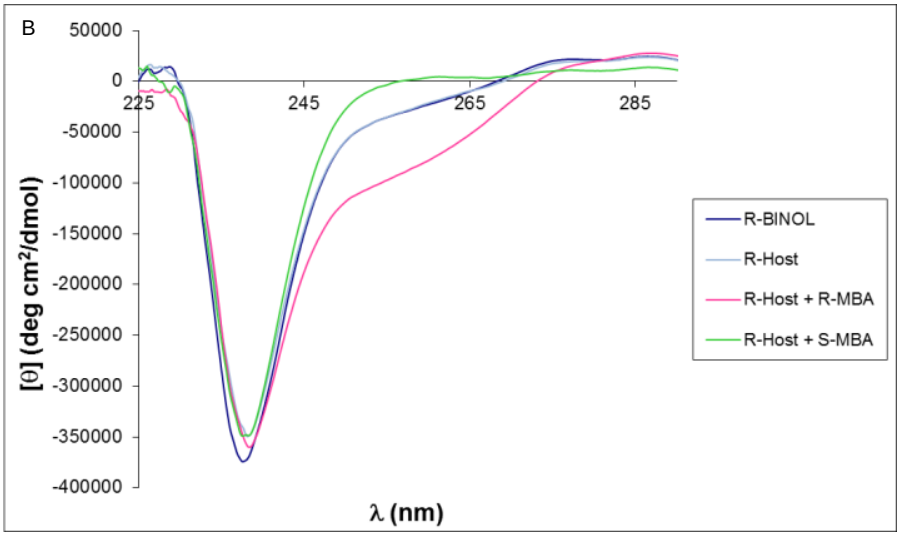

Figure 4.3. A) CD spectra of the assembly with (*S*)-**BINOL**, B) CD spectra of the assembly with (*R*)-**BINOL**.

With these simple CD studies serving as a proof of principle, we next decided to

carry out CD titrations to determine the stoichiometry of the assembly reaction (Fig. 4.4A and 4.2B). The wavelength chosen for these titrations was 253 nm, since it consistently showed the greatest difference in signal between the (*R*)- and (*S*)-amines (i.e. 98941 deg*cm^2/dmol for the case of (*R*)- and (*S*)-**MBA**). As expected, the reaction reaches saturation when one equivalent of the amine is added to an equimolar mixture of **BINOL** and **FPBA**.

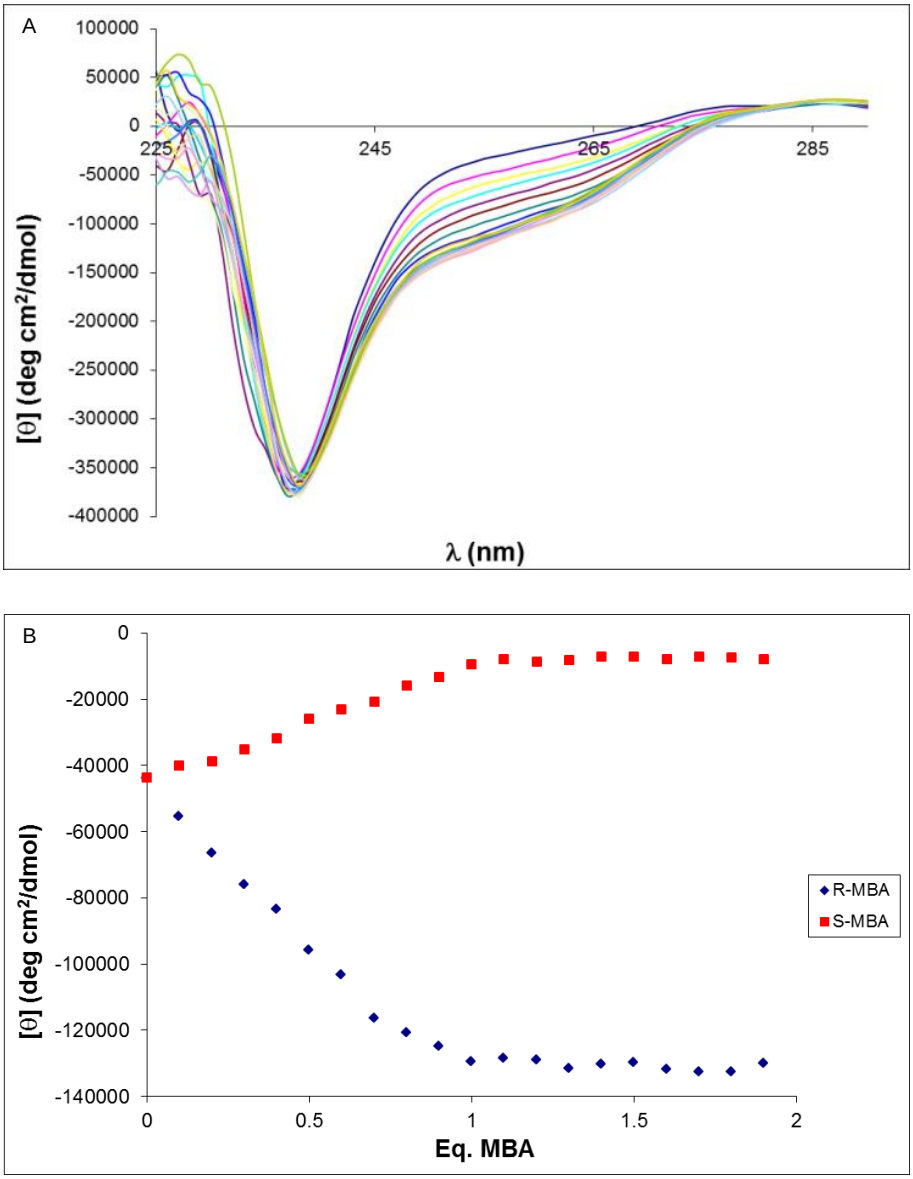

Figure 4.4. A) CD spectra for the titration of (*R*)-**MBA** into (*R*)-**BINOL**, B) CD titration. of (*R*)- and (*S*)-**MBA** into (*R*)-**BINOL**.

Upon examination of these results, it seemed evident that the signal that appears after completion of the assembly (between 250 nm and 265 nm) did not correspond to a significant variation in the twist angle of **BINOL** (whose characteristic Cotton Effect signal shows at around 240 nm[26] and modulates only slightly when the other two components are added). Molecular modelling experiments using Spartan confirmed that the dihedral angle of **BINOL** experienced no distortion in the product of assembly. We therefore concluded that the arising signal at 250 nm could be due to the aromatic ring in **FPBA** becoming CD-active upon formation of the imine-coordinated boronate ester. A simple CD experiment in which **FPBA** was combined with an equimolecular amount of (*R*)-**MBA** confirmed this second hypothesis when a signal with the expected negative sign appeared around 250 nm (Fig. 4.5).

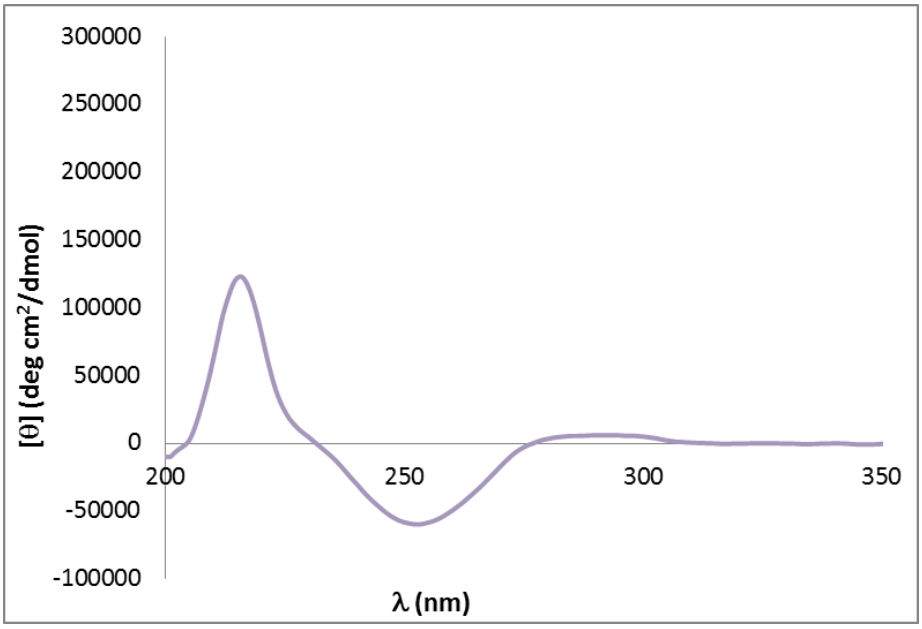

Figure 4.5. CD spectrum for an equimolecular mixture of **FPBA** and (*R*)-**MBA**.

4.2.2 A Chemo- and Enantioselective Differential Array

Once the assembly was found to differentiate the enantiomers of **MBA** *via* CD and the origin of the signal created was well understood, we sought to test the general utility by varying analytes and hosts. A series of commercially available α-chiral primary amines was used to explore the viability and limitations: cyclohexylethylamine (**CHEA**), 2-aminoheptane (**AH**), 1-(1-naphthyl)-ethylamine (**NEA**), α,4-dimethylbenzylamine (**DMBA**), and isopinocampheylamine (**IPCA**). These analytes were chosen to include a variety of α-primary amine structures; from those containing linear aliphatic substituents to others with aromatic groups attached to the stereocenter of the amine. The assembly reaction with these guests was verified *via* ^{1}H NMR spectroscopy at one equivalent of amine, and the CD spectra showed responses similar to **MBA** although with intensity and shape differences (See Experimental Section).

With the goal of obtaining an assembly that would provide amine and chirality differentiation, we tested the reaction with a collection of **BINOL** analogues. The ^{1}H-NMR spectroscopy tests showed that for **4.4** and **4.5** the assembly went to completion with one equivalent of the amine, while **4.6** proved too sterically constrained to lead to assembly.

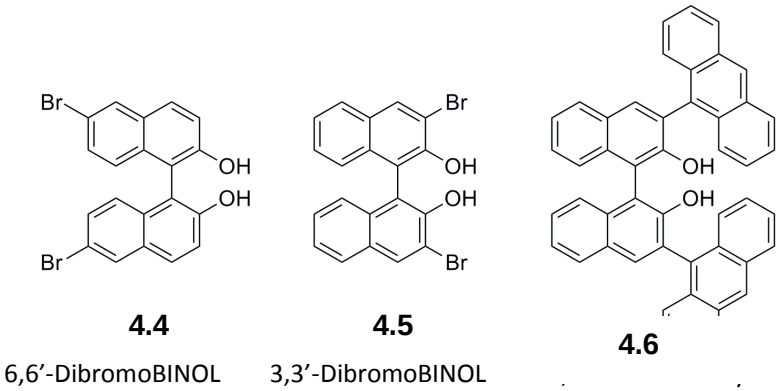

4.4 6,6′-DibromoBINOL

4.5 3,3′-DibromoBINOL

4.6

Figure 4.6. **BINOL** analogues tested.

For the case of **4.4**, the CD spectra have a distinctive shape pattern different from the one assigned to the assemblies with regular **BINOL** (Fig. 4.7), which adds variance to the system. This further variance meant a series of sensing units utilizing BINOL analogues could form an array to provide a deeper level of amine differentiation. The presence of the bromine atoms in the naphthalenic rings of this **BINOL** analogue are believed to cause the signal that appeared around 255 nm in the case of regular **BINOL** to shift towards longer wavelengths, be it by virtue of a resonance or inductive effect.

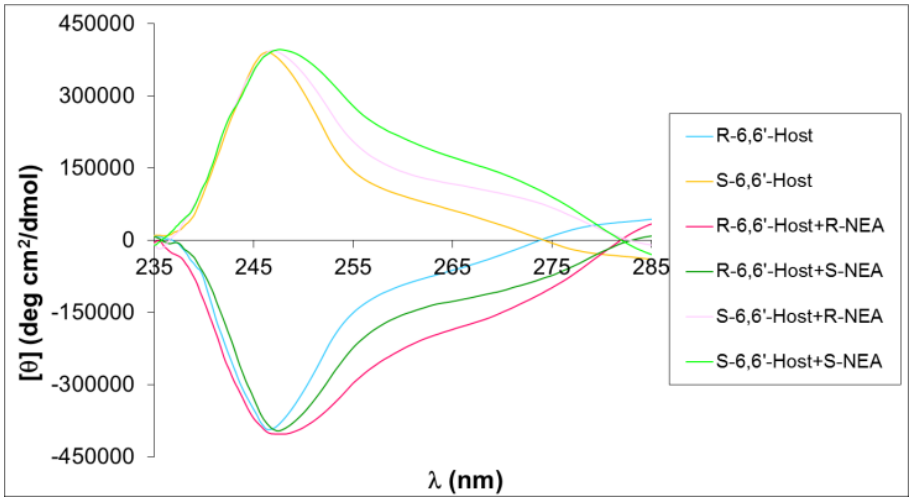

Figure 4.7. CD spectra for the assembly of **4.4**, **FPBA** and **NEA**.

When **4.5** was used in the assembly the signal for the **BINOL** moiety is greatly increased (Fig. 4.8). A plausible explanation for this phenomenon could be that the two bromine substituents in positions 3 and 3' are bulky enough and close enough to the two hydroxyl groups in 2 and 2' that completion of the assembly reaction does indeed cause a distortion between the two naphthalenic rings in accordance with our original hypothesis.

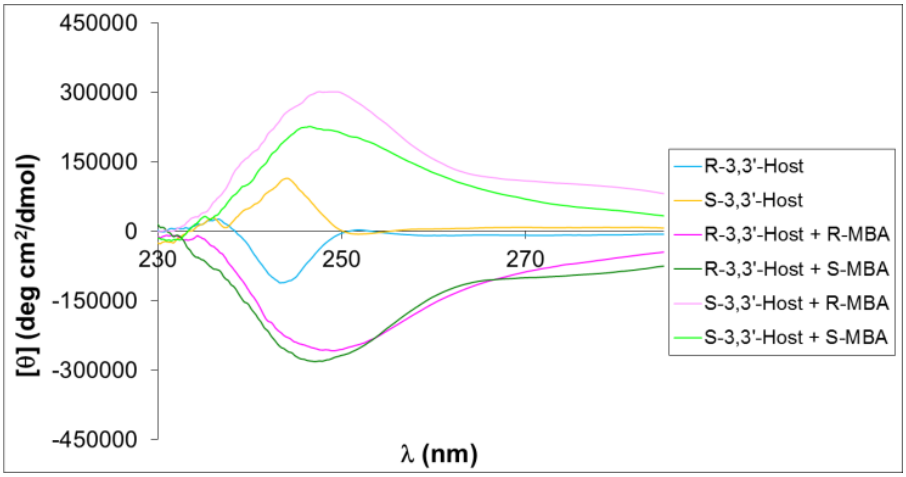

Figure 4.8. CD spectra for the assembly of **4.5**, **FPBA**, and **MBA**.

With an array of sensors in hand that give different signals for the amine analytes, it was possible to gather data to discriminate them based on their identities and handedness. The data generated with a series of receptors is often processed using supervised and unsupervised statistical analysis tools. In order to analyze the data obtained using the combination of our three sensors and six analytes we employed two different chemometric tools: principal component analysis and linear discriminant analysis.

Principal component analysis (PCA) is an unsupervised technique (meaning the data is entered without a previous identification step) that is used to reduce the dimensionality of the data space. It achieves this by employing linear algebra to create a number of orthogonal axes called components that represent decreasing extents of variance within the system. The first component is responsible for the most variance, the second component has the next most variance, and so forth.[27,28] The data gathered for these analyses came from equimolecular mixtures of all the amines, **FPBA**, and three **BINOL**s: (*R*)-**BINOL**, (*S*)-**4.4**, and (*R*)-**4.5**. All experiments where repeated 5 times to ensure reproducibility and the signal at three different wavelengths for each **BINOL** analogue was recorded. The different amines showed effective separation of all like groups (Fig. 4.9). All the *R* enantiomers were located on the left half of the graph with respect to F1 with all the *S* enantiomers on the right side; the only outlier being **AH**. On the basis of these observations, discrimination of these analytes based on absolute configuration is possible. Further, PCA finds that the system can also separate the amines based on their identity, with those containing aromatic rings as substituents appearing

separated from those with aliphatic groups due to greater modulation in the intensity of the CD signals. In fact, upon further inspection of the 2D PCA graphs it can be determined that the main component corresponds to chirality, with F2 and F3 representing variance amongst amines with aromatic and aliphatic groups (See Experimental Section).

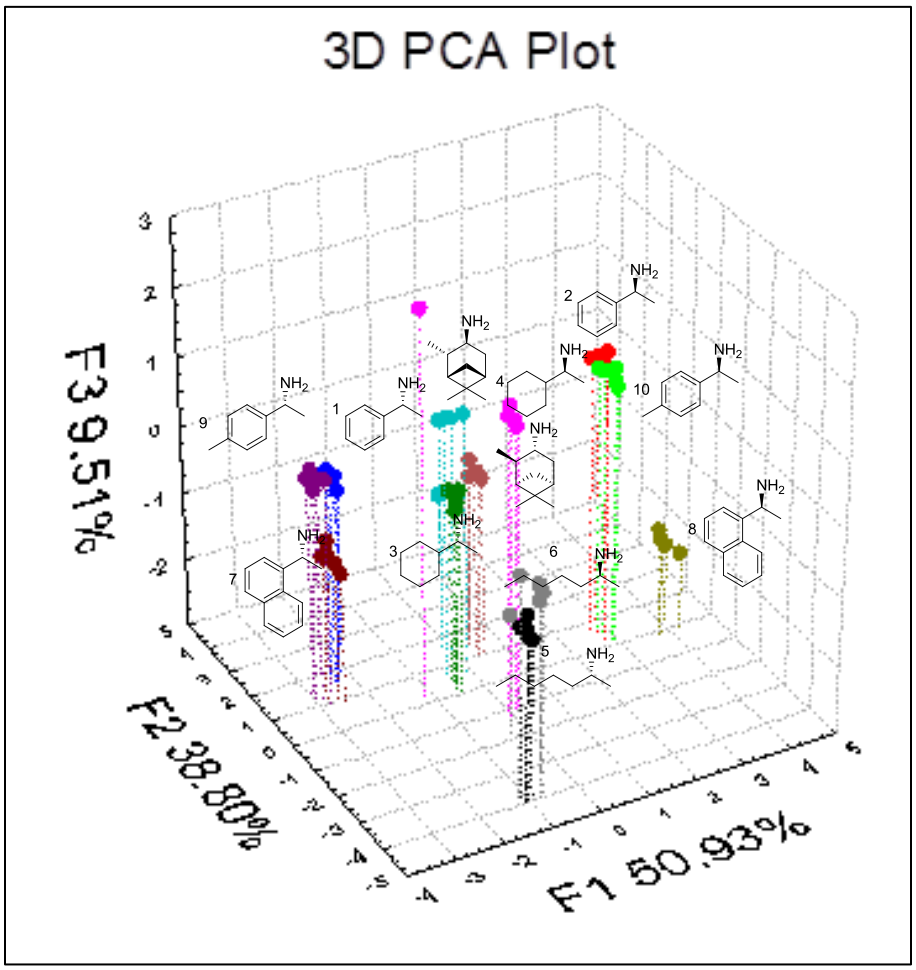

Figure 4.9. Principal component analysis plot.

Linear discriminant analysis (LDA) is another technique we used to process this data. This technique creates a series of linear equations that maximize the separation between different classes of analytes and minimize the separation within those classes. This is known as a supervised technique, in that it requires that the analytes be assigned to a particular group before starting the analysis.[29]

Using the same conditions and data space collected for the PCA case, the LDA plot showed tight clustering of each group, a visual indicator that the system was able to discriminate α–chiral primary amines both chemo- and enantioselectively (Fig. 4.10). It is also important to point out the fact that this chemometric tool provides a clear graphic differentiation between enantiomers (along horizontal axis) indicating that clusters are formed mostly based on chirality. In order to assess the predictive power of this LDA study, a jackknife analysis test was performed and showed 100% predictive power. In this type of self-evaluation tool, the program leaves out one data point while the rest of the data space is used to create a classification system. The excluded point is then assigned to a group using the system created. This process is repeated for every data point and the overall outcome translated into a confidence level. A score of 100% in the jackknife analysis indicates that our system, thanks to the incorporation of three different sensing assemblies and taking into account the shape of the signal (by using readings at three separate wavelengths for each ensemble) can effectively identify and classify the target amines.

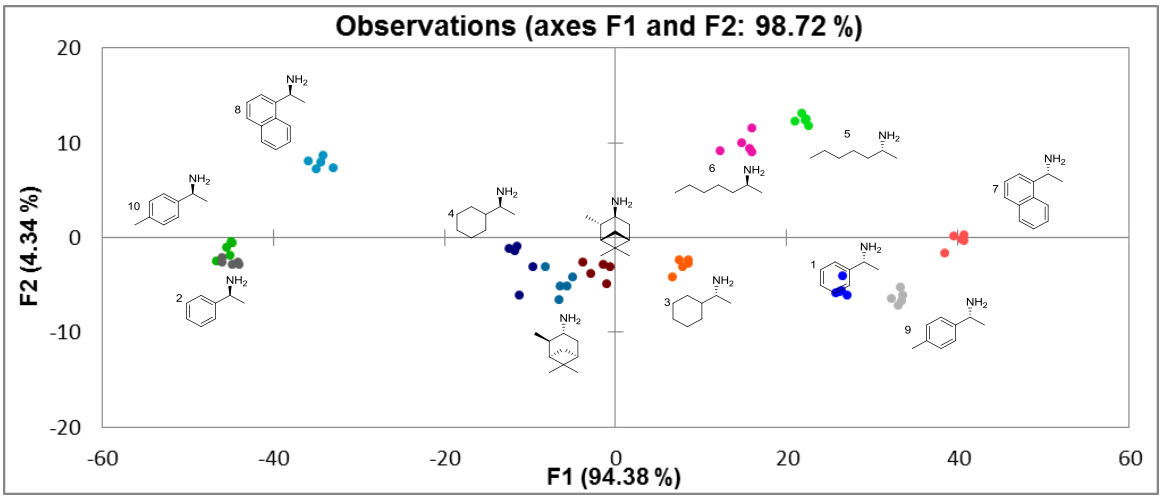

Figure 4.10. Linear discriminant analysis plot.

4.2.3 *Ee* Determination

As mentioned in the introduction, one goal of this project was to improve our previous primary amine *ee* analysis system. In order to determine *ee* with the approach discussed here a calibration curve was obtained by plotting the CD readings of a series of samples of known enantiomeric composition versus their *ee* values using (*R*)-**BINOL**, **FPBA** and **MBA** (Scheme 4.3), and employing 5 replicates of each data point for reproducibility purposes (Fig. 4.11). Once a linear equation was fit to the data a number of "unknown" samples were analyzed using the system. The *ee* results obtained using the sensor were then compared to the actual values (known from mixing commercially available enantiopure amines), with an average absolute error of 5.8% (Table 4.1). The

greatest errors that we encountered corresponded to samples with low *ee* values. These low *ee* values are of the least practical importance when trying to optimize performance of asymmetric catalysts.

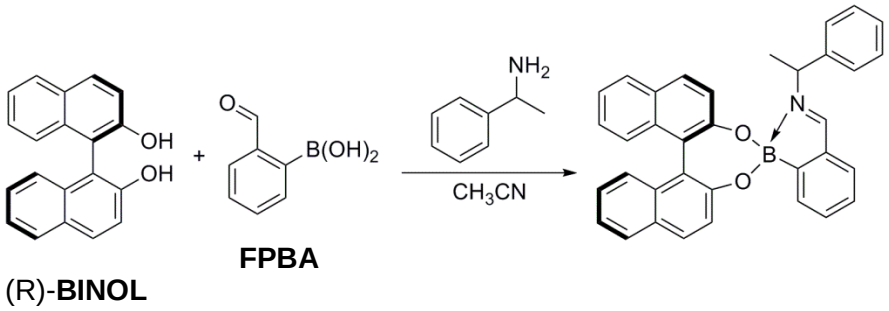

Scheme 4.3. Reaction used for calibration curve.

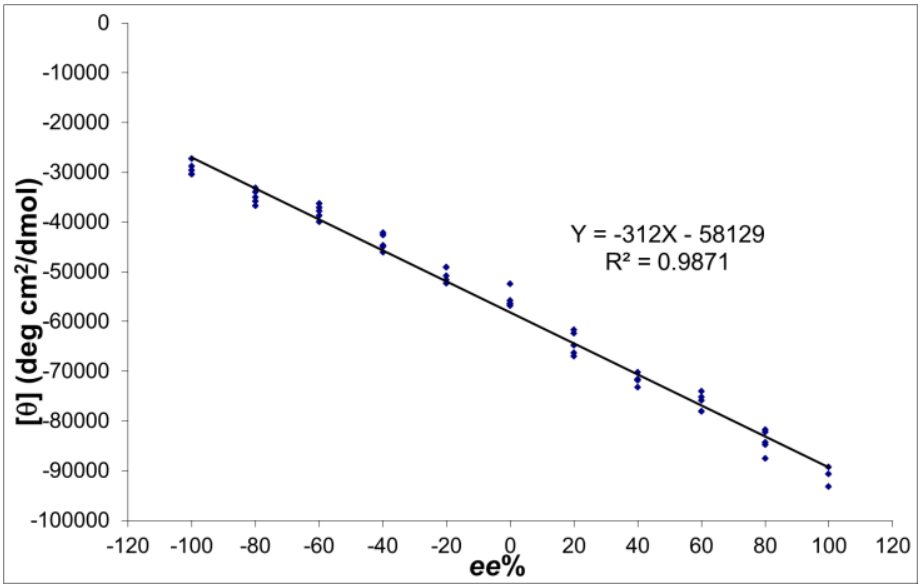

Figure 4.11. Calibration curve for **MBA**.

Sample	Real *ee*%	Calculated *ee*%
1	-10	-1.5
2	30	36.3
3	-70	-62.3
4	80	78.2
5	-50	-48.6

Table 4.1. Comparison of the results for *ee*% determination.

It is also noteworthy that the assembly only takes around 10 minutes to achieve completion and can be run in parallel for all unknowns. Another advantageous property of this system is the fact that as long as the saturation point (1 equivalent; Fig. 4.4B) is reached, the concentration of amine has no influence on the *ee* analysis. Finally, the analysis step takes about 3 minutes per sample, which effectively places this method in the realm of very rapid analysis.

4.3 CONCLUSIONS

We have described a technique that discriminates α-chiral primary amines based on chemical identity and chirality. This system is also able to determine *ee* for amine samples of unknown enantioenrichment. Using the optical technique of circular dichroism spectroscopy, an array of sensing ensembles was easily obtained by taking

advantage of the one-step, fast, and simple three-component assembly of the target amine with enantiopure **BINOL**s and an achiral boronic acid. The variance of the optical data when processed by the statistical analysis techniques of LDA and PCA allows fingerprinting of the amines both chemo- and enantioselectively. We have also proven that the system could be used to determine the *ee* of the parent amines with high accuracy, in reasonably short amount of time, while using relatively cheap commercially available materials.

4.4 Experimental Details

4.4.1 Materials and Methods

All reagents and solvents were used as purchased from commercial sources. Software used to carry out principal component analysis (PCA) and linear discriminant analysis (LDA) studies was XLSTAT 2011. ^{1}H NMR spectra were recorded on a Varian Mercury 400 MHz spectrometer. All CD measurements were performed at 25°C on a Jasco J-815 circular dichroism spectropolarimeter using a quartz cuvette of 0.1 cm light path.

4.4.2 Experimental Procedures for CD Spectra

4 mM stock solutions of **FPBA**, **BINOL** and derivatives and all α-chiral primary amines (**MBA**, **CHEA**, **AH**, **NEA**, **DMBA**, and **IPCA**) were prepared by stirring the appropriate mass or volume in HPLC grade acetonitrile. All CD spectra were collected after a dilution step to make all samples 0.4 mM, with the 3-component assembly being prepared by mixing 100μL of the **FPBA**, **BINOL**-type species and amine stock solutions and adding HPLC grade acetonitrile until achieving a volume of 1mL for each sample. Prior to each use, the CD instrument was purged with nitrogen for 20 min. Spectra were collected between 200 and 500 nm with a standard sensitivity of 100 mdeg, a data pitch of 0.5 nm, a band width of 0.5 nm, a scanning speed of 1000 nm s^{-1} and a response of 0.5 s. The titration experiments were performed by measuring the CD signal for a collection of samples of 0.4 mM in **FPBA** and **BINOL** and varying concentrations of the amine. The solutions of known *ee*% were prepared by mixing the appropriate amounts of enantiopure amines and the *ee*% values used for the final error determination calculated accordingly.

4.4.3 Characterization data

(*S*)-BINOL + FPBA + (*R*)-AH assembly product: ^{1}H-NMR (400MHz, $CDCl_3$) δ 8.8 (s, 1H), 8.5 (d, 2H), 8.1 (d, 2H), 7.9 (m, 3H), 7.6 (m, 7H), 7.1 (d, 2H), 3.4 (m, 1H), 1.7 (m, 2H), 1.4 (m, 5H), 1.3 (m, 4H), 0.9 (t, 3H); *m/z* (ESI-MS) 495.5 $[M]^+$.

(*S*)-4.4 + FPBA + (*S*)-CHEA assembly product: ^{1}H-NMR (400MHz, $CDCl_3$) δ 8.7 (s, 1H), 8.1 (d, 2H), 7.8 (m, 5H), 7.7 (d, 2H), 7.5 (m, 3H), 7.1 (d, 2H), 3.3 (m, 1H), 1.5 (m, 11H), 1.3 (d, 3H); *m/z* (ESI-MS) 667.0 $[M]^{+}$.

4.4.4 Additional CD Spectra for Assembly and PCA graphs

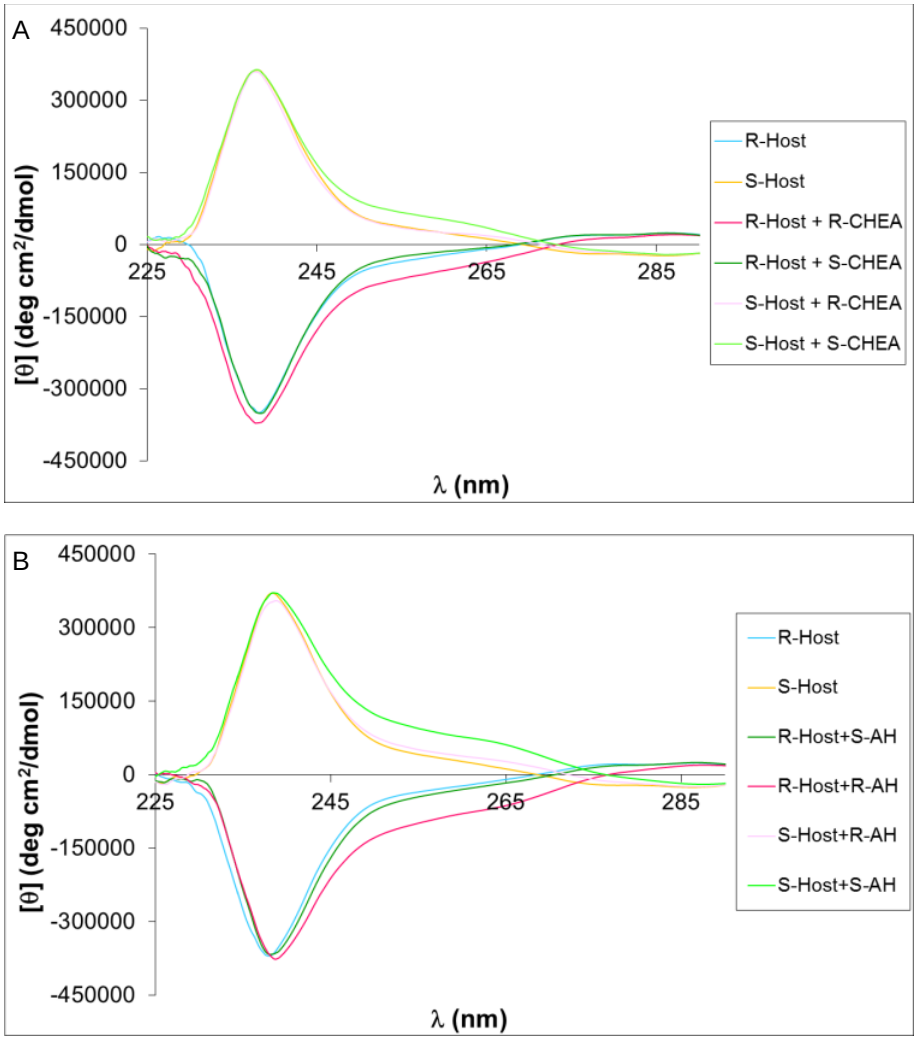

Figure 4.12. CD spectra for the assembly of **BINOL**, **FPBA** and A) **CHEA**, B) **AH**, C) **NEA**, D) **DMBA** and E) **IPCA**.

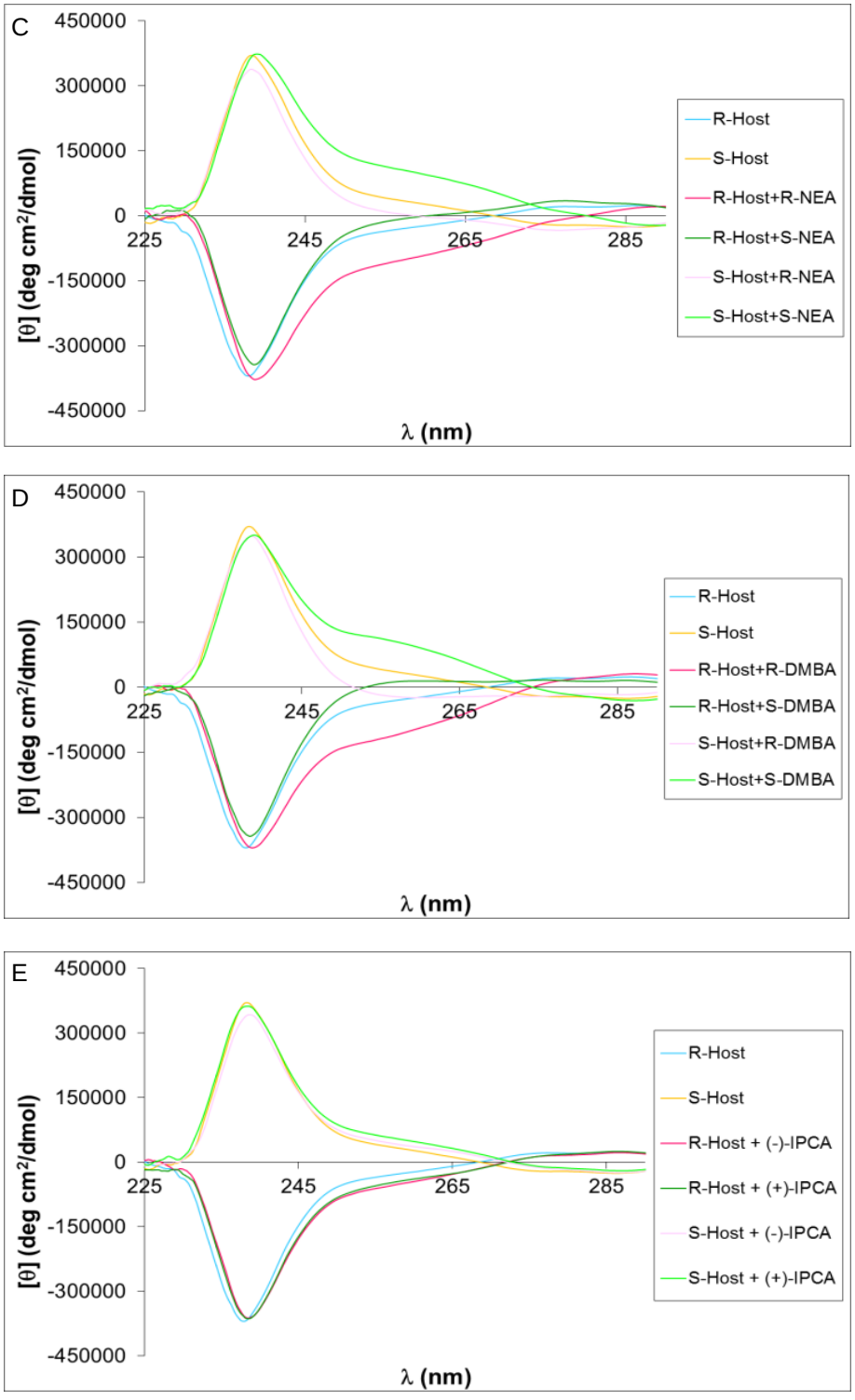

Figure 4.12. CD spectra for the assembly of **BINOL**, **FPBA** and A) **CHEA**, B) **AH**, C) **NEA**, D) **DMBA** and E) **IPCA** (Cont.).

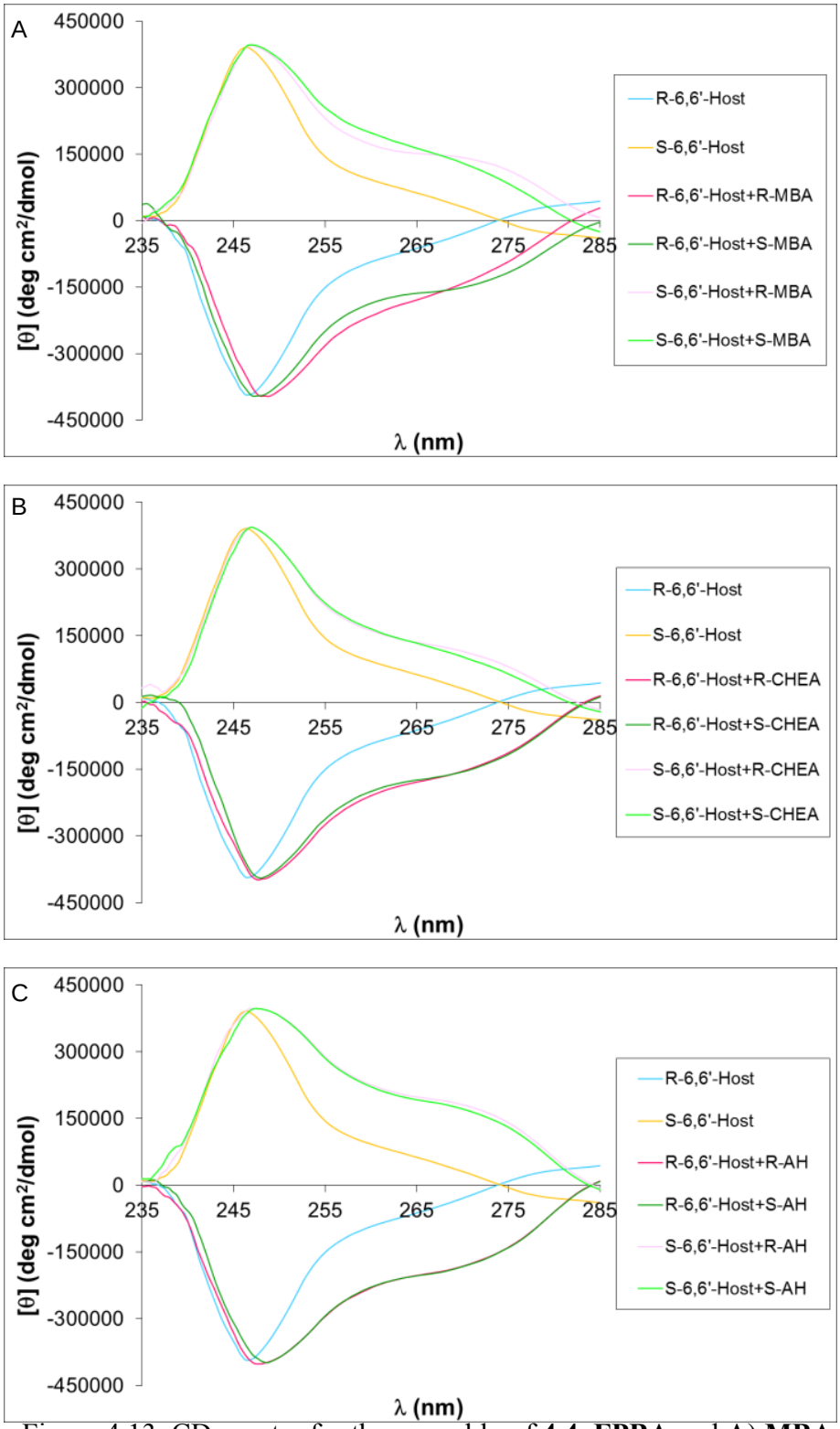

Figure 4.13. CD spectra for the assembly of **4.4**, **FPBA** and A) **MBA**, B) **CHEA**, C) **AH**, D) **DMBA** and E) **IPCA**.

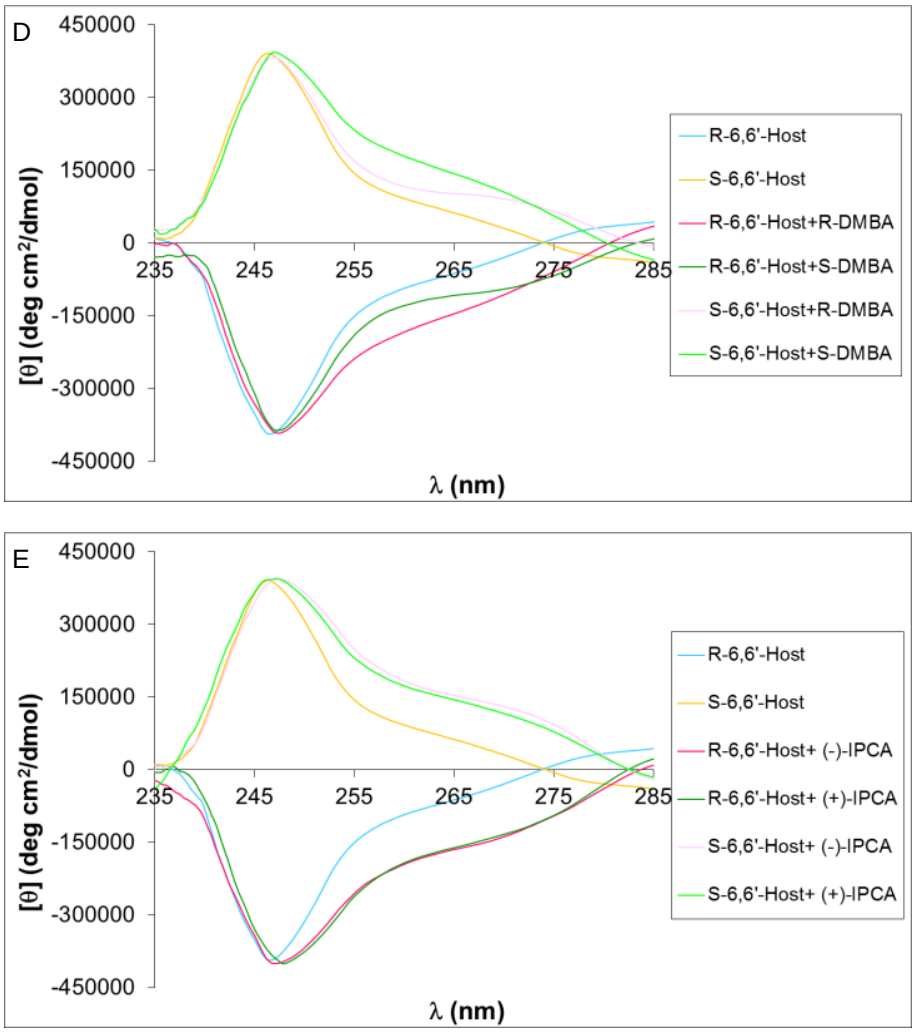

Figure 4.13. CD spectra for the assembly of **4.4**, **FPBA** and A) **MBA**, B) **CHEA**, C) **AH**, D) **DMBA** and E) **IPCA** (Cont.).

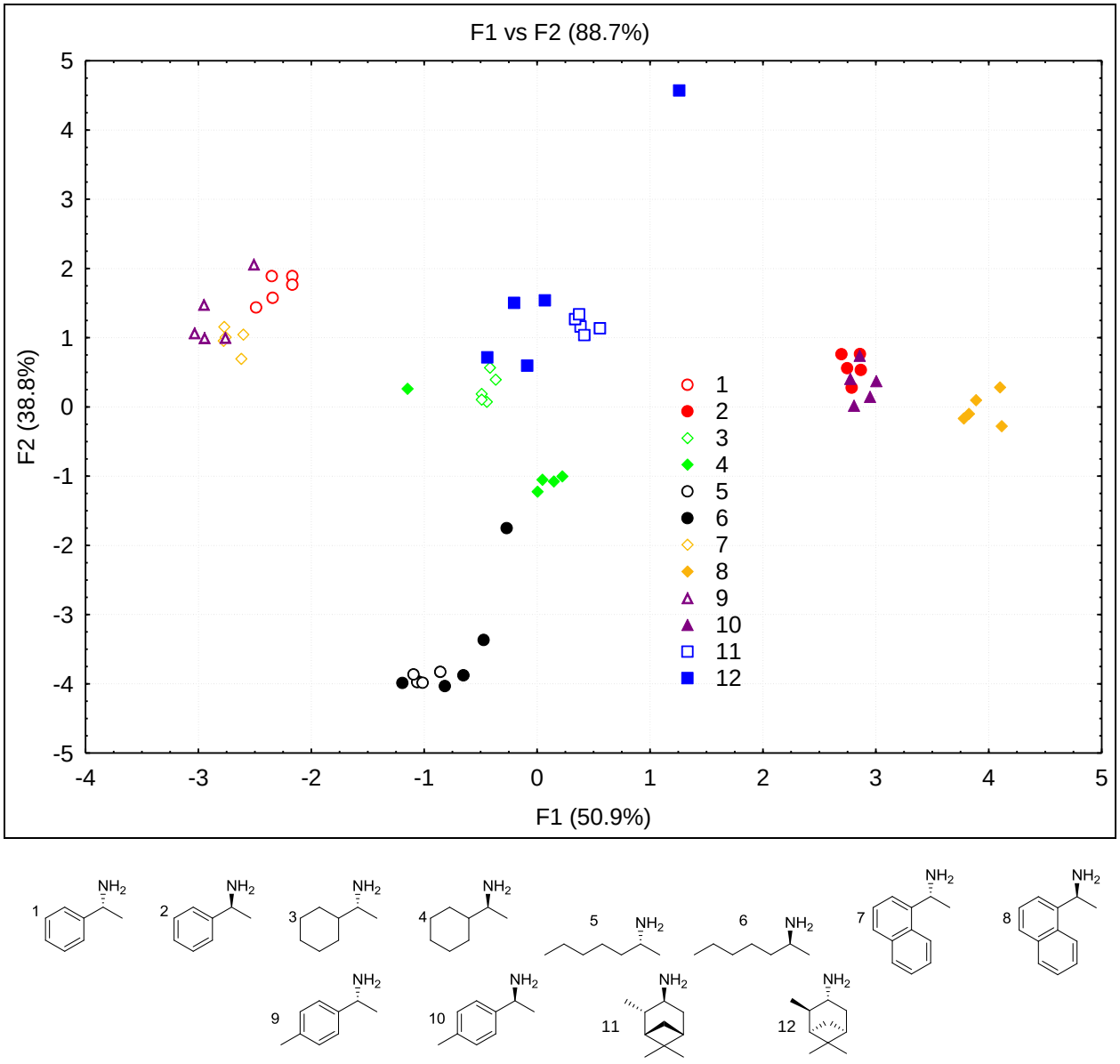

Figure 4.14. 2D PCA plot using **BINOL** and **4.4**.

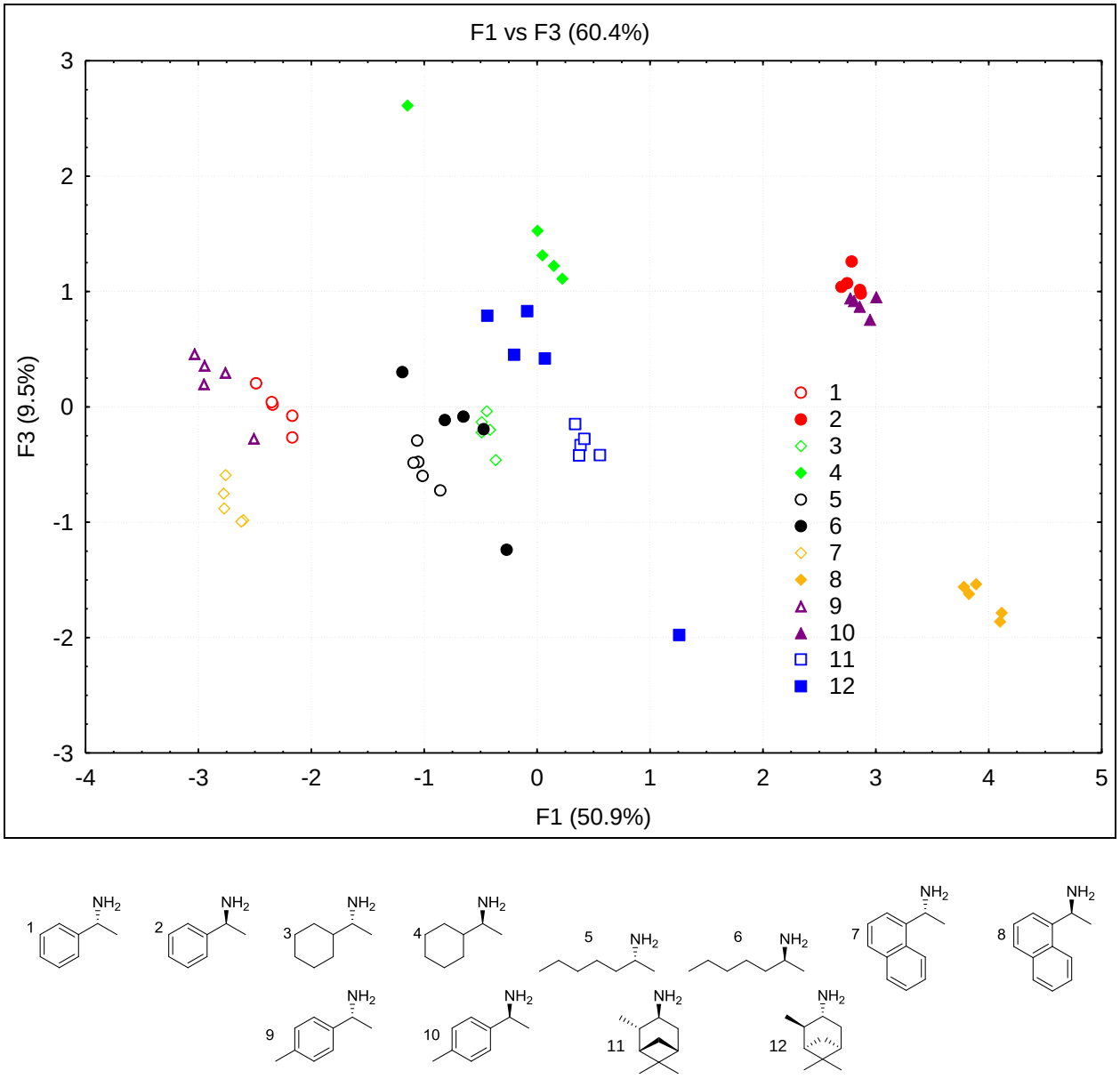

Figure 4.15. 2D PCA plot using **4.4** and **4.5**.

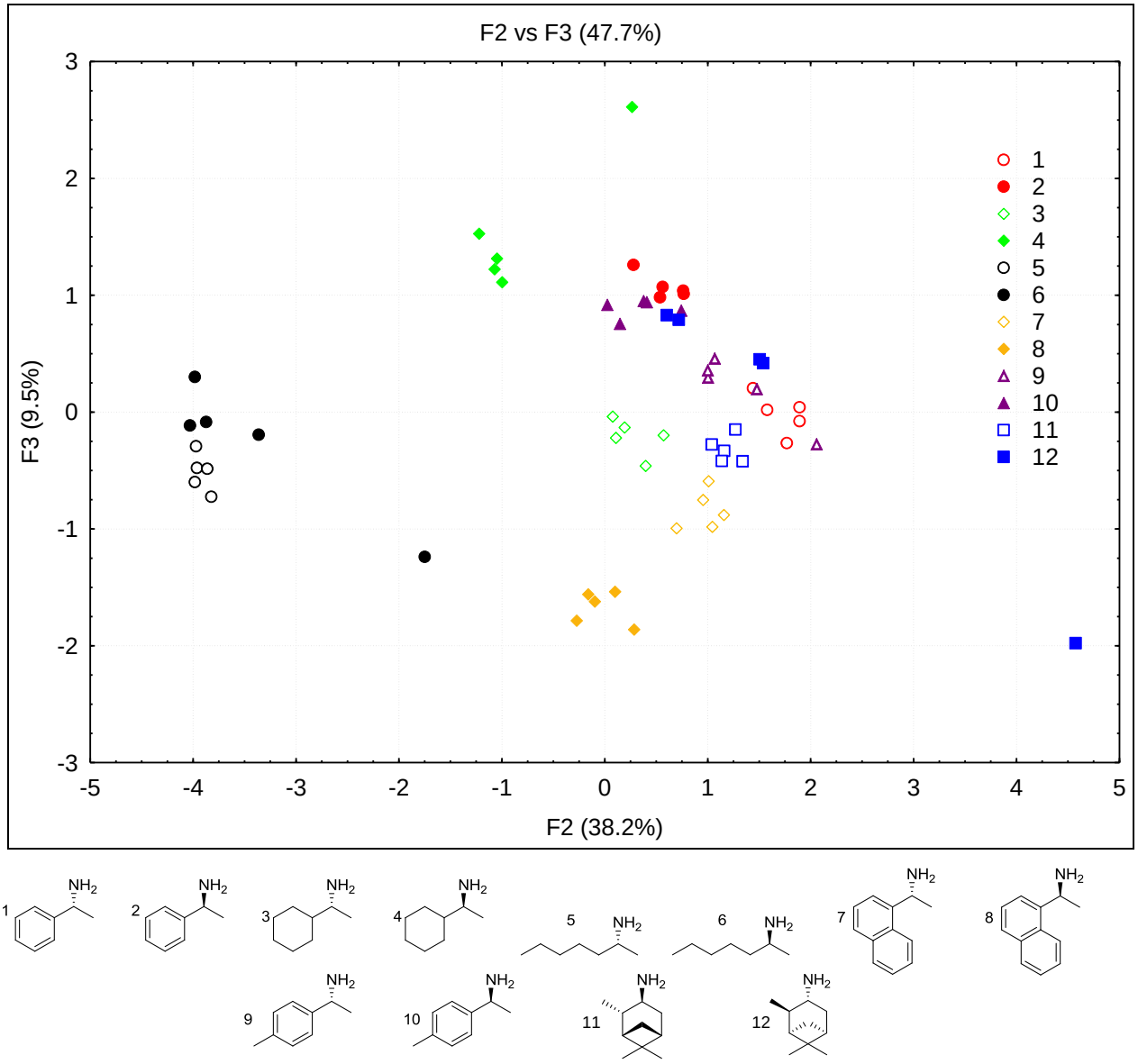

Figure 4.16. 2D PCA plot using **BINOL** and **4.5**.

4.5 REFERENCES

1 Wahler, D.; Reymond, J.-L. *Curr. Opin. Biotechnol.* **2001**, *12*, 535–544.

2 Stambuli. J. P.; Hartwig, J. F. *Curr. Opin. Chem. Biol.* **2003**, *7*, 420–426.

3 Gennari, C.; Piarulli, U. *Chem. Rev*. **2003**, *103*, 3071–3100.

4 Welch, C. J.; Szczerba, T.; Perrin, S. R. J. *J. Chromatogr. A* **1997**, *758*, 93–98.

5 Welch, C. J.; Grau, B.; Moore, J.; Mathre, D. J. *J. Org. Chem.* **2001**, *66*, 6836–6837.

6 Welch, C. J.; Fleitz, F.; Antia, F.; Yehl, P.; Waters, R.; Ikemoto, N.; Armstrong, I. J. D.; Mathre, D. J. *J. Org. Process Res. Dev.* **2004**, *8*, 186–191.

7 Sigman, M. S.; Jacobsen, E. N. *J. Am. Chem. Soc.* **1998**, *120*, 4901–4902.

8 Wol,f C.; Hawes, P. A. J. Org. Chem. **2002**, *67*, 2727–2729.

9 Lin, J.; Zhang, H. C.; Pu, L. *Org. Lett.* **2002**, *4*, 3297–3300.

10 Lee, S. J.; Lin, W. *J. Am. Chem. Soc.* **2002**, *124*, 4554–4555.

11 Ahn, K. H.; Ku, H.-Y.; Kim, Y.; Kim, S.-G.; Kim, Y. K.; Son, H. S.; Ku, J. K. *Org. Lett.* **2003**, *5*, 1419–1422.

12 Corradini, R.; Paganuzzi, C.; Marchelli, R.; Pagliari, S.; Sforza, S.; Dossena, A.; Galaverna, G.; Duchateau, A. *J. Mater. Chem.* **2005**, *15*, 2741–2746.

13 Liu, S.; Pestano, J. P. C.; Wolf, C. *J. Org. Chem.* **2008**, *73*, 4267–4270.

14 Gadamasetti, K. G.; Braish, T. *Process Chemistry in the Pharmaceutical Industry*; Vol. 2, CRC Press, New York, **1973**.

15 Hou, G.; Gosselin, F.; Li, W.; McWilliams, C.; Sun, Y.; Weisel, M.; O'Shea, P. D.; Chen, C.; Davies, I. W.; Zhang, X. *J. Am. Chem. Soc.* **2009**, *131*, 9882 – 9883.

16 Braun, H.; Felber, H.; Knesse, G.; Ritter, A.; Schmidtchen, F. P.; Schneider, A. *Tetrahedron* **2001**, *57*, 3313–3328.

17 Kadyrov, R.; Riermeier, T. H. *Angew. Chem.* 2003, **115**, 5630–5632; *Angew. Chem. Int. Ed.* **2003**, *42*, 5472–5474.

18 Huang, X.; Ortiz-Marciales, M.; Huang, K.; Stepanenko, V.; Merced, F. G.; Ayala, A. M.; Correa, W.; De Jesus, M. *Org. Lett.* **2007**, *9*, 1793–1795.

19 Lin, G.-Q.; Xu, M.-H.; Zhong, Y.-W.; Sun, X.-W. *Acc. Chem. Res.* **2008**, *41*, 831–840.

20 Hili, R.; Baktharaman, S.; Yudin, A. K. *Eur. J. Org. Chem*. **2008**, *31*, 5201–5213.

21 Nakanishi, K.; Berova, N.; Woody, R. W. *Circular Dichroism: Principles and Aplications*; Wiley-VCH, **2000**.

22 Nieto, S.; Dragna, J. M.; Anslyn, E. V. *Chem. Eur. J.* **2010**, *16*, 227-232.

23 Perez-Fuertes, Y.; Kelly, A. M.; Arimori, S.; Bull, S. D.; James T. D. *Org. Lett.*, **2006**, *8*, 1971-1974.

24 Perez-Fuertes, Y.; Kelly, A. M.; Fossey, J. S.; Powell, M. E.; Bull, S. D.; James, T. D. *Nat. Protoc.* **2008**, *3*, 210–214.

25 Mirri, G.; Bull, S. D.; Horton, P. N.; James, T. D.; Male L.; Tucker, J. H. R. *J. Am. Chem. Soc.* **2010**, *132*, 8903-8905.

26 Hanazaki, I.; Akimoto; H. *J. Am. Chem. Soc.* **1972**, *94*, 4102-4106.

27 Jurs, P. C.; Bakken, G. A.; McClellan, H. E. *Chem. Rev*. **2000**, *100*, 2649-2678.

28 Joliffe, I. T. *Principal Component Analysis*, 2nd ed; Springer-Verlag: New York, **2002**.

29 Johnson R. A.; Winchern, D. W. *Applied Multivariate Statistical Analysis*; Prentice-Hall: Englewood Cliffs, N. J., **1982**.

Chapter 5: Sensor Development and Application to Real High-Throughput Settings

5.1 INTRODUCTION

Of all the existing methods for the determination of the enantiomeric excess (*ee*) of a sample, chiral HPLC and GC remain the most widely used.[1-5] While the analytical chromatography methodologies are the gold standard for analysis of chiral analytes, they are serial and slow techniques. The demand for simple, fast assays for the determination of *ee* has increased dramatically over the last several years. At the root of this demand is the development of high-throughput screening (HTS) protocols for reaction development in synthetic laboratories and the pharmaceutical industry.[6-10] The most common example of the benefits of HTS in asymmetric reaction discovery involves the rapid evaluation/screening of a library of organometallic catalysts. This approach can exploit commercially available ligands or those obtained through modular construction, and/or a series of reaction conditions.[11-21] Parallel synthesis may vary experimental parameters such as metal centers, chiral ligands, acids/bases, temperature, solvent, pH, reaction time, as well as interrelationships among these variables. Parallel synthesis has rapidly expanded following the advent of microwell plates, microreactors, miniblock reactors, and automated liquid handlers.[22,23]

Given the synthetic efficiency of parallel syntheses, the limiting step in asymmetric catalyst discovery is the required determination of the *ee*% and yields of the products. This task cannot at the present time take place as quickly as the results are generated. *Bona fide* HTS analyzes thousands of samples per day.[24,25] For instance,

Takacs[26] employed a combinatorial approach in a series of catalytic asymmetric palladium-catalyzed cyclizations. He showed that optimization of the interdependence of reaction variables was necessary for achieving the highest *ee* values. However, due to time constraints, he could not test all the interdependences. Similarly, Whiting[27] monitored the effects of using four metals, three chiral ligands, two additives, and three solvents (144 combinations) in an asymmetric aza-Diels-Alder reaction. Using a chiral HPLC it took 168 hours of labor (spread over a few months) to determine the *ee* of each combination. Clearly, standard chiral HPLC is not compatible with HTS. It is understood that optical methods, like those based on UV-vis, circular dichroism (CD), fluorescence spectroscopy, etc. are better suited for rapid analysis.

The Anslyn group has utilized colorimetric indicator displacement assays[28], that require only 1 to 10 minutes to read a 96-well plate using a UV-vis spectrophotometer. The range is determined by the number of wavelengths that need to be analyzed. This reduces the time for analysis of 1000 samples to around 10 to 100 minutes (without including the time involved switching automated plates). These speeds represent true HTS.

No one has analyzed a 96-well plate for CD analogously since the technology does not exist, meaning all analyses are currently performed by hand resulting in high costs in both time and money. HTS CD spectropolarimetry would benefit the asymmetric synthesis community because a growing number of the assays being currently created for HTS of *ee* involve CD spectroscropy.[29] For example, Anslyn and Wolf have developed and tested CD methods for the analysis of chiral analytes, including amino acids[30], alcohols,[31] amino alcohols[32,33] carboxylates[34] and amines.[35-38] Yet, there is a lacuna in the instrumental world that prevents the implementation of these methods to rapid automated analysis; currently all samples need to be manually processed and analyzed serially. The

design and construction of an apparatus able to perform the sampling operations and read a 96-well plate automatically may bring CD into the realm of HTS.

Besides having a strong need in the organic chemistry synthetic community, the biological/biochemical sciences field could greatly benefit from a CD spectrometer that can read 96-well plates. CD spectroscopy is a sensitive technique for recognizing structural features and polymorphism of macromolecules of biological relevance, such as peptides, proteins and nucleic acids.[39,40] It is traditionally understood that CD can determine distortions in both the secondary and tertiary structure of these natural products. Comparison with previous cases and development of theoretical studies currently allow for an easier and more comprehensive determination of the relationship between the CD spectrum and molecular structure.[39,40] Further, CD is also a useful tool for determining the existence of a binding interaction between a macromolecule and small molecule substances like drugs, dyes, guests, or ligands. In addition, CD is used to characterize the site of interaction and local structure using a relatively small amount of sample and without loss of the sample.[39-41] Examples of the latter application include circumstances under which certain compounds change their preferred binding mode to DNA, either in the minor groove, major groove binding, or by intercalation.[42] A rapid, automated CD measurement system, will actualize the screening of drug interactions both from a qualitative and quantitative point of view if available to the numerous research collectives that focus on drug design. The principle behind the allure of this proposed application is the rapid manner in which drug candidates could be screened as agonists and antagonists of enzyme and protein activity. This would lead to an easy analysis of high volumes of prospective drugs and the determination of trends in binding for different drug candidate groups, which in turn would facilitate and hasten development of these drugs.

Although the main companies responsible for the manufacture of CD spectrometers have tried to streamline the acquisition of data by designing autosamplers or robotic injectors, the fluid dynamics and hydraulics involved only marginally hasten the reading process. The instrumentation for these sampling systems is also highly sensitive to non-aqueous media, malfunctioning frequently when common organic solvents are employed. Even when the apparatus performs ideally, the time/sample rates are nowhere near those observed for plate readers available for UV-vis spectroscopy. They are not true plate readers but automated flow injectors, drawing each sample and injecting it sequentially.

Why is a HTS-CD spectrometer not currently available? The reason is simply stated. Plastic multi-well plates (and even higher optical quality plates with glass or fused silica bottoms) are not necessarily optically isotropic. They are burdened with strain linear birefringence (LB), or different refractive indexes within the material. Parasitic LB has plagued measurements of the CD of anisotropic media for decades.[43-49]

Optical activity was discovered by Arago in 1811 when he passed linearly polarized light along the high-symmetry *c*-axis of quartz.[50-52] However, the determination of the *anisotropy* (the complete tensors) of optical activity in oriented systems by making off-axis measurements is still challenging.[53,54] This is because linear birefringence (LB) and linear dichroism (LD), non-zero along the low-symmetry directions, can be $\sim 10^4$ times larger than circular birefringence (CB or optical rotation) and CD. The minor chiroptical perturbation to the polarization state of light in anisotropic media is of the same order of magnitude as parasitic ellipticities from imperfect samples and polarimeter optical components. The year 2011 marked the 200th anniversary of an ongoing struggle to measure CB and CD in organized systems.[55,56]

This work takes advantage of professor Bart Kahr's recent experience in building polarimeters using as many of four photoelastic modulators simultaneously.[57,58] Multiple modulators provide the strategy for separating and eliminating contributions to the change in the polarization of light due to parasitic linear anisotropies that have traditionally given rise to artificial chiral signatures.

CD spectropolarimeters typically modulate between left and right circular polarization states by using a single photoelastic modulator before the sample. The differential transmission is recorded but the true value of CD can be grossly affected by the admixture of linear polarization in the input light. This linear polarization can strongly couple to unwanted anisotropies of the sample or its container. The remedy for this is the use of a second photoelastic modulator which is placed after the sample.

Photoelastic modulators (PEMs) are the key optical elements in many polarization measurement techniques including the following: ellipsometry, circular dichroism, Faraday rotation, fluorescence anisotropy, and the magneto-optic Kerr effect. Most of these techniques rely on the measurement of certain elements of the so-called Mueller matrix of a sample, the linear operator that contains all of the information about the polarization transforming properties of an analyte. Increasingly complex samples spread the desired optical effects over all 16 elements of the Mueller matrix. The distinctive advantage of instruments based on PEMs with respect to other sources of polarization modulation is their high sensitivity. Modern PEMs as constructed today by Hinds Instruments have high modulation purity and efficiency, broad spectral range, high power handling capability, large acceptance angle, large useful aperture, and high retardation stability.

In 1997, Jellison and Modine introduced a polarimeter with two freely running PEMs.[59,60] Their instrument simultaneously delivered eight elements of the Mueller

matrix. The complete matrix was obtained by combining results from distinct optical configurations. In 2011, Arteaga et al. at New York University introduced a polarimeter using four PEMs that measures simultaneously all Mueller matrix elements without reconfiguration, thus avoiding errors associated with moving optical components.[57,58] This instrument was extraordinarily fast, sensitive, and accurate, and presented the best option for testing the viability of a high-speed automated plate reader.

Also with the objective of bringing CD-based analytical methods to the scientific community, a major focus of our group is on translational research with chemists involved in asymmetric methodology development. We have been cognizant from the start that most synthetic methodology chemists are not thoroughly versed in supramolecular chemistry and chemometrics, and therefore would benefit from our assistance to adopt our methods. Analogously, we realize that our group is not specialized in synthetic organic methodology development, and hence we cannot as effectively use our own assays as could synthetic chemists. In other words, the goal of this particular series of projects is to implement our assays in the research laboratories of "card-carrying" organic methodology chemists like Drs. Xumu Zhang, Scott Miller, and Michael Krische. These collaborative efforts would test the utility and generality of our methods, while also highlighting the power of supramolecular chemistry to assist synthetic organic chemists. Achieving the stated goals would establish a new paradigm for *ee* determination, and would transition this paradigm out of our academic laboratories and into the real world.

In this particular body of work, we describe the preliminary results of a collaboration between our group and that of Dr. Xumu Zhang at Rutgers University, targeting chiral amines as the particular analyte. As one of most efficient approaches to prepare these compounds, the asymmetric hydrogenation of enamines and imines has

received particular attention. Although a small number of catalytic systems has been successfully applied to the industrial production, this is still a largely underdeveloped area in direct contrast with the great advances in asymmetric hydrogenation of olefins and ketones.[61-63] Compared with enamines and N-protected imines, asymmetric hydrogenation of prochiral iminium salts is a more atom economical and challenging method. This approach eliminates the extra steps of protection and deprotection of the amine group. However, the only examples of this methodology were reported by the Zhang group with well-established Ir-based catalysts.[64-66] They currently aim to develop a novel and efficient Rh-based catalytic system for this transformation, and the implementation of one of our fast *ee* determination protocols for screening of their samples could potentially facilitate this development process.

With this binary goal of testing the performance a multiple modulator polarimeter and screening the actual samples produced by the Zhang labs in mind, the Anslyn group chose an already-validated CD method for *ee* determination of α-chiral amines.[35] In this protocol, aldehyde **5.1** reacts with the amine under study to give a bidentate imine **5.2**. Fe(II) can, in turn, bind 3 equivalents of that imine to give octahedral complex **5.3**, with a helical chirality dictated by the handedness of the original amine (Scheme 5.1).

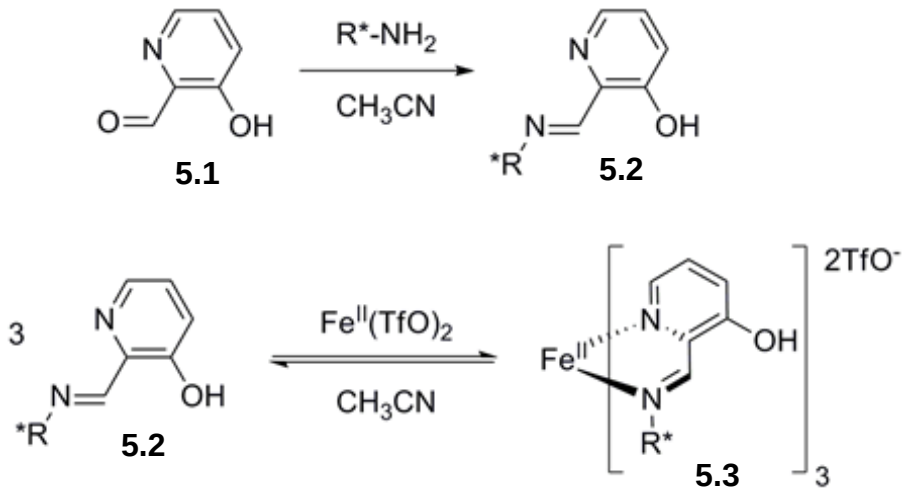

Scheme 5.1 Two-step assembly that leads to the CD-active Fe(II) complex used to report the *ee* of chiral amines.

The strong metal-to-ligand charge transfer bands that arise upon formation of **5.3** are measured by CD and related back to the enantioenrichment of the amine analyte. This reaction is fast, simple, and relies on commercially available reagents. As an added benefit, it does not require any work-up or purification steps and takes place *in situ*. It leads to highly reproducible readings, making it ideal as a test of instrumental performance and for implementation in a real synthetic setting.

5.2 Results and Discussion for the Plate Reader Analyses

The Stokes-Mueller calculus tracks the transformation of the state of polarization of light passing through the 4-PEM spectropolarimeter and will be used to describe the polarization modulation generated by the PEMs. A Mueller matrix (M) is a linear operator that represents an optical element or sample. Elements M_{03} and M_{30} are most related to CD and thus are highlighted in red.

$$M = \begin{bmatrix} M_{00} & M_{01} & M_{02} & M_{03} \\ M_{10} & M_{11} & M_{12} & M_{13} \\ M_{20} & M_{21} & M_{22} & M_{23} \\ M_{30} & M_{31} & M_{32} & M_{33} \end{bmatrix}$$

M transforms the polarization state of the input light expressed as a Stokes vector (S) whose components are sums and differences of the intensities of various polarization states (linear polarization states: I_x, I_y, $I_{\pm 45}$; circular polarization states: I_R, I_L) into output light with a polarization state defined as some other Stokes vector, $S_{out} = MS_{in}$.

The 4-PEM is designed with two symmetric arms that are called the polarization state generator (PSG) and the polarization state analyzer (PSA). Each arm is composed of a PEM and a polarizer. Using the Stokes-Mueller formalism, the optical response of the both the PSG and PSA can be represented as follows:

$$S_{PSG} = R(-\theta_{m0}) * M_{m0} * R(\theta_{m0}) * R(-\theta_{p0}) * M_{p0} * R(\theta_{p0}) * \begin{bmatrix} 1 \\ 0 \\ 0 \\ 0 \end{bmatrix}$$

$$S_{PSA} = \begin{bmatrix} 1 \\ 0 \\ 0 \\ 0 \end{bmatrix}^T * R(-\theta_{p1}) * M_{p1} * R(\theta_{p1}) * R(-\theta_{m1}) * M_{m1} * R(\theta_{m1})$$

where M_p is the Mueller matrix of a polarizer, M_m the Mueller matrix of a PEM, and $R(\theta)$ is a the rotation matrix. These three matrices are:

$$M_p = \begin{bmatrix} 1 & 1 & 0 & 0 \\ 1 & 1 & 0 & 0 \\ 0 & 0 & 0 & 0 \\ 0 & 0 & 0 & 0 \end{bmatrix} \quad R(q_x) = \begin{bmatrix} 1 & 0 & 0 & 0 \\ 0 & \cos(2q) & \sin(2q) & 0 \\ 0 & -\sin(2q) & \cos(2q) & 0 \\ 0 & 0 & 0 & 1 \end{bmatrix} \quad M_m = \begin{bmatrix} 1 & 0 & 0 & 0 \\ 0 & 1 & 0 & 0 \\ 0 & 0 & \cos(d) & \sin(d) \\ 0 & 0 & -\sin(d) & \cos(d) \end{bmatrix}.$$

The Mueller matrix of the modulator, *Mm*, changes with its time varying retardation. The nested trigonometric functions need to be expanded as an infinite sum of Bessel functions, now embedded into S_{PSG} and S_{PSA}. The time varying intensity is then calculated as: $I(t)=S_{PSA}*M_{sample}*S_{PSG}$; The ultimate objective of the instrument is to determine the elements of M_{sample} from the time-varying intensity measured at the detector $I(t)$. In the most general case (an anisotropic, absorbing, optically active sample) the optical properties of interest are related to M_{sample} through a complicated set of relations requiring that all elements of M_{sample} are known. But, it has previously been shown that for small linear anisotropies (less than ~0.5 rad) and negligible depolarization, the matrix M_{sample} can be expressed as:

$$\begin{pmatrix} 1+\frac{1}{2}(LD'^2+LD^2) & -LD & -LD' & CD+\frac{1}{2}(LBLD'+LB'LD) \\ -LD & 1+\frac{1}{2}(LD^2+LB'^2) & CB+\frac{1}{2}(LBLB'+LDLD') & LB' \\ -LD' & -CB+\frac{1}{2}(LBLB'+LDLD') & 1+\frac{1}{2}(LD'^2-LB^2) & -LB \\ CD-\frac{1}{2}(LBLD'+LB'LD) & -LB' & LB & 1-\frac{1}{2}(LB^2+LB'^2) \end{pmatrix}$$

In the absence of linear anisotropies (*LD*, *LD'*, *LB*, and *LB'*), *CD* can be taken directly from either the M_{03} or M_{30} elements. Commercial CD spectrometers typically measure M_{03} using a single PEM positioned before the sample. However, even very small linear birefringence in the sample holder will couple to residual LD, either intrinsic or from the solution meniscus and other interfaces, to give artifacts comparable to the magnitude of typical CD values (±1/2(LBLD'+LB'LD). To measure CD in the presence of linear anisotropies, both M_{03} and M_{30} must be measured, with two (or four in this case) PEMs, and the values averaged to remove the artifactual terms. Figure 5.1 illustrate the large deviations from the actual that result from measurement of only M_{03} or M_{30}.

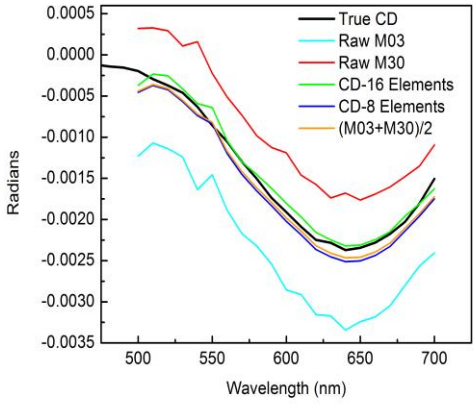

Figure 5.1. CD errors when using only one PEM. A solution of Cu(II) tartrate measured without (True CD) and with (all other spectra) a birefringent material placed after the solution cuvette using the 4-PEM.[f]

The Kahr group prepared a sample that emulates a well-plate measurement by placing a circularly dichroic solution contained in a high quality cuvette just before a transparent birefringent material (a piece of adhesive tape). The complete M was measured with the 4-PEM polarimeter. As expected, M_{03} and M_{30} by themselves did not match the CD measured directly in the quartz cuvette without the interfering linearly birefringent tape. But, $(M_{03}+M_{30})/2$ matched quite well.

5.2.1 Calibration Curves

Four different commercially available amines were tested using the instrumental set-up and derivatization method described above. The analytes chosen span a range of

[f] A 1-PEM instrument can only measure raw M_{03} or M_{30}, while a 2-PEM instrument can accurately measure CD by averaging these two elements, or by performing analytic inversion on a MM constructed from all 8 elements measured with a 2-PEM instrument. The CD calculated from all 16 discretely measured elements is shown for comparison.

chemical properties designed to test the viability and reproducibility of the system when dealing with a variety of situations, by including aliphatic and aromatic amines with different degrees of substitution and electronic distribution (Figure 5.2).

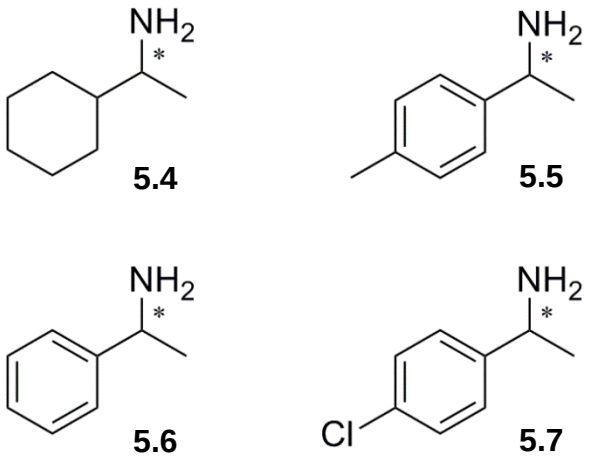

Figure 5.2. Amine analytes chosen for the study.

All four amines were derivatized and loaded into a 96-well plate. The plate was sealed with a thin glass cover, secured with elastic bands. The reason for this configuration is that the polarimeter at New York University used for this test had a horizontal light path. Therefore, the well plate had to be mounted upright, requiring a method to secure the fluid in the wells. Our reagents and common organic solvents used in synthesis reacted with glues. A glass plate and rubber bands sealed the well plate without leakage (Figure 5.3).

A

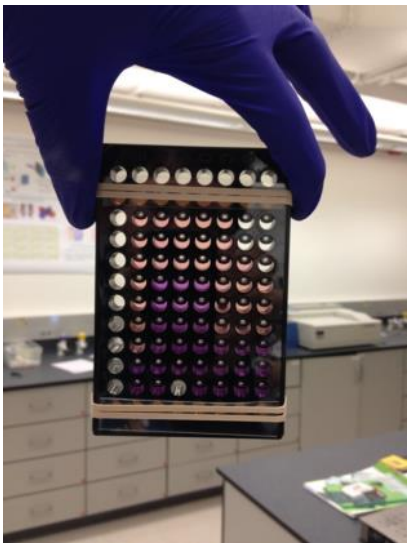

B

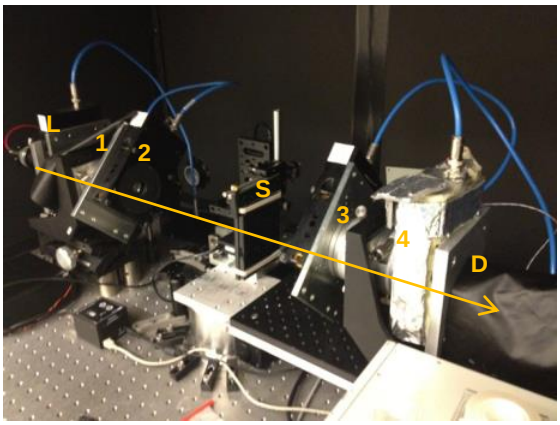

Figure 5.3. A) 96-well plate containing the solutions intended for obtaining calibration curves, B) Horizontal 4PEM with optical train indicated by yellow arrow. L = light source, (1,2,3,4) = PEMs, S = sample plate, D = detector.

The range of *ee*% values was chosen in order to obtain a CD calibration curve that faithfully describes the behavior of the system. Thus, we began by plotting the CD

readings of a series of samples of known enantiomeric composition versus their *ee*% values (Figures 5.4-5.7). Positive 100% is taken as 100% of the *R* enantiomer of the amine while -100% represents a reaction with only the *S* enantiomer of the amine.

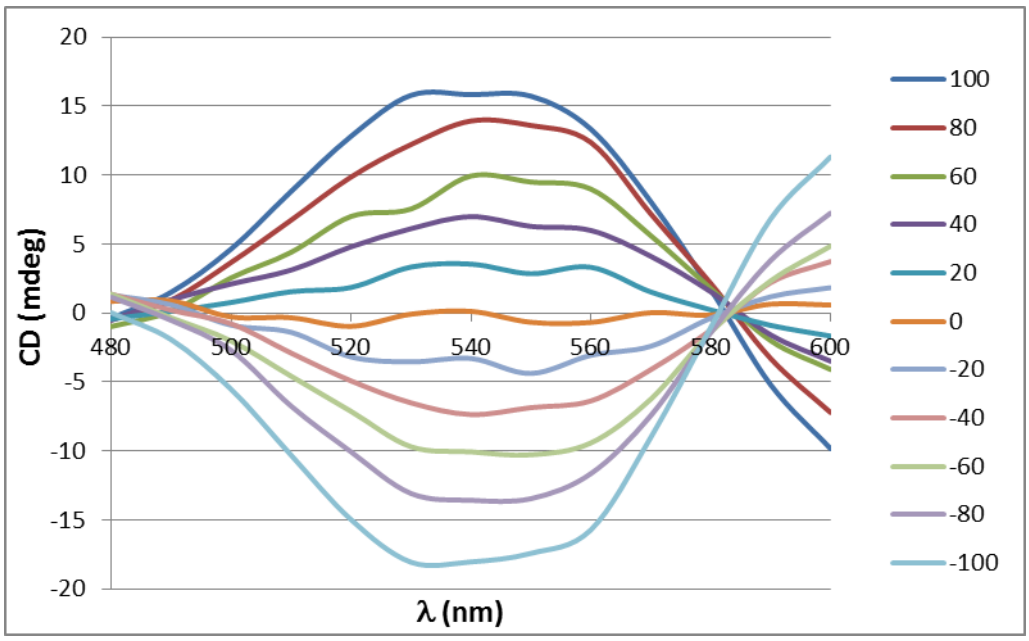

Figure 5.4. CD spectra for the assembly with **5.4**.

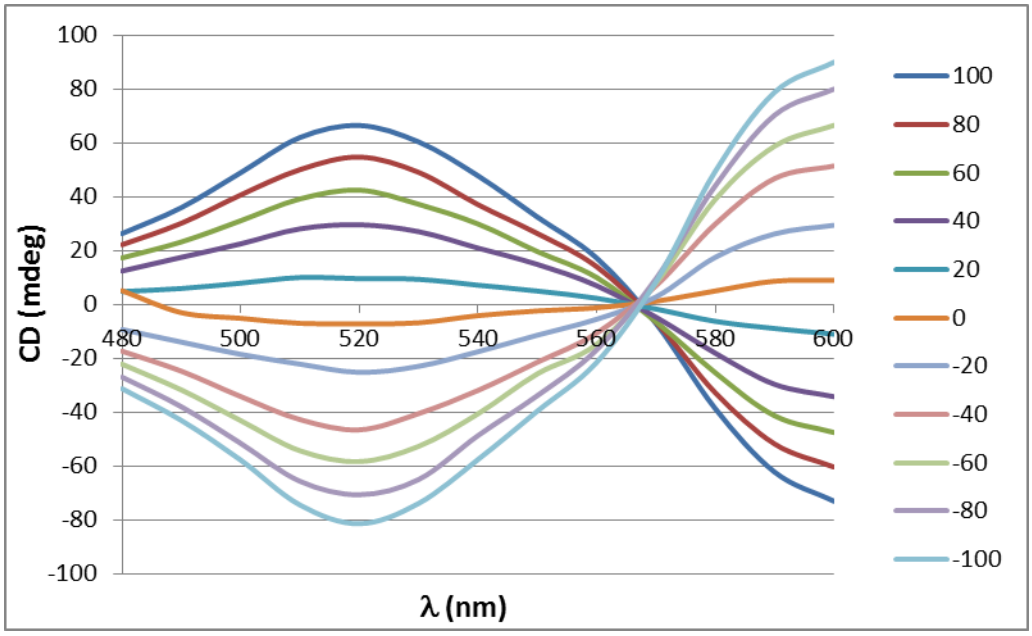

Figure 5.5. CD spectra for the assembly with **5.5**.

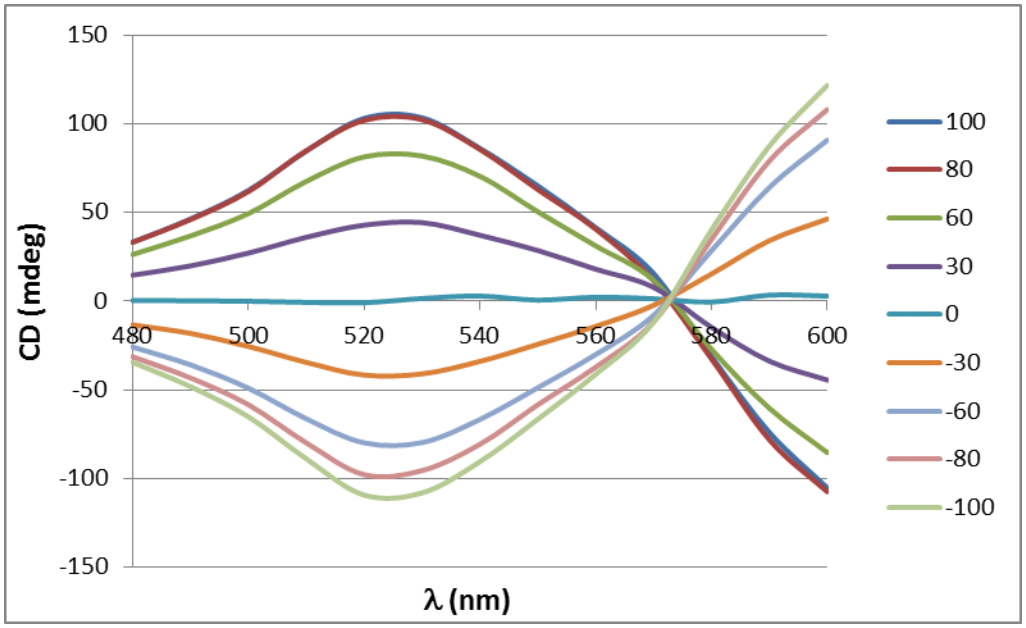

Figure 5.6. CD spectra for the assembly with **5.6**.

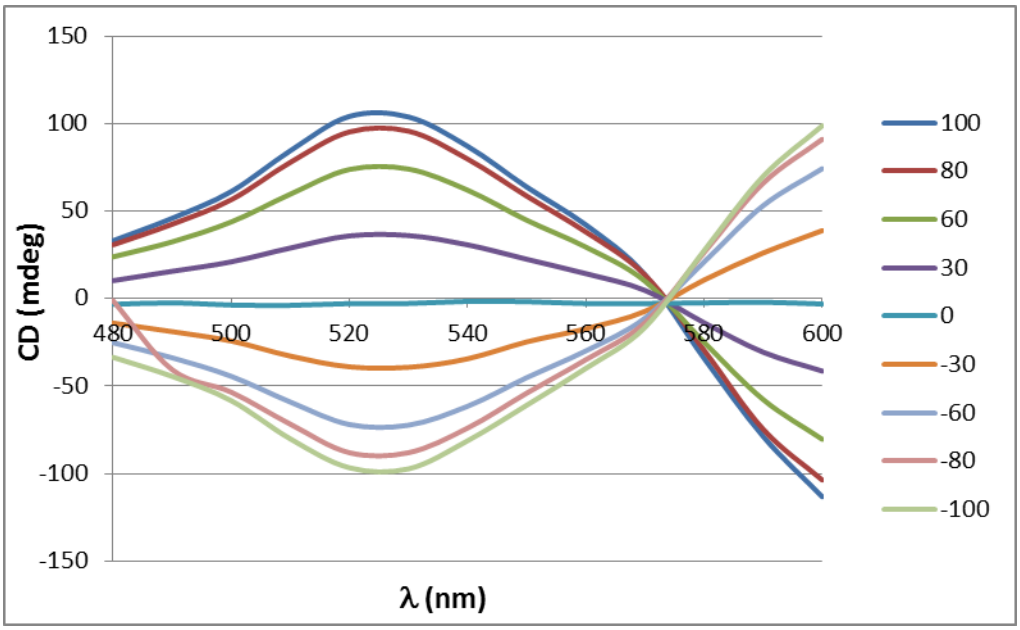

Figure 5.7. CD spectra for the assembly with **5.7**.

Upon gathering the data from the CD scans, the wavelength that exhibited maximum signal intensity was chosen for building four calibration curves. When the CD values were plotted against the known *ee*%'s a third-degree polynomial that connects the two variables (CD and *ee%*) was defined for each case (Figures 5.8-5.11).

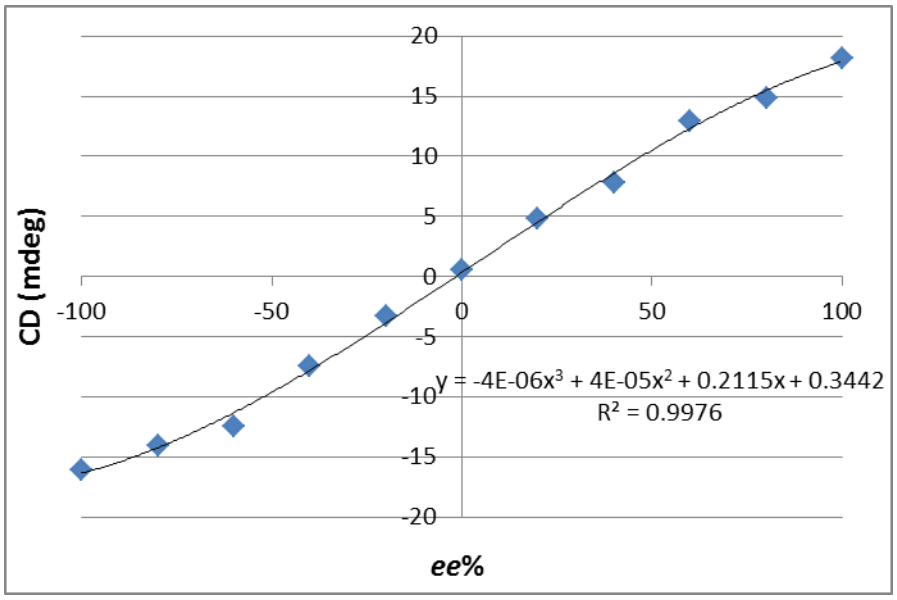

Figure 5.8. Calibration curve for the assembly with **5.4** at 530 nm.

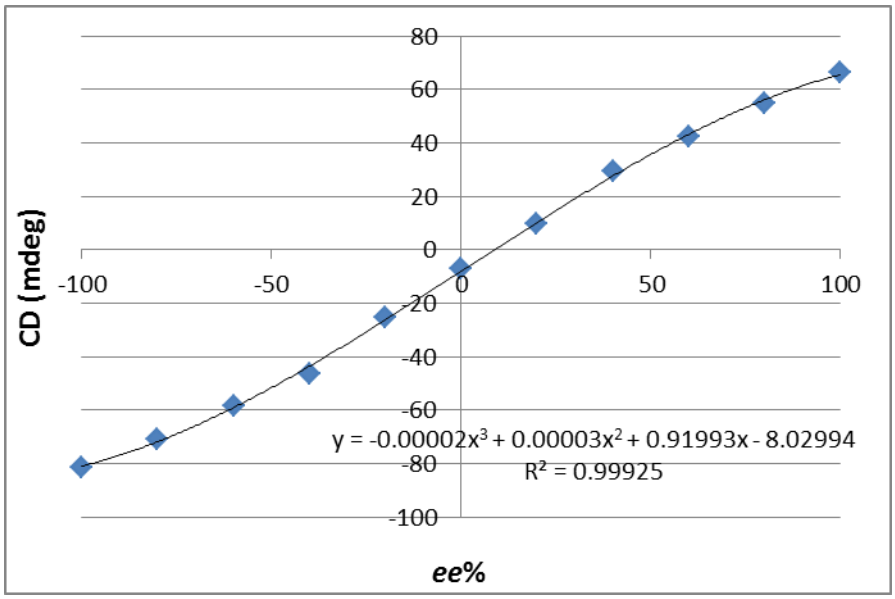

Figure 5.9. Calibration curve for the assembly with **5.5** at 520 nm.

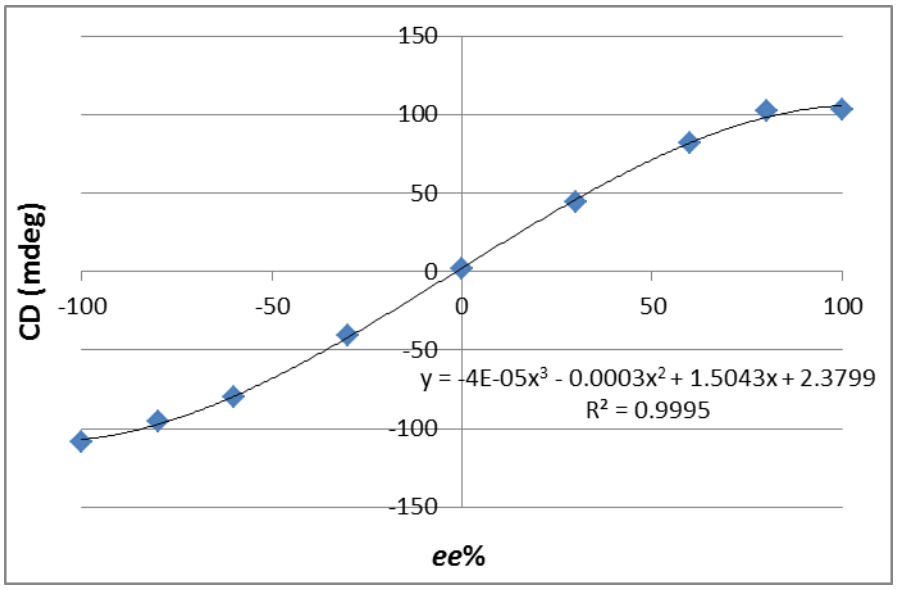

Figure 5.10. Calibration curve for the assembly with **5.6** at 530 nm.

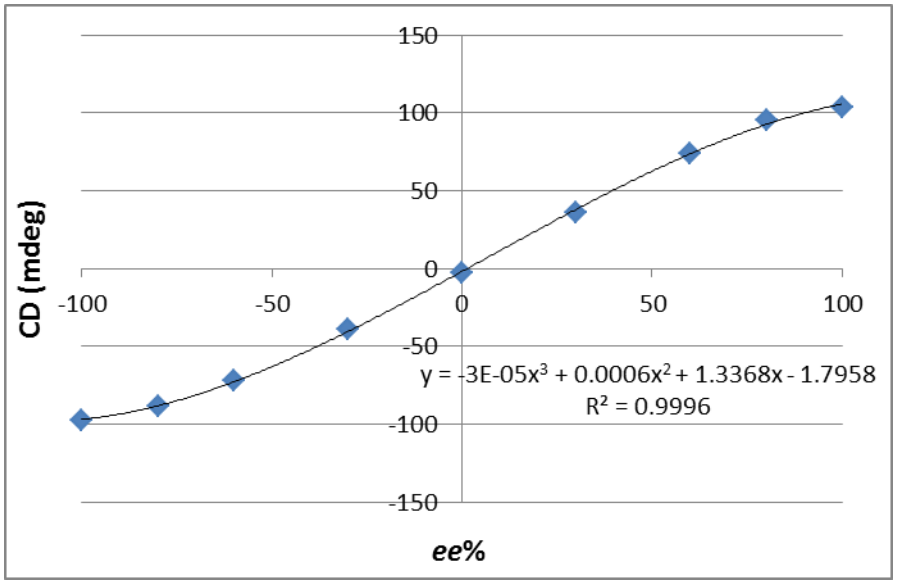

Figure 5.11. Calibration curve for the assembly with **5.7** at 530 nm.

All amine guests responded in a manner analogous to that observed for the experiments that had been previously conducted manually.[35] The sigmoidal shape of these calibration curves is also in agreement with the behavior previously determined for this system. It was found that the characteristic shape is not a sign of cooperativity (as it shows no dependence on concentration) and rather a result of the statistical distribution of the enantiomers around Fe(II).

Also remarkable is that even though the aliphatic amine yields weaker signals, the shape of the calibration curve and its correlation index indicate satisfactory performance.

5.2.2 Enantiomeric Excess Determination

Once the calibration curves that relate CD signal intensity to *ee*% for each amine were obtained, a number of "unknown" samples were analyzed. These samples were prepared by using a known proportion of each of the amine enantiomers. After derivatizating and procuring a reading for these solutions, the CD values were input into the equation relating CD with *ee*% and these calculated values were then compared to the actual values (Tables 5.1-4).

Calculated *ee*%	Real *ee*%	Error
18.58	20	1.42
82.2	90	7.8
-43.98	-50	6.02
-23.39	-30	6.61
-57.31	-70	12.69
11.22	10	1.22
-74.91	-80	5.09
	Average Error	5.84

Table 5.1 List of experimental values of *ee*% compared to the actual values for the studies with **5.4**.

Calculated *ee*%	Real *ee*%	Error
-12.45	-10	2.45
-44.12	-40	4.12
-72.35	-90	17.65
66.04	70	3.96
59.5	50	9.5
-64.31	-60	4.31
	Average Error	7.00

Table 5.2 List of experimental values of *ee*% compared to the actual values for the studies with **5.5**.

Calculated *ee*%	Real *ee*%	Error
-22.04	-20	2.04
56.12	50	6.12
91.46	90	1.46
-94.07	-80	14.07
-41.95	-40	1.95
	Average Error	5.13

Table 5.3 List of experimental values of *ee*% compared to the actual values for the studies with **5.6**.

Calculated *ee*%	Real *ee*%	Error
20.88	20	0.88
-27.61	-30	2.39
-67.51	-80	12.49
73.01	90	16.99
-60.75	-70	9.25
	Average Error	8.40

Table 5.4 List of experimental values of *ee*% compared to the actual values for the studies with **5.7**.

These error values are consistent with those found when measuring such samples individually and fall within the range of accuracy that is expected for a HTS method. The end goal for our methods is serving as an initial screening identify possible hits among a multitude of result and then applying chiral chromatography to those samples that seem promising upon the initial analysis. As we do not aim to replace chiral chromatography

with optical HTS but to provide a supplementary technique to screen large number of samples, we can accept less than perfect accuracies.

5.3 Results and Discussion for the Experiments with Real Samples

Thioureas have been widely used as a H-bond donor in organocatalysis.[67-69] Most research in this area focuses on the direct activation of neutral substrates by H-bonding, while more recent efforts take advantage of the anion binding of ion-paring intermediates.[70-72] Previous work by the Zhang labs at Rutgers University explored the activation of nitroalkenes by thioureas *via* proposed H-bonding interactions in the enantioselective hydrogenation (Scheme 5.1).[73] Inspired by the powerful strategies developed in ion-pairing catalysis,[74-82] they sought to extend the anion-binding catalysis concept to the field of asymmetric hydrogenation. Based on the reports in anion-binding catalysis, especially the enantioselective reactions of iminium ions[83] and the mechanistic study[84], they envisioned that the thiourea could interact with the counteranion in the catalytic pathway (Scheme 5.1). This would be the first example of Rh/bisphosphine-thiourea-catalyzed asymmetric hydrogenation of N-H imines assisted by anion binding.

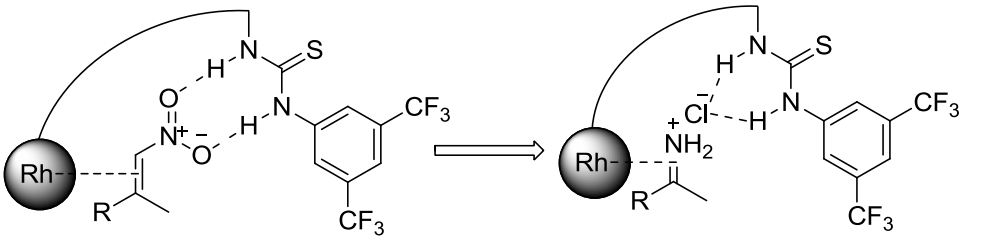

Scheme 5.1. Extension of the Rh/Bisphosphine-Thiourea catalytic system.

With the ultimate goal being the fast screening of a large number of samples, the initial stages of this collaborative work would include the testing of several samples originated from the Zhang group. After they had been synthesized, the *ee*% values obtained by our method would be contrasted with those recorded with the standard accepted techniques of chiral GC to quantify the level of accuracy and reliability. Once the reproducibility and quality of our faster protocol were established, actual screening of arrays of samples could begin.

5.3.1 Adaptation of the Method to Real Samples

Actual synthetic samples pose a challenging problem to sensing, since they are often mixtures of several components. These components make the analysis more difficult than pure products tested in the proof of concept and require some additional triaging prior to analysis. The first step to processing the samples produced by the Zhang group with our *ee* determination protocol involved a series of tests to assess the performance of our method when the analyte comes from the crude product of an actual synthetic process as opposed to from a mixture of commercially available pure enantiomers.

Upon initial treatment of the first samples (analyte **5.6**) received, it became evident that the active assembly product was not being formed to a significant degree. The reason for this issue was determined to be reduced purity of the amine synthesized, leading to the formation of side products (with unreacted starting material, catalyst, chiral auxiliaries, etc.) and interferences with the CD readings.

In order to remedy this problem, we devised a series of experiments aimed to define viable stoichiometries for the three components of the reaction that would allow reproducible readings. The idea is that if a functional threshold ratio is established for the amine, the system will generate satisfactory results even if the total concentration of the amine is unknown. This is not only a solution for this specific case of the Zhang amines, but can also be framed within the general goal of hastening the analysis step, as it eliminates the need for knowing the exact amount of analyte.

Using **5.6** as the amine analyte and leaving the concentration of the metal center constant and varying that of **5.1** and **5.6**, it was possible to find a trend in the CD response as a function of the proportions between the three components (Figure 5.12).

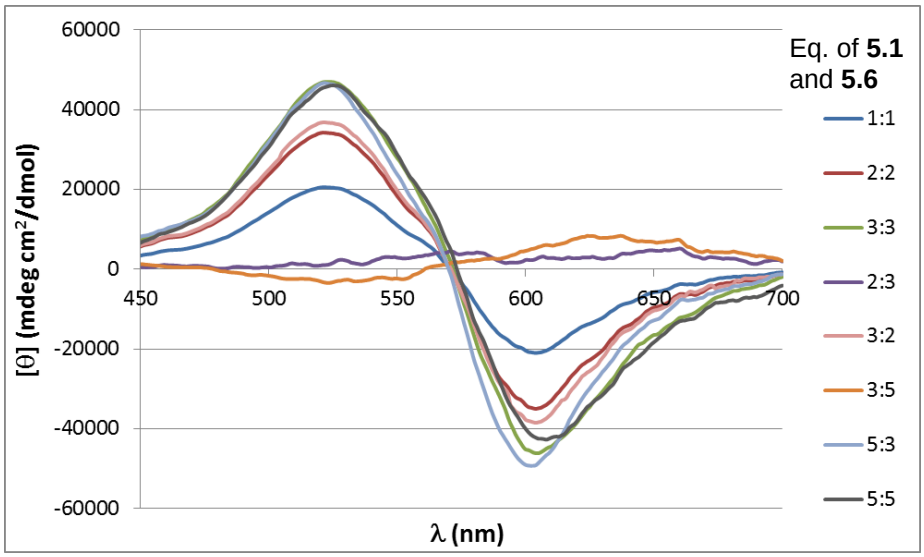

Figure 5.12. CD signal as a function of the equivalents of aldehyde **5.1** and amine **5.6** used with respect to Fe(II) (1 mM).

From this experiment it was concluded that at λ_{max}=525 nm the CD signal is reproducibly maximized as long as there are three equivalents of the imine present without an excess of amine **5.6**. In order to further test this principle we performed a titration of **5.6** into the system containing an equivalent of Fe(II) and 8 equivalents of **5.1** (Figure 5.13).

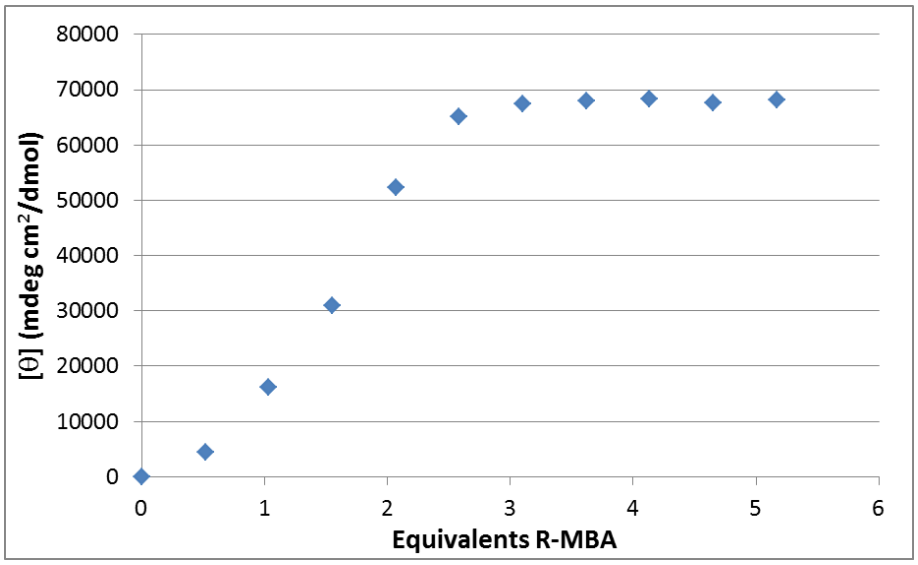

Figure 5.13 CD titration of **5.6** into a system containing 1 equivalent (1 mM) of Fe(II) and 8 equivalents of **5.1** at 525 nm.

The experimental evidence that indicated a functional range of amine concentration as long as the other two components are maintained at a certain values allowed us to start processing crude samples and obviated the requirement for determination of the exact concentration.

5.3.2 Enantiomeric Excess Determination in Real Samples

With a set of conditions that allowed reliable screening we processed a batch of reaction crudes provided by the Zhang labs with analytes **5.5** and **5.6**. The samples were worked up according to the protocol previously used by the Zhang group. Calibration curves were generated using the same derivatization conditions and stoichiometries as determined above of the commercially available amines, Fe(II) and **5.1** (Figure 5.14).

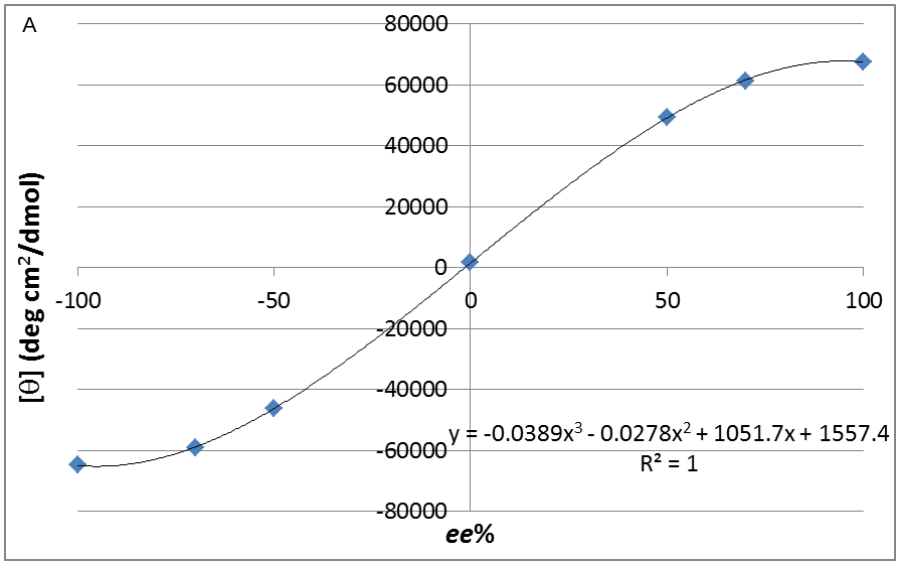

Figure 5.14. A) CD calibration curve for the assembly with Fe(II) (1 mM), **5.1** (8 mM) and **5.5** (5 mM) in CH_3CN at 521 nm. B) CD calibration curve for the assembly with Fe(II) (1 mM), **5.1** (8 mM) and **5.6** (5 mM) in CH_3CN at 525 nm.

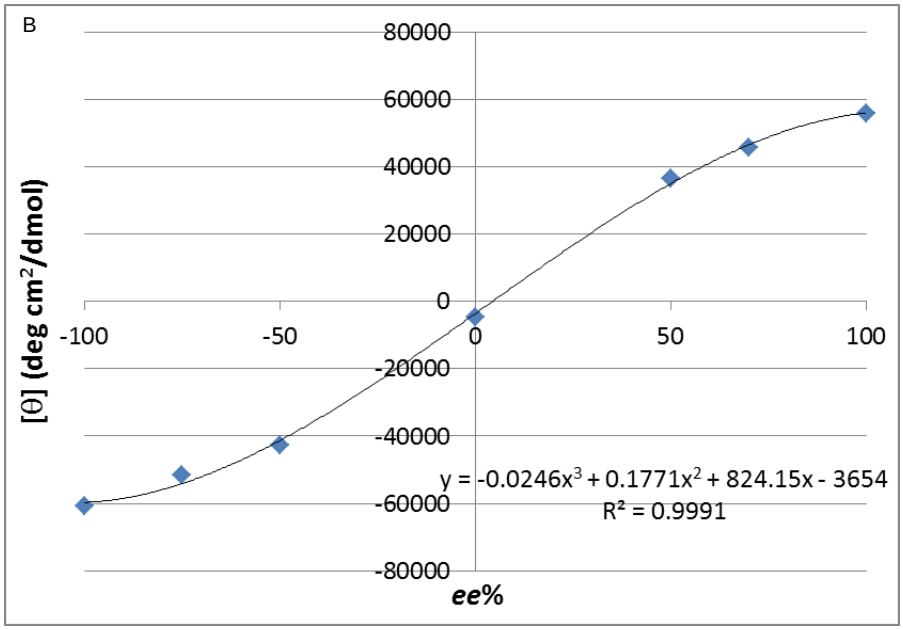

Figure 5.14. A) CD calibration curve for the assembly with Fe(II) (1 mM), **5.1** (8 mM) and **5.5** (5 mM) in CH_3CN at 521 nm. B) CD calibration curve for the assembly with Fe(II) (1 mM), **5.1** (8 mM) and **5.6** (5 mM) in CH_3CN at 525 nm (Cont.).

Using the equations defined by these calibration curves, the samples obtained by the Zhang group were analyzed and the results compared with those *ee*% values determined through chiral GC (Tables 5.5 and 5.6).

Calculated *ee*%	Chiral GC *ee*%	Error
109.2	90	19.2
3.1	-1	4.1
-35.9	-38.9	3.0
	Average Error	8.8

Table 5.5 List of experimental values of *ee*% compared to the actual GC values for the studies of the samples containing **5.5**.

Calculated *ee*%	Chiral GC *ee*%	Error
-1.9	-4.0	2.1
-45.1	-69.0	23.9
82.8	94.0	11.2
-29.1	-35.0	5.9
	Average Error	10.8

Table 5.6 List of experimental values of *ee*% compared to the actual GC values for the studies of the samples containing **5.6**.

While the degree of accuracy in the results yielded by this original analyses is not ideal, it is close enough to the values determined using the standard technique in the field, with much faster analysis rates. Each chiral GC analysis took an average of 30 minutes, compared to our method which took less than 3 hours for all samples (2 hours for the derivatization reaction + 50 minutes to analyze all samples and data points in the calibration curves). For the purposes of our HTS methodology, these numbers would allow the synthetic chemist to identify trends in enantioenrichment within potentially numerous arrays of samples. The trends affecting enantioselectivity can be found, then the reaction conditions that produced high *ee*% values could be examined in more detail.

5.4 CONCLUSIONS

With this novel instrumental design it becomes possible to read CD values of multiple samples in a multi-well plate format. The technology has been tested with an

existing sensing ensemble and the results proven consistent with bibliographic data. With average reading times of 3 seconds for a single wavelength value and around 50 seconds for a 120 nm scan per sample, the rate of CD analysis can truly be called high-throughput. Besides, as evidenced by the high correlation coefficients in the calibration curves (even when defined by few data points), this improvement in run-time speeds does not mean a loss in reproducibility. As an additional testament to the robustness to the method and the applicability to the instrument, the average error for *ee*% values in all amines tested is well within the limit associated with HTS.[35]

For the case of the implementation of the method into a catalytic discovery process, major headway is reported. We defined a protocol for working with a range of total analyte concentration that eliminates a purity control step and makes analysis of crude samples faster. Furthermore, a first set of real samples obtained from a synthetic group was obtained with satisfactory result.

Future work in this area involves expanding the scope of the method now that we have demonstrated its efficiency outside the sphere of commercially available pure materials into wider screenings of real samples. In the near future, we aim to process both more diverse species and heavier volumes of analytes from the Zhang group. Targeting larger numbers of samples to be screened will strongly showcase the increased speed of the method and emphasize its utility as a tool for understanding trends and causality in reaction conditions.

5.5 EXPERIMENTAL DETAILS

5.5.1 Materials and Methods

All reagents were purchased from commercial sources and used as received with the exception of aldehyde **5.1**, which was purified by sublimation under high vacuum with mild heat (60-70^{o}C) using a cold finger apparatus before use in the assay.

The so-called New York Univeristy four photoelastic modulator polarimeter was previously described.[57,58] In brief, light was incident on the sample at normal incidence. The transmitted light was detected with a photomultiplier. This instruments measures the 16 parameters of a normalized Mueller matrix at each wavelength. Briefly, the polarization state generator (PSG) and the polarizer state analyzer (PSA) are composed of two photoelastic modulators (PEMs) (Hinds Instruments) each operating at a different frequency, and a polarizer. The PEMs were set at relative orientations of ±45◦. A Xe arc lamp coupled to the monochromator allows spectroscopic measurements in a range from 290 nm to 850 nm. The advantage of this setup over other Mueller matrix polarimeters is that measurements are obtained without any moving parts.

5.5.2 CD Calibration Curves and Test Sample Experimental

All solutions intended for the plate reader experiments were prepared using the same method: 100 μL of the appropriate amine combination (obtained by mixing 3 mM solutions of the two enantiomers of each analyte in the necessary ratios) were mixed with 100 μL of a 3 mM solution of aldehyde 1 for 10 minutes. Then 100 μL of a 1 mM

solution of $Fe(OTf)_2$ were added to the mixture and the system was allowed to equilibrate for 2 hours, effectively making the concentration of host-guest complex 0.33 mM. The solvent used was HPLC grade acetonitrile. Upon completion of the reaction 30 μL of each solution were incorporated into each well of the 96 well-plate and 270 μL of HPLC grade acetonitrile added, leaving the final concentration of the active complex at 0.033 mM. This dilution step is necessary to account for the particular path length of the well-plate. When the path the beam has to pass through the sample (from the 0.1cm cuvettes used historically by our group) is increased to 12mm as in the 96 well plates, the concentration of the active species must be lowered accordingly. The degree of dilution necessary was determined experimentally by testing several concentrations on different wells for a known assembly until replicating previous results.

The solutions for the amine concentration determination were prepared by mixing 100 μL of a stock solution of amine **5.6** of the appropriate concentration (3 mM, 6 mM, 9 mM and 15 mM) with 100 μL of a stock solution of aldehyde 5.1 of the appropriate concentration (3 mM, 6 mM, 9 mM and 15 mM). Then 100 μL of a 3 mM solution of $Fe(OTf)_2$ were added to each solution and the CD measurements taken. For the titration of the amine into the system with an excess of aldehyde, the data points correspond to solutions prepared by mixing 100 μL of a 24mM solution of **5.1** with 100 μL of solutions of **5.6** of increasing concentrations (1.5 mM, 3 mM, 4.5 mM, 6 mM, 7.5 mM, 9 mM, 10.5 mM, 12 mM, 13.5 mM and 15 mM), with 100 μL of a solution of $Fe(OTf)_2$ at 3 mM added afterwards. For the calibration curves we mixed 100 μL of a 24mM solution of **5.1** with 100 μL of 15 mM solutions of amines **5.5** and **5.6** in varying proportions of the two enantiomers to achieve the desired *ee* values, to subsequently add 100 μL of a solution of $Fe(OTf)_2$ (3 mM). The actual samples were worked up by stirring them in 5 mL of $NaHCO_3$ to then extract with DCM (3x2 mL) and dry over anhydrous Na_2SO_4 and filter,

to finally eliminate the solvent in vacuum. The resulting solid was processed into the *ee* determination protocol in analogous conditions as those used for the calibration curves and assuming 100% purity. All of these CD measurements were performed at 25°C on a Jasco J-815 circular dichroism spectropolarimeter using a quartz cuvette of 0.1 cm light path. The CD instrument was purged prior to each use with nitrogen for 20 min. Spectra were collected between 200 and 700 nm with a standard sensitivity of 100 mdeg, a data pitch of 0.5 nm, a band width of 0.5 nm, a scanning speed of 1000 nm s^{-1} and a response of 0.5 s.

All curves were fit using the spreadsheet software Microsoft® Excel® and the physically relevant roots of the corresponding third-degree polynomial equations calculated *via* Wolfram Mathematica software.

5.6 REFERENCES

1 Alves, G.; Fortuna, A.; Falcao, A. *Trends Chromatogr*. **2008**, *4*, 1-10.

2 Stambuli, J. P.; Hartwig, J. F. *Curr. Opin. Chem. Biol.* **2003**, *7*, 420.

3 Shimizu, K. D.; Snapper, M. L.; Hoveyda, A. H. *Chem-Eur J.* **1998**, *4*, 1885.

4 Shabbir, S. H.; Regan, C. J.; Anslyn, E. V. *Natl Acad Sci USA* **2009**, *106*, 10487.

5 Reetz, M. T. *Angew. Chem. Int. Edit*. **2002**, *41*, 1335.

6 Traverse, J. F.; Snapper, M. L. *Drug Discov. Today*. **2002**, *7(19)*, 1002-12.

7 Jaekel, C.; Paciello, R. *Chem. Rev.* **2006**, *106(7)*, 2912-42.

8 Gennari, C.; Piarulli, U. *Chem. Rev*. **2003**, *103(8)*, 3071-100.

9 Wahler, D.; Reymond, J.- L. *Curr Opin Biotechnol*. **2001**, *12(6)*, 535-44.

10 Stambuli, J. P.; Hartwig, J. F. *Curr. Opin. Chem. Biol*. **2003**, *7(3)*, 420-6.

11 de Vries, J. G.; Lefort, L. *Chem. Eur. J.* **2006**, *12(18)*, 4722-34.

12 Ding, K. *Chem. Commun*. **2008**, *8*, 909-21.

13 Lefort, L.; Boogers, J. A. F.; de Vries, A. H. M.; de Vries, J. G. *Top. Catal*. **2006**, *40(1-4)*, 185-91.

14 Minnaard, A. J.; Feringa, B. L.; Lefort, L. de Vries, J. G. *Acc. Chem. Res.* **2007**, *40(12)*, 1267-77.

15 Seiche, W.; Breit, B. *Catalysts with Chiral Self-assembling Ligands in Phosphorus Ligands in Asymmetric Catalysis*, ed. A. Börner, Wiley-VCH, Weinheim **2008.**

16 Sakthivel, K.; Notz, W.; Bui, T.; Barbas, C. F. *J. Am. Chem. Soc*. **2001**, *123(22)*, 5260-7.

17 Lefort, L.; Boogers, J. A. F.; De Vries, A. H. M.; De Vries, J. G. *Org. Lett.* **2004**, *6(11)*, 1733-5.

18 Feringa, B. L. *Acc. Chem. Res.* **2000**, *33(6)*, 346-53.

19 Pamies, O.; Dieguez, M. *Chem. Eur. J.* **2008**, *14(3)*, 944-60.

20 Pescarmona, P. P.; Van der Waal, J. C.; Maxwell, I. E.; Maschmeyer, T. *Catal. Lett.* **1999**, *63(1,2)*, 1-11.

21 Crabtree, R. H. *Chem. Commun*. **1999**, *17*, 1611-6.

22 Powers, D. G.; Coffen, D. L. *Drug Discov. Today* **1999**, *4(8)*, 377-83.

23 Jagt, R. B. C.; Toullec, P. Y.; Schudde, E. P.; De Vries, J. G.; Feringa, B. L.; Minnaard, A. J. *J. Comb. Chem*. **2007**, *9(3)*, 407-14.

24 Tarasow, T. M.; Tarasow, S. L.; Eaton, B. E. *Nature* **1997**, *389(6646)*, 54-7

25 Reetz, M. T.; Kuhling, K. M.; Wilensek, S.; Husmann, H.; Hausig, U. W.; Hermes, M. *Catal. Today* **2001**, *67(4)*, 389-96.

26 Takacs, J. M.; Han, J. *Org. Lett*. **2004**, *6(18)*, 3099-102.

27 Bromidge, S.; Wilson, P. C.; Whiting, A. *Tetrahedron Lett*. **1998**, *39(48)*, 8905-8.

28 Leung, D.; Anslyn, E. V. *J. Am. Chem. Soc*. **2008**, *130(37)*, 12328-12333.

29 Wolf, C.; Bentley, K. W. *Chem. Soc. Rev*. **2013**.

30 Ghosn, M. W.; Wolf, C. *Tetrahedron*, **2010**, *66(23)*, 3989-3994.

31 You, L.; Berman, J. S.; Anslyn, E. V. *Nat. Chem*. **2011**, *3(12)*, 943-948.

32 Ghosn, M. W.; Wolf, C. *J. Am. Chem. Soc*. **2009**, *131(45)*, 16360-16361.

33 Iwaniuk, D. P.; Bentley, K. W.; Wolf, C. *Chirality*, **2012**, *24(7)*, 584.

34 Joyce, L. A.; Maynor, M. S.; Dragna, J. M.; da Cruz, G. M.; Lynch, V. M.; Canary, J. W.; Anslyn, E. V. *J. Am. Chem. Soc.* **2011**, *133(34)*, 13746-13752.

35 Dragna, J. M.; Pescitelli, G.; Tran, L.; Lynch, V. M.; Anslyn, E. V.; Di Bari, L. *J. Am. Chem. Soc.* **2012**, *134(9)*, 4398-4407.

36 Metola, P.; Anslyn, E. V.; James, T. D.; Bull, S. D. *Chem. Sci.* **2011**, *3(1)*, 156-161.

37 Ghosn, M. W.; Wolf, C. *Tetrahedron*, **2011**, *67(36)*, 6799-6803.

38 Iwaniuk, D. P.; Wolf, C. *Org. Lett*. **2011**, *13(10)*, 2602-2605.

39 Berova, N.; Nakanishi, K.; Woody, R. W. *Circular dichroism: principles and applications.* New York: Wiley-VCH, **2000**.

40 Purdie, N.; Brittain, H. G. *Analytical applications of circular dichroism*. **1993**.

41 Eriksson, M.; Nordén, B. *Meth. Enzymol*. **2001**, *340*, 68-98.

42 Nordén, B.; Kurucsev, T. J. *Mol. Recognit.* **1994**, *7(2)*, 141-155.

43 Hipps, K. W.; Crosby, G. A. *J. Phys. Chem*. **1979**, *83*, 555-562.

44 Schellman, J.; Jensen, H. P. *Chem. Rev*. **1987**, *87*, 1359-1399.

45 Michl, J.; Thulstrup, E. W. *Spectroscopy with Polarized Light*, VCH: New York, **1986**.

46 Kuroda, R.; Harada, T.; Shindo, Y. *Rev. Sci. Instrum*. **2001**, *72*, 3802-3810.

47 Maestre, M. F.; Salzman, G. C.; Tobey, R. A.; Bustamante, C. *Biochemistry*, **1985**, *24*, 5152-5157.

48 Moxon, J. R. L.; Renshaw, A. R. *J. Phys.: Condens. Matter*, **1990**, *2*, 6807-6836.

49 Kremers, M.; Meekes, H. *J. Phys. D: Appl. Phys.* **1995**, *28*, 1212-1224.

50 Arago, F. *Mem. Inst. Fr.* **1811**, *1*, 93-134.

51 O'Loane, J. K. *Chem. Rev.* **1980**, *80*, 41-61.

52 Applequist, *J. Am. Sci.* **1987**, *75*, 59-68.

53 Kobayashi, J.; Asahi, T.; Takahashi, S.; Glazer, A. M. *J. Appl. Crystallogr*. **1988**, *21*, 479-484.

54 Arteaga, O.; Canillas, A.; Jellison, Jr. G. E. *Appl. Opt.* **2009**, *48*, 5307-5317.

55 Kaminsky, W. *Rep. Prog. Phys*. **2000**, *63*, 1575-1640.

56 Kahr, B.; Arteaga, O. *Chemphyschem*, **2012**, *16*, 79-88.

57 Arteaga, O.; Freudenghtal, J.; Wang, B.; Nichols, S.; Kahr, B. *Chim. Oggi*. **2012**, *30*, 31-36.

58 Arteaga, O.; Freudenthal, J.; Wang, B.; Kahr, B. *Appl. Opt*. **2012**, *51*, 6805-6817.

59 Jellison, G. E., & Modine, F. A. *Appl. Opt.* **1997**, *36(31)*, 8184-8189.

60 Jellison, G. E., & Modine, F. A. *Appl. Opt.* **1997**, *36(31)*, 8190-8198.

61 Church, T. L.; Andersson, P. G. *Chiral Amine Synthesis*; Wiley-VCH Verlag GmbH & Co. KGaA: **2010**.

62 Zhang, W.; Zhang, X. *Comprehensive Chirality*; Editors-in-Chief: Erick, M. C., Hisashi, Y., Eds.; Elsevier: Amsterdam, **2012**, 301-317.

63 Xie, J.-H.; Zhu, S.-F.; Zhou, Q.-L. *Chem. Rev*. **2010**, *111*, 1713-1760.

64 Hou, G.; Gosselin, F.; Li, W.; McWilliams, J. C.; Sun, Y.; Weisel, M.; O'Shea, P. D.; Chen, C.-y.; Davies, I. W.; Zhang, X. *J. Am. Chem. Soc.* **2009**, *131*, 9882-9883.

65 Hou, G.; Li, W.; Ma, M.; Zhang, X.; Zhang, X. *J. Am. Chem. Soc*. **2010**, *132*, 12844-12846.

66 Hou, G.; Tao, R.; Sun, Y.; Zhang, X.; Gosselin, F. *J. Am. Chem. Soc*. **2010**, *132*, 2124-2125.

67 Knowles, R. R.; Jacobsen, E. N. *Proc. Natl. Acad. Sci. U. S. A.* **2010**, *107*, 20678-20685.

68 Takemoto, Y. *Chem. Pharm. Bull.* **2010**, *58*, 593-601.

69 Zhang, Z.; Schreiner, P. R. *Chem. Soc. Rev.* **2009**, *38*, 1187-1198.

70 Phipps, R. J.; Hamilton, G. L.; Toste, F. D. *Nat. Chem.* **2012**, *4*, 603-614.

71 Brak, K.; Jacobsen, E. N. *Angew. Chem. Int. Ed*. **2013**, *52*, 534-561.

72 Mahlau, M.; List, B. *Angew. Chem. Int. Ed.* **2013**, *52*, 518-533.

73 Zhao, Q.; Li, S.; Huang, K.; Wang, R.; Zhang, X. *Org. Lett*. **2013**, *15*, 4014-4017.

74 Taylor, M. S.; Jacobsen, E. N. *J. Am. Chem. Soc*. **2004**, *126*, 10558-10559.

75 Taylor, M. S.; Tokunaga, N.; Jacobsen, E. N. *Angew. Chem. Int. Ed*. **2005**, *44*, 6700-6704.

76 Knowles, R. R.; Lin, S.; Jacobsen, E. N. *J. Am. Chem. Soc.* **2010**, *132*, 5030-5032.

77 Xu, H.; Zuend, S. J.; Woll, M. G.; Tao, Y.; Jacobsen, E. N. *Science* **2010**, *327*, 986-990.

78 Birrell, J. A.; Desrosiers, J.-N.; Jacobsen, E. N. *J. Am. Chem. Soc.* **2011**, *133*, 13872-13875.

79 Burns, N. Z.; Witten, M. R.; Jacobsen, E. N. *J. Am. Chem. Soc.* **2011**, *133*, 14578-14581.

80 Lin, S.; Jacobsen, E. N. *Nat. Chem.* **2012**, *4*, 817-824.

81 Lalonde, M. P.; McGowan, M. A.; Rajapaksa, N. S.; Jacobsen, E. N. *J. Am. Chem. Soc.* **2013**.

82 De, C. K.; Klauber, E. G.; Seidel, D. *J. Am. Chem. Soc.* **2009**, *131*, 17060-17061.

83 Lee, Y. S.; Alam, M. M.; Keri, R. S. *Chem.Asian J.* **2013**.

84 Zuend, S. J.; Jacobsen, E. N. *J. Am. Chem. Soc.* **2009**, *131*, 15358-15374.

Bibliography

Adamczyk-Woźniak, A.; Cyrański, M. K.; Jakubczyk, M.; Klimentowska, P.; Koll, A.; Kołodziejczak, J.; Pojmaj, G.; Żubrowska, A.; Żukowska, G. Z.; Sporzyński, A. *J. Phys. Chem. A* **2010**, *114*, 2324-2330.

Ahn, K. H.; Ku, H.-Y.; Kim, Y.; Kim, S.-G.; Kim, Y. K.; Son, H. S.; Ku, J. K. *Org. Lett.* **2003**, *5*, 1419–1422.

Alves, G.; Fortuna, A.; Falcao, A. *Trends Chromatogr*. **2008**, *4*, 1-10.

Al-Zoubi, R. M.; Marion, O.; Hall, D. G. *Angew. Chem. Int. Ed*. **2008**, *47*, 2876-2879.

Anslyn, E. V.; Dougherty, D. A. Chapter 11. *Modern physical organic chemistry*. University Science Books. **2006**.

Applequist, *J. Am. Sci.* **1987**, *75*, 59-68.

Arago, F. *Mem. Inst. Fr.* **1811**, *1*, 93-134.

Arnal-Hérault, C.; Pasc, A.; Michau, M.; Cot, D.; Petit, E.; Barboiu, M. *Angew. Chem. Int. Ed.* **2007**, *46*, 8409-8413.

Arnal-Hérault, C.; Pasc, A.; Michau, M.; Cot, D.; Petit, E.; Barboiu, M. *Angew. Chem. Int. Ed*. **2007**, *46(44)*, 8409-8413.

Arteaga, O.; Canillas, A.; Jellison, Jr. G. E. *Appl. Opt*. **2009**, *48*, 5307-5317.

Arteaga, O.; Freudenghtal, J.; Wang, B.; Nichols, S.; Kahr, B. *Chim. Oggi*. **2012**, *30*, 31-36.

Arteaga, O.; Freudenthal, J.; Wang, B.; Kahr, B. *Appl. Opt*. **2012**, *51*, 6805-6817.

Berova, N.; Nakanishi, K.; Woody, R. W. *Circular dichroism: principles and applications.* New York: Wiley-VCH, **2000**.

Bicker, K. L.; Sun, J.; Harrell, M.; Zhang, Y.; Pena, M. M.; Thompson, P. R.; Lavigne, J. J. *Chem. Sci.* **2012**, *3*, 1147–1156.

Bielecki, M.; Eggert, H.; Norrild, J. C. *J. Chem. Soc., Perkin Trans. 2*, **1999**, *3*, 449-456.

Birrell, J. A.; Desrosiers, J.-N.; Jacobsen, E. N. *J. Am. Chem. Soc.* **2011**, *133*, 13872-13875.

Bissell, R.; Prasanna de Silva, A.; Nimal Gunaratne, H.; Mark Lynch, P.; Maguire, G.; McCoy, C.; Samankumara Sandanayake, K. *Top. Curr. Chem*. **1993**, *168*, 223-264.

Brak, K.; Jacobsen, E. N. *Angew. Chem. Int. Ed*. **2013**, *52*, 534-561.

Braun, H.; Felber, H.; Knesse, G.; Ritter, A.; Schmidtchen, F. P.; Schneider, A. *Tetrahedron* **2001**, *57*, 3313–3328.

Bromidge, S.; Wilson, P. C.; Whiting, A. *Tetrahedron Lett*. **1998**, *39(48)*, 8905-8.

Brown HC, Zaidlewicz M. *Organic Syntheses via Boranes. Vol. 2*. Milwaukee, WI: Aldrich Chemical; **2001**.

Brown HC. *Organic Syntheses via Boranes. Vol. 1*. Milwaukee, WI: Aldrich Chemical; **1997**.

Brown, H. C.; B. Nazer, B.;Cha, J. S.;Sikorski, J. A. *J. Org. Chem*. **1986**, *51*, 5264.

Brown, H. C.; Cole, T. E.; Srebnick, M.; Kim, K. –W. *J. Org. Chem*. **1986**, *51*, 4925.

Brown, H. C.; Kramer, G. W.; Hubbard, J. L.; Krishnamurthy, S. *J. Organometal. Chem*. **1980**, *188*, 1.

Brown, H. C.; Sinclair, J. A. *J. Organometal. Chem*. **1977**, *131*, 163.

Bukhtiyarova, M.; Rizzo, C. J.; Kettner, C. A.; Korant, B. D.; Scarnati, H. T.; King, R. W. *Antiviral Chem. Chemother*. **2002**, *12*, 367-373.

Burns, N. Z.; Witten, M. R.; Jacobsen, E. N. *J. Am. Chem. Soc.* **2011**, *133*, 14578-14581.

Cao, H.; Heagy, M. D. *J. Fluoresc*. **2004**, *14*, 569–584.

Cesàro, A. *Thermodynamic Data for Biochemistry and Biotechnology*; Hinz, H. J., Ed.; Springer-Verlag: Berlin, **1986**.

Chaberek, S.; Courtney, R. C.; Martell, A. E. *J. Am. Chem. Soc*. **1952**, *74*, 5057.

Chandrasekharan, J.; Brown, H. C. *J. Org. Chem*. **1985**, *50*, 518.

Church, T. L.; Andersson, P. G. *Chiral Amine Synthesis*; Wiley-VCH Verlag GmbH & Co. KGaA: **2010**.

Collins, B. E.; Metola, P.; Anslyn, E. V. *Supramol. Chem.* **2013**, *25(2)*, 79-86.

Collins, B. E.; Sorey, S.; Hargrove, A. E.; Shabbir, S. H.; Lynch, V. M.; Anslyn, E. V. *J. Org. Chem*. **2009**, *74*, 4055–4060.

Collins, B. E.; Sorey, S.; Hargrove, A. E.; Shabbir, S. H.; Lynch, V. M.; Anslyn, E. V. *J. Org. Chem.* **2009** *74(11)*, 4055-4060.

Cooper, C. R.; James, T. D. *Chem. Lett* **1998**, 883–884.

Cooper, C. R.; Spencer, N.; James, T. D. *Chem. Commun*. **1998**, 1365-1366.

Corbett, P. T.; Vial, L.; West, K. R.; Wietor, J.-L.; Sanders, J. K. M.; Otto, S. *Chem. Rev*. **2006**, *106*, 3652.

Corradini, R.; Paganuzzi, C.; Marchelli, R.; Pagliari, S.; Sforza, S.; Dossena, A.; Galaverna, G.; Duchateau, A. *J. Mater. Chem.* **2005**, *15*, 2741–2746.

Côté, A. P.; Benin, A. I.; Ockwig, N. W.; O'Keeffe, M.; Matzger, A. J.; Yaghi, O. M. *Science* **2005**, *310*, 1166-1170.

Cougnon, F. B. L.; Sanders, J. K. M. *Acc. Chem. Res*., Article ASAP

Crabtree, R. H. *Chem. Commun*. **1999**, *17*, 1611-6.

Dai, C.; Cazares, L.H.; Wang, L.; Chu, Y.; Troyer, D.A.; Semmes, O.J.; Drake, R.R. Wang, B. *Chem. Commun.* **2011**, *47*, 10338-10340.

de Silva, A. P.; Gunnlaugsson, T.; Rice, T. E. *Analyst*, **1996**, *121(12)*, 1759-1762.

de Vries, J. G.; Lefort, L. *Chem. Eur. J.* **2006**, *12(18)*, 4722-34.

De, C. K.; Klauber, E. G.; Seidel, D. *J. Am. Chem. Soc.* **2009**, *131*, 17060-17061.

DeMoor, J. E.; Van der Kelen, G. P. *J. Organomet. Chem*. **1966**, *6*, 235.

Dewar, M. J. S.; Jones, R. *J. Am. Chem. Soc*. **1967**, *89*, 4251.

Ding, K. *Chem. Commun*. **2008**, *8*, 909-21.

Dragna, J. M.; Pescitelli, G.; Tran, L.; Lynch, V. M.; Anslyn, E. V.; Di Bari, L. *J. Am. Chem. Soc.* **2012**, *134(9)*, 4398-4407.

Dunsdon, R. M.; Greening, J. R.; Jones, P. S.; Jordan, S.; Wilson, F. X. *Bioorg. Med. Chem. Lett.* **2000**, *10*, 1577-1579.

Eaton, G. R. *J. Chem. Ed*. **1969**, *46*, 547.

Edwards, N. Y.; Sager, T. W.; McDevitt, J. T.; Anslyn, E. V. *J. Am. Chem. Soc*. **2007**, *129*, 13575–13583.

El-Kaderi, H. M.; Hunt, J. R.; Mendoza-Cortés, J. L.; Côté, A. P.; Taylor, R. E.; O'Keeffe, M.; Yaghi, O. M. *Science* **2007**, *316*, 268-272.

Eriksson, M.; Nordén, B. *Meth. Enzymol*. **2001**, *340*, 68-98.

Fang, H.; Kaur, G.; Wang, B. *J. Fluoresc.* **2004**, *14(5)*, 481-489.

Fedoak, R. N.; Gershon, M. D.; Field, M. *Gastroenterology* **1989**, *96*, 37.

Feringa, B. L. *Acc. Chem. Res.* **2000**, *33(6)*, 346-53.

Ferrand, Y.; Crump, M. P.; Davis, A. P. *Science*, **2007**, *318(5850)*, 619-622.

Flentke, G. R.; Munoz, E.; Huber, B. T.; Plaut, A. G.; Kettner, C. A.; Bachovchin, W. W. *Proc. Natl. Acad. Sci. U. S. A.* **1991**, *88*, 1556-1559.

Franks, F. *Pure Appl. Chem.* **1987**, *59*, 1189–1202.

Franzen, S.; Ni, W.; Wang, B. *J. Phys. Chem. B* **2003**, *107*, 12942−12948

G. Wulff; *Pure Appl. Chem.* **1982**, *54*, 2093-2102.

Gadamasetti, K. G.; Braish, T. *Process Chemistry in the Pharmaceutical Industry*; Vol. 2, CRC Press, New York, **1973**.

Galbraith, E.; Kelly, A. M.; Fossey, J. S.; Kociok-Köhn, G.; Davidson, M. G.; Bull, S. D.; James, T. D. *New J. Chem*. **2009**, *33(1)*, 181-185.

Gamsey, S.; Miller, A.; Olmstead, M. M.; Beavers, C. M.; Hirayama, L. C.; Pradhan, S.; Wessling, R. A.; Singaram, B. *J. Am. Chem. Soc.* **2007**, *129*, 1278–1286.

Gennari, C.; Piarulli, U. *Chem. Rev*. **2003**, *103(8)*, 3071-100.

Ghosn, M. W.; Wolf, C. *Tetrahedron*, **2010**, *66(23)*, 3989-3994.

Ghosn, M. W.; Wolf, C. *Tetrahedron*, **2011**, *67(36)*, 6799-6803.

Ghosn, M. W.; Wolf, C. *J. Am. Chem. Soc*. **2009**, *131(45)*, 16360-16361.

Goldberg, R. N.; Tewari, Y. B. *J. Phys. Chem. Ref. Data* **1989**, *18*, 809−880.

Good, C. D.; Ritter, D. M. Ritter *J. Am. Chem. Soc*. **1962**, *84*, 1162.

Gray Jr, C. W.; Houston, T. A. *J. Org. Chem*. **2002**, *67(15)*, 5426-5428.

Gray, C. W., Jr.; Houston, T. A. *J. Org. Chem.* **2002**, *67*, 5426–5428.

Gutierrez-Moreno, N. J.; Medrano, F.; Yatsimirsky, A. K. *Org. Biomol. Chem.* **2012**, *10*, 6960-6972.

Hall, D. G. *Boronic Acids: Preparation and Applications in Organic Synthesis and Medicine*, Wiley-VCH, Weinheim, **2005**.

Hanazaki, I.; Akimoto; H. *J. Am. Chem. Soc.* **1972**, *94*, 4102-4106.

Hargrove, A. E.; Zhong, Z.; Sessler, J. L.; Anslyn, E. V. *New J. Chem*. **2012**, *34(2)*, 348-354.

Hili, R.; Baktharaman, S.; Yudin, A. K. *Eur. J. Org. Chem*. **2008**, *31*, 5201–5213.

Hipps, K. W.; Crosby, G. A. *J. Phys. Chem*. **1979**, *83*, 555-562.

Hiratake, J.; Oda, J. *Biosci. Biotech. Biochem*. **1997**, *61*, 211-218.

Hou, G.; Gosselin, F.; Li, W.; McWilliams, J. C.; Sun, Y.; Weisel, M.; O'Shea, P. D.; Chen, C.-y.; Davies, I. W.; Zhang, X. *J. Am. Chem. Soc.* **2009**, *131*, 9882-9883.

Hou, G.; Li, W.; Ma, M.; Zhang, X.; Zhang, X. *J. Am. Chem. Soc*. **2010**, *132*, 12844-12846.

Hou, G.; Tao, R.; Sun, Y.; Zhang, X.; Gosselin, F. *J. Am. Chem. Soc*. **2010**, *132*, 2124-2125.

Huang, C. Y.; Cabell, L. A.; Anslyn, E. V. *J. Am. Chem. Soc.* **1994**, *116(7)*, 2778-2792.

Huang, X.; Ortiz-Marciales, M.; Huang, K.; Stepanenko, V.; Merced, F. G.; Ayala, A. M.; Correa, W.; De Jesus, M. *Org. Lett.* **2007**, *9*, 1793–1795.

Hutin, M.; Bernardinelli, G.; Nitschke, J. R. *Chem.-Eur. J.* **2008**, *14(15)*, 4585-4593.

Iwaniuk, D. P.; Bentley, K. W.; Wolf, C. *Chirality*, **2012**, *24(7)*, 584.

Iwaniuk, D. P.; Wolf, C. *Org. Lett*. **2011**, *13(10)*, 2602-2605.

Jaekel, C.; Paciello, R. *Chem. Rev.* **2006**, *106(7)*, 2912-42.

Jagt, R. B. C.; Toullec, P. Y.; Schudde, E. P.; De Vries, J. G.; Feringa, B. L.; Minnaard, A. J. *J. Comb. Chem*. **2007**, *9(3)*, 407-14.

James, B. D.; Nanda, R. K.; Wallbridge, M. G. H. *J. Chem. Soc. A*, **1966**, 182.

James, T. D. *Creative Chemical Sensor Systems*. Springer Berlin Heidelberg, **2007**.

James, T. D. *Top Curr. Chem*. **2007**, *277*, 107-152.

James, T. D.; Linnane, P.; Shinkai, S. *Chem. Commun*. **1996**, *3*, 281-288.

James, T. D.; Phillips, M. D.; Shinkai, S. *Boronic Acids in Saccharide Recognition*, RSC Publishing, Cambridge, **2006**.

James, T. D.; Sandanayake, K. R. A. S.; Shinkai, S. *Angew. Chem. Int. Ed.* **1994**, *33*, 2207.

James, T. D.; Sandanayake, K. R. A. S.; Shinkai, S. *Angew. Chem., Int. Ed. Engl.* **1996**, *35*, 1910–1922.

James, T. D.; Sandanayake, K. R. A. S.; Shinkai, S. *J. Chem. Soc., Chem. Commun*. **1994**, 477.

James, T. D.; Sandanayake, K. R. A. S.; Shinkai, S. *Nature*, **1995**, *374*, 345-347.

James, T. D.; Sandanayake, K. R. A.; Shinkai, S. *Angew. Chem. Int. Ed*. **2003**, *35(17)*, 1910-1922.

James, T. D.; Sandanayake, K. R. A.; Shinkai, S. *Angew. Chem. Int. Ed.* **1996**, *35(17)*, 1910-1922.

James, T. D.; Shinkai, S.; *Top. Curr. Chem*. **2002**, *218*, 159–200.

Jellison, G. E., & Modine, F. A. *Appl. Opt.* **1997**, *36(31)*, 8190-8198.

Jin, S.; Cheng, Y.; Reid, S.; Li, M.; Wang, B. *Med. Res. Rev*. **2010**, *30*, 171–257.

Johnson R. A.; Winchern, D. W. *Applied Multivariate Statistical Analysis*; Prentice-Hall: Englewood Cliffs, N. J., **1982**.

Joliffe, I. T. *Principal Component Analysis*, 2nd ed; Springer-Verlag: New York, **2002**.

Joyce, L. A.; Maynor, M. S.; Dragna, J. M.; da Cruz, G. M.; Lynch, V. M.; Canary, J. W.; Anslyn, E. V. *J. Am. Chem. Soc.* **2011**, *133(34)*, 13746-13752.

Jurs, P. C.; Bakken, G. A.; McClellan, H. E. *Chem. Rev*. **2000**, *100*, 2649-2678.

Kadyrov, R.; Riermeier, T. H. *Angew. Chem.* 2003, **115**, 5630–5632; *Angew. Chem. Int. Ed.* **2003**, *42*, 5472–5474.

Kahr, B.; Arteaga, O. *Chemphyschem*, **2012**, *16*, 79-88.

Kaminsky, W. *Rep. Prog. Phys*. **2000**, *63*, 1575-1640.

Kelly, A. M.; Perez-Fuertes, Y.; Arimori, S.; Bull, S. D.; James, T. D. *Org. Lett.* **2006**, *8*, 1971–1974.

Kelly, A. M.; Pérez-Fuertes, Y.; Fossey, J. S.; Yeste, S. L.; Bull, S. D.; James, T. D. *Nat. Protoc.* **2008**, *3(2)*, 215-219.

Kettner, C.; Mersinger, L.; Knabb, R. *J. Biol. Chem*. **1990**, *265*, 18289-18297.

Kitamura, M.; Suzuki, T.; Abe, R.; Ueno, T.; Aoki, S. *Inorg. Chem.* **2011**, *50(22)*, 11568-11580.

Knowles, R. R.; Jacobsen, E. N. *Proc. Natl. Acad. Sci. U. S. A.* **2010**, *107*, 20678-20685.

Knowles, R. R.; Lin, S.; Jacobsen, E. N. *J. Am. Chem. Soc.* **2010**, *132*, 5030-5032.

Kobayashi, J.; Asahi, T.; Takahashi, S.; Glazer, A. M. *J. Appl. Crystallogr*. **1988**, *21*, 479-484.

Korich, A. L.; Iovine, P. M. *Dalton Trans*. **2010**, *39*, 1423-1431.

Kremers, M.; Meekes, H. *J. Phys. D: Appl. Phys.* **1995**, *28*, 1212-1224.

Kuivila, H. G.; Keough, A. H.; Soboczenski, E. J. *J. Org. Chem.* **1954**, *19*, 780-783.

Kuroda, R.; Harada, T.; Shindo, Y. *Rev. Sci. Instrum*. **2001**, *72*, 3802-3810.

Lalonde, M. P.; McGowan, M. A.; Rajapaksa, N. S.; Jacobsen, E. N. *J. Am. Chem. Soc.* **2013**.

Larkin, J.D.; Fossey, J.S.; James, T.D.; Brooks, B.R.; Bock, C.W. *J. Phys. Chem. A* **2010**, *114*, 12531-12539.

Lavigne, J. J.; Anslyn, E. V. *Angew. Chem., Int. Ed.* **1999**, *38(24)*, 3666-3669.

Lee, J. W.; Lee, J.-S.; Chang, Y.-T. *Angew. Chem. Int. Ed*. **2006**, *45*, 6485–6487.

Lee, S. J.; Lin, W. *J. Am. Chem. Soc.* **2002**, *124*, 4554–4555.

Lee, Y. S.; Alam, M. M.; Keri, R. S. *Chem.Asian J.* **2013**.

Lefort, L.; Boogers, J. A. F.; De Vries, A. H. M.; De Vries, J. G. *Org. Lett.* **2004**, *6(11)*, 1733-5.

Lefort, L.; Boogers, J. A. F.; de Vries, A. H. M.; de Vries, J. G. *Top. Catal*. **2006**, *40(1-4)*, 185-91.

Lehn, J.-M. *Chem. Soc. Rev*. **2007**, *36*, 151.

Lehn, J.-M. *Supramolecular Chemistry: Concepts and Perspectives*; VCH: Weinheim, **1995**.

Leung, D.; Anslyn, E. V. *J. Am. Chem. Soc*. **2008**, *130(37)*, 12328-12333.

Li, H.; Liu, Y.; Liu, J.; Liu, Z. *Chem. Commun*. **2011**, *47(28)*, 8169-8171.

Lin, G.-Q.; Xu, M.-H.; Zhong, Y.-W.; Sun, X.-W. *Acc. Chem. Res.* **2008**, *41*, 831–840.

Lin, J.; Zhang, H. C.; Pu, L. *Org. Lett.* **2002**, *4*, 3297–3300.

Lin, S.; Jacobsen, E. N. *Nat. Chem.* **2012**, *4*, 817-824.

Liu, S.; Pestano, J. P. C.; Wolf, C. *J. Org. Chem.* **2008**, *73*, 4267–4270.

Lorand, J. P.; Edwards, J. O. *J. Org. Chem*. **1959**, *24(6)*, 769-774.

Maestre, M. F.; Salzman, G. C.; Tobey, R. A.; Bustamante, C. *Biochemistry*, **1985**, *24*, 5152-5157.

Mahlau, M.; List, B. *Angew. Chem. Int. Ed.* **2013**, *52*, 518-533.

Mallia, A. K.; Hermanson, G. T.; Krohn, R. I.; Fujimoto, E. K.; Smith, P. K. *Anal. Lett.* **1981**, *14(8)*, 649-661.

Martinez-Aguirre, M. A.; Villamil-Ramos, R.; Guerrero-Alvarez, J. A.; Yatsimirsky, A. K. *J. Org. Chem*. **2013**, *78*, 4674-4684.

Matsumura, T.; Iwatsuki, S.; Ishihara, K. *Inorg. Chem. Commun*. **2005**, *8(8)*, 713-716.

Maue, M.; Schrader, T. *Angew. Chem., Int. Ed.* **2005**, *44*, 2265–2270.

Metola, P.; Anslyn, E. V.; James, T. D.; Bull, S. D. *Chem. Sci.* **2011**, *3(1)*, 156-161.

Michl, J.; Thulstrup, E. W. *Spectroscopy with Polarized Light*, VCH: New York, **1986**.

Mikhailov, B. M.; Kuimova, M. E. *Zh. Obshch. Khim*. **1971**, *41*, 1721.

Minnaard, A. J.; Feringa, B. L.; Lefort, L. de Vries, J. G. *Acc. Chem. Res.* **2007**, *40(12)*, 1267-77.

Mirri, G.; Bull, S. D.; Horton, P. N.; James, T. D.; Male L.; Tucker, J. H. R. *J. Am. Chem. Soc.* **2010**, *132*, 8903-8905.

Miyaura, N.; Suzuki, A. *Chem. Rev*. **1995**, *95*, 2457-2483.

Miyaura, N.; Yamada, K.; Suzuki, A. *Tetrahedron Lett*. **1979**, *20*, 3437-3440.

Miyazaki, Y.; Fujimori, T.; Okita, H.; Hirano, T.; Yoshimura, K. *Dalton Trans*. **2013**, *42*, 10473-10486.

Miyazaki, Y.; Matsuo, H.; Fujimori, T.; Takemura, H.; Matsuoka, S.; Okobira, T.; Uezu, K.; Yoshimura, K. *Polyhedron*, **2008**, *27*, 2785-2790.

Moulin, E.; Cormosw, G.; Giuseppone, N. *Chem. Soc. Rev*. **2012**, *41*,1031.

Moxon, J. R. L.; Renshaw, A. R. *J. Phys.: Condens. Matter*, **1990**, *2*, 6807-6836.

Musto, C. J.; Lim, S. H.; Suslick, K. S. *Anal. Chem*. **2009**, *81*, 6526–6533.

Nagai, Y.; Kobayashi, K.; Toi, H.; Aoyama, Y. *Bull. Chem. Soc. Jpn.* **1993**, *66*, 2965−2971.

Nakanishi, K.; Berova, N.; Woody, R. W. *Circular Dichroism: Principles and Aplications*; Wiley-VCH, **2000**.

Nguyen, B. T.; Wiskur, S. L.; Anslyn, E. V. *Org. Lett.* **2004**, *6*, 2499–2501.

Ni, W.; Kaur, G.; Springsteen, G.; Wang, B.; Franzen, S. *Bioorg. Chem*. **2004**, *32*, 571−581.

Nieto, S.; Dragna, J. M.; Anslyn, E. V. *Chem. Eur. J.* **2010**, *16*, 227-232.

Nordén, B.; Kurucsev, T. J. *Mol. Recognit.* **1994**, *7(2)*, 141-155.

Norrild, J. C.; Eggert, H. *J. Chem. Soc., Perkin Trans. 2*, **1996**, *12*, 2583-2588.

Nöth, H.; Vahrenkamp, H. *Chem. Ber.* **1966**, *99*, 1049.

Nöth, H.; Vahrenkamp, H. *Chem. Ber*. **1967**, *100*, 3353.

Nöth, H.; Wrackmeyer, B. *Nuclear Magnetic Resonance Spectroscopy of Boron Compounds*, Springer-Verlag: Berlin, **1978**. .

O'Loane, J. K. *Chem. Rev.* **1980**, *80*, 41-61.

Onak, T. P.; Landesman, H.; Willams, R. E. *J. Phys. Chem*. **1959**, *63*, 1533.

Paetzold, P. I.; Hansen, H. -J Z. *Inorg. Chem*. **1966**, *345*, 79.

Pamies, O.; Dieguez, M. *Chem. Eur. J.* **2008**, *14(3)*, 944-60.

Paugam, M.-F.; Bien, J. T.; Smith, B. D.; Chrisstoffels, L. A. J.; de Jong, F.; Reinhoudt, D. N. *J. Am. Chem. Soc.* **1996**, *118*, 9820–9825.

Paugam, M.-F.; Valencia, L. S.; Bogges, B.; Smith, B. D. *J. Am. Chem. Soc.* **1994**, *116*, 11203–11204.

Perez-Fuertes, Y.; Kelly, A. M.; Arimori, S.; Bull, S. D.; James T. D. *Org. Lett.*, **2006**, *8*, 1971-1974.

Perez-Fuertes, Y.; Kelly, A. M.; Fossey, J. S.; Powell, M. E.; Bull, S. D.; James, T. D. *Nat. Protoc.* **2008**, *3*, 210–214.

Perez-Fuertes, Y.; Kelly, A. M.; Johnson, A. L.; Arimori, S.; Bull, S. D.; James, T. D. *Org. Lett*. **2006**, *8*, 609–612.

Pescarmona, P. P.; Van der Waal, J. C.; Maxwell, I. E.; Maschmeyer, T. *Catal. Lett.* **1999**, *63(1,2)*, 1-11.

Phillips, M. D.; James, T. D. *J. Fluoresc.* **2004**, *14*, 549–559.

Phillips, W. D; Miller, H. C.; Mutterties, E. L. *J. Am. Chem. Soc*. **1959**, *81*, 4496.

Phipps, R. J.; Hamilton, G. L.; Toste, F. D. *Nat. Chem.* **2012**, *4*, 603-614.

Pizer, R.; Tihal, C. *Inorg. Chem*. **1992**, *31*, 3243-3241.

Pizer, R.; Tihal, C. *Polyhedron* **1996**, *15(19)*, 3411-3416.

Powers, D. G.; Coffen, D. L. *Drug Discov. Today* **1999**, *4(8)*, 377-83.

Purdie, N.; Brittain, H. G. *Analytical applications of circular dichroism*. **1993**.

Rambo, B. M.; Lavigne, J. *J. Chem. Mater*. **2007**, *19*, 3732-3739.

Reetz, M. T. *Angew. Chem. Int. Edit*. **2002**, *41*, 1335.

Reetz, M. T.; Kuhling, K. M.; Wilensek, S.; Husmann, H.; Hausig, U. W.; Hermes, M. *Catal. Today* **2001**, *67(4)*, 389-96.

Rowan, S. J.; Cantrill, S. J.; Cousins, G. R. L.; Sanders, J. K. M.; Stoddart, J. F. *Angew. Chem., Int. Ed*. **2002**, *41*,898.

Sakthivel, K.; Notz, W.; Bui, T.; Barbas, C. F. *J. Am. Chem. Soc*. **2001**, *123(22)*, 5260-7.

Schaeffer, R.; Todd, L. J. *J. Am. Chem. Soc.* **1965**, *87*, 488.

Schellman, J.; Jensen, H. P. *Chem. Rev*. **1987**, *87*, 1359-1399.

Schiller, A.; Wessling, R. A.; Singaram, B. *Angew. Chem. Int. Ed*. **2007**, *46*, 6457–6459.

Secor, K. E.; Glass, T. E. *Org. Lett.* **2004**, *6*, 3727–3730.

Seiche, W.; Breit, B. *Catalysts with Chiral Self-assembling Ligands in Phosphorus Ligands in Asymmetric Catalysis*, ed. A. Börner, Wiley-VCH, Weinheim **2008.**

Shabbir, S. H.; Regan, C. J.; Anslyn, E. V. *Natl Acad Sci USA* **2009**, *106*, 10487.

Shimizu, K. D.; Snapper, M. L.; Hoveyda, A. H. *Chem-Eur J.* **1998**, *4*, 1885.

Siedle, A. R. *Annu. Rep. NMR Spectrosc.* **1982**, *12*, 177-261.

Siedle, A. R. *Annu. Rep. NMR Spectrosc*. **1988**, *20*, 205-314.

Sigman, M. S.; Jacobsen, E. N. *J. Am. Chem. Soc.* **1998**, *120*, 4901–4902.

Smith, B. M.; Owens, J. L.; Bowman, C. N.; Todd, P. *Carbohydr. Res.* **1998**, *308*, 173-179.

Smith, W. L. *J. Chem. Ed*. **1977**, *54*, 469.

Spencer, J.; Burd, A. P.; Goodwin, C. A.; Mérette, S. A. M.; Scully, M. F.; Adatia, T.; Deadman, J. J. *Tetrahedron* **2002**, *58*, 1551-1556.

Springsteen, G.; Deeter, S.; Gao, X.; Wang, B. *Tetrahedron*, **2002**, *58*, 5291–5300.

Springsteen, G.; Wang, B. *Tetrahedron* **2002**, *58(26)*, 5291-5300.

Stambuli, J. P.; Hartwig, J. F. *Curr. Opin. Chem. Biol*. **2003**, *7(3)*, 420-6.

Striegler, S. *Curr. Org. Chem*. **2003**, *7*, 81–102.

Strynadka, N. C. J.; Adachi, H.; Jensen, S. E.; Johns, K.; Sielecki, A.; Betzel, C.; Sutoh, K.; James, M. N. G. *Nature* **1992**, *359*, 700-705.

Suzuki A, Brown HC. *Organic Syntheses via Boranes. Vol. 3*. Milwaukee, WI: Aldrich Chemical; **2003**.

Suzuki, A. *J. Organomet. Chem.* **1999**, *576*, 147-168.

Takacs, J. M.; Han, J. *Org. Lett*. **2004**, *6(18)*, 3099-102.

Takaya, Y.; Ogasawara, M.; Hayashi, T.; Sakai, M.; Miyaura, N. *J. Am. Chem. Soc.* **1998**, *120*, 5579–5580.

Takemoto, Y. *Chem. Pharm. Bull.* **2010**, *58*, 593-601.

Tarasow, T. M.; Tarasow, S. L.; Eaton, B. E. *Nature* **1997**, *389(6646)*, 54-7

Taylor, M. S.; Jacobsen, E. N. *J. Am. Chem. Soc*. **2004**, *126*, 10558-10559.

Taylor, M. S.; Tokunaga, N.; Jacobsen, E. N. *Angew. Chem. Int. Ed*. **2005**, *44*, 6700-6704.

Thompson, R. J.; Davis, J. C. *J. Inorg. Chem*. **1965**, *4*, 1464.

Toporcer, L. H.; Dessy, R. E.; Green, S. I. E. *Inorg. Chem*. **1965**, *4*, 1649.

Traverse, J. F.; Snapper, M. L. *Drug Discov. Today*. **2002**, *7(19)*, 1002-12.

Varki, A.; Cummings, R. D.; Esko, J. D. et al., editors. *Essentials of Glycobiology*. 2nd edition. Cold Spring Harbor (NY): Cold Spring Harbor Laboratory Press; **2009**.

Wahler, D.; Reymond, J.- L. *Curr Opin Biotechnol*. **2001**, *12(6)*, 535-44.

Wang, W.; Gao, X.; Wang, B. *Curr. Org. Chem.* **2002**, *6*, 1285–1317.

Weith, H.; Wiebers, J.; Gilham, P. *Biochem*. **1970**, *9*, 4396.

Welch, C. J.; Szczerba, T.; Perrin, S. R. J. *J. Chromatogr. A* **1997**, *758*, 93–98.

Welch, C. J.; Fleitz, F.; Antia, F.; Yehl, P.; Waters, R.; Ikemoto, N.; Armstrong, I. J. D.; Mathre, D. J. *J. Org. Process Res. Dev.* **2004**, *8*, 186–191.

Welch, C. J.; Grau, B.; Moore, J.; Mathre, D. J. *J. Org. Chem.* **2001**, *66*, 6836–6837.

Wilson, M. E.; Najdi, S.; Krochta, J. M. Hsieh, J-L.; Kurth, M. *J. Macromolecules* **1998**, *31*, 4486-4492.

Wiskur, S. L.; Lavigne, J. J.; Ait-Haddou, H.; Lynch, V.; Chiu, Y. H.; Canary, J. W.; Anslyn, E. V. *Org. Lett.* **2001**, *3(9)*, 1311-1314.

Wiskur, S. L.; Lavigne, J. J.; Matzger, A.; Tobey, S. L.; Lynch, V. M.; Anslyn, E. V. *Chem.-Eur. J.* **2004**, *10*, 3792–3804.

Wol,f C.; Hawes, P. A. J. Org. Chem. **2002**, *67*, 2727–2729.

Wolf, C.; Bentley, K. W. *Chem. Soc. Rev*. **2013**.

Wrackmeyer, B. *Annu. Rep. NMR Spectrosc*. **1988**, *20*, 61-203.

Wright, A. T.; Griffin, M. J.; Zhong, Z.; McCleskey, S. C.; Anslyn, E. V.; McDevitt, J. T. *Angew. Chem., Int. Ed.* **2005**, *44*, 6375–6378.

Wulff, G. *Pure Appl. Chem.* **1982**, *54*, 2093-2102

Wulff, G., Dederichs, W., Grotstollen, R., Jupe, C. *On the chemistry of binding sites, Part II: Specific binding of substances to polymers by fast and reversible covalent interactions, in Affinity Chromatography and Related Techniques*, Gribnau, T. C. J., Visser, J., Nivard, R. J. F., Eds., Elsevier, Amsterdam, **1982**.

Wulff, G.; Lauer, M.; Böhnke, H. *Angew. Chem. Int. Ed*. **1984**, *23(9)*, 741–742.

Xie, J.-H.; Zhu, S.-F.; Zhou, Q.-L. *Chem. Rev*. **2010**, *111*, 1713-1760.

Xing, Z.; Wang, H. C.; Cheng, Y.; Zhu, C.; James, T. D.; Zhao, J. *Eur. J. Org. Chem.* **2012**, *6*, 1223-1229.

Xu, H.; Zuend, S. J.; Woll, M. G.; Tao, Y.; Jacobsen, E. N. *Science* **2010**, *327*, 986-990.

Yang, W.; Gao, S.; Gao, X.; Karnati, V.R.; Ni, W.; Wang, B.; Hooks, W.B.; Carson, J.; Weston, B. *Bioorg. Med. Chem. Lett*. **2002**, *12*, 2175-2177.

Yang, W.; Gao, X.; Wang, B. *Med. Res. Rev.* **2003**, *23(3)*, 346-368.

Yang, W.; Lin, L.; Wang, B. *Tett. Lett.* **2005**, *46*, 7981–7984.

Yasuda, H.; Kurokawa, T.; Fuji, Y.; Yamashita, A.; Ishibashi, S. *Biochim. Biophys. Acta* **1990**, *1021*, 114.

Yeste, S. L.; Powell, M. E.; Bull, S. D.; James, T. D. *J. Org. Chem.* **2008**, *74(1)*, 427-430.

You, L.; Berman, J. S.; Anslyn, E. V. *Nat. Chem.* **2011**, *3(12)*, 943-948.

Zaubitzer, F.; Buryak, A.; Severin, K.; *Chem. Eur. J.* **2006**, *12*, 3928–3934.

Zhang, T.; Anslyn, E. V. *Org. Lett.* **2007**, *9*, 1627–1629.

Zhang, W.; Zhang, X. *Comprehensive Chirality*; Editors-in-Chief: Erick, M. C., Hisashi, Y., Eds.; Elsevier: Amsterdam, **2012**, 301-317.

Zhang, X.; You, L.; Anslyn, E. V.; Qian, X. *Chem. Eur. J.* **2012**, *18*, 1102–1110.

Zhang, Z.; Schreiner, P. R. *Chem. Soc. Rev.* **2009**, *38*, 1187-1198.

Zhao, J.; Davidson, M. G.; Mahon, M. F.; Kociok-Kohn, G.; James, T. D. *J. Am. Chem. Soc.* **2004**, *126*, 16179–16186.

Zhao, J.; Fyles, T. M.; James, T. D. *Angew. Chem., Int. Ed.* **2004**, *43*, 3461–3464.

Zhao, Q.; Li, S.; Huang, K.; Wang, R.; Zhang, X. *Org. Lett.* **2013**, *15*, 4014-4017.

Zhu, L.; Anslyn, E. V. *J. Am. Chem. Soc.* **2004**, *126*, 3676–3677.

Zhu, L.; Shabbir, S. H.; Gray, M.; Lynch, V. M.; Sorey, S.; Anslyn, E. V. *J. Am. Chem. Soc.* **2006**, *128*, 1222-1232.

Zhu, L.; Zhong, Z.; Anslyn, E. V. *J. Am. Chem. Soc.* **2005**, *127*, 4260–4269.

Zuend, S. J.; Jacobsen, E. N. *J. Am. Chem. Soc.* **2009**, *131*, 15358-15374.